Characterisation of Subsidiary Pacemaker Tissue in an *Ex Vivo* Model of Sick Sinus Syndrome and its Utility for Biopacemaking.

A thesis submitted to The University of Manchester for the degree of Doctor of Philosophy in the Faculty of Medical and Human Sciences

2010

Dr Gwilym Matthew Morris

School of Medicine

Contents

Word count 50,893

List of tables

List of figures

Abstract

Dr Gwilym Matthew Morris

Submission for the degree of Doctor of Philosophy, The University of Manchester

Ion Channel Expression in the Pacemaker of the Heart, the Sinoatrial Node

September 2010

Background: Sick sinus syndrome (SSS) is common and may require electronic pacemaker implantation, gene therapy (biopacemaking) may be an alternative. For SSS, repair may be better than the generation of a *de novo* biopacemaker, due to the complex nature of the sinoatrial node (SAN). We hypothesised that an *ex vivo* model of SSS could be created by the identification of a subsidiary pacemaker in the SAN region, and that expression of a pacemaker channel (HCN4 or HCN212) in this region would accelerate the pacing rate.

Methods: A bradycardic SSS model was generated by the removal of the upper two thirds of a rat SAN and a system to record the intrinsic activity during tissue culture was developed. The leading pacemaker site of the SSS preparations were identified by activation mapping then characterised by I_f blockade, β-adrenergic stimulation, histology and immunohistochemistry. Further SSS preparations were injected in this region with recombinant adenovirus (RAd) expressing no functional ion channel (Ad5-GFP or Ad5-GFP-HCN4Δ); or RAd expressing a functional I_f channel (Ad5-HCN212 or Ad5-PREK-HCN4). During tissue culture electrical activity was monitored using bipolar electrodes.

Results: Tissue culture and monitoring of the rat SAN is feasible and does not induce significant changes in HCN4 or connexin-43 expression. The uninjected SSS preparations displayed a slower rate than the control SAN ($p<0.001$). In 5/6 cases the subsidiary pacemaker was HCN4 –ve and Connexin-43 +ve (in contrast to the SAN) and was close to the superior aspect of the inferior vena cava. The cell size of the subsidiary pacemaker was comparable to that of the SAN and smaller than working myocardium ($p<0.001$). Pacing was responsive to β-adrenergic stimulation and was partially dependent on I_f current. The pacing rate of the AdHCN212-injected SSS preparations was significantly faster than the uninjected SSS preparations ($p<0.001$). The remaining RAd did not significantly affect the pacing rate of the SSS model.

Conclusions: There is subsidiary pacemaker tissue close to the superior aspect of the IVC that shares some characteristics of the SAN. These results suggest that adenovirus-mediated expression of HCN channels in subsidiary pacemaker tissue of the right atrium may be a useful strategy in biopacemaking for SSS.

Declaration

No portion of the work referred to in the thesis has been submitted in support of an application for another degree or qualification of this or any other university or institute of learning.

Copyright statement

Acknowledgements

Though my name alone is printed on the spine of this thesis, its inception and realisation would not have been possible without a great many people. I offer great thanks to my principle supervisor, Professor Mark Boyett, for the initial idea and ongoing encouragement during the (many) times when experimental success appeared an impossible goal. I'm also indebted to his exacting proof reading of this document. Thank you to my other supervisors: Dr Paul Kingston for his guidance in ushering new forms of viral life into this world, to Dr Halina Dobryzinski for her unmatched expertise in immunohistochemistry and to Dr Ming Lei for his keen eye for the fine detail of cellular electrophysiology.

Thank you to all of the members of the laboratory from September 2006 – 2009 who guided and assisted me during my faltering transition from physician to clinician scientist. I am grateful to the wider scientific community of the University of Manchester and to the cardiovascular scientists I have met from across the world, all of whom have reminded me how fascinated I am by basic science.

Thanks to my family, who with their lifelong support have lead me to this juncture; you instilled in me a sense of self-belief that allowed me to pursue my interests unfettered by doubt, but (I hope) with a humility that will always help me to learn from all those around me.

Most importantly, this thesis is dedicated to my wife Michaela, who has been with me through all of the most difficult times. Always there to remind me of what is most important, with unflinching love and support. I couldn't have done any of this without you.

Lastly, no thanks to Mark Twain, who puts me in mind of the viva that awaits, "better to remain silent and be thought a fool than to speak out and remove all doubt".

List of abbreviations

AAV	Adeno-assosciated virus
Ad	Adenovirus
Ad5	Human adenovirus serotype 5
AF	Atrial fibrillation
Amp	Ampicillin
ANP	Atrial natriuretic peptide
AP	Action potential
AVN	Atrioventricular node
bp	Base pairs
bpm	Beats per minute
cAMP	3'-5'-cyclic adenosine monophosphate
CAR	Coxsakie and adenovirus receptor
CCS	Cardiac conduction system
cGMP	3'-5'-cyclic guanosine monophosphate
CICR	Calcium induced calcium release
CPE	Cytopathological effect
CS	Coronary sinus
CT	Crista terminalis
Cx	Connexin
DD	Diastolic depolarization
dH_2O	Distilled water
DMSO	Dimethyl sulphoxide
ECG	Electrocardiogram
EDTA	Ethylenediaminetetraacetic acid
ES	Encapsidation signal
EtOH	Ethanol
FLAG	Epitope tag N-DYKDDDDK-C
FO	Fossa ovalis
HCN	Hyperpolarisation-activated cyclic nucleotide gated

hMSC	Human mesenchymal stem cells
hrGFP	Humanised renilla green fluorescent protein
IRES	Internal ribosomal entry site
IVC	Inferior vena cava
Kan	Kanamycin
kb	Kilobases
LB	Luria Bertani
MCS	Multiple cloning site
MDP	Maximum diastolic potential
MIEmCMV	Major immediate-early murine cytomegalovirus enhancer/promoter
MOI	Multiplicity of infection
NCX	Na^{+}/ Ca^{2+} exchanger
OCT	Optimum cutting temperature compound
pBR322 ori	Bacterial origin of replication
PBS	Phosphate buffered saline
pfu	Plaque forming units
pS	Picoseivert
R/L arm	Right/Left region of homologous recombination
R/L-ITR	Right/Left inverted terminal repeat
RA	Right atrium
RAd	Recombinant adenovirus
RE	Restriction endonuclease
RYR	Ryanodine receptors
SAN	Sinoatrial node
SDS	Sodium dodecyl sulphate
Sep	Interatrial septum
SERCA	Sarcoplasmic/endoplasmic reticulum Ca^{2+} ATPase
SNRT	Sinus node recovery time
SOCC	Store-operated Ca^{2+} channels

SR	Sarcoplasmic reticulum
SSS	Sick sinus syndrome
Sv40 pA	Sv40 polyadenylation signal
SVC	Superior vena cava
WPRE	Woodchuck hepatitis post-transcriptional regulatory element

1. Introduction

1.1 The origin of the heart beat

The heart has been imbued with great philosophical and spiritual significance for thousands of years. In the second century A.D. Claudius Galen noted the heart would continue to beat when removed from the thorax, thus establishing that the heart did not require external stimulation to beat. This lead to his conclusion that the heart was "as it were, the hearthstone and source of the innate heat by which the animal is governed".[1] We now know that the beating of the heart relies on the generation and coordinated propagation of electrical impulses through the heart by specialised tissues termed the cardiac conduction system (CCS). This was discovered and defined by late 19th and early 20th century anatomists (figure 1).

Walter Gaskell (1847 – 1914) performed an extensive series of experiments that established the basis of the heart beat and the mode of propagation. He noted that strips of cardiac muscle would continue to beat in isolation, establishing the principle of intrinsic automaticity.[2] In the tortoise heart he observed a peristaltic wave of activity that commenced at the sinus venosus, spreading to the atrioventricular (AV) groove and then on to the ventricle.[2] Histological examination of the sinus venosus revealed an area of thin tissue with a lack of cross striations and large nuclei, what we now know to be the sinoatrial node (SAN). Furthermore, he laid the foundations for the discovery of the mechanism of AV conduction. He noted a ring like sheet of muscular connections in the frog and tortoise heart that could be transected at specific locations to induce varying degrees of conduction block; second degree (Mobitz II) AV block and third degree (complete) AV block with a ventricular escape rhythm.[3]

The nature of this connection between the atria and ventricles was elucidated by Wilhelm His, Jr (1863 – 1934). Examination of the embryological development of the heart revealed the insertion of a connective tissue sheet between the atria and ventricles with the preservation of a muscular tract that bridged the connective tissue before splitting into right and left bundles.[4] He was further able to

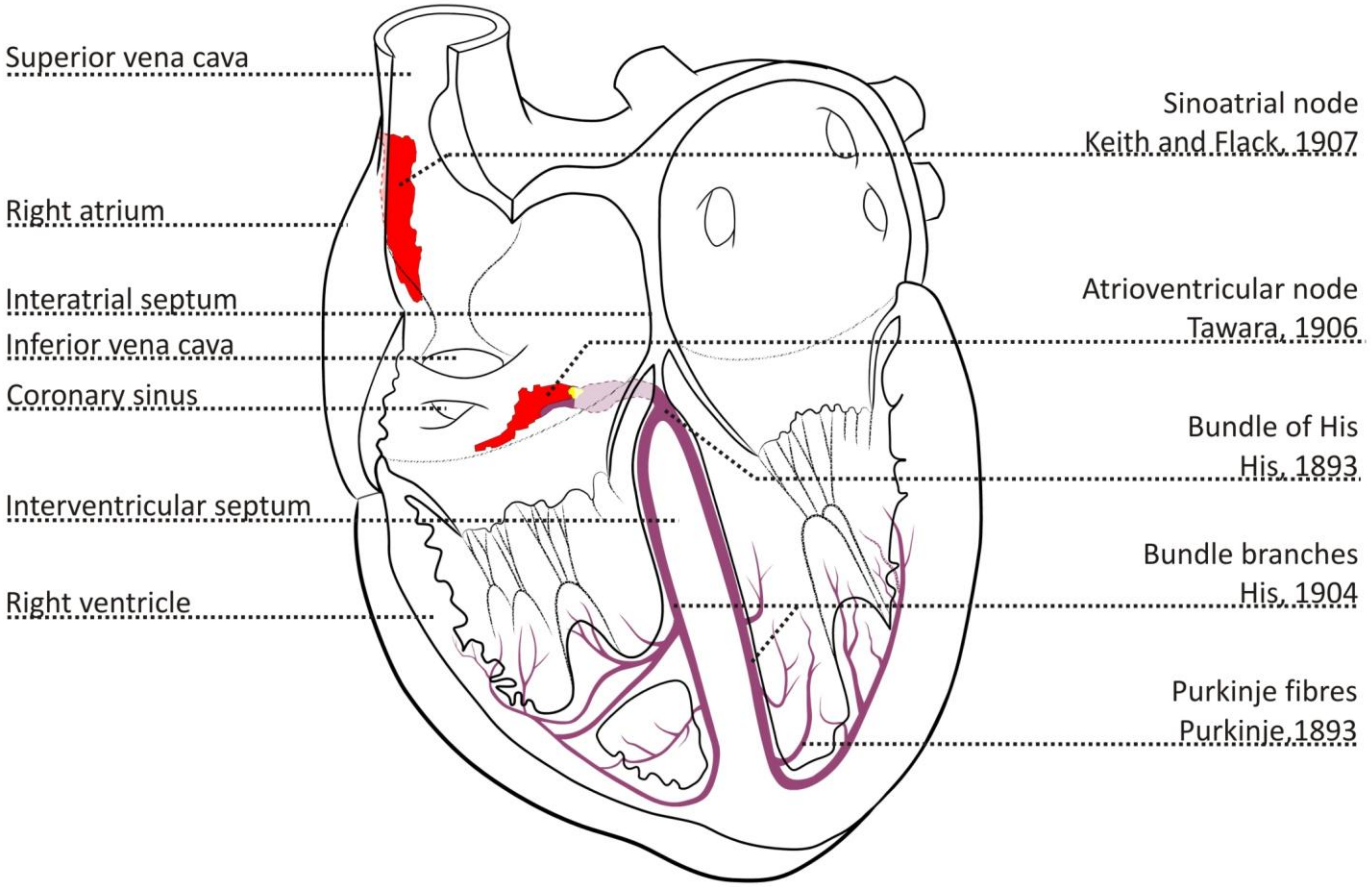

Figure 1. Schematic representation of the cardiac conduction system of the heart with annotation to show the discovery of each component. The sinoatrial and atrioventricular nodes, shown in red, are derived from detailed reconstructions. The remainder is schematic.

demonstrate that division of the eponymously named 'bundle of His' could lead to asynchronous contraction of the atria and ventricles.

The recognition of a unified AV conducting system is credited to Sunao Tawara (1873 – 1952). Working in the laboratory of Ludwig Aschoff, Tawara identified the AV node (AVN) at the base of the interventricular septum and traced its connection to the bundle of His, the right and left bundle branches and on to the Purkinje fibres.[5] Tawara realised that the network of fibres described in 1839 by Jan Purkinje (1787 – 1869) was part of the terminal section of an integrated electrical conduction system.[6]

The origin of the cardiac impulse was elucidated by Sir Arthur Keith (1866 – 1955) and Martin Flack (1882 – 1931). Aware that the origin of the peristalsis of the heart muscle appeared near the sinus venosus they set out to study this area in microscopic detail. While examining the heart of a mole, Flack noted a small structure at the junction of the right atrium (RA) and the superior vena cava (SVC). This was similar in appearance to the AVN described by Tawara, had a distinct blood supply and was densely innervated by the autonomic nervous system.[7] Subsequent electrical recording of the exposed endocardium confirmed that this structure, the SAN, was the primary (leading) pacemaker of the heart.[8]

1.2 The embryological development of the cardiac conduction system

The development of the CCS remains incompletely understood, however, recent work has begun to elucidate the genes responsible for the formation of this specialised conducting cardiac tissue.[9] Consideration of the embryology of the heart explains some of the relationships of the different elements of the CCS and also the existence of ectopic arrhythmic foci and subsidiary pacemakers in the adult heart.[10]

The primitive embryonic heart tube with poorly differentiated primary myocardium displays a slowly conducted sinusoidal electrocardiogram (ECG) initiated in the caudal area, reflected as slow peristaltic waves.[11] By the stage of development of the chamber heart a recognisable ECG has developed.[12] The molecular programme directs the upregulation of high conduction gap junctions so that there are

contractile rapidly conducting myocardial segments (atria and ventricles) and slow conducting non contractile areas (caudal, sinus venosus; mid, atrioventricular canal; dorsal, outflow tract).[13] The further specialisation of these tissues is species-dependent. Higher vertebrates, including most mammals, have a clearly identifiable CCS. It is particularly well developed in hoofed mammals, less so in rodents, with humans somewhere in between.[13]

All of the cardiac tissue is derived from lateral plate mesoderm that fuses during the gastrulation stage in mammalian embryos to form the heart tube. Some of the medial mesodermal cells form progenitor pools that localise to the caudal and dorsal poles of the heart tube serving to proliferate myocardium of the developing heart.[14] In the primitive heart the primary pacemaker activity is located at the caudal pole and remains confined to the most recently added caudal myocytes.[15] Consistent with this observation, this area expresses the pacemaker channel HCN4 (hyperpolarisation-activated cyclic nucleotide gated 4) and there is evidence of repression of high conductance gap junction and ion channel genes (Connexin [Cx]40, Cx43 and SCN5A; see below).[9]

This can be explained by the principle that the 'default' cardiac development pathway is directed by the cardiac homeobox gene *Nkx-2.5* to make contractile myocardium. Repression of this program allows the specialisation and localisation of the CCS. During the development of the caudal (venous) pole of the heart *Nkx-2.5* is repressed; this allows the activation of the transcription factor *Tbx3* and the HCN4 gene, thus directing the development of pacemaker tissue.[16] This area eventually differentiates into the sinus horns and the SAN. Most of the remainder of the developing myocardium expresses *Nkx-2.5* with consequent activation of Cx40, and suppression of the 'pacemaker program'.[10] Later in development the right/left specialisation of the heart is directed by *Pitx2c* with repression of the pacemaker phenotype in the left heart; consequently *Pitx2c* deficient foetuses have SANs in both the right and left atria.[16, 17]

Another important part of the CCS to be considered is the AVN that develops from the atrioventricular canal. While the surrounding myocardium of the heart tube

develops a mature fast conducting phenotype under the direction of *Nkx-2.5* the atrioventricular canal retains a slow conducting embryonic nature. Central to this process is a well defined, evolutionarily conserved pathway. The extracellular signalling molecule Bmp2 activates *Tbx2* which, along with *Tbx3,* represses the expression of Cx40, Cx43 and Scn5a.[18-21] Thus the atrioventricular canal and subsequent AVN is delineated by a Bmp2-Tbx2-Notch-Hey1/2 signalling cascade.[22, 23]

The understanding of the developmental process of the CCS leads to some understanding of the cardiac tissues most prone to causing ectopic pacemaker or arrhythmia in the adult heart and provides a molecular basis for the existence of subsidiary pacemakers. The persistent areas of slow conducting embryological myocardium expressing *Tbx3* are shown in figure 2. Ectopic atrial tachycardias have been demonstrated to arise from the coronary sinus ostium which forms, along with the tricuspid and mitral rings, from the floor of the embryonic atrium which in turn is derived from the atrioventricular canal.[10, 24] Furthermore, 'cristal tachycardia' arising from the crista terminalis (CT) are also likely to originate from this tract of *Tbx3* positive tissue.[25] It may be hypothesised that the repression of the pacemaker program (including HCN4 and *Tbx3*) may be incomplete in these areas so that the tissue is not fully differentiated into fast conducting secondary myocardium, retaining some embryonic characteristics and therefore a propensity to automaticity and arrhythmia.

1.3 The histology of the sinoatrial node

The histologically defined SAN sits near the junction of the SVC and RA.[26] The SAN histology differs from the surrounding myocardium. This was first noted by Gaskell even before the existence of the nodal structure was found by Keith and Flack.[2,7] Gaskell described an area in the sinus venosus lacking in muscle striations and possessing large cell nuclei. In all mammalian species the ultrastructure of SAN cells differs from working myocardium. They are small, pale and have poorly developed sarcomeres and sarcoplasmic reticulum (SR).[27-30] These cells are densely packed in

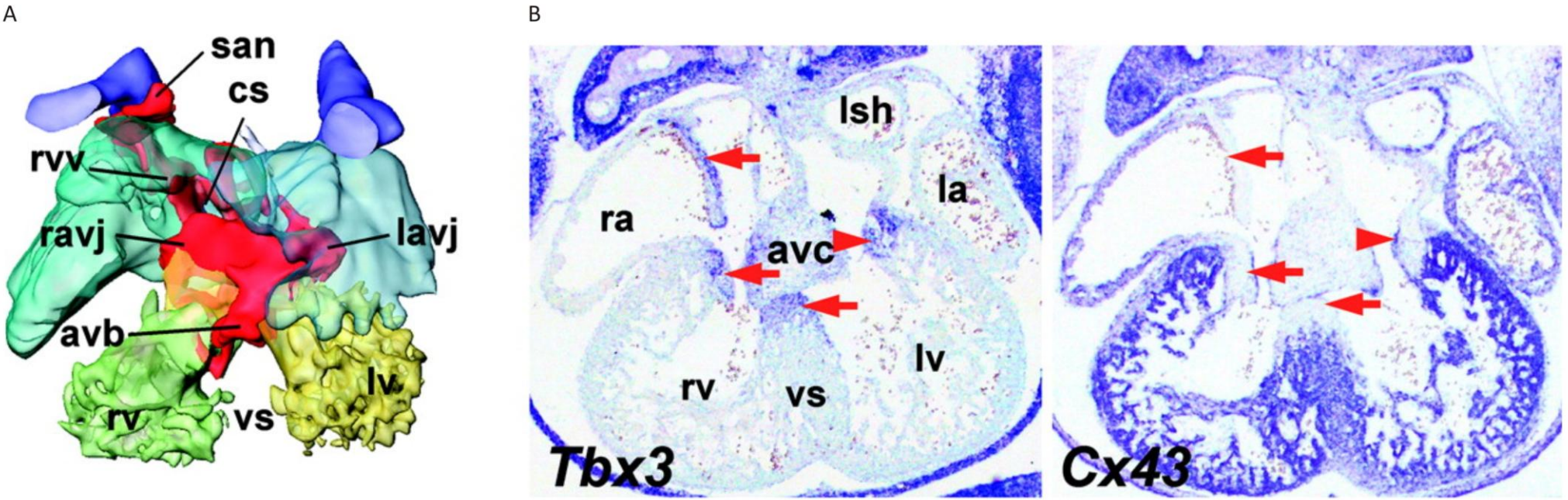

Figure 2. Persistent Tbx3 expression defines the cardiac conduction system driving the development of nodal tissue and internodal tracts. A) Reconstruction of Tbx3 expression in the sinoatrial node of mouse heart. The myocardium has been removed to reveal the Tbx3-expressing area in red. The lumens of the atria, left and right ventricles are shown in blue, green and yellow respectively. B) Sections of an embryonic mouse heart showing that expression of Tbx3 correlates with the absence of Cx43, i.e. with nodal tissue rather than working myocardium. SAN, sinoatrial node; CS, coronary sinus; RVV, right venous valve; AVB, atrioventricular bundle; R/LAVJ, right/left atrioventricular junction; R/LV, right/left ventricle; VS, interventricular septum; LSH, left sinus horn; R/LA right / left atrium; AVC, atrioventricular canal. From Christoffels et al.[9]

an area of highly fibrous connective tissue but interdigitate with the surrounding myocardium (figure 3).[26, 31] The proportion of collagen in the SAN varies between species, apparently increasing with the size of the animal. In small mammals such as the rat or rabbit the SAN is 50% collagen; in the pig and human the node is comprised of 70 – 75% collagen. [32, 33] An increase in extracellular matrix may be required for physical support in the larger SAN. Within the connective tissue the cells are single or organised into small groups of interweaving cells surrounded by a basement membrane.[30]

Traditionally the SAN in the human has been depicted as a small discrete area at the junction of the SVC and RA. This view is based on early histological reconstructions of the SAN that showed it to be a limited structure in this area.[34, 35] However, it is clear that the electrophysiologically-defined SAN extends well beyond this area (see section 1.4).[36] Recent studies using electron microscopy have found the node to be a more extensive structure.[26, 37] Construction of an anatomically detailed model of the rabbit SAN using a combination of histology, electrical mapping and immunohistochemistry supports the view of the extensive nature of the node.[38] The most common position of the human SAN is close to the SVC, 0.1-1 mm subepicardial within the terminal atrial groove (body), extending superiorly (head) and inferiorly (tail) in parallel with the CT. If the SAN artery is taken as a 'signpost' for the position of the SAN then there is large anatomical variation around this point. The position is a variable distance from the CT, the usual shape is crescentic with overall dimensions varying from 8-21.5 mm length, 3.4-13.3 mm height and 1.1-6.6 mm width.[26] The position of the SAN artery within the SAN is not well conserved; the body of the SAN is reliably penetrated by the artery. From here the course is usually central throughout the node but may be eccentric with the artery not extending fully to the tail of the node before coursing between the SAN and epicardium.[26] This large anatomical variation is reflected in functional aspects of the SAN discussed below in section 1.4.

The centre of the SAN is usually the site of first activation (the leading pacemaker site).[39] The central cells are typical nodal pacemaker 'P' cells - they are small (5-10

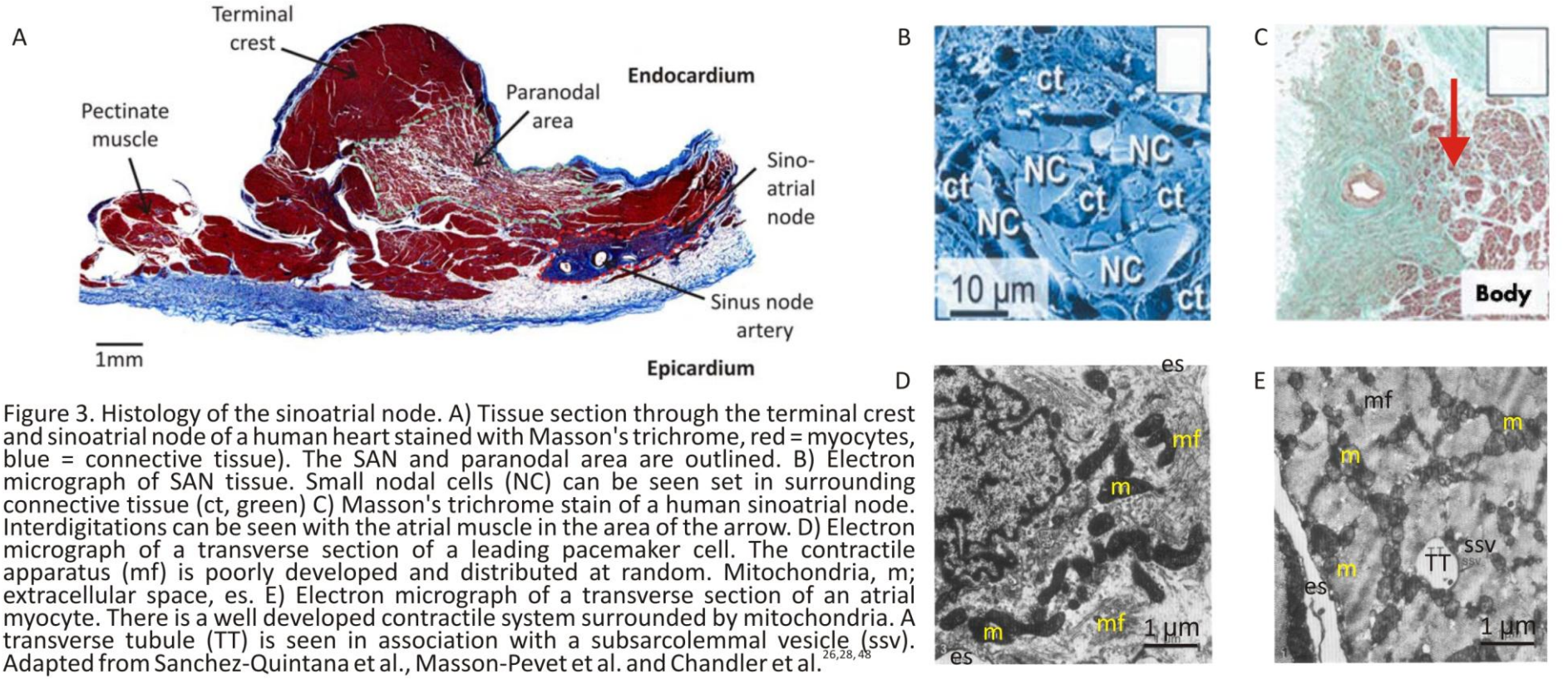

Figure 3. Histology of the sinoatrial node. A) Tissue section through the terminal crest and sinoatrial node of a human heart stained with Masson's trichrome, red = myocytes, blue = connective tissue). The SAN and paranodal area are outlined. B) Electron micrograph of SAN tissue. Small nodal cells (NC) can be seen set in surrounding connective tissue (ct, green) C) Masson's trichrome stain of a human sinoatrial node. Interdigitations can be seen with the atrial muscle in the area of the arrow. D) Electron micrograph of a transverse section of a leading pacemaker cell. The contractile apparatus (mf) is poorly developed and distributed at random. Mitochondria, m; extracellular space, es. E) Electron micrograph of a transverse section of an atrial myocyte. There is a well developed contractile system surrounded by mitochondria. A transverse tubule (TT) is seen in association with a subsarcolemmal vesicle (ssv). Adapted from Sanchez-Quintana et al., Masson-Pevet et al. and Chandler et al.[26,28,48]

µm diameter in canine and human), 'empty' (they contain only a few myofilaments) and spindle shaped.[27] These central cells are orientated perpendicular to the CT and are grouped in islets with interconnecting cytoplasmic bridges.[40, 41] There is a gradual transition of cell type towards the periphery of the SAN, with the appearance and intermingling of cells that are intermediate in morphology between nodal and atrial cells.[27, 38, 42] In the periphery of the SAN the cells are orientated in parallel to the CT.[40] The cell alignment may aid the propagation of the action potential (AP) to the atrial muscle by presenting a planar wavefront which is more likely to be conducted than a convex wavefront.[43] From hereon large atrial muscle cells run parallel to the CT to form a preferential conduction pathway to the AVN.[40]

The precise interaction of the SAN with the surrounding muscle is not known. In the canine and human there is evidence of discrete superior and inferior exit pathways from the SAN with functional block zones laterally.[44] Study of the rabbit SAN suggests that there is an insulating connective tissue sheath around the SAN.[38, 40] However, histological examination of human SAN suggests it is not physically insulated from the surrounding myocardium.[26] While there may be a proliferation of fibro-fatty tissue in older specimens there is no definitive anatomical plane between the SAN and the myocardium in most human hearts studied. There are multiple interdigitating areas of SAN and atrial muscle throughout the border of the SAN and RA muscle (figure 3).[26] Conceptually these two observations could be reconciled by the presence of functional block zones.

In conclusion, the histology of the SAN is complex and varies across species. This arrangement is thought to facilitate the function of the node to reliably drive the surrounding atrial muscle. The discrete exit pathways possibly serve to insulate the SAN from the hyperpolarizing effect of the atrial muscle and protect it from reciprocating tachycardias.

1.4 Electrical activity of pacemaker tissue

It has been known since the 1940s that the hallmark of spontaneously active cardiac tissue is diastolic depolarization (DD), originally termed the 'pacemaker

potential'.[45] AP morphology differs throughout the heart with the AP of the SAN differing markedly from that of the working myocardium (figure 4). Furthermore, the SAN has a relatively depolarized (less negative) membrane potential during phase 4 (diastole) with a slower phase 0 (upstroke) and smaller overshoot (figure 5).[46]

1.4.1 Cellular mechanisms of pacemaking

The genesis of phase 4 DD is central to the pacemaker function of the SAN. It is incompletely understood, but is known to be dependent on the interaction of primary membrane generated potentials (the membrane [M] clock), and intracellular calcium dynamics (the calcium [Ca^{2+}] clock) (figure 6).

1.4.1.1 The membrane clock and associated ion channels

1.4.1.1.1 Delayed rectifier potassium current

Working myocardium has a stable phase 4 resting potential (figure 5), this is generated by an outward current, the 'inward rectifier' K^+ current, $I_{K,1}$, carried by $K_{ir}2$ channels, such as $K_{ir}2.1$.[47] The essential tenet of SAN pacemaking is that it has no stable resting potential, essentially because it lacks $K_{ir}2.1$ and thus $I_{K,1}$.[48] Indeed in ventricular muscle, simply knocking out $K_{ir}2.1$ allows a degree of pacemaking to occur.[49] During the action potential the 'delayed rectifier' K^+ current (I_K) is activated in the SAN and is responsible for repolarization of the SAN myocyte at the end of the action potential. There are three types of I_K known to be present in the SAN; slow ($I_{K,s}$), rapid ($I_{K,r}$) and ultra-rapid ($I_{K,ur}$).[50-54] After the action potential, I_K decays allowing depolarization of the SAN cell. Work has shown that at dominant pacemaker potentials of -55 to -40 mV patch clamp can detect I_K tails, while there is no significant activation of the large depolarizing inward 'funny current' (I_f, see below) until more negative potentials of -80 to -70 mV.[55] Thus the decay of I_K is believed to be responsible for the early pacemaker potential (figures 5 and 6).

$I_{K,r}$ is the most prominent of these currents in the SAN carried by a voltage gated K^+ channel $K_v11.1$ (previously known as the hERG channel); complete and specific pharmacologic blockage can be achieved with E-4031.[39, 47, 53] The use of 0.2-1 μM

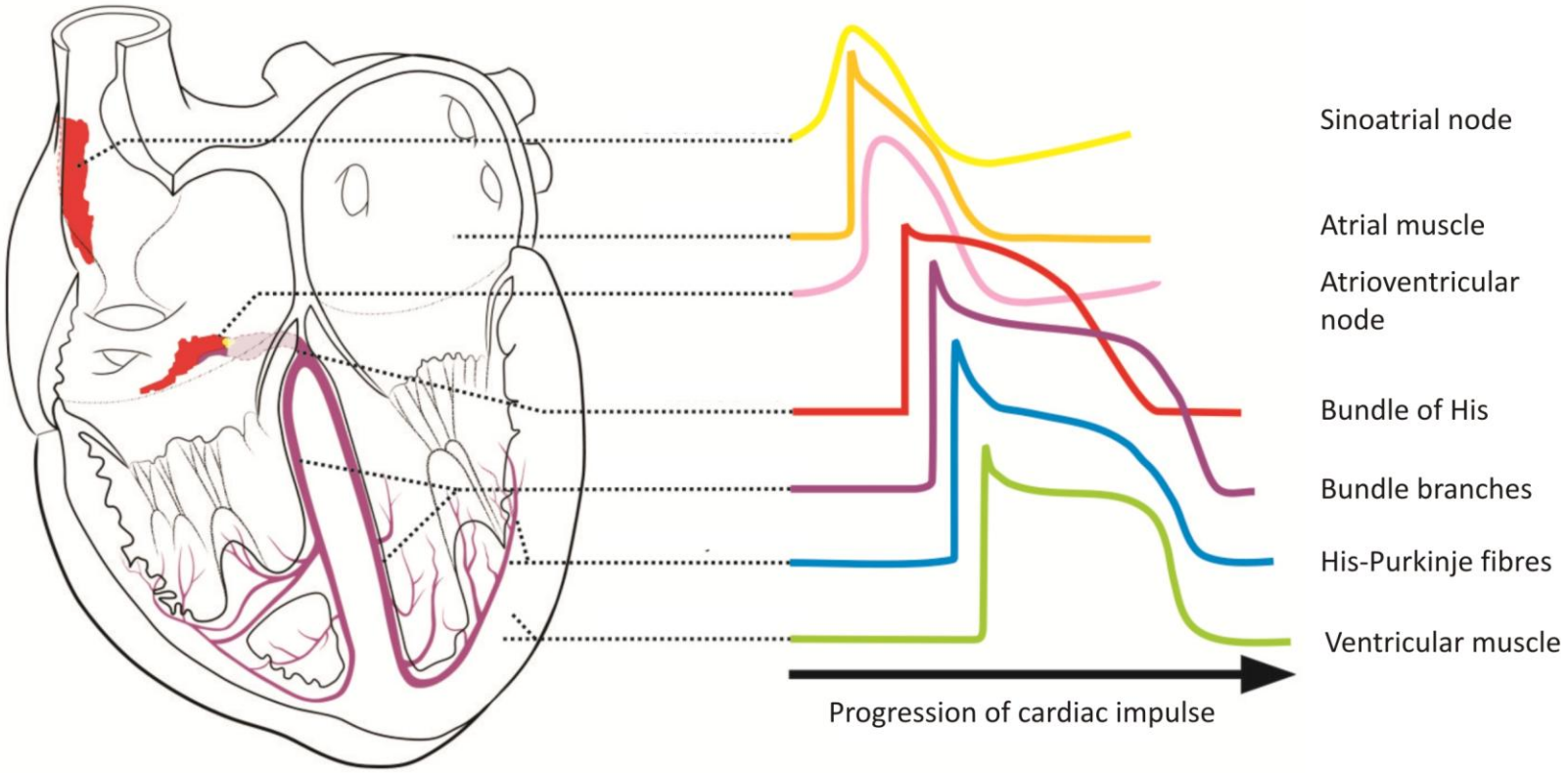

Figure 4. Schematic representation of the cardiac conduction system of the heart, surrounding structures and representative action potential morphologies. The sinoatrial node and atrioventricular node shown in red are based on accurate reconstructions. The His-Purkinje system and action potentials are schematic, though based on published data.

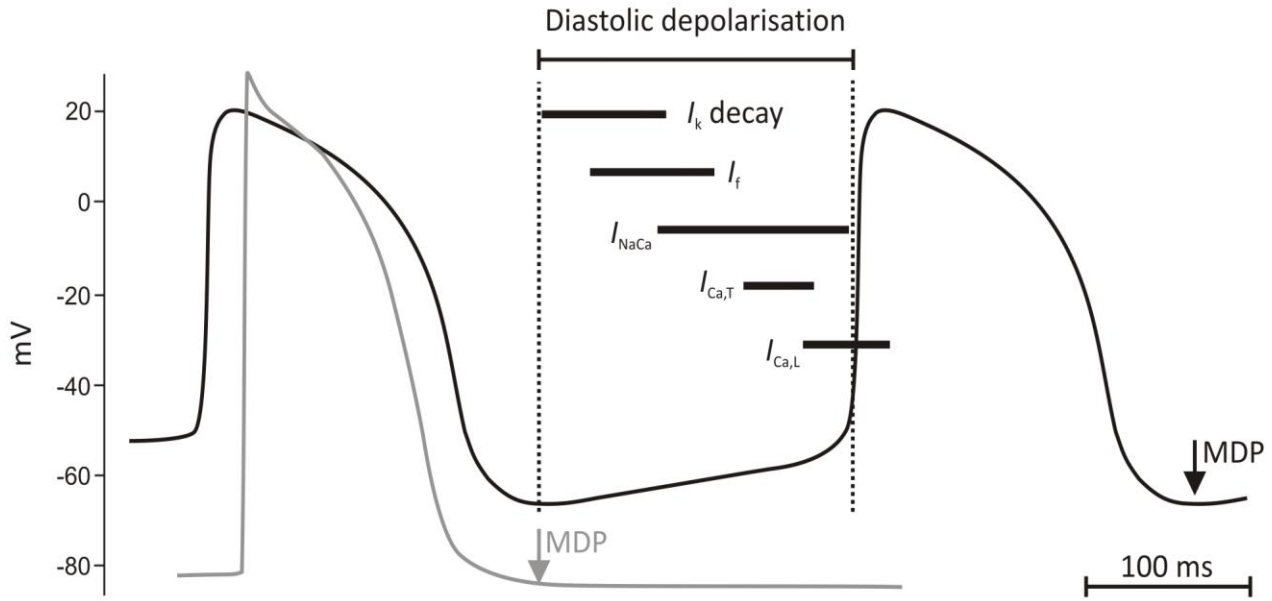

Figure 5. Typical action potentials recorded from atrial muscle (light grey) and the centre of the SAN (black). The temporal contributions of the main ionic currents to the pacemaker potential are shown by the black bars. Adapted from Boyett et al.[40]

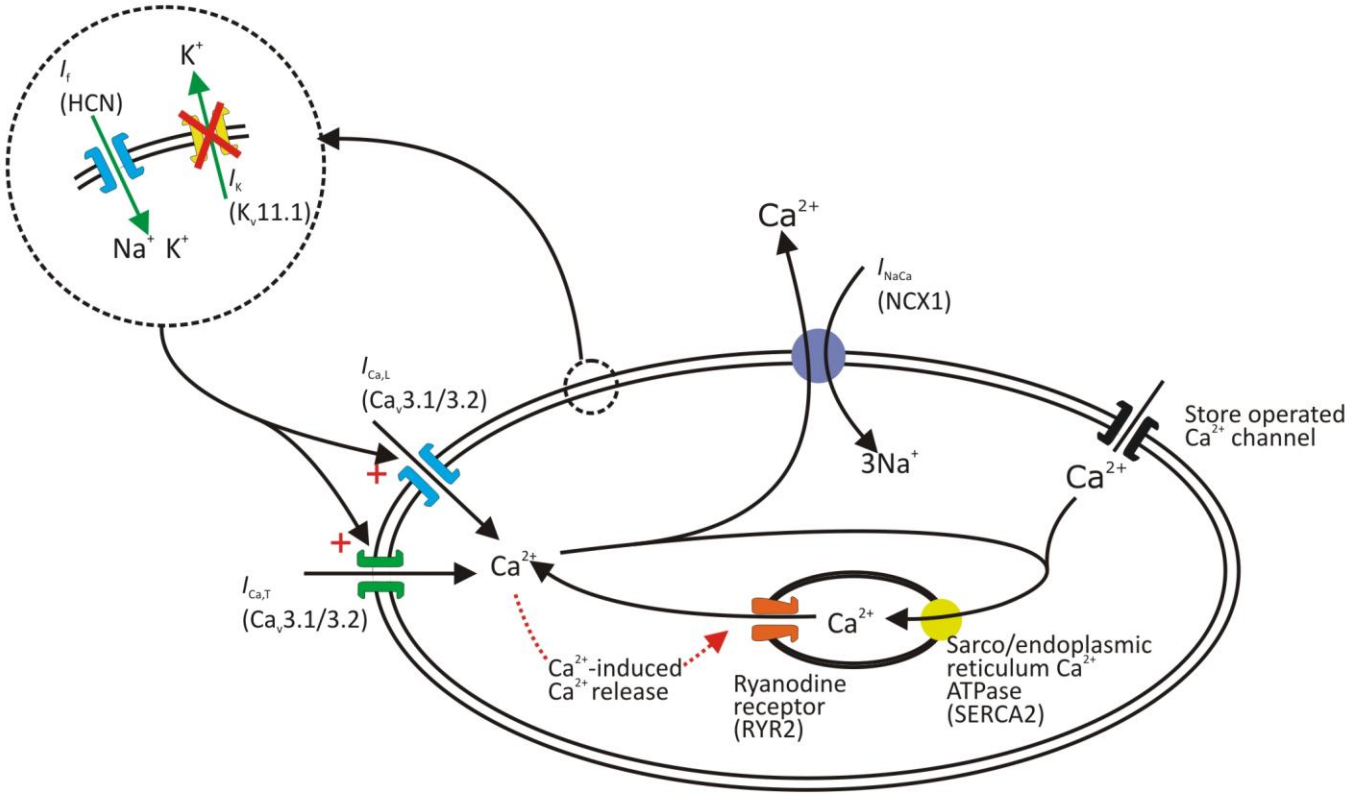

Figure 6. Ionic currents involved in SAN pacemaking. A SAN myocyte is shown. Membrane clock: during the pacemaker potential, there is a voltage-dependent decay of outward current (I_K or outward rectifier K^+ current) and a voltage-dependent activation of at least three inward currents, I_f, $I_{Ca,L}$ and $I_{Ca,T}$. Calcium clock: during the final phase of the pacemaker potential, there is an activation of inward I_{NaCa} in response to a spontaneous release of Ca^{2+} from the sarcoplasmic reticulum via the ryanodine receptor (RyR2). Ca^{2+} release from the sarcoplasmic reticulum also occurs as a result of Ca^{2+}-induced Ca^{2+} release in response to Ca^{2+} entry into the cell via $I_{Ca,L}$ and $I_{Ca,T}$. The sarcoplasmic reticulum is replenished with Ca^{2+} by reuptake via SERCA2. Store-operated Ca^{2+} channels (SOCC) at the cell surface membrane may also help to replenish the sarcoplasmic reticulum with Ca^{2+}. For references see text.

E-4031 on intact rabbit SAN tissue increases the cycle length as well as reducing the slope of phase 0 depolarization, prolonging the action potential and decreasing the maximum diastolic potential (MDP, figure 7).[54, 56] This effect is more pronounced in central SAN tissue with a large proportion of small 'typical' SAN cells. Consistent with this observation it has been demonstrated that complete block of $I_{K,r}$ with 1 µM E-4031 causes cessation of activity in all SAN tissue, while 0.1 µM E-4031 stops pacemaker activity in central tissue only.[50, 54] It is likely that the increased sensitivity to E-4031 represents a reduced density of the K_v11.1 protein in the central areas, immunohistochemical examination of the distribution of the ERG channel shows that the level is high close to the CT (peripheral SAN) and falls away towards the intercaval area (central SAN).[57]

Given that the evidence supports that the decay of I_K is responsible for early DD, why then should blockade of the current stop or slow pacing? Furthermore if reduction of I_K by E-4031 slows pacing, why then is there reduced density of the channel in leading (faster) pacemaker regions? The role of I_K in pacemaking is to repolarise the cell and thus activate the hyperpolarisation-activated current responsible for early to mid DD (I_f), then to decay rapidly so that the depolarization of the cell is not opposed. Therefore complete block of I_K will prevent repolarization of the cell and consequent activation of depolarizing currents. In central SAN areas the density of other ionic currents are reduced (I_{to}, I_{Na} and I_f – see below[39]), so reduced I_K current density may be sufficient to repolarise the cell. Furthermore, reduced I_K must be expected to prevent a disproportionate repolarising drive on the cell causing a stable resting membrane potential. Human adenovirus serotype 5 (Ad5) mediated expression of I_f (HCN1) and $I_{K,1}$ (K*ir*2.1) in guinea-pig left ventricular cardiomyocytes has demonstrated that modulation of pacemaker rate by changing I_f density is dependent on an $I_{K,1}$ density between -2 pA/pF and -4 pA/pF at -60mV.[58] With $I_{K,1}$ outside these parameters cycle length, DD slope and APD_{90} do not correlate with I_f density (figure 7). If I_f is similarly fixed then changing $I_{K,1}$ density does not change cycle length. Although the outward K^+ current in these experiments was $I_{K,1}$ rather than $I_{K,r}$ this supports the notion that the role of I_K in

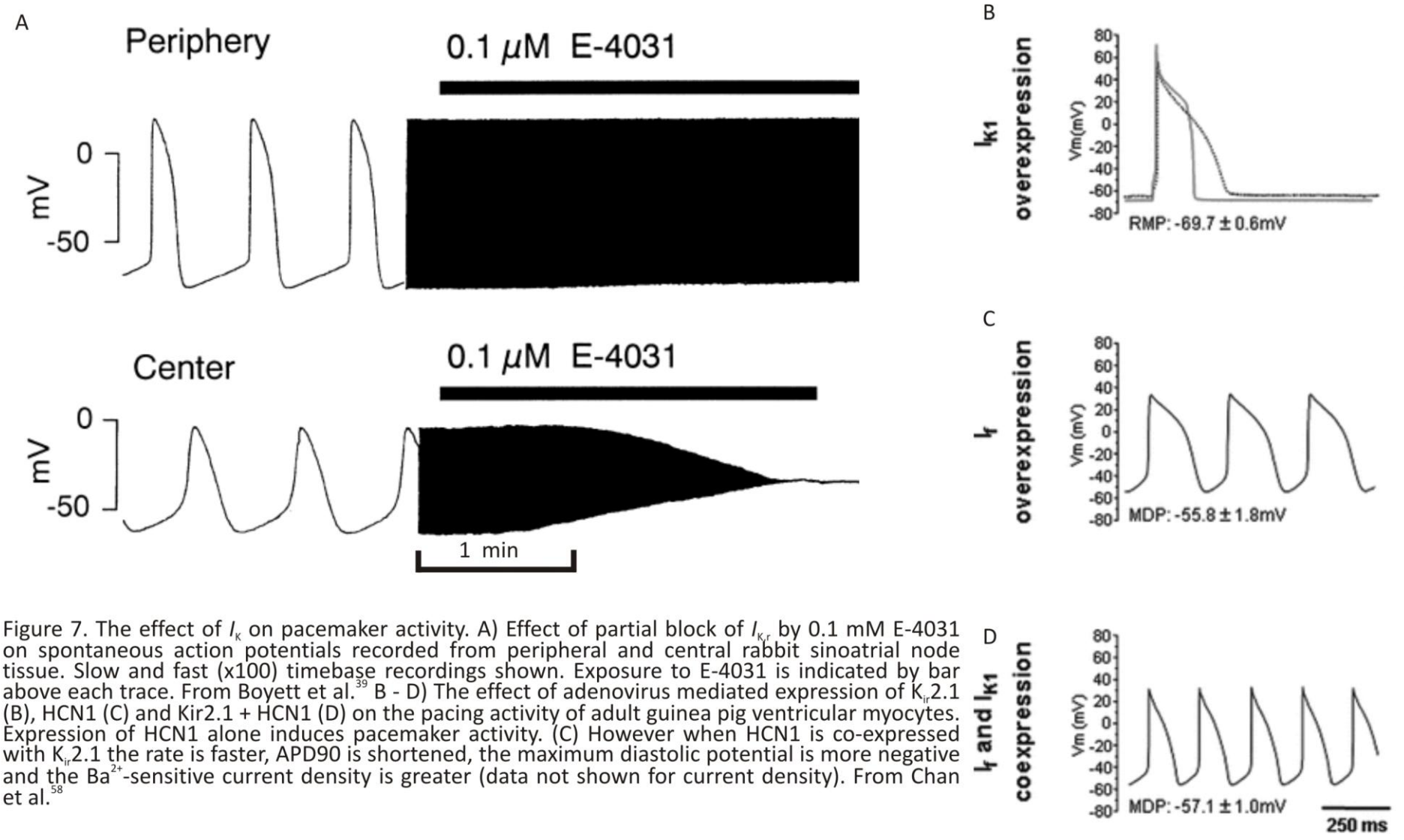

Figure 7. The effect of I_K on pacemaker activity. A) Effect of partial block of $I_{K,r}$ by 0.1 mM E-4031 on spontaneous action potentials recorded from peripheral and central rabbit sinoatrial node tissue. Slow and fast (x100) timebase recordings shown. Exposure to E-4031 is indicated by bar above each trace. From Boyett et al.[39] B - D) The effect of adenovirus mediated expression of $K_{ir}2.1$ (B), HCN1 (C) and Kir2.1 + HCN1 (D) on the pacing activity of adult guinea pig ventricular myocytes. Expression of HCN1 alone induces pacemaker activity. (C) However when HCN1 is co-expressed with $K_{ir}2.1$ the rate is faster, APD90 is shortened, the maximum diastolic potential is more negative and the Ba^{2+}-sensitive current density is greater (data not shown for current density). From Chan et al.[58]

pacemaking is to set the maximum diastolic potential (i.e. beginning of phase 4) to a level at which I_f is most effective.

Much is known about the structure and function of K_v11.1. It has a central role in the generation of inherited and drug-induced long QT syndromes that may lead to torsades de pointes; it has therefore received considerable research interest.[59] The K_v11.1 protein is an 1159 amino acid K^+ channel that is the molecular correlate of $I_{K,r}$.[60, 61] Like most K^+ channels it is a six transmembrane domain voltage-gated K^+ channel, four identical subunits combine to form the functional channel.[62] In addition to the presence in the SAN, K_v11.1 (and $I_{K,r}$) is present in the ventricular muscle.[63, 64] $I_{K,r}$ recorded from ventricular myocytes closely resembles that recorded from pacemaker cells.[64, 65] Patch clamp of recombinant K_v11.1 expressed in mammalian cell lines shows that $I_{K,r}$ contributes mainly to the late part of repolarization during an action potential.[66, 67] Consideration of the properties of K_v11.1 that lead to the current pattern of $I_{K,r}$ aids in the understanding of the contribution of this current to SAN cell repolarization and the current decay in early DD. It is activated by depolarization, but with decreasing outward current at voltages above ~0 mV it displays a significant tail current at negative voltages which is important for pacemaking as described above.[60, 61] It is rapidly deactivated by a fast voltage-dependent 'C-type' (pore collapse) mechanism meaning that current is limited during positive potentials during the phase 2 plateau of the AP.[68, 69] As the membrane repolarises, the rapid recovery of the channels returns them to a conducting state providing a repolarising outward K^+ current; this in turn again rapidly deactivates (forming the tail current) and thus is unable to provide a stable resting potential.

1.4.1.1.2 The funny current

The initial study of the mechanism of pacemaking in Purkinje cells seemed to identify the deactivation of an outward K^+ current ($I_{K,2}$) on hyperpolarization as the primary mechanism behind DD - this was partly based on fact that the reversal potential of $I_{K,2}$ was close to that of a pure K^+ current.[70] However, the study of

pacemaking mechanisms in SAN cells identified an inward current, the 'funny' current (I_f) specifically activated (unlike most voltage gated channels) by hyperpolarization.[71] Following the discovery of I_f it was realised that the initial interpretation of $I_{K,2}$ was flawed due to the presence of $I_{K,1}$ in Purkinje cells and block of $I_{K,1}$ with Ba^{2+} revealed '$I_{K,2}$' to be identical to I_f.[72] There is now a wealth of evidence that I_f is one of the central mechanisms of pacemaker activity: a) the current is activated at SAN pacemaker potentials, around -40 to -65 mV; b) hyperpolarization current can induce pacing activity in non-SAN cells; c) blockage or deficiency of I_f reduces the pacing rate of intact SAN; d) I_f is able to modulate the pacing rate response to sympathetic and parasympathetic stimulation; e) the molecular correlate of I_f are voltage-gated cyclic nucleotide-regulated ion channels, the HCN channels, and they are found in both embryonic and adult SAN tissue.[9, 47, 73-79] This evidence, and the nature of I_f will be discussed in this section.

Expression of I_f (also known as hyperpolarization-activated current, I_h) has been recorded and studied in pacemaker tissues of the heart as well as neurons.[80] Though there is wide variation in the kinetics of I_f recorded from different cells and tissues (time constants varying by orders of magnitude from tens to hundreds of ms) there are recognised features of the current.[78, 80-83] Following hyperpolarization negative to -50 mV there is an instantaneous voltage-independent current leak, followed by delayed activation of the current then achievement of steady-state. This results in a characteristic sigmoidal current waveform.[84, 85] The time constant of activation and the magnitude of the inward current are voltage-dependent; increasing hyperpolarization accelerates activation and increases the inward current.[84, 86] Removal of the hyperpolarizing step results in deactivation of I_f. Study of the tail currents of I_f is complicated by the presence of other voltage-dependent currents; however the deactivation of I_f appears to be influenced by the membrane depolarization such that increasing membrane depolarization accelerates the kinetics of deactivation.[86, 87]

I_f in the mammalian SAN is activated at potentials negative to -50 mV with a time constant of 2 – 4 s at -70 mV and saturates at -100 mV.[88-90] The I_f reversal potential is -25 mV suggesting a mixed cation selectivity.[89] Over the negative part of the

pacemaker range (-40 mV to -65 mV) the predominant contribution to I_f will be Na^+, but the use of Na^+ free solutions has been used to demonstrate a role for K^+.[90, 91] Accurate characterisation of native I_f has been difficult. The single channel conductance of I_f is very small, around 1 pS, making the measurement of single channel events extremely difficult.[88] Furthermore, the measured characteristics of I_f vary widely, perhaps even between areas and cells within a single SAN of an individual animal.[39, 90, 92-95] This variation is in part due to the nature of the f-channels which are known to assemble from multiple subunits, associate with many cell proteins and are strongly modified by cell messengers. Study of I_f by pharmacological blockade of I_f has, until recently, been incomplete and non-specific. For example the blockers Cs^+ and Rb^+ also interact with other ion channels.[78, 96] New pharmacological agents such as ivabradine demonstrate greater channel specificity for I_f.[74] Administration of ivabradine to human subjects causes significant slowing of the heart rate providing evidence for the importance of I_f for heart rate control *in vivo*.[97] Furthermore, a mutant zebrafish expressing very little I_f is profoundly bradycardic; and mice deficient in I_f die in utero having hearts that show slowed cardiac conduction and an absence of primitive pacemaker cells.[75, 98] In humans heterozygous dominant-negative mutations of I_f have been reported to be associated with significant sinus bradycardia.[99-101]

The molecular correlates of I_f are the HCN channels 1-4.[102] Amino acid sequence homology identifies them as members of the K_v superfamily.[47] Four subunits combine to form a functional channel. Each subunit consists of six transmembrane domains with a positively-charged S4 voltage sensor, pore-forming P region and CYG K^+ selectivity filter.[80] The transmembrane domains are highly conserved between the isoforms with 80 – 90% homology.[102-104] The cytoplasmic carboxy terminus of the HCN channels contains a 120 amino acid 3'-5'-cyclic adenosine monophosphate (cAMP) binding domain that bears similarity to the cAMP and 3'-5'-cyclic guanosine monophosphate (cGMP) binding domains of other cyclic nucleotide binding proteins.[102, 105, 106] Deletion of this region suggests it functions to inhibit the channel, slowing the kinetics.[106] Thus binding of cAMP in response to adrenergic stimulation removes this inhibition and provides a mechanism to

increase I_f and therefore speed DD and pacemaking.[73, 107] The corollary is also true for muscarinic-mediated parasympathetic slowing of the heart rate. This was thought to depend on the activation of a K^+ current, $I_{K,ACh}$. However, acetylcholine reduces I_f at a dose 20 times lower than that required to activate $I_{K,ACh}$ and this lower dose of acetylcholine is capable of slowing the rate of spontaneously beating SAN cells.[108] Single f-channel recordings show that these changes in I_f are mediated by an alteration in the activation curve, hence an increase in the single channel open probability rather than an affect on the channel conductance.[88, 109] Interestingly this is a direct cAMP binding effect and not dependent on phosphorylation.[107] An important feature of the modulation of pacing rate by I_f is that it acts entirely via a change in the slope of DD as first demonstrated by Brown et al.[73] The AP threshold and duration are not altered.[78]

HCN channels expressed in mammalian cell lines assemble into homotetramers or heterotetramers and produce current similar, but not identical to, I_f.[110] This quantitative difference in comparison to I_f conducted through native f-channels is one of the obstacles in determining the features of I_f, but has offered a signpost to the fact that f-channels *in vivo* are probably heterotetramers and are associated with other molecules that modulate their function, so called context dependence.[111] In addition to cAMP binding, further alteration of the function of native f-channels has been demonstrated by the subunit MiRP1; association with caveolae, β2 adrenoreceptors and membrane phospholipids; and phosphorylation by serene/threonine and tyrosine kinases.[112-117] HCNs 1, 2 and 4 are expressed in the heart. The properties of each channel vary; HCN2 displays the largest change in activity in response to cAMP, the speed of activation kinetics vary in the order HCN 1 > 2 > 4 (fast activation time constant 30 ms, 184 ms, 461 ms respectively).[118] HCN4 is the dominant isoform in the SAN of most mammalian species accounting for over 80% of total HCN mRNA.[77, 118, 119] The levels of HCN1 and HCN2 vary according to species. The second most prevalent isoform is HCN1 in humans and rabbits and HCN2 in dogs and mice.[77, 118-120] Thus 'native I_f' is in fact a heterogeneous current, highlighting one of the difficulties in studying this current. In addition HCN channels display current-voltage hysteresis under non-equilibrium

conditions and the degree of hysteresis varies between each isoform, thus potentially altering the contribution to pacemaking under varying cardiac pacing or experimental conditions.[121]

In summary, this mixed Na^+/K^+ current is activated after the action potential by the hyperpolarisation induced by $I_{K,r}$ (see above, section 1.4.1.1.1). As the membrane voltage becomes increasingly negative the open probability of the f-channel increases and the activation kinetics quicken, rapidly increasing the overall magnitude of I_f. At the same time $I_{K,r}$ is deactivating and thus equilibrium is reached at the point of the MDP; following this net cation current becomes inward and DD begins.

1.4.1.2 The calcium clock and associated ion channels

The precise definition of the 'calcium clock' can be disputed as it is a fairly new concept. In this context the components of the calcium clock will be taken to be any of the molecules or processes involved with calcium handling in the SAN cell that contribute to, or impact upon pacemaking activity. The fundamental concept is that calcium contributes significantly to late DD by processes that are linked to, but partially independent from, I_f.[122, 123]

1.4.1.2.1 T-type calcium current

The presence of a transient type (T-type) Ca^{2+} current has been demonstrated by recording I_{Ca} in SAN cells in the presence of nifedipine.[124] $I_{Ca,T}$ is activated at negative membrane potentials (-80 mV), has a small amplitude and is blocked by $NiCl_2$.[124] $I_{Ca,T}$ is dependent on the voltage-gated Ca^{2+} channels, $Ca_v3.1$ and $Ca_v3.2$, and has been found in all cardiac myocytes displaying automaticity, including SAN myocytes.[47, 55, 77] The kinetics of expressed $Ca_v3.1$ and $Ca_v3.2$ closely resemble native $I_{Ca,T}$.[125] These channels are significantly more abundant in the SAN than the working myocardium and in concordance with this the current density is around 10 times larger in SAN cells than atrial or ventricular cells.[48, 124] The activation range and abundance of $I_{Ca,T}$ in the SAN suggests a role in pacemaking but the contribution of $I_{Ca,T}$ to pacemaking varies between species. The current is not detected in porcine SAN cells but the presence of $Ca_v3.1$ has been demonstrated in

the human SAN.[77, 126] Block of $I_{Ca,T}$ with Ni^{2+} prolongs the cycle length by 14% in rabbit and knockout of the $Ca_v3.1$ gene in the mouse leads to bradycardia and increased SAN recovery time.[124, 127] Importantly this effect is primarily through a reduction in the slope of the late phase of DD. This supports a mechanism whereby early linear DD is initiated and maintained by $I_{K,r}$ decay and activation of I_f; with late exponential DD and subsequent AP triggering dependant on Ca^{2+} currents, the first of which is $I_{Ca,T}$ activated by I_f-mediated membrane depolarization.

T-type Ca^{2+} channels have α_1 subunits with four transmembrane domains that confer pore selectivity; these are highly conserved between $Ca_v3.1$ and $Ca_v3.2$.[125, 128] A beta subunit (β_{1b}) improves membrane trafficking and current through $Ca_v3.1$ and $Ca_v3.2$, but other subunits do not appear to significantly alter the channel function.[125, 129] The channels deactivate rapidly, the process of $Ca_v3.1$ deactivation is not dependent on the movement of charged particles and is thought the depend on a 'ball and chain' mechanism.[125, 130]

Given that the current amplitude is small and the channel inactivation is rapid, how can $I_{Ca,T}$ contribute so significantly to pacemaking? This can be explained by the recruitment of Ca^{2+}-induced Ca^{2+}-release (CICR) by ryanodine receptors (RYR) on the sarcoplasmic reticulum which amplifies the contribution of $I_{Ca,T}$ and thus initiates the Ca^{2+} clock.

1.4.1.2.2 Ryanodine receptors, oscillatory calcium events and sodium/calcium exchange

While the process of CICR is a well accepted phenomenon in cardiac cells, it has been studied mainly in ventricular myocytes.[131, 132] In these cells the process of CICR is tightly controlled and regulated by the tight juxtaposition of membrane L-type Ca^{2+} channels and sarcolemmal RYRs in transverse(t)-tubules.[133-135] The RYR subunit contains a transmembrane pore forming domain with cytosolic sites for Ca^{2+} binding, calmodulin binding and phosphorylation.[136] The functional channels are homotetramers.[136] There are thousands of organised Ca^{2+} release units per cell generating Ca^{2+}sparks that allow the coordinated release of Ca^{2+}throughout the cell.[137]

In contrast SAN cells do not possess t-tubules and therefore the regulation of Ca^{2+} release might be expected to differ.[138] The use of FLUO-4 and confocal microscopy has allowed detailed temporal and spatial examination of the Ca^{2+} dynamics of cardiac cells. The existence of an intracellular independent Ca^{2+} clock has been proposed. The SR possesses Ca^{2+} release channels (RYR) and a pump to replenish stores (Sarcoplasmic/Endoplasmic reticulum Ca^{2+} ATPase, SERCA). Spontaneous Ca^{2+} release has been observed under non-physiological conditions (e.g. high [Ca^{2+}] or low [K^{+}]) in Purkinje fibres and SAN cells.[139] Spontaneous Ca^{2+} is release also seen when the SR is disconnected from the cell membrane by 'skinning' cells, study of cell fragments or isolated SR vesicles reveals.[140-142] Unlike the global Ca^{2+} release seen in ventricular myocytes in response to an AP, this activity is seen as localised Ca^{2+} release manifesting as sparks or wavelets.[143-145]

However, study of Ca^{2+} release under physiological conditions in whole SAN cells suggests, as might be expected, that Ca^{2+} is tightly regulated and linked to the membrane potential. Ca^{2+} sparks increase with membrane depolarization between -60 mV and -40 mV and are seen in the subsarcolemmal space (figure 8).[146] Hence it seems there is local control of CICR located at the cell membrane of SAN cells in a manner analogous to that seen in the t-tubules of ventricular myocytes, a theory supported by the peripheral distribution of RYR in SAN cells.[147, 148]

Evidence that the late phase 4 Ca^{2+} release is orchestrated by $I_{Ca,T}$ comes partly from the voltage activation characteristics - activation occurs between -60 mV and -40 mV and is therefore termed low voltage Ca^{2+} release.[146] Furthermore, low voltage Ca^{2+} release is abolished by Ni^{2+} block of $I_{Ca,T}$.[149] The importance of the localised Ca^{2+} release events in pacemaking is suggested by the speed of the 'ticking' of the Ca^{2+}clock. The speed of Ca^{2+} restitution determines the speed at which the clock resets. In ventricular cells this is extremely slow (~10 s), in SAN cells it is rapid (~0.5 s).[140]

Further spontaneous Ca^{2+} sparks are generated when the SR Ca^{2+}reaches a critical level, thus the Ca^{2+} clock frequency is determined in part by the speed by which

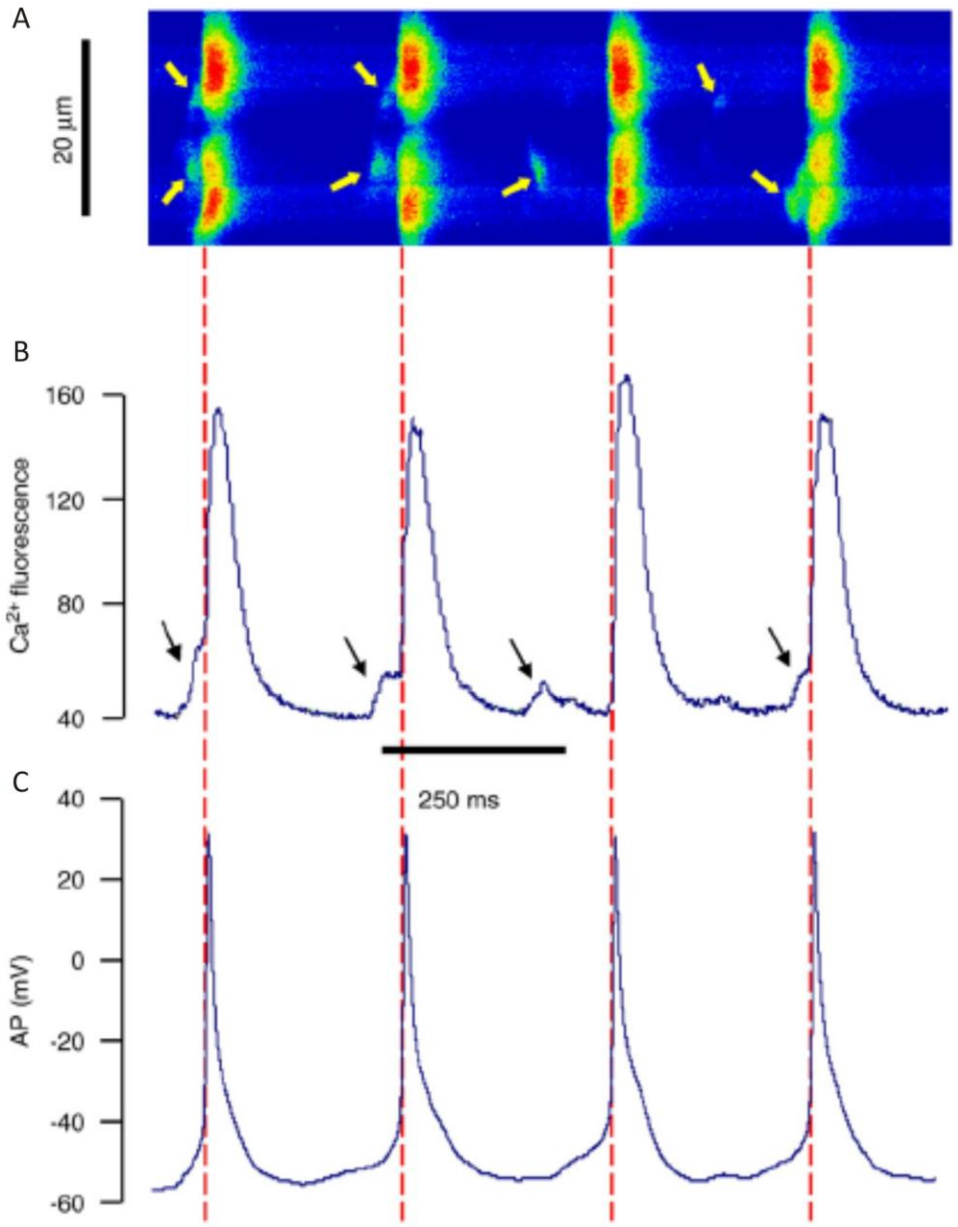

Figure 8. Sarcoplasmic Ca^{2+} sparks are linked to the membrane action potential in sinoatrial node cells. A) Confocal line-scan Ca^{2+} imaging in a SAN cell loaded with Fluo-4 pentapotassium. Arrows denote localised Ca^{2+} sparks that precede the action potential upstroke and Ca^{2+} transients. Localized Ca^{2+} release events were not always captured prior to each Ca^{2+} transient, this is probably due to the technical limitations of the confocal line scanning technique. B) Spatial averaging of Ca^{2+} signals from A. C) The corresponding membrane potential recording. During the patch clamp and Ca^{2+} recordings there was no stimulus applied; the data represent spontaneous events. From Chen et al.[146]

cytoplasmic Ca^{2+} is pumped back into the SR by SERCA. The availability of cytosolic Ca^{2+} may be regulated in part by store-operated Ca^{2+} channels (SOCC) at the cell membrane. The transient receptor potential channels, TRPC1 and TRPC3, appear to act as SOCC and are detected in the SAN.[47, 150-152] The application of SOCC blockers Gd^{3+} and SKF-96365 reduces the pacing rate of mouse SAN cells around one quarter though the exact mechanism is unclear.[152] Another explanation of the increased rate of Ca^{2+} cycling in SAN cells is that basal cAMP levels are high in comparison to ventricular myocytes, even in the absence of β-adrenergic stimulation.[153] This is likely to enhance the action of $I_{Ca,L}$, RYR and SERCA.[122] However, as discussed above, this high basal cAMP will also increase I_f.[107] Interestingly, phosphodiesterase activity is also high in SAN cells, perhaps facilitating rapid and sensitive changes in response to sympathetic or parasympathetic stimulation.[154]

Following amplification of the small $I_{Ca,T}$ via CICR, the elevated intracellular Ca^{2+} is translated into membrane current by the electrogenic forward mode activity (movement of one Ca^{2+} out of the cell for three Na^+ into the cell) of the Na^+/ Ca^{2+} exchanger, NCX1, generating the inward current, I_{NCX}.[155] NCX1 consists of nine transmembrane domains containing α-repeat sequences that facilitate ion transport, and a large cytoplasmic loop containing Ca^{2+}-binding sites.[156, 157] The substrates Ca^{2+} and Na^+ directly activate and regulate NCX1; nanomolar concentrations of intracellular Ca^{2+} promote recovery of the exchanger from the 'I_2 inactivation' state.[157]

The importance of the interaction of RYR/NCX1 and the specific cellular organisation of localised Ca^{2+}release in SAN cells is demonstrated by the close apposition of RYR and NCX1 within SAN cells. As shown in figure 9, confocal microscopy has demonstrated that expression of the two are topographically related.[148] Furthermore, blockage of CICR in SAN cells using ryanodine or blockage of I_{NCX} using Li^+ reduces the inward current by a similar amount when DD is simulated by voltage clamp.[144] The importance of NCX1 in the generation of the membrane current is suggested by the fact that in these experiments Li^+ can abolish spontaneous pacing and ryanodine can slow the pacing rate.[144]

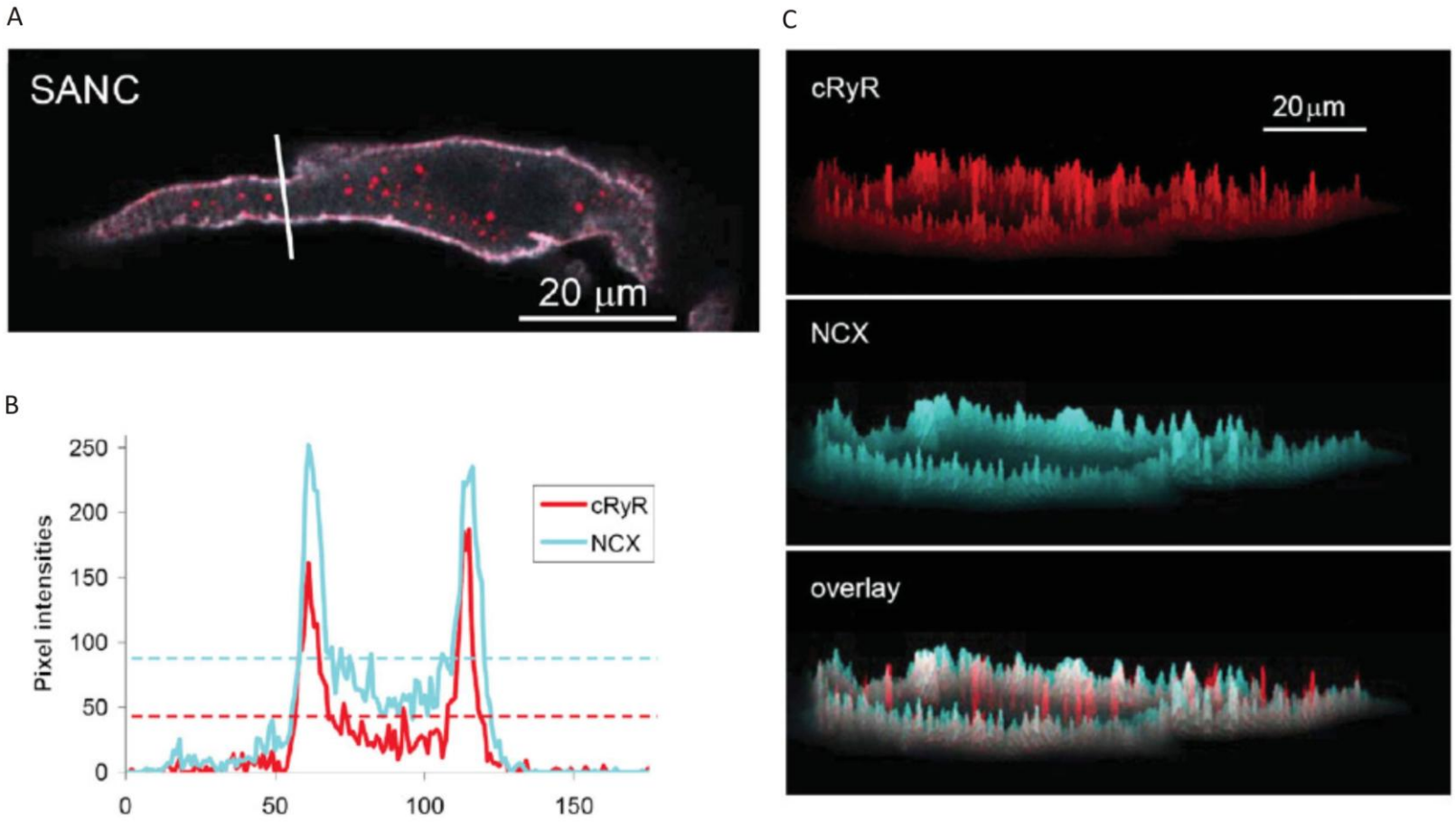

Figure 9. The spatial integration of the sarcoplasmic ryanodine receptor and the surface membrane NCX exchanger as revealed by quantitative immunohistochemistry. A) Laser scanning confocal microscope image of a whole sinoatrial node cell immunolabeled for NCX and RyR. B) Fluorescence intensity of labelling along a line indicated by the thick white line in A. The horizontal dashed lines represent the average pixel intensity. C) Topographical profiles of the pixel intensity levels of each antibody fluorescence. The maximum height represents the brightest pixel; less bright pixels are scaled to a smaller height. From Lyashkov et al.[148]

1.4.1.3 Phase 0, the action potential upstroke

Recordings from the SAN show that phase 0 of the AP is slow in comparison to ventricular muscle (figure 5).[46] Firing of the AP is the end of the specific pacemaking phase, however the unique properties of the SAN AP merit mention. The action potential upstroke in the SAN is carried by $I_{Ca,L}$, thus block of this current with nifedipine abolishes pacemaking.[158, 159] L-type Ca^{2+} channels are formed by isoforms of the pore forming α_1 subunits: α_{1S} ($Ca_v1.1$), α_{1C} ($Ca_v1.2$), α_{1D} ($Ca_v1.3$), and α_{1F} ($Ca_v1.4$).[160] $I_{Ca,L}$ in the SAN is dependent on $Ca_v1.3$, whilst in the working myocardium it is exclusively $Ca_v1.2$ that carries this current.[158] $Ca_v1.3$ has a more negative threshold activation potential than $Ca_v1.2$ and so is more suited to pacemaking tissues, because it is activated earlier by DD. Hence in wild-type mice $I_{Ca,L}$ is activated at -50 mV but in Cav1.3-/- mice $I_{Ca,L}$ is not detected until -20mV.[161] Cav1.3-/- mice display sinus bradycardia and arrhythmia. The AP upstroke and continued pacing in these mice may be dependent on $Ca_v1.2$ or $Na_v1.5$.[47, 161, 162]

The inward Na^+ current (I_{Na}) is important in the working myocardium where it is responsible for the fast upstroke of the action potential, it is carried by the $Na_v1.5$ channel. The $Na_v1.5$ channel is the main α-subunit of the functional channel containing the pore domains, it is known to associate with a number of β-subunits.[163] I_{Na} is abundant in the working myocardium and in the periphery of the SAN, but is absent from the centre of the SAN explaining the slower upstroke of the action potential seen here.[164-166] Despite the documented absence of $Na_v1.5$ from the centre of the SAN, $Na_v1.5$ knockout mice still show bradycardia, long SAN conduction times and SAN conduction block. [48, 167] Likewise, mutations in the gene for $Na_v1.5$ (SCN5A) in humans have been associated with sick sinus syndrome (SSS) [168-172] These effects are surprising given the lack of $Na_v1.5$ in the centre of the node, but are postulated to arise from impaired channel function at the periphery of the SAN.[164] Human SAN myocytes excised from a patient with inappropriate sinus tachycardia showed a large inward current resembling I_{Na}.[173] These myocytes might represent transitional (peripheral) myocytes rather than true central SAN

myocytes, but this finding might also suggest that I_{Na} may be more important in the human SAN than previously thought.

1.4.2 Gap junctions and electrical coupling in the sinoatrial node

Gap junctions facilitate electrical coupling between cardiac myocytes and thus allow propagation of the AP throughout the heart. Vertebrate gap junctions are formed by membrane proteins from the connexin gene family (abbreviated as Cx followed by the mass of the protein in kilodaltons, e.g., Cx43).[174] They are hexameric proteins with subunits consisting of four transmembrane domains, two extracellular loops and a cytoplasmic loop.[175] The hexamers assemble in gap junction plates and allow the intercellular passage of ions and metabolites.[175, 176] Their function may be regulated by phosphorylation of the C-terminal domain.[177]

Cx43 and Cx40 are expressed throughout the atrial working myocardium forming high conductance gap junctions allowing rapid conduction velocity of the AP in this tissue. In contrast, Cx43 and Cx40 are not expressed in the centre of the SAN.[48, 178] Cx45 is expressed in the SAN, where it forms low conductance gap junctions with consequent poor electrical coupling.[178] As a result, the conduction velocity of the AP in the centre of the SAN is slow and the centre of the SAN is electrically insulated from the surrounding atrial muscle.[178] This is important because the hyperpolarizing influence of the resting potential of RA myocardium could suppress the pacemaker activity of the SAN.[178] Towards the periphery of the SAN, the electrical coupling improves; expression of Cx43 and Cx45 has been demonstrated in the peripheral rabbit SAN.[178] As discussed in section 1.3, interdigitations between SAN and atrial myocytes are seen in the periphery, theoretically facilitating the propagation of the action potential from the SAN into the surrounding atrial muscle.[26, 178] The importance of appropriate connexin subtype expression for normal pacemaking is demonstrated by the effects of connexin mutations on normal pacemaking; Cx40 knockout mice and Cx40/Cx43 knockout mice are bradycardic with SAN exit and entry block, as well as a prolongation of SAN conduction time.[179-181] Connexin mutations result in significant disease in humans including oligodentodigital

dysplasia caused by a Cx43 mutation that leads to, among other features, atrioseptal defects, AV block and ventricular tachycardia.[182]

1.4.3 Mapping and characterisation of sinoatrial node electrical activity

1.4.3.1 The leading pacemaker site and the sinoatrial node activation sequence

The activation sequence and propagation of the action potential in the SAN has been extensively studied. The site of first activation, the leading pacemaker site, is typically in a central nodal position close to the SVC. This area is a small volume of less than 1% of the total nodal volume, estimated at around 5000 cells.[183] The site of the leading pacemaker is variable between species. In humans and dogs the site of first activation may vary from a superior to inferior position and there may even be multiple simultaneous leading pacemakers.[36, 184] Interestingly the leading pacemaker, as defined by extracellular potential recording, may not directly correlate with the area of primary negativity when the endocardium is removed allowing direct recordings from the SAN cells.[185] This may have important implications for the accurate identification of the site of arrhythmia in clinical electrophysiology.

Even within a single animal the leading pacemaker site is dynamic, a phenomenon known as pacemaker shift (figure 10).[186, 187] Study of the SAN of the rabbit has clearly demonstrated the variable nature of the leading pacemaker.[186] Pacemaker shift may be a mechanism for mediating heart rate modulation. Alterations in p-wave morphology on the surface ECG can be seen in response to variation in heart rate in humans and dogs (figure 10).[36, 188, 189] This correlates with variation in the exit site from the SAN which in turn may be dependent on the location of the leading pacemaker. Pacemaker shift is mediated by electrical heterogeneity of the SAN. Computer modelling and study of isolated balls of SAN tissue demonstrated that nifedipine (which decreases the heart rate) has a greater effect on central rather than peripheral SAN tissue, and thus the leading pacemaker site shifts from a central to a peripheral location.[38, 190] It is hypothesised that there is a gradient in cell type from ‘typical’ nodal cells at the centre of the SAN, to atrial cells at the

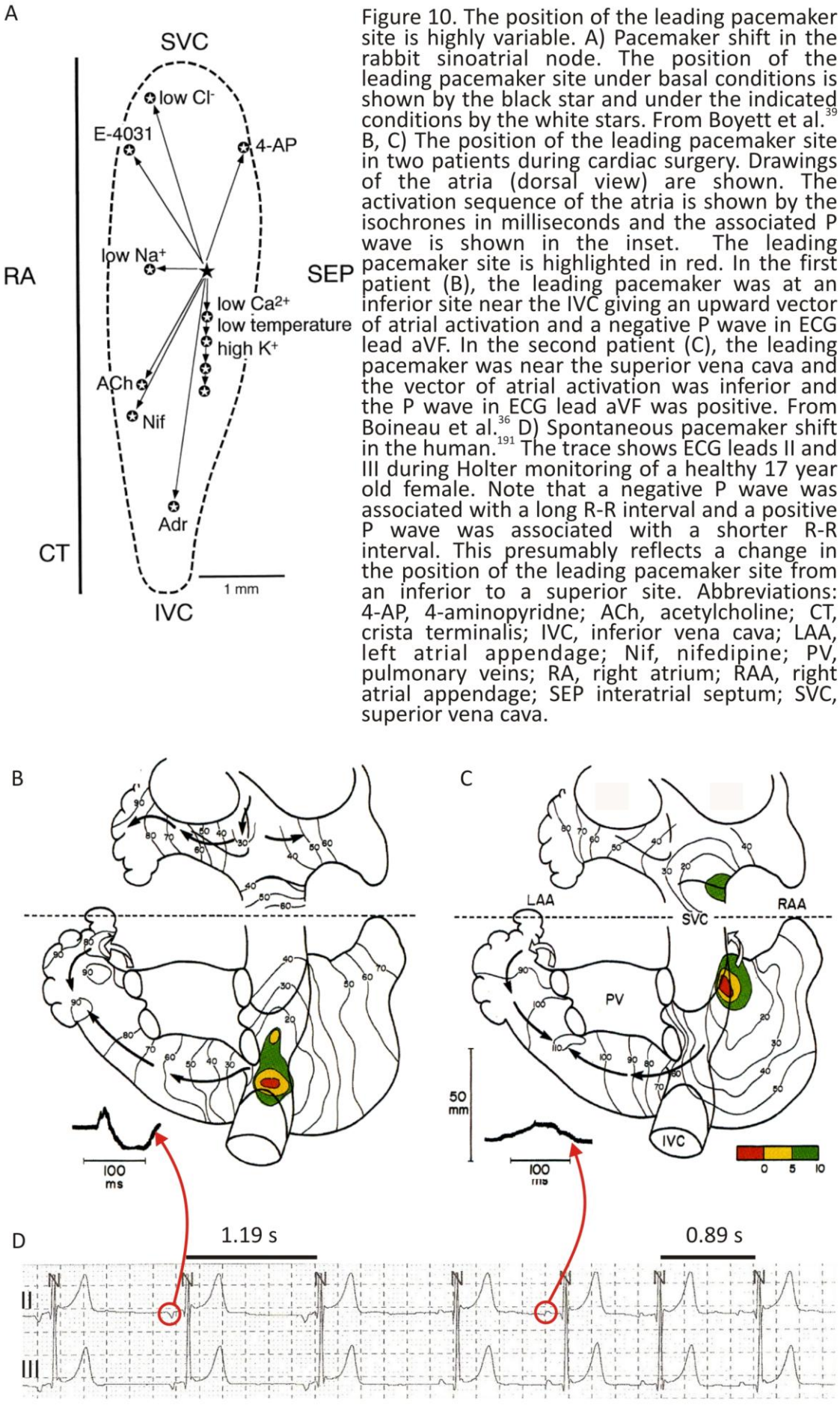

Figure 10. The position of the leading pacemaker site is highly variable. A) Pacemaker shift in the rabbit sinoatrial node. The position of the leading pacemaker site under basal conditions is shown by the black star and under the indicated conditions by the white stars. From Boyett et al.[39] B, C) The position of the leading pacemaker site in two patients during cardiac surgery. Drawings of the atria (dorsal view) are shown. The activation sequence of the atria is shown by the isochrones in milliseconds and the associated P wave is shown in the inset. The leading pacemaker site is highlighted in red. In the first patient (B), the leading pacemaker was at an inferior site near the IVC giving an upward vector of atrial activation and a negative P wave in ECG lead aVF. In the second patient (C), the leading pacemaker was near the superior vena cava and the vector of atrial activation was inferior and the P wave in ECG lead aVF was positive. From Boineau et al.[36] D) Spontaneous pacemaker shift in the human.[191] The trace shows ECG leads II and III during Holter monitoring of a healthy 17 year old female. Note that a negative P wave was associated with a long R-R interval and a positive P wave was associated with a shorter R-R interval. This presumably reflects a change in the position of the leading pacemaker site from an inferior to a superior site. Abbreviations: 4-AP, 4-aminopyridne; ACh, acetylcholine; CT, crista terminalis; IVC, inferior vena cava; LAA, left atrial appendage; Nif, nifedipine; PV, pulmonary veins; RA, right atrium; RAA, right atrial appendage; SEP interatrial septum; SVC, superior vena cava.

periphery.[192] In support of this theory there is an increase in cell size from the centre to the periphery of the SAN.[193] Furthermore smaller cells (as defined by small cell capacitance) are more typically nodal with a slow action potential upstroke (10 V/s compared to 60 V/s for larger SAN cells) and typical SAN current phenotype (e.g. absence of I_{Na}).[194]

1.4.3.2 Exit sites from the sinoatrial node

In the rabbit the AP impulse propagates from the leading pacemaker preferentially in an oblique cranial direction towards the CT.[183] This is thought to facilitate reliable exit from the SAN as the AP waveform will arrive as a broad front to the atrial muscle. However there is evidence for discrete exit pathways from the SAN. A medial block zone (towards the interatrial septum) has been demonstrated in all species studied (cat, rabbit, pig and monkey).[31, 39, 195, 196] Extracellular potential mapping in the dog showed cranial and caudal exit sites and ablation of these discrete sites caused SAN exit block.[185] Optical mapping of the activation sequence of canine SAN and atria confirmed these findings and demonstrated medial (interatrial septum) and lateral (CT) block zones.[44] The propagation of APs recorded in these experiments showed preferential rapid conduction in the supero-inferior axis and slow transverse AP propagation that does not exit the SAN. Perhaps the SAN is surrounded by a loop of blood vessels and connective tissue leading to anatomical and physiological conduction block? Such an arrangement would contribute to electrical insulation from the surrounding hyperpolarizing influences of the atrial muscle, but predispose to SAN exit block if these discrete pathways are compromised.

However, the most comprehensive anatomical studies of human SAN histology to date failed to demonstrate any evidence for an anatomical block in any direction.[26, 197] Indeed, multiple radiations of nodal tissue interdigitating with normal atrial myocardium were noted, suggesting the potential for multiple sites of nodal wavefront breakthrough (figure 3). Thus conduction block around the SAN may be a functional phenomenon (see section 1.5).

1.4.3.3 Overdrive suppression of pacemaker tissues

An important feature of the SAN is the lack of overdrive suppression, i.e. suppression of activity in response to rapid stimulation. The $SNRT_{max}$ (the time to resumption of SAN activity) after fast atrial pacing is of the order of one second in normal human subjects.[198] However other cardiac cells that display some pacemaking activity may be profoundly affected by such stimulation. Purkinje fibre activity may be suppressed for up to one minute by rapid electrical stimulation which would have disastrous consequences for the primary cardiac pacemaker.[199] This is mainly due to the lack of $Na_v1.5$ within the SAN.[39]

1.4.4 Subsidiary pacemaker tissue

As previously discussed, detailed anatomical reconstruction of the rabbit SAN reveals that it is an extensive structure traversing the distance between the SVC and inferior vena cava (IVC) (figure 11).[38] This is in keeping with the observed electrophysiology and embryology of the SAN (see sections 1.2 and 1.4.3).[10, 186] In the rat, node-like tissue has been demonstrated in the interatrial groove and in the atrioventricular ring bundle surrounding the tricuspid valve.[200] In the guinea-pig there is a 'retroaortic node' in the interatrial septum (figure 11).[201] Focal atrial tachycardia in the human is well documented as originating from the pulmonary vein sleeves, coronary sinus ostium, CT, atrial appendages, interatrial septum, left atrium and mitral valve annulus.[24, 25, 202-206] Three-dimensional mapping of the RA in a patient with SSS has recently demonstrated the ability of subsidiary pacemaker tissue at the interatrial septum to support what clinically appeared to be a sinus bradycardia.[207] Intrinsic automaticity has been demonstrated in the inferior portion of the canine RA.[208] This tissue displays reduced sensitivity to Acetylcholine (ACh) but increased sensitivity to noradrenaline and overdrive pacing.[209] Subsidiary pacemaker cells isolated from the Eustachian ridge of the cat (inferior border of the IVC) show intrinsic automaticity with slow DD similar to SAN cells.[210]

There is indirect evidence via pharmacological blockade that both the membrane and Ca^{2+} clocks contribute to pacemaking mechanisms in subsidiary pacemaker tissue.[211] I_K decay and I_f activation has been recorded in these cells.[212, 213] However,

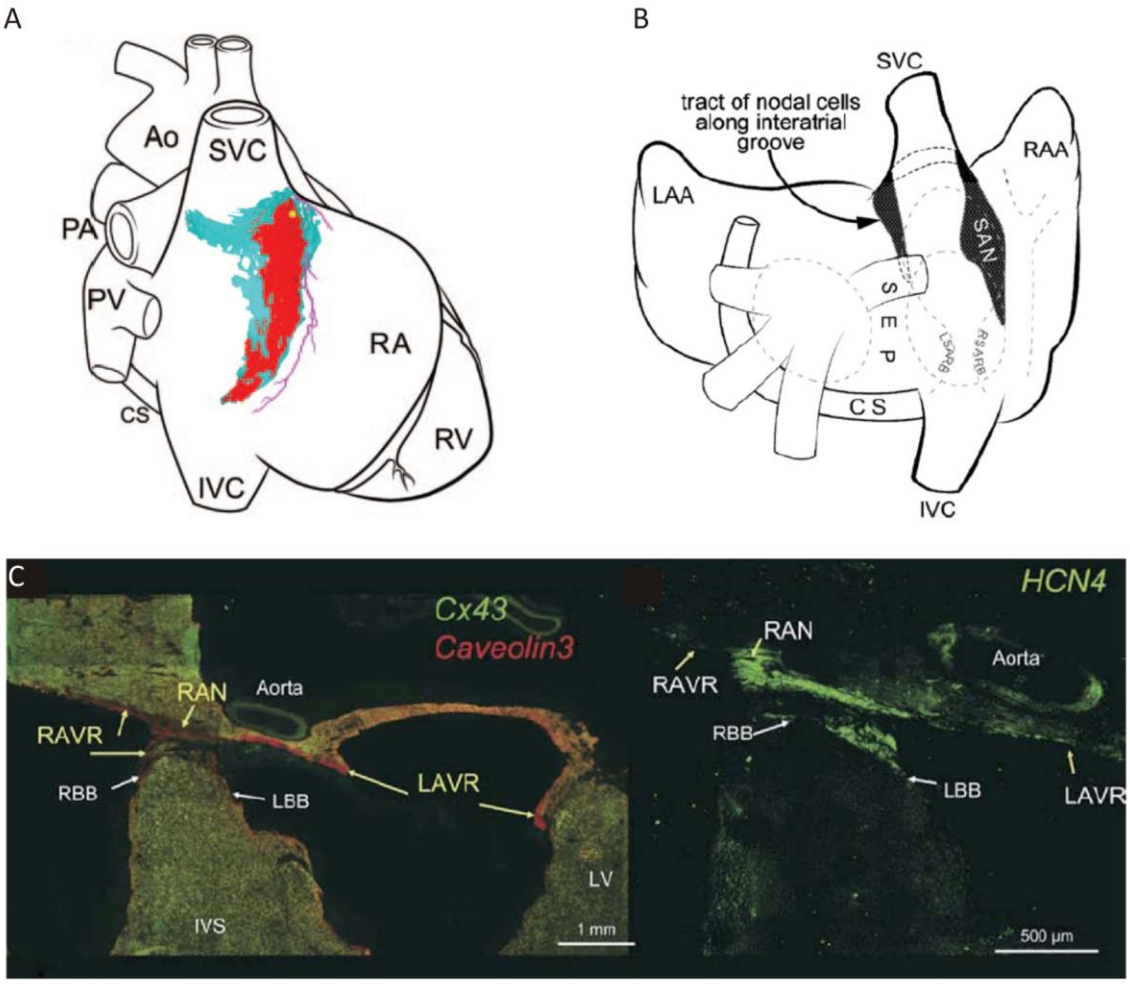

Figure 11. The extent of the sinoatrial node and subsidiary pacemaker tissues. A) Computer 3-dimensional reconstruction of the rabbit sinoatrial node. B) The extent of HCN4 positive tissue in the rat. Note the tract of HCN4 positive cells extending along the interatrial groove. C) The position of the retroaortic node (Cx43 negative, HCN4 positive) in the guinea-pig. From Dobrzynski et al., Yamamoto et al., and Yanni et al., respectively.[38, 200, 201] Ao, aorta; SVC, superior vena cava; PA, pulmonary artery; PV, pulmonary vein; CS, coronary sinus; IVC, inferior vena cava; RA, right atrium; RV, right ventricle; LAA, left atrial appendage; sep, interatrial septum; RAA, right atrial appendage; L/RSARB, left/right sinoatrial ring bundle; RAN, retroarotic node; IVS, interventricular septum; AR, aortic root; LAVR, left atrioventricular ring; R/LBBB, right/left bundle branch; LAVR, left (mitral) atrioventricular ring; RAVR, right (tricuspid) atrioventricular ring.

I_f displays a long time course of activation and small amplitude, perhaps due to a HCN isoform switch? Fluorescence confocal microscopy has demonstrated diastolic Ca^{2+} efflux from subsidiary pacemaker cells, and reduction of Ca^{2+} flux by SERCA or NCX inhibition slows their pacing activity.[211, 214, 215] Although the pacemaker mechanisms are similar to the SAN, the cycle length is approximately double that of SAN cells (perhaps due to reduced I_f) and electron microscopy reveals subtle ultrastructural differences of these cells from true SAN cells.[210]

In the human heart there is an extensive structure within the CT close to but distinct from the SAN, the paranodal area.[77] This area comprises loosely packed myocytes that are mixed in phenotype between typical RA and SAN. There is a unique pattern of ion channel expression in the paranodal area, particularly regarding K^+ channels. There is a high level of expression of $K_v4.2$, $K_{ir}6.1$, TASK1, SK2 and MiRP2 with low levels of $K_{ir}2.1$.[77] The function of this area is not known. It is suggested that the ion channel expression will lead to a relative depolarization in comparison to RA cells. This may be necessary for the facilitation of propagation of the SAN AP to the RA. The paranodal area may also be an important focus of ectopic atrial tachycardias.

1.5 Molecular architecture of the sinoatrial node

As discussed in section 1.4.1, the generation of DD requires ion currents specifically suitable for this role, and these currents differ from those in the working myocardium. These differences are, of course, a result of the expression of specific ion channel 'signatures' within nodal versus working myocardial tissue. The presence or absence of ion channel subtypes has been extensively investigated using quantitative PCR, *in-situ* hybridisation and immunohistochemistry. The generally accepted markers for SAN tissue are the presence of HCN (2 or 4) and Cx45; the absence of $Na_v1.5$, Cx43 and atrial natriuretic peptide (ANP).[40, 41, 158, 216] This has provided a framework for the study of other ion channel subtypes within the SAN.[38] Pacemaker mechanisms vary between species; for example I_f in rabbit is ~ 4 times greater in magnitude when compared to humans.[217, 218] Thus the ion channel signature should be expected to differ between species and indeed this is

the case.[219] In this section the molecular structure of the human and rat SAN will be discussed due to their relevance to clinical problems and the experimental model respectively.

1.5.1 Molecular architecture of the sinoatrial node of *Homo sapiens*

The intrinsic heart rate of humans is 60-80 beats per minute (bpm). APs have been recorded from human SAN; in accordance with data from other species they display DD and a slow phase 0 depolarization.[218] There are little functional data available for the human SAN due to the paucity of experimental tissue. I_f has been directly recorded from human SAN cells and the importance of I_f, $I_{Ca,L}$ and $I_{Ca,T}$ in humans can be inferred from the *in vivo* heart rate lowering effect of ivabradine and diltiazem and mibefradil respectively.[97, 218, 220, 221]

The detailed ion channel structure of the human SAN was recently elucidated.[77] The membrane clock in the human involves the inwardly rectifying K^+ channels $K_{ir}2.1$ and $K_{ir}2.3$ which are present in both the RA and SAN in humans; however levels of both are lower in the SAN than RA which is to be expected as there is no stable resting potential in the SAN.[77, 218] In humans, f-channels comprise HCN4 and HCN1 which are highly expressed in the SAN but not RA - HCN2 was detected in the RA with negligible levels in the SAN (figure 12).[77, 218]

The components of the Ca^{2+} clock are also present. As observed in other mammalian species the T-type Ca^{2+} channel $Ca_v3.1$ is the most abundant and levels are higher in the SAN than RA.[40, 77] SERCA2a and RYR2 are expressed at lower levels in the SAN than RA.[77] Interestingly TRPC6 (SOCC) mRNA is significantly higher in SAN cells than RA, as is RYR3 (though the overall level of RYR3 compared to RYR2 is very low).[77] How high levels of TRPC6 and RYR3 interact with significantly lower levels of SERCA and RYR2 is not clear. These data suggest that the generation of Ca^{2+} sparks in SAN cells may differ from the working myocardium - mechanistic differences in Ca^{2+} spark generation in muscle cells expressing RYR1 and RYR3 have been observed to differ from cardiac muscle expressing RYR2 only.[222]

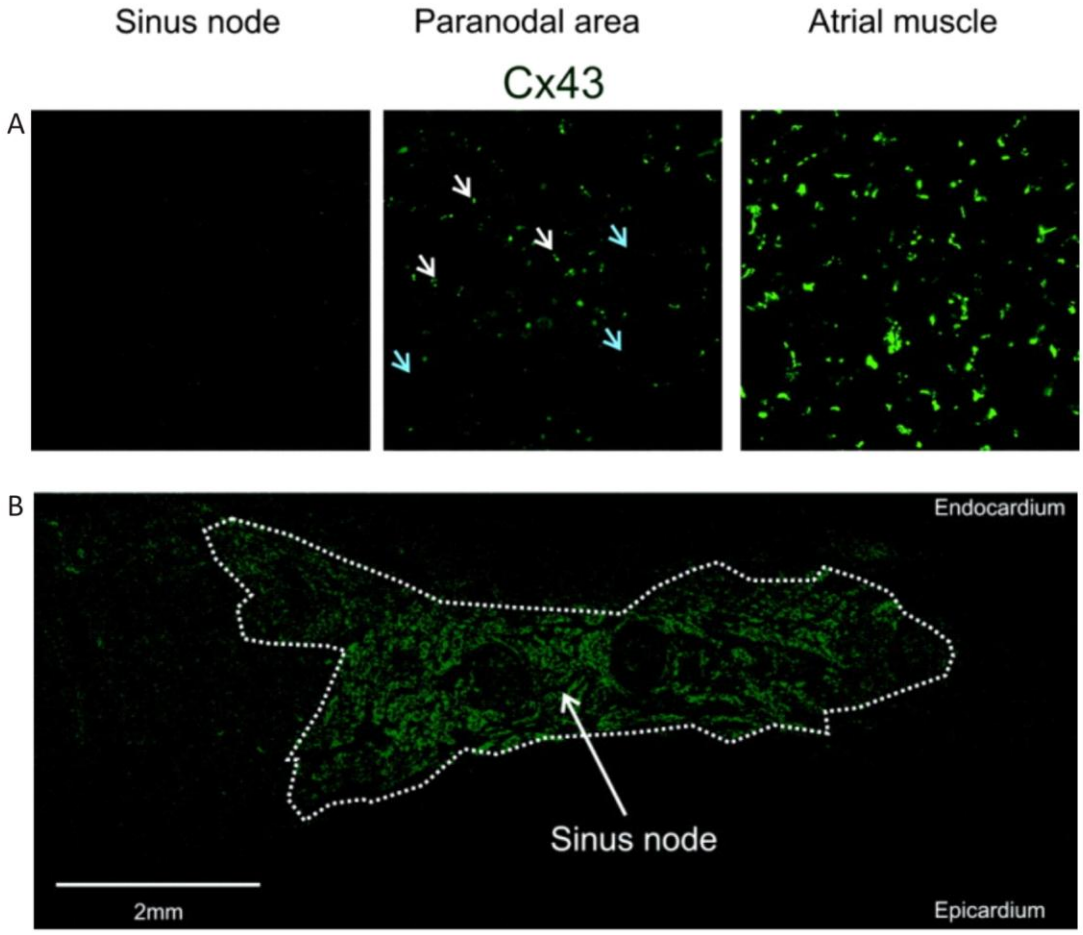

Figure 12. The characteristics of the human sinoatrial node and paranodal area. A) Connexin 43 expression in the SAN, paranodal area and atrial muscle. Cx43 expression is shown by immunohistochemistry in green. For the paranodal area, Cx43 positive cells are denoted by the white arrows and Cx43 negative cells by the blue arrows. B) HCN4 expression in the human SAN revealed by immunohistochemistry. For definition of the areas sampled see figure 3. From Chandler et al.[77]

As expected from the slow phase 0 depolarization, the human SAN does not express $Na_v1.5$ and there is an isoform switch of the L-type Ca^{2+} channel from Cav1.2 to Cav1.3.[77] However other data suggests the presence of I_{Na} in human SAN cells though these may be peripheral rather than central SAN cells.[173] With respect to early repolarization, transient outward K^+ channels are differentially expressed in the SAN: $K_v4.3$ is the predominant isoform in both the RA and SAN, but with lower expression levels in the SAN than RA. There are higher levels of $K_v4.2$ in the SAN than RA, with equal levels of $K_v1.4$.[77] All of the K^+ delayed rectifier channels are expressed at lower levels in the SAN than RA including $K_v1.5$, $K_v11.1$ (ERG) and $K_v7.1$ (K_vLQT1).[77] This suggests that there is a downward gradient in AP duration away from the SAN similar to that noted in rabbits.[223] Accessory subunits are expressed at broadly similar levels in RA and SAN, other than KChIP2 (K^+ channel interacting protein 2) which is highly expressed in the SAN only.[77] Clearly, complex regulatory mechanisms are present and further work will be required to understand why the regulatory subunits should be present at similar or higher levels in the SAN when the K^+ channels themselves are present at lower levels. As expected, the high conductance gap junction proteins Cx40 and Cx43 are absent from the human SAN.[77]

1.5.2 Molecular architecture of the sinoatrial node of *Rattus rattus*

The intrinsic heart rate of the rat is ~390 bpm.[224] Much less data are available regarding the molecular structure of the rat SAN. As in other species, the rat SAN is characterised by absence of Cx43 and $Na_v1.5$, and the presence of HCN4 and Cx45.[200, 225] The f-channels of the rat comprise HCN2 and HCN4 - HCN2 is reported to be the predominant isoform, HCN1 and HCN3 are not detectable.[226] There is broad distribution of pacemaker tissue: the SAN is made up of a large 'head' located in the anterior wall of the SVC; HCN4 and Cx45 positive tissue extends down the side of the CT with a second smaller tail extending down the interatrial groove.[200, 225] HCN4 and Cx45 positive cells are also detectable in the atrioventricular ring bundle round the tricuspid valve but not the mitral valve.[200] Details of K^+ channel and Ca^{2+}-handling protein expression in the rat SAN are not known.

1.6 Disease and remodelling of the sinoatrial node

SAN disease includes a spectrum of clinical disorders. Recognised primary SAN disorders include sinoatrial node re-entry, inappropriate sinus tachycardia and SSS. Of these only SSS causes bradycardia requiring pacing. SSS is a common syndrome causing syncope and presyncope; the ECG may show SAN exit block, sinus arrest, alternating sinus tachycardia or bradycardia and atrial fibrillation (AF). It is a common problem in clinical cardiology and one of the commonest indications for insertion of permanent pacing systems.[227] There are a number of rare causes of SSS, but 'idiopathic' SSS is by far the commonest description and the prevalence increases with advancing age.[228, 229] The cause of SSS is controversial, early histological studies led to a belief that progressive SAN fibrosis and loss of SAN cells underlies the disorder.[230, 231]However, there is also evidence of electrical remodelling as a molecular pathology in SSS, age related changes of the SAN occur with an area of slow action potential upstroke velocity extending into the peripheral SAN are seen with advancing age in the cat and rabbit.[232] Consideration of the anatomical and molecular remodelling of the SAN in different disease states suggests that SSS is a broad and, in some cases, plastic clinical entity.

1.6.1 Idiopathic sinoatrial node disease and ageing

Ageing has long been associated with SAN dysfunction, causing a decrease in the overall intrinsic heart rate, and an increase in SAN conduction time.[164, 232, 233] These changes in humans appear to be preceded by a period of detectable but clinically silent atrial remodelling, this is particularly apparent around the region of the CT leading to slowing of conduction, voltage loss and a decrease in SAN reserve.[234] As may be expected in a bradycardic remodelled SAN, an inferior shift in the leading pacemaker site has been demonstrated in aged rats and humans with SAN dysfunction.[164, 225] However, the site of the leading pacemaker site does not appear to be affected by age in rabbits and cats.[235] Histological studies previously attributed SSS to SAN fibrosis.[232, 236, 237] Indeed it can be shown that ageing leads to significant extracellular matrix remodelling in the SAN of the rat.[225]

However, more recent histological analysis of the SAN in ageing found a decreased SAN volume with fatty infiltration in old human SAN but not young.[238] While other groups have replicated the findings of fatty infiltration around the sinus venosus and SAN, the reduction in SAN volume has not been confirmed in animals or humans.[197, 232] While the reported increase in connective tissue in the SAN with age has not been seen by all groups, there is a redistribution of connective tissue to surround individual nodal cells, or small cell clusters. When combined with observed nodal cell atrophy this gives the illusion of increasing connective tissue area.[33, 232, 238]

There is clearer evidence of electrical remodelling in the pathology of SSS. Ion channel expression is known to display temporal plasticity; in the neonatal rabbit I_{Na} is present throughout the SAN, but in the adult it is absent from the centre; furthermore the area of slow action potential upstroke velocity extends into the peripheral SAN with advancing age in the cat and rabbit. [194, 235, 239] These results suggest an age-dependent downregulation of peripheral $Na_v1.5$ - indeed this has been demonstrated in aged rats along with an age-dependent hypertrophy of SAN cells.[225] This could lead to exit block from the SAN and an inability of the node to drive the surrounding tissue.

Other electrophysiological changes occur. $K_v1.5$ (partly responsible for I_K) is known to decrease with aging in the rat SAN, which could explain the observed age-related increase in AP duration.[235, 240] Decreased expression of Cx43 in the vicinity of the SAN may account for the observed increase in SAN conduction time and SAN exit block seen with ageing.[241] It has also been noted in the guinea-pig that Cav1.2 expression declines during aging.[242]

1.6.2 Ischaemic sinoatrial node dysfunction

Up to a third of the cases of idiopathic SSS may be due to chronic ischaemia of the SAN.[243] Sinus bradycardia and sinus arrest are commonly seen in the acute phases of myocardial infarction due to altered neurological influences on the heart.[244] However, in one study of patients presenting for permanent pacemaker implantation for symptomatic bradycardia, significant coronary artery stenoses

were found in 71% of patients, suggesting that ischaemia may have a significant role in the development of SAN dysfunction.[245]

1.6.3 Inherited sinoatrial node dysfunction

As well as in the elderly, SAN disease occurs in children and young adults, most of these cases are associated with structural heart disease.[246-248] However, a significant number have no clear structural reason for developing SSS.[249, 250] In these patients, genetic aetiology is assumed. Familial mutations affecting I_f and I_{Na} have been demonstrated to cause inherited SSS in humans as discussed in sections 1.4.1.1.2 and 1.4.1.3 respectively.[99-101, 168-172] Mutations of calsequestrin (CASQ2) causing autosomal recessive catecholaminergic polymorphic ventricular tachycardia are also associated with SAN dysfunction, presumably perturbation of SR Ca^{2+} impairs CICR and thus the Ca^{2+} clock.[251]

1.6.4 Sinoatrial node dysfunction and heart failure

Fatal bradycardia contributes a significant burden in heart failure, accounting for ~42% of in-hospital heart failure sudden deaths.[164, 252-254] These bradyarrhythmias arise because heart failure causes diseases of the CCS, including SSS.[240] A rat model of post-infarction heart failure shows SAN dysfunction (decrease of the intrinsic heart rate and prolongation of the SAN recovery time [SNRT]).[240] SAN dysfunction has been demonstrated in human heart failure patients - they exhibited sinus bradycardia, increased SAN recovery time, inferior localisation of the leading pacemaker, prolongation of SAN conduction time and abnormal circuitous propagation of the sinus impulse.[255] The SAN remodelling may be due to abnormal haemodynamics of the RA in heart failure and as such represent a right atrial cardiomyopathy. Consistent with this concept SAN dysfunction in humans (evidenced by increased SNRT) has been observed in association with conditions leading to RA pressure and volume overload, including dysynchronous AV pacing and chronic atrial septal defect.[256, 257] Cellular electrical remodelling of the SAN by downregulation of HCN channels has been implicated in this process.[258]

1.6.5 Sinoatrial node dysfunction and atrial tachycardia

Chronic ectopic atrial tachycardia leads to remodelling and dysfunction of the SAN. Canine models of AF utilising chronic atrial tachycardia (20 Hz) pacing demonstrate increased SNRT, reduced maximal SAN rate and reduced intrinsic heart rate.[259] Furthermore, prolongation in SNRT has been noted in patients following DC cardioversion of chronic AF, though this does not predict the long term success of this intervention.[260, 261] Even short periods of atrial tachycardia induce functional SAN remodelling.[262] Once again cellular electrical remodelling may be responsible for this process - atrial tachycardia pacing induces abnormalities of the Ca^{2+} clock (evidenced by altered CICR, caffeine sensitivity and RYR expression) and the membrane clock (evidenced by reduced HCN4, HCN2 and minK expression with reduction in the I_f and $I_{K,s}$ currents).[263, 264] The plasticity of this process is demonstrated by reverse remodelling of SAN function seen after restoration of sinus rhythm by AF ablation.[265]

1.6.6 Sinoatrial node dysfunction in endurance athletes

Endurance athletes display a resting sinus bradycardia. For example, the heart rate of elite cyclists has been reported to be ~30 bpm.[266] The received knowledge is that this is due to high vagal tone.[267] However, experimental studies have shown a decrease in the intrinsic heart rate, and thus a decrease in the intrinsic pacemaker activity of the SAN.[267] This suggests that the bradycardia is due to electrical remodelling of the SAN, furthermore the athletic resting bradycardia persists after physical de-conditioning, suggesting that the changes are intrinsic to the node rather than a function of short-to-medium term autonomic modulation.[268] Pilot data suggests that athletic training in rats leads to an intrinsic slowing of the heart rate during Langendorff heart experiments.[224] In humans endurance training leads to remodelling throughout the CCS with prolonged SAN cycle length, SNRT, AVN Wenckebach cycle length and AVN effective refractory period both at baseline and following autonomic blockade with atropine and propranolol.[269]

It could be hypothesised that the remodelling is reactive to the chronic sinus tachycardia associated with endurance exercise, a form of tissue or cellular

homeostasis. However rats and dogs who were trained following cardiac denervation failed to develop any resting or intrinsic bradycardia.[270, 271] Thus the initial response to training seems to be mediated by the autonomic nervous system with subsequent chronic mechano-electrical feedback leading to intrinsic changes of the SAN and other regions of the CCS.[269]

1.6.7 Sinoatrial node dysfunction and diabetes mellitus

SSS has been observed in diabetic patients as well as in the streptozotocin rat model of diabetes.[272] SAN dysfunction in diabetes mellitus may be a consequence of microvascular dysfunction or hyperinsulinaemia associated with peripheral insulin resistance (in type II diabetes mellitus).[272, 273] Soon after diabetes induction streptozoticin-treated rats showed a marked sinus bradycardia both *in vivo* and during Langendorff experiments.[274-276] Furthermore, expression levels of Cx40, Cx43 and Cx45 were increased in the SAN of diabetic rats.[277]

1.7 What is a 'biopacemaker' and why do we need them?

Advances in pharmacology and invasive cardiology have led to a vast improvement in mortality and morbidity in a number of cardiovascular conditions. However, for most conditions modern cardiology is unable to offer lasting cures (i.e. without need for ongoing pharmacotherapy or presence of a prosthetic implant). Most relevant to this discussion is a consideration of the spectrum of bradyarrhythmic disorders. Bradyarrhythmias are a common problem; an inappropriately low heart rate may lead to haemodynamic collapse and syncope. This may be caused by SAN dysfunction (as above) or conduction block distally in the CCS. Many of these conditions are currently treated by the implantation of electronic cardiac pacemakers that reduce mortality and morbidity in carefully selected patient groups.[278]

1.7.1 Current use and limitations of implantable electronic pacemakers

Pacemaker implantation is a common procedure with over 32000 patients treated in 2006 in the United Kingdom.[227] Modern technological innovation has vastly reduced the size, and increased the functionality of cardiac pacemakers. Standard

pacemaker systems pace via the right heart, either single chamber (RA or RV), or dual chamber (RA and RV), and may be programmed to suppress activity in response to intrinsic heart rhythms. By estimating activity level via accelerometers, respiratory rate or venous oxygenation, rate responsive systems allow some degree of chronotropic response to physiological demands.[279]

There are several well known complications associated with cardiac pacemakers. In the United Kingdom in 2006 the total mortality directly attributed to the pacemaker system was 0.36% (118 patients), and 1.26% patients suffered complications severe enough to require removal of the pacemaker system (413 patients).[227] The overall complication rate is certainly higher than this, causing significant morbidity, including a 1.6%-2.6% rate of pneumothorax, 2.6% incidence of lead fracture, and 5% incidence of infection. [280-282]

It is clear that the cardiac impulse initiated by standard electronic pacemaker systems is not truly physiological. Surface electrocardiogram will show a left bundle branch block pattern with prolonged QRS complex duration, and concomitant cardiac ventricular dyssynchrony as the impulse spreads from the right to the left ventricle. This phenomenon leads to impairment of the systolic and diastolic functions of the heart. *In vivo* studies of pacing in dogs confirmed that left ventricular function was impaired by RV pacing, as evidenced by reduced maximal LV pressure, and systemic systolic blood pressure.[283, 284] A criticism of the above studies is that the loss of the atrial component of the cardiac cycle may account in part for the findings as atrioventricular sequential pacing shows an increase in peak systolic pressure and left ventricular fractional shortening when compared to RV pacing in the canine heart.[285]

However, similar results have been obtained in humans, when AV sequential pacing was compared to RA pacing - the rate of increase in left ventricular pressure (dP/dt), peak systolic pressure, ejection fraction and stroke volume were decreased, suggesting that cardiac dyssynchrony induced by RV pacing causes a reduction in left ventricular efficiency. [286] RV pacing also affects cardiac diastolic function in dogs, and humans.[285, 287-289] Reduction in diastolic function (as measured

by left ventricular relaxation [dP/dt] or the diastolic relaxation time constant [Tau]) due to age and hypertensive heart disease is a major cause of heart failure.[290] Furthermore there is evidence that long term pacing via the RV causes remodelling evidenced via myocyte disarray and fibrosis which may cause a progressive deterioration in cardiac function.[291, 292] A study utilising B-type natriuretic peptide as a marker of atrial stretch and degree of heart failure suggested that even in structurally normal hearts RV pacing induces physiologically significant heart failure, although the study groups were not well matched with respect to underlying pathology and this was not a prospective randomised controlled trial.[293] In the same study diastolic function was assessed using the Tei index (a transthoracic echocardiographic calculation of isovolumic relaxation time divided by ejection time), and was found to be impaired by increased pacing demand. Previously the Tei index has been used as a prognostic marker in cardiac amyloidosis and dilated cardiomyopathy, which may imply that increased pacing dependence may indicate poor prognostic outlook due to the deleterious effects of RV pacing, although this has not been specifically studied.[294, 295] These limitations have led to an ongoing search for an alternative pacing site, such as the interventricular septum or RV outflow tract, that provide better physiological and clinical outcomes.[296]

1.7.3 The hypothetical ideal biopacemaker

Some of the problems with electronic pacemakers discussed above could be circumvented if the natural pacemaker could be rejuvenated or recreated. Knowledge of the ionic and genetic basis of the generation of the pacemaker current (sections 1.2 and 1.4) has allowed a number of groups to undertake proof of concept experiments, showing that enhancing the chronotropy of cardiac cells can allow them to serve as an independent pacemaker, the so called biopacemaker.

As discussed above, the SAN has a complex molecular and electrical structure that allows it to perform its normal function.[39] The ideal biopacemaker would therefore be able to replicate these conditions, affording protection from overdrive suppression and re-entry as well as allowing predictable and coordinated propagation of the action potential down the His-Purkinje system, with appropriate

response to autonomic regulation. The easiest way to create a biopacemaker with a physiological rate, autonomic response and synchronous AV conduction would be to create the biopacemaker in the region of a previously dysfunctional SAN. However, this may provide an effective treatment for SAN disease such as SSS, but not for AVN block. Current United Kingdom epidemiological data would suggest that the SAN would be a viable site for implantation of a biopacemaker in approximately 27% of cases.[227] Longitudinal studies of patients receiving atrial pacemakers for SAN disease (without ventricular back up) suggests that with careful screening this is a safe strategy.[297]

AVN block accounts for the majority of pacemaker implantation (48.5%), and so we would expect that biopacemakers should be developed to treat such conditions by rejuvenation of the AVN, or implantation of the biopacemaker below the level of block. In fact most experimental work has concentrated on animal models of AVN block with the implantation of the biopacemaker into ventricular myocardium or the left bundle branch (see section 1.7.4).[227] Such an approach could be considered analogous to a VVIR electronic pacemaker (see table 1 for summary of pacing modes), which remains the most common implanted pacemaker at 41%, but are also known to have a higher incidence of pacemaker syndrome (symptomatic haemodynamic disturbance) due to atrioventricular dys-synchrony.[227, 298] Furthermore asynchronous atrioventricular pacing (which is delivered by a VVI pacemaker) has been demonstrated to induce electrical remodelling of the SAN and RA myocardium causing increased SNRT and effective refractory periods respectively.[256] Patients in this study that received VVI rather than DDD (synchronous atrioventricular) pacing had a higher incidence of AF.

Additional evidence of the detrimental effect of a lone ventricular pacing site could be gained by demonstrating clinical superiority of DDD pacing compared with VVI pacing. The Canadian trial of physiologic pacing (CTOPP) and the mode selection trial (MOST) suggest reduced morbidity and lower rates of AF in dual chamber pacing modes. [229, 282] These findings are disputed by some, but small benefits in these cohorts may be obscured by the high mortality, advanced age and comorbidity of most pacemaker patients, and in fact the placement of the right

Mode R = rate responsive	**VVI (R)** Ventricular pacing and sensing, inhibitory response to intrinsic sensed beat	**DDD (R)** Atrial ± ventricular (dual) pacing and sensing, inhibitory or triggered (dual) response to sensed activity	**AAI (R)** Atrial pacing and sensing, inhibitory response to intrinsic sensed beat
Leads	Right ventricular	Right atrial Right ventricular	Right atrial
Physiological sequential AV pacing	No	Yes	Yes
Response to intrinsic atrial activity	None	Atrial pacing suppressed ± triggered ventricular pacing	Pacemaker suppressed
Response to intrinsic ventricular activity	Pacemaker suppressed	Ventricular pacing suppressed	None

Table 1. The common electronic pacing modes showing the lead placements, sensing and pacing activity

ventricular lead may have a stronger effect on morbidity and mortality than the pacemaker mode.

It must be remembered that pacing, whether electrical or biological, from the RV apex or RV outflow tract will produce ventricular dyssynchrony and atrioventricular dissociation, which have limitations as discussed above. It is likely that biopacemakers at ectopic sites will be prone to high levels of overdrive suppression due to the presence of the $Na_v1.5$ current in working myocytes and be susceptible to re-entrant tachycardia due to the absence of an appropriate cellular environment and low conductance connexins.[39, 199] Furthermore, the maximum rate of ventricular biopacemakers appears to be limited by the substrate (i.e. the ventricular myocardium).[299] Ventricular biopacemakers may even be a nidus for ventricular arrhythmia – in the ventricular myocytes of hypertensive and heart failure rats upregulation of I_f has been demonstrated and this has been proposed to be one of the cellular substrates for the ventricular arrhythmias seen in these clinical syndromes.[300-304]

It is important that any engineered pacemaker is responsive to the autonomic nervous system. It is likely that any pacemaker employing HCN genes will be responsive via cAMP-dependent pathways.[106] However the density of innervation of the SAN, the presence of RyR/I_{NCX} coupling which is enhanced by adrenergic stimulation, and modulation of the resting membrane potential by acetylcholine-responsive I_{KACh} suggests that biopacemakers sited in the SAN region may be more responsive than those at other sites.

1.7.4 Biopacemakers, the state of the art

In 1998 Edelberg et al. demonstrated chronotropic enhancement of mouse myocyte contraction rate, and murine heart rate by injection of a plasmid expression vector containing the cDNA of human β2 adrenergic receptor.[305] By transfection into neonatal myocytes, *ex vivo* heart preparations and transplanted hearts they demonstrated that gene transfer was a potential method of manipulation of the native heart rate. The same approach was used to investigate the enhancement of chronotropicity in pigs, by the injection of human β2 receptor

plasmid cDNA into the RA of pigs.[306] Using percutaneous recording electrodes with injecting needles, the plasmid was injected at the site of earliest atrial action potential (presumed SAN). Compared to control animals, injected pigs showed significantly enhanced chronotropy. The effect was transient and maximal on day two, demonstrating that naked DNA is not an efficient system for the production of stable transgene expression. However, this was not truly a *de novo* biopacemaker, but enhancement of intrinsic rate. Furthermore, in neither species was pathological bradycardia or atrioventricular block modelled.

1.7.4.1 Ventricular biopacemaker via suppression of I_K

The first true biopacemaker was created in guinea pigs via the suppression $I_{K,1}$ ($K_{ir}2.1$). All embryonic cardiac cells possess pacemaking activity, with an action potential upstroke carried by L-type calcium channels in a manner similar to the SAN action potential.[307] The hyperpolarized resting membrane potential seen in adult ventricular myocytes is highly dependent on $I_{K,1}$, and thus the expression of a dominant negative mutant form of $K_{ir}2.1$ causes a partial depolarization of the ventricular myocytes unmasking their latent pacemaker potential.[49]

Injection of a dominant negative mutant of $K_{ir}2.1$ ($K_{ir}2.1$ AAA) in an adenoviral vector induced partial depolarization of the ventricular myocytes, shifting the resting potential from -80 mV to -60 mV. Spontaneous action potentials were observed with similar morphology to genuine SAN cells and these cells showed a chronotropic responsive to β-adrenergic stimulation by isoprenaline (figure 13).

1.7.4.2 Ventricular and left atrial biopacemakers via expression of I_f using native and engineered HCN channels

Further work has concentrated on the use of HCN channels. These channels are the ideal candidate for the creation of a biopacemaker as they are responsible for I_f, are highly expressed in the SAN and are central to the pacemaker potential plus the chronotropic response to catecholamines.[76] In a mouse model of atrioventricular block, injection of plasmid DNA containing cDNA encoding both HCN2 and β2

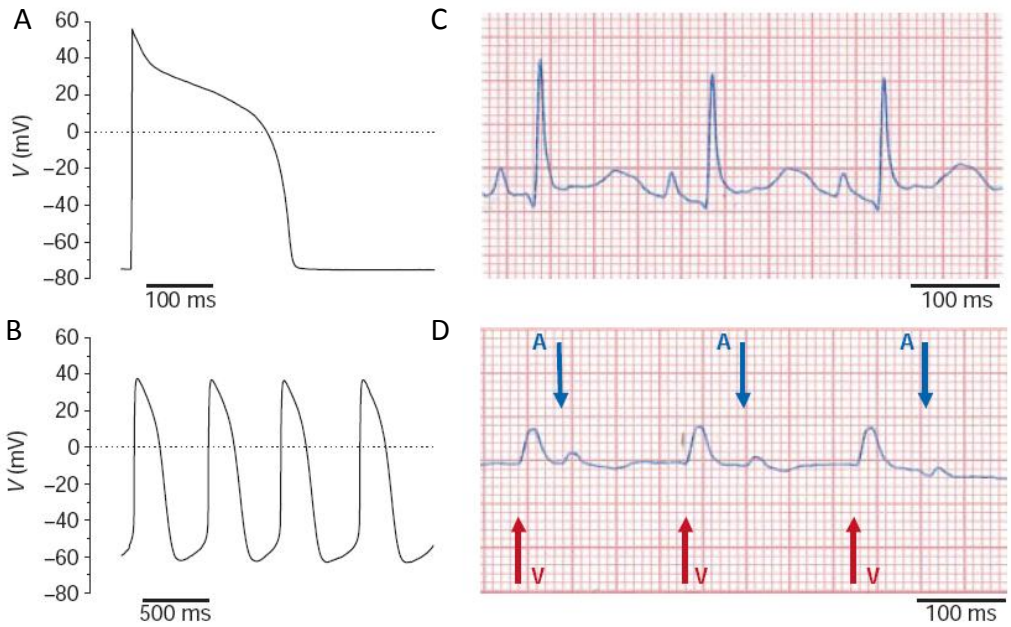

Figure 13. Biopacemaker created by suppression of $I_{K,1}$ in the ventricular myocardium of guinea pig. A) Action potentials evoked by external stimuli in control ventricular myocytes (i.e. no spontaneous depolarization). B) Spontaneous depolarization in myocytes transduced with Kir2.1AAA causing suppression of $I_{K,1}$. C) Control surface electrocardiogram showing normal sinus rhythm. D) Independent atrial (A) and ventricular (V) pacemakers in guinea pigs with Kir2.1AAA injected into the left ventricular free wall. From Miake et al.[49]

adrenergic receptor into the left ventricle increases the rate of escape rhythms and improves survival.[308]

Recombinant adenovirus (RAd) containing the cDNA sequence for the channel HCN2 has been injected into the left atrial myocardium of dogs with experimentally induced SAN arrest.[309] The consequent expression of HCN2 at this ectopic site was shown to induce independent catecholamine-sensitive pacemaking activity. Left atrial cells harvested from these animals expressed I_f of 7 ± 4 pA at -130 mV in 4 of 5 cells studied, implying that the infection of mHCN2 to left atrial cells induces sufficient hyperpolarisation-activated current to produce a slow diastolic depolarization. No recordings of action potentials from spontaneously beating cells were presented.

Although not specifically reported in the papers, the rate calculated from the published ECGs was relatively slow (30 – 40 beats per minute). The reason for this slow rate is most probably that the cellular environment of working myocardium differs significantly from the SAN, HCN channels behave differently in different cell types.[310] The basis of this context dependence is not fully understood but may depend on differing molecular chaperones, basal cAMP levels or cellular electrophysiology.[153, 311] For example I_K modulates the pacing rate induced by I_f when expressed in ventricular cardiomyocytes.[58] In fact, while transfection of HCN2 has been shown to hasten the firing rate of cells expressing endogenous I_f they are not able to induce measured I_f in adult ventricular myocytes.[312]

In an attempt to reduce the influence of context dependence and improve the rate of pacemaking, HCN2 has been expressed in the left bundle branch of dogs.[313] The left bundle branch of dogs was identified by electrocardiographic recording via cardiac catheterisation, and an adenoviral vector containing mHCN2 driven by CMV promoter was injected using a modified catheter. Between 4 and 7 days later the dogs were studied under anaesthesia using RV and LV recording electrodes to allow the assessment of the rate and origin of escape rhythms under atrioventricular block produced by vagal stimulation. Escape rhythms were clearly shown to

originate from the left bundle in the study animals (with early left ventricular activation), but in control animals right ventricular activation occurred earlier in the QRS complex providing further evidence that the biopacemaker was the primary pacemaker under these experimental conditions.

Evidence that the biopacemaking was the result of the over-expression of HCN2 is provided by the significant increase in measured I_f in the experimental group, and immunohistochemical staining of the injection site for HCN2. The same HCN isoform as the above study provided an improved pacemaking rate when expressed in the left bundle branch. However, the problems associated with atrioventricular disassociation and left bundle branch block were discussed in section 1.7.1, and haemodynamic assessments were not presented here.

Current animal models employ a 'tandem' electronic pacemaker and biopacemaker system in anticipation that any future human trials of bio-pacemaking would require this. This model has been used to test HCN channels that have been engineered to provide improved pacing rates when expressed in the working myocardium. The use of these mutant channels (engineered HCN2, mE324A) has reduced (but not ameliorated) the dependence on electronic 'backup' pacing when expressed in the canine left bundle branch.[314]

RAd containing wild-type mHCN2 or mutant mHCN2 (mE324a) was injected into the left bundle branch of dogs, with simultaneous implantation of an electronic pacemaker (VVI) programmed to provide backup pacing at rates less than 45 bpm; normal saline injection was used as a control. Complete atrioventricular block was induced by radiofrequency ablation. The biopacemaker groups (mHCN2 and mE324A) demonstrated reduced dependence on backup electronic pacing and improved epinephrine responsiveness.

It is also reported that there was no evidence of increased overdrive suppression in either group, post-pacing pauses were 1 to 5 seconds with no significant difference between the groups. However, the validity of this result is doubtful. The overdrive pacing rate was probably too slow at 80 bpm (previous studies have used rates of 90 – 200 bpm; increasing pause length is seen with increasing rates). Furthermore,

no group in this study had a measured native SAN pause with which to compare the biopacemaker pause. The corrected SNRT (CNSRT) can be used compare the biopacemaker overdrive suppression to that of a normal SAN.[198, 315] In humans the normal CNSRT is less than 550 ms, and in the dog less than 127 ms (for pacing rate of 200 bpm).[315, 316] Using the reported escape times and resting heart rate of the dogs in this study the CNSRT for the biopacemakers is between 0 to 4000 ms.

In the above study the comparison of mutant mHCN2 (mE324a) to mHCN2 is of particular importance.[314] The kinetics of mutant mHCN2 (mE324a) are faster than wild-type mHCN2 and results of patch clamp experiments in rat ventricular myocytes presented also show that mutant mHCN2 (mE324a) has a faster and more positive pacemaker depolarization.[312, 317] It may be hypothesised therefore that it would provide faster pacemaking *in vivo* which would raise the possibility of engineering HCN channels with kinetics that would allow fine tuning of the pacing rate. However, there was no significant difference in the rates between the mutant mHCN2 (mE324a) and mHCN2 groups. Western blot analysis and measured current densities suggest that mutant mHCN2 (mE324a) was expressed at lower levels than mHN2 which may account for these findings. Alternatively the context dependence in non SAN cells may limit the rate that is achievable by transfection of HCN channels; it may prove necessary to co-express a construct that suppresses $I_{K,1}$ although this may prove pro-arrhythmic by prolonging the action potential.

RAd containing mHCN1ΔΔΔ (mHCN1-*EVY235-7*ΔΔΔ created by deletion of residues 235 – 237 of the S3 – S4 linker to favour channel opening) has been demonstrated to induce I_f rather than merely enhance pacemaking.[318] APs recorded from spontaneously firing guinea-pig left ventricular cardiomyocytes expressing mHCN1ΔΔΔ clearly show a diastolic depolarization and increased firing rate compared to control cells, although they retain the Na^+-driven rapid action potential upstroke and overshoot of ventricular cells. mHCN1ΔΔΔ was then injected into the left atrial appendage of pigs at thoracotomy. Using a tandem biological and electronic pacemaker system, a porcine model of SSS was developed by guided radiofrequency ablation of the SAN. The elevation in intrinsic rate in the

biopacemaker group reduced the need for electronic pacing from 69 ± 18% to only 14 ± 15% (p = 0.02) (figure 14).

While providing improved pacing rates, these engineered pacemaker channels are not without problems. For example, a chimaeric channel HCN212 has been engineered containing the extracellular and intracellular domains of HCN2 with the transmembrane domain of HCN1 to provide enhanced pacing in working myocardium, but with the superior catecholamine sensitivity of HCN2.[319] Expression of HCN212 in canine left bundle branch resulted in episodic ventricular tachycardia in all animals.[319] The arrhythmia was effectively suppressed by Ivabradine infusion; note that Ivabradine has a higher efficacy in blocking HCN1 channels than other isoforms - this may be an important lesson in the choice of HCN isoform for any human trials so that any unexpected deleterious effects of the biopacemaker can be modulated pharmacologically.[320]

1.7.4.3 Left ventricular biopacemakers via cell transplantation

Another method of inducing spontaneous activity in quiescent cells is fusion of fibroblasts containing mHCN1 with cultured ventricular myocytes. When such cells were fused using poly-ethylene glycol, the myocytes became spontaneously active.[321] I_f was recorded from these cells and upon injection into the left ventricle of guinea pigs with atrioventricular block the rate of the escape rhythm was increased. This ectopic activity could be blocked using the I_f blocker ZD7288.

Human mesenchymal stem cells (derived from human blastocyts) can be differentiated into beating groups of cells termed embryoid bodies that will integrate with ventricular myocytes *in vitro*.[322-324] The pacing activity of these cells is responsive to autonomic modulation and is dependent on the presence of hyperpolarisation-activated current, low expression of I_K and a high density of Na^+ current.[325, 326] Implantation of 40 – 150 embryoid bodies into the left ventricular free wall of a swine model of atrioventricular block induced pacing activity in 11 of 13 animals, though the pacing was intermittent and unreliable.[323] Human mesenchymal stem cells have also been used as a delivery vector for mHCN2.[327, 328]

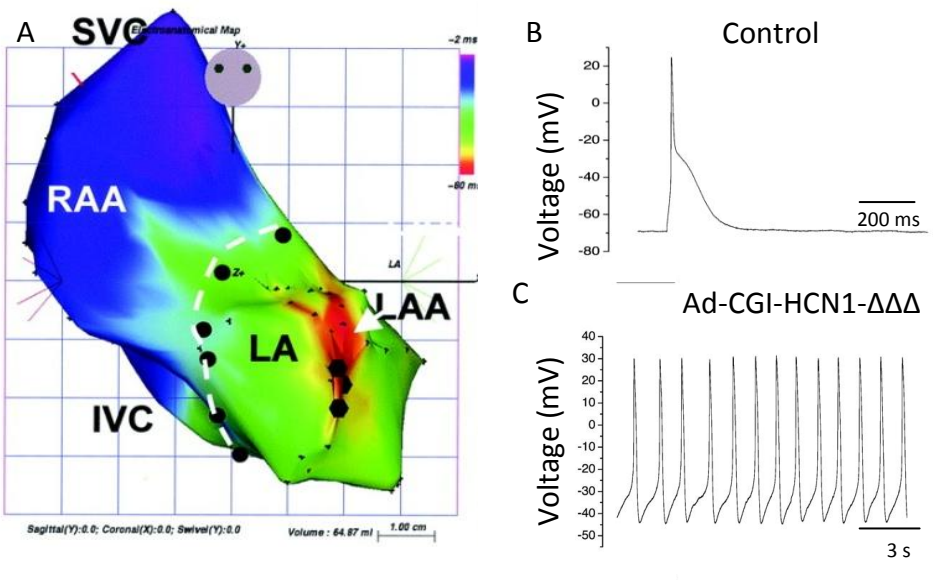

Figure 14. Biopacemaker in the left atrium of the pig. A) Electroanatomic (CARTO) map of pig atria following sinoatrial node ablation and injection of HCN1ΔΔΔ (white arrow) into the left atrial appendage (LAA). The LAA showed earliest activation (red) SVC, superior vena cava; LA, left atrium; SVC, superior vena cava; IVC, inferior vena cava; RAA, right atrial appendage. B and C) Action potentials recorded from control LAA cells (B) and Ad-CGI-HCN1-ΔΔΔ transduced LAA cells, demonstrating that HCN1-ΔΔΔ can induce spontaneous activity in working LAA myocytes. From Tse et al.[318]

Xenografts to the left ventricle of human mesenchymal stem cells (hMSCs) electroporated with mHCN2 were shown to express I_f. Escape rhythms were pace mapped to the implantation site, though the rate was very slow and not physiologically acceptable.[327]

Spontaneously active RA neonatal cells have been transplanted into the left ventricle of pigs with AV block.[329] This approach was technically successful; escape rhythms were within the physiological range (89 ± 13 bpm), were isoprenaline responsive and formed gap junctions with adult LV cardiomyocytes via Cx43. The improved rates seen are probably due to the presence of neonatal SAN cells in the 'transplant'. Thus the pacemaker cells in this model are true SAN cells and do not solely have an upregulation of I_f, though no immunohistochemical or electrophysiological evidence is presented to support this claim. The clinical application of this approach is clearly limited by the availability of neonatal tissue.

1.7.5 Mode of delivery of the biopacemaker product

Arguably the main obstacle to overcome regarding human clinical trials of biopacemakers is the mode of delivery. In human trials of gene therapy it has been difficult to replicate the results from animal models. Part of the problem stems from the widespread use of viruses as vectors for the transfer of the gene therapy product. Unlike laboratory animals, most humans have been exposed to common viruses in their lifetime which leads to a degree of immune memory and an unpredictable immune response. This was graphically demonstrated by the death of a patient in a phase one clinical trial of a hepatic gene therapy product within an adenoviral vector, probably secondary to a massive immune response associated with disseminated intravascular coagulation and multiple organ failure. [330] A patient in the same trial receiving the same dose was unaffected.

RAd and adeno-associated virus (AAV) are popular vectors in laboratory research, mainly due to the high efficiency of infection and transgene transfer, which is of the order of 30-360 times more effective than plasmid DNA-based approaches.[331] Both of these vectors have been used successfully to infect myocardial cells.[332] The use of RAd is severely limited by the host immune response; hence gene expression

peaks around one week, and progressively declines thereafter.[332-334] Improvement in gene expression and reduction of RAd immunogenicity has been achieved by the production of RAd vectors encoding less viral coat proteins and early genes, which also allows the inclusion of larger genes of interest; there are also attempts to induce immune tolerance to RAd.[335, 336]

Although displaying similar levels of immunogenicity to RAd, interest in AAV has been stimulated by the demonstration of stable gene expression in the heart over several months.[337, 338] Furthermore engineering of the caspids of AAV (which affects cell surface binding *in vivo*) and use of a 1.5-kilobase (kb) cardiac myosin light chain promoter (CMV(enh)/MLC1.5 promoter) can increase the specificity of the virus for cardiac tissue, which reduces the transduction of hepatic cells if the AAV enters the circulation.[339] Other viruses that may allow stable gene expression are retroviruses that utilise reverse transcriptase to integrate into the host genome. Included in this family are HIV-derived lentiviruses that have the additional ability to integrate into post mitotic cells. Effective transduction of cardiac myocytes has been demonstrated with this virus. [340, 341] Unfortunately, while not entirely random, the site of integration into the genome cannot yet be predicted or controlled. Clinical trials using retroviral therapy have caused leukaemia via integration into oncogenes.[342]

Specific regional infection and gene expression is one of the challenges for gene delivery in the creation of a biopacemaker. The transgene needs to be delivered to a region, such as the SAN, left ventricle or bundle branch and be expressed in a small localised area. The most obvious approach is direct injection of the material during heart catheterisation guided by electrophysiological mapping. It has been demonstrated that local infection of Ad5 can be seen around the needle track in the myocardium in pigs, and this approach has also been used effectively for naked plasmid DNA.[343, 344] The delivery of a biopacemaker to a ventricular or Hissian site is easily practicable with current clinical radiological and electrophysiological techniques.[345] Identification of the SAN *in vivo* may be more difficult as electrophysiological mapping of the RA has revealed multiple leading pacemaker sites with wide variation in anatomical sites.[346] This approach has the disadvantage

of requiring an invasive procedure requiring central venous access and large diameter electrophysiology catheters.

More sophisticated approaches may include the use of cardiac or regional cardiac specific promoters, and the use of microbubbles to allow non invasive targeting of the transgene or vector. Many groups have used cardiac specific promoters with transgenes in viral vectors to cause cardiac specific gene expression despite the detection of vector in other organ systems.[332] This could be a powerful technique for the delivery of a biopacemaker gene to the SAN or AVN because unique gene expression occurs in these regions due to their specialised nature (see sections 1.2 – 1.4). Perhaps Tbx3 or HCN4 associated promoters could be used to maximise expression in the SAN? Ultrasound contrast media containing microbubbles can be engineered to contain viral vectors or naked plasmid DNA; high frequency ultrasound is then used to disrupt the bubbles at the point of interest. Using this approach a high concentration of gene product can be delivered to the region of interest with less concern of infection of other organs. With this technology significant concentrations of viral vectors have been obtained in cardiac capillaries, and this may also be effective for naked DNA, albeit with lower transduction efficiency. [332, 347] However, it is unlikely that this method will be effective for most biopacemaker applications as electrophysiological mapping will be required to guide site selection.

A different approach to gene delivery is the use of cell allografts based on the techniques discussed in section 1.7.4.3. The problems of immune rejection remain and this approach may require long term immunosupression for success.[327, 348] Embryoid bodies have low graft viability, have been reported to form malignant teratomas *in vivo* and are susceptible to ischaemia.[348-350] Much of the focus of cardiac stem cell therapy in humans is heart failure and myocardial infarction.[348] In these conditions a degree of differentiation and migration of the stem cells is desirable, but would be problematic for biological pacing where a localised concentration of pacemaker cells is required. The long term stability and degree of migration of stem cells in this application is unknown.

1.8 Overview and aims of the work presented

The overall aim was to establish proof of concept for the use of biopacemaking in SSS. There are no established experimental models of SSS. SAN modification has been used *in vivo,* but this approach will result in a heterogeneous study population.[318] Therefore the initial challenge was to develop and characterise an *ex vivo* model of bradycardia in sick sinus syndrome. This required the modification of the SAN dissection technique to ensure sterility, fabrication of an electronic system to continuously record extracellular potentials from the tissue while in culture and assessment of the response of the pacemaker tissue to the culture environment.

The maintenance of a SSS model in an *ex vivo* environment also presented the opportunity to record the chronotropic response of the model to I_f blockade and β-adrenergic stimulation. Furthermore, by accurate identification of the leading pacemaker site it was possible characterise the histology, ion channel expression and gap junction expression in this region. To ensure that significant degredation of the tissue did not occur the cultured tissue was assessed for features of necrosis and apoptosis.

In accordance with previously published biopacemaker work the target genes chosen were HCN channels. It was therefore necessary to engineer viruses containing the HCN genes of interest. Although ion channel transgenes have been expressed in spontaneously active single cells in culture, expression of transgenes by intact SAN tissue has not been demonstrated. Therefore RAd mediated expression of marker genes and HCN2 was investigated. Subsequently the effect of RAd mediated gene expression on the pacing rate of the SSS model was assessed using infection by RAd containing HCN cDNA shown to encode functional channels compared to infection with RAd encoding a marker gene or a non-functional HCN channel.

The data were analysed with respect to the following 12 null hypotheses referred to in the discussion:

1. The sinoatrial node from the rat, *Rattus rattus,* cannot be cultured *ex vivo* and the pacemaker activity cannot be sustained and monitored

2. Tissue culture will induce no significant change in the level of ion channel and gap junction expression of the sinoatrial node

3. Tissue culture will induce no cellular apoptosis in the sinoatrial node

4. Tissue culture will induce no changes in cell or tissue histology of the sinoatrial node or right atrial myocardium

5. The spontaneous pacing rate of the sick sinus syndrome model is not significantly different to the intact (control) preparation

6. The primary histological and immunohistochemical features of the subsidiary pacemaker do not differ from that of the sinoatrial node

7. There is no significant contribution of I_f to pacemaker activity in the subsidiary pacemaker

8. The subsidiary pacemaker is not responsive to β-adrenergic stimulation

9. Adenovirus mediated gene expression in the sinoatrial node or subsidiary nodal tissue is not viable

10. The right atrium intercaval area is not receptive to adenovirus mediated ion channel expression

11. The spontaneous pacing rate of the sick sinus syndrome model will not be increased by injection of adenovirus that carries a transgene for a functional ion channel (Ad5-HCN212 or Ad5-PREK-HCN4)

12. The spontaneous pacing rate of the sick sinus syndrome model will not be increased by injection of adenovirus that does not carry a transgene for an active ion channel (Ad5-GFP or Ad5-GFP-HCN4Δ)

2. Methods

Details of media and reagents can be found in Appendix A1.

2.1 Overview of methods

2.1.1 Recombinant adenovirus

RAds were produced using the AdEasy system.[351] The HCN channel cDNA was sub-cloned from pCDNA3 into the shuttle vector pShuttle or pShuttle-IRES-hrGFP-1 (Appendix A4) using oligonucleotide sequences to introduce RE sites where necessary. Homologous recombination between the resultant shuttle vectors and pAd, containing the Ad5 genome, was performed in BJ5183 competent *Escherichia coli* to produce a plasmid containing the Ad5 genome and the HCN gene of interest or humanised renilla green fluorescent protein (hrGFP). This plasmid was linearised, transfected into Ad293 cells and then a primary virus stock was purified by Arklone P extraction.

The primary virus stock was amplified on a small scale and purified by Arklone P extraction. A small scale viral DNA extraction was prepared, the HindIII digest pattern was checked against the predicted pattern and a Southern blot was performed to confirm the presence of the HCN gene using a probe generated from the appropriate HCN channel cDNA. Cos7 cells were infected with the virus, after 48 h the presence of channel proteins at the cell membrane was confirmed by immunocytochemistry and patch clamp was performed to ensure the expected current could be recorded. Following these checks, a large virus stock was prepared by CsCl gradient centrifugation.

2.1.2 Sinoatrial node culture

The SAN was dissected from three month old Wistar Hannover rats at 37°C under sterile conditions. The SAN preparation comprised the posterior wall of the RA extending from the SVC to the IVC and from the interatrial septum to part of the right atrial appendage (RAA)). A recording system was developed using 0.15 mm diameter stainless steel needles and a 0.5 mm silver wire earth insulated to within 3-4 mm of the tip. The electrodes were pinned near the SAN and recording

electrodes were connected to a Neurolog system (Digitimer) with 50 Hz filter and low pass/high pass filters. The setup was transferred to 293 medium (Appendix A1) in a 37°C/5% CO_2 incubator. Extracellular potentials were continuously recorded using Powerlab and Chart software. The 30 s average rate was calculated via the detection of a deflection greater than 2 SD as a paced beat.

The effect of tissue culture on the SAN tissue was assessed at 48 h. The SAN was removed from culture and frozen in optimal cutting temperature compound (OCT, Prolabo) . 16 µm cryosections were prepared and histological staining with Masson's trichrome or quantitative immunohistochemistry for HCN4 and Cx43 was performed. The presence of apoptosis was detected by immunohistochemical staining for activated caspase-3, an enzyme cleaved early in the apoptotic cascade.[352] Apoptosis was induced by culture with 6 µm camptothecin (inhibitor of topoisomerase) to assess the effect of apoptosis on the histology of the tissue and to serve as a positive control for the immunohistochemistry experiments.[353] The effect of culture on cell size was investigated; the cell membrane of myocytes was marked using antibody to caveolin-3 so that cell diameter could be measured by confocal microscopy. Statistical analysis was performed by unpaired t-test, 1-way or 2-way ANOVA as appropriate.

2.1.3 Sick sinus syndrome model

The SAN of three month old Wistar Hanover rats were dissected under sterile conditions. To create the SSS model the upper two thirds of the preparation was removed by transverse incision at the level of the fossa ovalis. The SSS preparation was transferred to SAN medium and incubated at 37°C/5% CO_2 and the pacing rate was monitored as above. Rates were averaged over 6 h and compared to the control by 2-way ANOVA.

The leading pacemaker of the SSS preparation was identified by activation mapping using a pair of bipolar electrodes and calibrated micromanipulators. The position of the leading pacemaker site was recorded with reference to the bifurcation of the SAN artery in the control preparations, and to the superior aspect of the IVC in the SSS preparations. The rate responses to β-adrenergic stimulation (using

isoprenaline) and I_f blockade (using CsCl) were assessed and compared by paired t-test. The tissue was then frozen in OCT compound and 16 µm cryosections were prepared. The nature of the leading pacemaker was assessed using Masson's trichrome staining and immunohistochemistry for HCN4 and Cx43. Cell size was assessed using Cav3 as above; the cell size was compared to that of the body of the SAN using unpaired t-test.

2.1.4 Adenovirus mediated transgene expression in cardiac tissue

The SSS preparation was dissected under sterile conditions. Initially lacZ was used as a marker gene due to the ease and reliability of the X-gal assay. $1x10^8$ pfu of the adenovirus Ad5-PREP-lacZ was injected at three sites into the intercaval region of the RA. This virus has been previously demonstrated to produce high levels of transgene expression in the porcine vascular endothelium.[354] After 48 h the presence of β-galactosidase was determined by a whole tissue X-gal assay. The experiment was repeated and after 48 h the SAN tissue was frozen in OCT compound and 16 µm cryosections were prepared. The X-gal assay was performed on the tissue sections followed by immunohistochemistry using primary antibodies to HCN4 and atrial natriuretic peptide (ANP).

The virus Ad5-GFP-HCN2 was used to study transgenic ion channel expression in the SSS model. This bicistronic vector allows co-expression of GFP and HCN2. 1×10^8 pfu Ad5-GFP-HCN2 was injected into the most common subsidiary pacemaker site, superior to the IVC. After 48 h culture the whole tissue was fixed directly for immunohistochemistry or frozen in OCT compound and 16 µm cryosections were prepared. Immunohistochemistry using a primary antibody against HCN2 was used for detection and images were obtained using confocal fluorescence microscopy.

2.1.5 Biopacemaking

The SSS model was prepared as described. Using a graduated syringe and micromanipulator, 1-2 µl of the RAd of interest was injected into the superior aspect of the SVC. In total ~ 1×10^7 pfu of the RAd was injected per experiment. RAd containing cDNA for functional HCN channels (Ad5-HCN212 and Ad5-PREK-HCN4) were compared to RAd containing cDNA for a marker gene (Ad5-GFP) or a

non functional HCN channel (Ad5-GFP-HCN4Δ). The recording electrodes were inserted and the preparation was transferred to a 37°C/5% CO_2 incubator for monitoring of the spontaneous pacing rate. The rate was averaged over one hour or six hours and compared to the control and uninjected SSS syndrome using 1- or 2-way ANOVA as appropriate.

2.2 Amplification of plasmid DNA

2.2.1 Bacterial transformation

50 µl of plasmid mix was prepared on ice using 5-10 ng plasmid DNA and diluent distilled water (dH_2O). Competent DH5α *Escherichia coli* (Invitrogen) were removed from the -80°C storage to ice and allowed to thaw. 10 -50 µl of the plasmid mix was added to 50 µl of the DH5α. dH_2O was used as a negative control, if the transformation was to be performed using ligated DNA, uncut pcDNA3.1 was included as a positive control. The mixture was left on ice for 1 h, heat shocked at 42°C for 45 s, then returned to ice for 10 min. The transformed bacteria were added to 700 µl of sterile Luria Bertani (LB) broth (without antibiotic) and incubated at 37°C with vigorous rotational shaking for 1 h. Following incubation, 200 µl of the bacteria were spread onto selective LB agar plates and incubated at 37°C overnight.

2.2.2 Plasmid DNA amplification

2.2.2.1 Small scale DNA amplification: 'miniprep'

Small amounts of DNA (up to 20 µg in 40 µl) were extracted using the Qiagen miniprep system (Qiagen).[355] A single colony from a selective agar plate was inoculated into 5 ml LB medium containing the appropriate antibiotic and incubated for 6 -12 h with vigorous shaking. Cultures were numbered and prior to harvesting a small amount of each culture was streaked onto a numbered section of a selective agar plate. The plate was incubated at 37°C overnight then stored at 4°C until required. Bacterial cells from the cultures were harvested by centrifugation at 5400 x *g* for 15 min at 4°C and the supernatant was drained. The following steps were performed according to the manufacturers' instructions with the standard commercially available buffers.[355] The cell pellet was resuspended in 250 µl P1

buffer containing RNase A before cell lysis by addition of an equal volume of P2 buffer. Neutralisation was achieved by addition of 350 µl P3 buffer and the resulting cell debris precipitate was pelleted by centrifugation at 13000 x g for 10 min. The DNA-containing supernatant was decanted into a QIAprep spin column and DNA was bound to the membrane by centrifugation at 13000 x *g* for 1 min, the membrane was washed using 0.75 ml PE buffer containing ethanol (EtOH). The DNA was eluted using 40-50 µl dH_2O.

2.2.2.2 Medium and large scale DNA amplification: 'midiprep' and 'maxiprep'

Medium (up to 100 µg in 50 µl) and large (up to 500 µg in 100 µl) scale plasmid DNA preparation was performed using the midiprep and maxiprep procedures respectively (Qiagen).[355] The two protocols are identical other than the reagent volumes used, thus the procedures are described giving volumes for midiprep/maxiprep respectively when they differ. A starter culture was prepared using a single colony from a selective agar plate (usually the numbered miniprep plate) inoculated into 10 ml LB medium containing the appropriate antibiotic and incubated for 6-8 h with vigorous shaking. The contents of the starter culture were added to 100 ml/400 ml LB medium containing the appropriate antibiotic and incubated overnight with vigorous shaking. Cells were harvested by centrifugation at 6000 x *g* for 15 min at 4 °C.

The following steps were performed according to the manufacturers' instructions with the standard commercially available buffers.[355] The cell pellet was resuspended in 4 ml/10 ml P1 buffer containing RNase A before cell lysis by addition of an equal volume of P2 buffer and mixing for 5 min. Neutralisation was achieved by addition of 4 ml/10 ml chilled P3 buffer with immediate mixing. The mixture was incubated on ice for 20 min and the resulting cell debris precipitate was pelleted by centrifugation at 20000 x *g* for 30 min. The DNA-containing supernatant was decanted into a fresh tube, mixed and centrifuged again at 20000 x *g* for 15 min.

A Qiagen-tip 100/400 was equilibrated with 4 ml/10 ml QBT buffer and the supernatant from the final centrifugation step was applied to the column so that

the plasmid DNA could bind to the membrane. The membrane was washed twice using 10 ml/30 ml QC buffer before the DNA was eluted using QF buffer. The DNA was precipitated using 3.5 ml/10.5 ml room temperature isopropanol (Sigma-Aldrich), the mixture was immediately centrifuged at 15000 x *g* for 30 min at 4 °C. The resulting DNA pellet was washed using 2 ml/5 ml 70% EtOH (Sigma-Aldrich) then centrifuged at 15000 x *g* for 10 min at 4 °C. The pellet was allowed to dry and then eluted in 50–100 µl dH_2O.

2.2.3 Quantification of DNA

2.2.3.1 Quantitative 1% agarose gel electrophoresis

1 µl of the DNA sample of interest was added to 8 µl dH_2O and 1 µl 10x loading buffer (Promega). The sample was loaded into 1% agarose gel alongside 15 µl of 1 kb Ladder Plus (Invitrogen) and run at 85 mV for 30 min-1 h until sufficient separation of the sample was achieved. Visual comparison of the relative fluorescence under UV light was used to quantify the mass of DNA in the 1 µl aliquot of sample DNA by comparison to the 1.6 Kb band of the ladder which is known to contain 60 ng DNA.

2.2.3.2 UV-Vis absorbance spectra microsample quantification

1 µl DNA was loaded onto the Nanodrop 1000 (Thermo Fisher Scientific). The DNA concentration was automatically calculated via optical absorbance at 280 nm.

2.3 Generic molecular biology and cell culture protocols

2.3.1 Cloning of the gene of interest into plasmid vectors

2.3.1.1 Restriction endonuclease DNA digestion

Restriction endonucleases (REs) and buffers were obtained from New England Biolabs or Promega. Buffers, incubation times and temperatures were selected according to the manufacturers' instructions. [356, 357] Small quantities of DNA (1-3 µg) for diagnostic digests were performed with 1-3 µl of each RE and 2 µl 10x buffer in a total volume of 20 µl. Larger quantities for DNA purification were performed with 5-10 µl of each RE and 5 µl 10x buffer in a total volume of 50 µl.

2.3.1.2 Agarose gel purification of restriction endonuclease digested DNA fragments

Following digestion DNA fragments were separated by 1% agarose gel electrophoresis at 85 mV as above; bands were quickly excised under UV light. DNA was then purified according to the QIAquick gel extraction kit protocol (Qiagen) using commercially available buffers.[355] The gel volume was quantified by weighing the slice, assuming a density of 1 g/ml, which was then dissolved in 3 volumes of QG buffer at 50 °C. When the gel was completely dissolved, the DNA was precipitated by the addition of one volume of room temperature isopropanol. The solution was added to a QIAquick spin column and the DNA bound to the membrane by centrifugation. The column was washed with PE buffer and the DNA eluted into 50 µl dH_2O by centrifugation. All centrifuge steps were performed at 17900 x *g* for 1 min.

2.3.1.3 Dephosphorylation of restriction endonuclease digested DNA fragments

If required (for blunt end ligation or compatible cohesive ends) dephosphorylation of the DNA fragments was performed prior to ligation. 5 µg DNA was added to 2 µl calf intestinal alkaline phosphatase (CIAP, Promega), 6 µl 10x CIAP buffer (Promega) and dH_2O to a total volume of 60 µl. The reaction was incubated at 37°C for 15 min and then deactivated at 56°C for 15 min. A further 2 µl CIAP, 1 µl 10x CIAP buffer and 7 µl dH_2O was added and the incubation step was repeated. The salts, enzyme and remaining phosphorylated DNA were removed using agarose gel purification (section 2.3.1.2).

2.3.1.4 Design and annealing of oligopeptides

When necessary, additional RE recognition sequences were introduced into the vectors to allow the generation of cohesive ends compatible with the gene insert fragment. The sequences were designed using the RE recognition sequences published by New England Biolabs.[356] Single strand oligopeptides were manufactured by MWG biotech; the sequences are available in Appendix A3.

Complementary single strand oligopeptides were annealed by heating to 95°C for 15 min and cooling gradually to 4 °C.

2.3.1.5 DNA ligation reactions

DNA ligation reactions were performed with an overall concentration of vector plus insert DNA between 0.001-0.010 µg/µl, 1.5 µl T4 DNA ligase (Promega) and 2 µl 10x T4 buffer (Promega) in a total volume of 20 µl. Molar ratios of insert to vector of 1:1, 3:1 and 5:1 were used, calculated using the following equation:

$$\frac{\textbf{vector mass} \times \textbf{insert size}}{\textbf{vector size}} \times \textbf{molar ratio} \left(\frac{\textbf{insert}}{\textbf{vector}}\right) = \textbf{insert mass}$$

RE-digested vector without insert, and re-ligated single cut vector were used as negative and positive controls respectively. Reactions proceeded at 4 °C overnight.

2.3.2 Eukaryotic cell culture

The cell lines used were derived from human embryonic kidney cells (293 and Ad293) and African green monkey kidney cells (Cos7). Protocols were identical for the two cell types.[358, 359]

2.3.2.1 Recovery of stored cells

A 50 µl aliquot of cells was removed from storage at -80°C and thawed rapidly at 37°C. After addition of 10 ml 293 medium (Appendix A1), the cells were pelleted by centrifugation at 300 x *g* for 5 min, the pellet was resuspended in 15 ml 293 medium, added to a cell culture flask with a surface area of 75 cm^2 and incubated at 37°C/5% CO_2. The medium was changed every 48–72 h.

2.3.2.2 Splitting cell cultures

The cell monolayer was observed using an inverted light microscope (Olympus). When the monolayer reached 70% confluence the cells were detached from the substrate by trypsinisation. The medium was removed and the cells washed gently with 5 ml phosphate buffered saline (PBS, Sigma-Aldrich). Sufficient prewarmed (37 °C) trypsin (0.25%), ethylenediaminetetraacetic acid (EDTA) $4Na^+$ (Gibco) solution was added to cover the cell layer, and then after 1 min the cells were disaggregated

by agitation and tituration. The cell suspension was transferred to a larger flask to expand the culture, or 20–30% was returned to the original flask to maintain the cell line.

2.4 Generation and validation of recombinant adenovirus

The generation of RAd was based on the Ad-Easy system (Stratagene).[351]

2.4.1 Generation of plasmid DNA

2.4.1.1 Shuttle plasmids

The gene of interest was purified and ligated into the multiple cloning site of pShuttle or pShuttle-IRES-hrGFP-1 (Stratagene). Insertion and correct orientation of the insert was confirmed by RE digest and 1% agarose gel electrophoresis. The shuttle plasmid was amplified and purified, linearised by *Pme*I digestion and dephosphorylated (section 2.3.1.3). The linear DNA was purified by 1% agarose gel electrophoresis (section 2.3.1.2).

2.4.1.2 Homologous recombination

Homologous recombination between the shuttle vector and pAdEasy-1 (Stratagene) was performed in BJ5183 competent *Escherichia coli* (Stratagene). The cells were thawed from -80°C on ice and 40 µl was added to a mixture of 1 µg shuttle vector and 100 ng of pAdEasy-1. A negative control was provided by 1 µg shuttle vector without pAdEasy-1. Electroporation was performed in pre-chilled cuvettes (0.2 cm gap) at 200 Ω, 2.5 kV, 25 µF. 1 ml sterile LB broth was added and the cell suspension was incubated at 37°C with vigorous shaking for 1 h. The recovered cells were then split (500 µl, 300 µl, 100 µl and 50 µl) between four LB-kanamycin plates and incubated at 37°C overnight.

2.4.1.3 Testing for recombinant Ad plasmids

Following overnight incubation, the plates generated in section 2.4.1.2 were examined and compared to the control. Successful recombinants appeared as tiny colonies; 10-15 of these were selected, added to 5 ml LB-kanamycin broth and incubated overnight at 37°C with vigorous shaking. DNA was extracted using the

miniprep procedure (section 2.2.2.1). PacI RE digest of 10 µl of the miniprep DNA was performed as described in section 2.3.1.1 and the resultant fragments were run on a 1% agarose gel at 85 mV. Potential recombinants were identified by the presence of a large ~30 kb band and smaller bands at 3 kb or 4.5 kb.

2.4.1.4 DNA extraction for the large recombinant Ad plasmids

A starter culture was prepared using a single colony from a numbered miniprep plate identified as a potential recombinant. This was inoculated into 10 ml LB-kanamycin and incubated for 6-8 h with vigorous shaking. The contents of the starter culture were added to 400 ml LB medium containing the appropriate antibiotic and incubated overnight with vigorous shaking. Cells were harvested by centrifugation at 6000 x *g* for 15 min at 4 °C. Bacteria were lysed and the DNA recovered using the maxiprep protocol described in section 2.2.2.2.

2.4.2 Generation and purification of virus

2.4.2.1 Preparation of linear DNA for transfection of Ad-293 cells

5 µg of linearised and dephosphorylated DNA was required for each transfection. The Ad plasmid DNA was linearised by PacI RE digestion as described in section 2.3.1.1.The linearised DNA was purified by agarose gel extraction as described in section 2.3.1.2. Linear Ad DNA was dephosphorlyated as described in section 2.3.1.3. Following dephosphorylation the enzyme and salts were removed using a modification of the Qiagen Genomic tip 20 protocol and commercially available buffers (Qiagen).[355]

The pH of the dephosphorylation reaction was adjusted by the addition of 900 µl QBT buffer, a further 1 ml QBT was used to equilibrate the genomic tip. The DNA sample was added to the column and allowed to flow through and bind to the membrane by gravity. The DNA was eluted into a polycarbonate centrifuge tube using 2 ml buffer QF warmed to 50 °C. DNA was precipitated by addition of 1.4 ml room temperature isopropanol and then centrifuged at 20,000 x *g* for 30 min at 4 °C. The supernatant was decanted and the DNA pellet washed with 70% EtOH at

4°C and then centrifuged at 20,000 x *g* for 15 min at 4 °C. The pellet was dried in air and resuspended in 50 µl dH_2O.

2.4.2.2 Transfection of Ad-293 cells

Eukaryotic cell transfection was performed using 293fectin (Invitrogen). Ad293 cells were split to ~50% confluence at 24 h prior to the experiment so that at transfection they were ~80 – 90% confluent on a 25 cm^2 surface (see section 2.3.2 for cell culture protocols). The cells were gently washed in PBS which was then replaced with 1 ml Optimem medium (Invitrogen). DNA complexes were prepared from the linearised dephosphorylated Ad DNA (section 2.4.2.1); in one microcentrifuge tube Optimem was added to 2 – 3 µg DNA to a total volume of 150 µl, and in another 2 µl 293fectin was added to 148 µl Optimem. After 5 min the two tubes were mixed. The mixture was incubated at 37°C for 20 min and then added to the Ad293 cells followed by a further incubation at 37 °C/5% CO_2 for 4 h. After this final incubation step the Optimem was replaced by 293 medium and the cell cultures returned to 37 °C/5% CO_2. After 72 h the medium was changed and the cells were inspected by inverted phase contrast microscopy on a daily basis for the development of cytopathological effect (CPE, figure 15).

2.4.2.3 Extraction and amplification of primary virus stock from cell culture

Cell cultures were monitored until 90 – 95% of cells showed CPE and then adherent cells were detached from the flasks by agitation and tituration. The resulting suspension was centrifuged at 300 x *g* for 5 min, the supernatant was discarded and the pellet resuspended in 1 ml PBS. Virus titre was maximised by freeze thawing or Arklone P extraction.[360] The stock was amplified (secondary stock) by infection of a total flask area of 350 cm^2 at 70 – 80% confluence with 500 µl primary stock; virus was extracted in the same manner as the primary stock.

2.4.2.3.1 Arklone P extraction

The cell suspension prepared in section 2.4.2.3 was added to 1 ml Arklone P (ICI) and mixed for 5 min, the mixture was centrifuged at 1000 x *g* for 10 min. The top

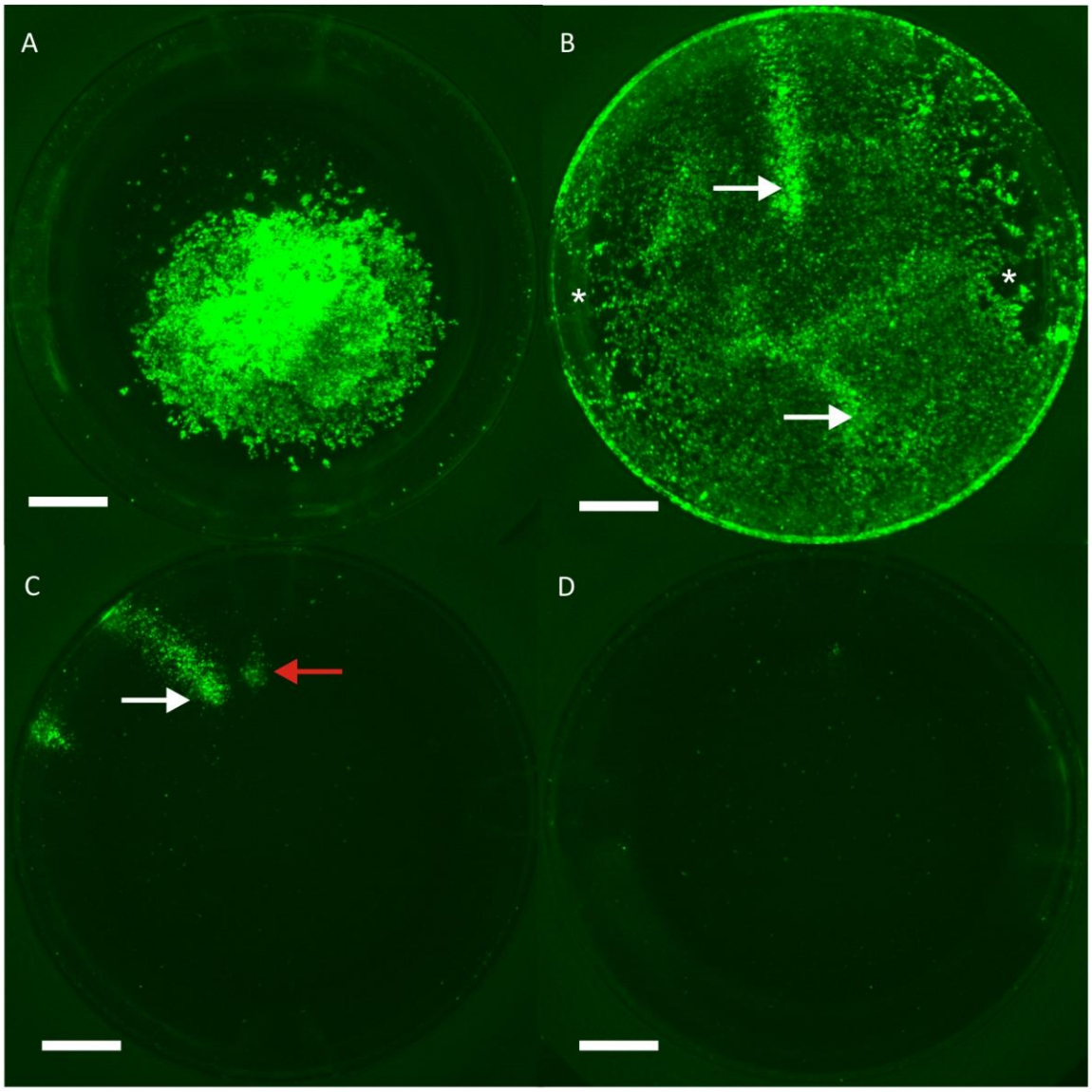

Figure 15. Cytopathological effect of adenovirus revealed by green fluorescent protein expression in Ad293 cells. A serial dilution end-point assay was prepared as described and the cells were infected with serial dilutions of Ad5-GFP, a RAd causing expression of hrGFP. Images were captured after eight days using confocal fluorescent microscopy. The panels demonstrate the range of CPE patterns seen. A) Rapid complete CPE with detachment of the cell layer (dilution 1 x 10^{-3}). B) Comprehensive CPE of the entire monolayer without detachment; areas of detachment are seen (white asterisk) along with comets (white arrow), (dilution 1 x 10^{-5}). C) Localised areas of CPE. A comet is seen (white arrow) along with an early comet that has not yet developed a full tail (red arrow), (dilution 1 x 10^{-10}). D)No significant CPE. Some background autofluorescence is noted, (dilution 1 x 10^{-11}). The titre of this virus was thus determined as 8.19 x 10^{10} pfu/ml. Note that the GFP is for demonstration purposes only. CPE was visualised by inverted phase contrast microscopy.

(aqueous) layer was carefully aliquoted into screw top microcentrifuge tubes and stored at -80 °C.

2.4.2.3.2 Freeze thawing

The cell suspension was aliquoted into screw top microcentrifuge tubes, frozen in liquid nitrogen then thawed rapidly at 37 °C. The freeze thaw cycle was repeated three times in total and the virus stock was stored at -80 °C.

2.4.2.4 Small scale viral DNA purification

A cell culture flask of 75 cm^2 area at 70-80% confluence was infected with 50 µl primary virus stock. The cells were resuspended at 50-75% CPE by tituration and pelleted by centrifugation at 300 x *g* for 5 min. The cell pellet was washed with 5 ml PBS and centrifuged for a further 5 min at 300 x *g*. The pellet was resuspended in 360 µl of 1x Tris-EDTA, pH 8 and transferred to a microcentrifuge tube. 25 µl of 10% sodium dodecyl sulphate (SDS), 8 µl of 0.5 M EDTA and 4 µl of Proteinase K (20 mg/ml) (all reagents Sigma-Aldrich) were added before incubation at 37 °C for 2 h. This was mixed vigorously with 100 µl of 5M NaCl (Sigma-Aldrich) and left on ice overnight before centrifugation at 15000 x *g* for 1 h at 4 °C. The resulting supernatant was harvested and added to an equal volume of phenol:chloroform:isoamylalchohol (Sigma-Aldrich) at a ratio of 25:24:1 and gently mixed. The top layer was carefully removed, added to two volumes of 95% EtOH and centrifuged at 15000 x *g* for 10 min. The resulting pellet was washed in 70% EtOH, respun at 15000 x *g* for 10 min then resuspended in 50 µl dH_2O containing RNase A (0.1 mg/ml, Invitrogen).[360]

2.4.2.5 Southern blot detection of insert DNA

Presence of the gene of interest in the viral DNA was confirmed using Southern blot analysis and digoxenin labelled probes generated from the plasmids from which the gene was originally cloned.

2.4.2.5.1 Synthesis of digoxenin labelled DNA probes

The target DNA (to which probes were to be made) was isolated by agarose gel extraction as previously described in section 2.3.1.2. DNA was then denatured by

heating to 95 °C for 10 min. The tube was cooled immediately on ice, then 2 µl hexanucleotide mixture, 2 µl deoxyribonucleotide triphosphate (dNTP) mixture and 1µl Klenow enzyme (all reagents Roche) were added. dH_2O was added to make a total volume of 20 µl before incubation at 37°C for 20 h.

2.4.2.5.2 Blotting DNA onto nitrocellulose membrane

A 1% agarose gel was prepared (Appendix A1) and electrophoresis of HindIII RE digested viral DNA was performed. The gel was rinsed with dH_2O and then placed in 0.25 M HCl (Sigma-Aldrich) on a shaker for 30 min to fragment the DNA. Following a further wash with dH_2O, the gel was soaked in 0.4 M NaOH (Sigma-Aldrich) on a shaker for 20 min to denature the DNA. Following a final wash in dH_2O a nitrocellulose membrane (Biodyne Plus 0.45 µm, PALL Life Sciences) was cut to exactly match the size of the agarose gel and the blotting equipment was assembled as shown in figure 16. The blot was left for 16 h to ensure maximal transfer of DNA from gel to membrane.

2.4.2.5.2 Pre-hybridisation

The nitrocellulose membrane was separated from the gel and washed in 5 x saline sodium citrate (SSC, Appendix A1) on a shaker for 5 min. The membrane was then incubated in pre-hybridisation solution (Appendix A1) in a sealed bag at 68°C for 2h.

2.4.2.5.3 Hybridisation

The digoxenin-labelled probe was denatured by heating at 95 °C for 10 min and 1 µg of the probe was added to the pre-hybridisation solution. The bag was re-sealed and the membrane was incubated for 16 h at 68 °C, before being washed in 2 x SSC/0.1% SDS (Sigma-Aldrich) at room temperature for 15 min and then in 0.1 x SSC/0.1% SDS at 65 °C for 30 min.

2.4.2.5.4 Immunodetection

Immunodetection was performed using anti-digoxenin/alkaline phosphatase conjugate (Roche) then the membrane was photographed. The series of washes are detailed in table 2. Details of the buffer solutions can be found in Appendix A1.

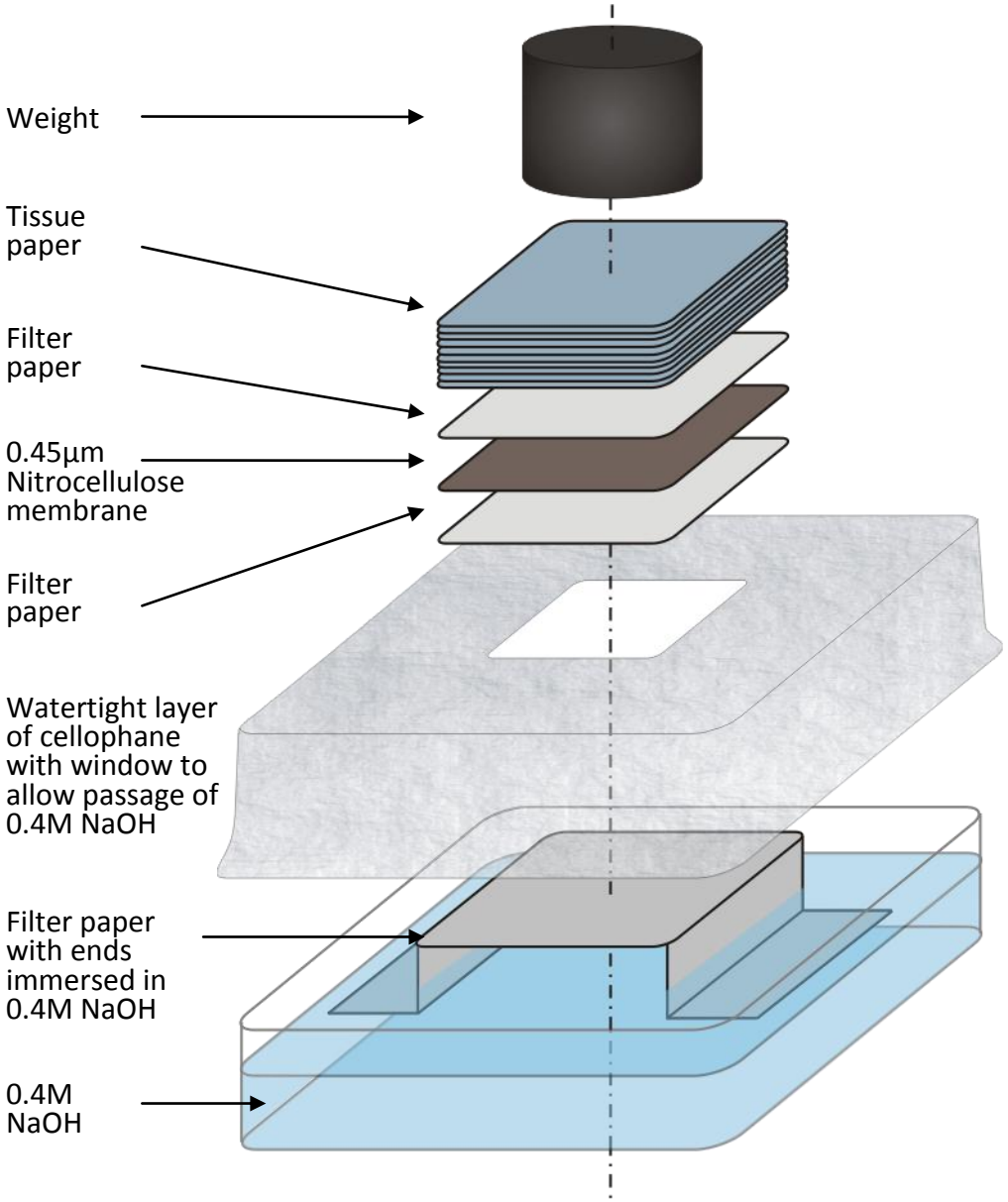

Figure 16. Assembly of equipment for the blotting of DNA from 1% agarose gel onto nitrocellulose membrane.

Step	Solution	Incubation time
1	Southern Buffer 1	1 min
2	Southern Buffer 2	30 min
3	Southern Buffer 1	5 min
4	Anti-digoxenin/alkaline phosphatase conjugate 150 mU/ml in Southern Buffer 1	30 min
5	Southern Buffer 1	30 min
6	Southern Buffer 3	2 min
7	Southern Colour substrate	12 h (in dark)
8	Southern Buffer 4	5 min

Table 2. Steps for immunodetection of a digoxenin labelled probe using anti-digoxenin/alkaline phosphatase conjugate

2.4.2.6 Caesium chloride gradient purification of large viral cultures

Once the correct viral DNA digestion pattern and probe binding had been confirmed, a larger culture of the virus was prepared. Ad293 cells at 80-90% confluence were infected at a multiplicity of infection (MOI) of ~5 using the secondary stock. The total flask area of was 5000-6000 cm^2. The cells were harvested by agitation and tituration when CPE was seen in >95% of the cell monolayer (usually ~48-72 h) and centrifuged at 1000 x *g* for 15 min at 4 °C. Arklone P extraction was performed using 5 ml PBS/5 ml Arklone P as described in section 2.4.2.3.1. CsCl (Sigma-Aldrich) solutions were prepared in dH_2O, 2.5 ml of 1.33 g/ml CsCl was layered on 1.5 ml of 1.45 g/ml CsCl, the arklone extracted virus was layered on top of this and the centrifuge tube was topped up with mineral oil (Sigma-Aldrich) and spun at 90,000 x *g* in an ultracentrifuge for 2 h at 4 C°.

The virus band was removed by side puncture of the centrifuge tube using a sterile 21 G needle. The part-purified virus was transferred to a 15 ml Falcon tube and diluted with 1 volume of Tris-EDTA pH 7.8 (Appendix A1). It was then layered on top of a second CsCl gradient prepared using 1 ml of 1.45g/ ml CsCl and 1.5 ml of 1.33g/ ml CsCl topped with mineral oil. The gradient was centrifuged at 100,000 x *g* for 18 h at 4°C. The virus band was removed using a sterile 21 G needle as before.

Visking tubing was prepared by boiling in 2% NaOH/1 mM EDTA for 10 min, then 1 mM EDTA for 10 min before stage at 4°C in 1 mM EDTA.[361] Prior to use the visking tubing was washed in sterile dH_2O and soaked in CsCl dialysis buffer A (Appendix A1). The virus band was transferred to the visking tubing which was sealed then dialysed against CsCl dialysis buffer A. After 1 h the buffer was replaced with fresh CsCl dialysis buffer A, then after a further hour the virus was dialysed against CsCl dialysis buffer B (Appendix A1) for 2 h. The purified virus was extracted from the dialysis tubing and aliquoted into screw top microcentrifuge tubes for storage at -80 °C.[360, 362]

2.4.3 Adenovirus titration by serial dilution end-point assay

293 cells were grown to 80% confluence on a total flask surface area of 75 cm^2 and then resuspended trypsinisation (section 2.3.2.2). The cell density was calculated using light microscopy and a haemocytometer (Bright Line) according to the manufacturer's instructions. 72 wells of a 96 well plate (flat bottomed, Corning) were inoculated with 5-7 x 10^3 293 cells each. 24 h after inoculation the medium was carefully removed and the cells were infected with 100 μl of the serially-diluted virus in fresh, pre-warmed 293 medium (the serial dilutions are shown in table3). Starting dilution was 10^{-2} continuing to 2.98 x 10^{-14}, each dilution was performed in triplicate. An additional 100 μl of fresh pre-warmed 293 medium was added 24 h later. The medium was changed every 3-5 days, whilst monitoring the wells regularly for evidence of CPE by inverted phase contrast microscopy. After eight days the end-point well was determined (table 3).

2.4.4 Infection and preparation of Cos7 cells for patch clamp and immunocytochemistry

Cos7 cells were grown to 80-90% confluence and total flask surface of 75 cm^2 and harvested by trypsinisation (see section 2.3.2). The cell density of the suspension was calculated using light microscopy and a haemocytometer according to the manufacturer's instructions. 3 x 10^4 cells were inoculated into each well of a 6 well flat bottomed plate (Gibco) containing small cover slips then incubated for 12 h at 37°C/5% CO_2, the virus of interest was then added at a MOI of 100-500. The cells were incubated for a further 24 h. For patch clamp experiments the cells were disaggregated using 0.5 mM EDTA, centrifuged at 300 x *g* for 5 min, resuspended in 1 ml 293 medium and returned to the wells. After 1 h incubation at 37°C/5% CO_2 the cover slips were taken from the wells for the patch clamp experiments.

2.5 Patch clamp

Patch clamp experiments for Ad5-GFP-HCN2 and Ad5-PREK-HCN4 were performed by Yalena Kryukova at Columbia University, New York, USA. The patch clamp

Well:	**1**	**2**	**3**	**4**	**5**	**6**	**7**	**8**	**9**	**10**	**11**	**12**
Dilution:	10^{-2}	10^{-3}	10^{-4}	10^{-5}	10^{-6}	$5x10^{-7}$	$2.5x10^{-7}$	$1.25x10^{-7}$	$6.25x10^{-8}$	$3.13x10^{-8}$	$1.56x10^{-8}$	$7.81x10^{-9}$
pfu/ml:	10^{3}	10^{4}	10^{5}	10^{6}	10^{7}	$2x10^{7}$	$4x10^{7}$	$8x10^{7}$	$1.6x10^{8}$	$3.2x10^{8}$	$6.4x10^{8}$	$1.28x10^{9}$

Well:	**13**	**14**	**15**	**16**	**17**	**18**	**19**	**20**	**21**
Dilution:	$3.91x10^{-9}$	$1.95x10^{-9}$	$9.77x10^{-10}$	$4.88x10^{-10}$	$2.44x10^{-10}$	$1.22x10^{-10}$	$6.10x10^{-11}$	$3.05x10^{-11}$	$1.53x10^{-11}$
pfu/ml:	$2.56x10^{9}$	$5.12x10^{9}$	$1.02x10^{10}$	$2.05x10^{10}$	$4.10x10^{10}$	$8.19x10^{10}$	$1.64x10^{11}$	$3.28x10^{11}$	$6.55x10^{11}$

Well:	**22**	**23**	**24**	**25**	**26**	**27**	**28**	**29**	**30**
Dilution:	$7.63x10^{-12}$	$3.81x10^{-12}$	$1.91x10^{-12}$	$9.52x10^{-13}$	$4.77x10^{-13}$	$2.38x10^{-13}$	$1.19x10^{-13}$	$5.96x10^{-14}$	$2.98x10^{-14}$
pfu/ml:	$1.31x10^{12}$	$2.62x10^{12}$	$5.24x10^{12}$	$1.05x10^{13}$	$2.10x10^{13}$	$4.19x10^{13}$	$8.39x10^{13}$	$1.68x10^{14}$	$3.36x10^{14}$

Table 3. Virus end point serial dilution table and corresponding plaque forming units (pfu) concentrations

experiments for Ad5-GFP-HCN4Δ were performed by Yunhong Gui, University of Manchester, UK. Details of the protocols are included in each figure legend.

2.6 Sinoatrial node culture and monitoring of extracellular potentials

2.6.1 Sinoatrial node tissue culture

Three month-old male Wistar Hanover rats were humanely euthanised by cervical dislocation in accordance with the United Kingdom Home Office schedule 1 animals (scientific procedures) act 1986.[363] The thorax was cleaned with ChloraPrep (2% chlorhexidine gluconate/70% isopropyl alcohol, CareFusion) and the heart was removed quickly under sterile conditions to sterile oxygenated Tyrode's solution (Appendix A1) at 37 °C. The SAN was quickly dissected while continuously bathed in sterile oxygenated Tyrode's solution at 37°C and then photographed using a dissecting microscope (Leica). To generate the SSS model the upper two thirds was removed by a transverse incision at the level of the fossa ovalis (FO), and the AVN and Eustachian ridge were removed as shown in figure 17. The SAN preparation was then transferred to SAN medium (Appendix A1) at 37 °C.

A recording system was fabricated using 0.2 mm diameter stainless steel needles (JCM Health). Two needles and a 0.5 mm silver wire (WPI) were soldered to shielded three core low resistance wire (generic). Silicon glue (Radio Spares) was used to insulate the needles to within 3-4 mm of the tip and also to enclose the solder (figure 18). The electrodes were pinned through the tissue periphery at opposite corners and the earth was secured in the tissue culture medium. The recording electrodes were connected to a Neurolog system (Digitimer) with 50 Hz filter and low pass/high pass filters adjusted to optimise the signal/noise ratio. The setup was transferred to a 37°C/5% CO_2 incubator on an oscillatory rocker. Extracellular potentials were continuously recorded using a PC with Powerlab and Chart software (ADInstruments). Chart software calculated the 30 s average rate via the detection of a deflection greater than 2 SD of the average amplitude as a paced beat. The medium was changed every 24 h. The rate was averaged over six hours and compared to the rate of the control preparation using 2-way ANOVA

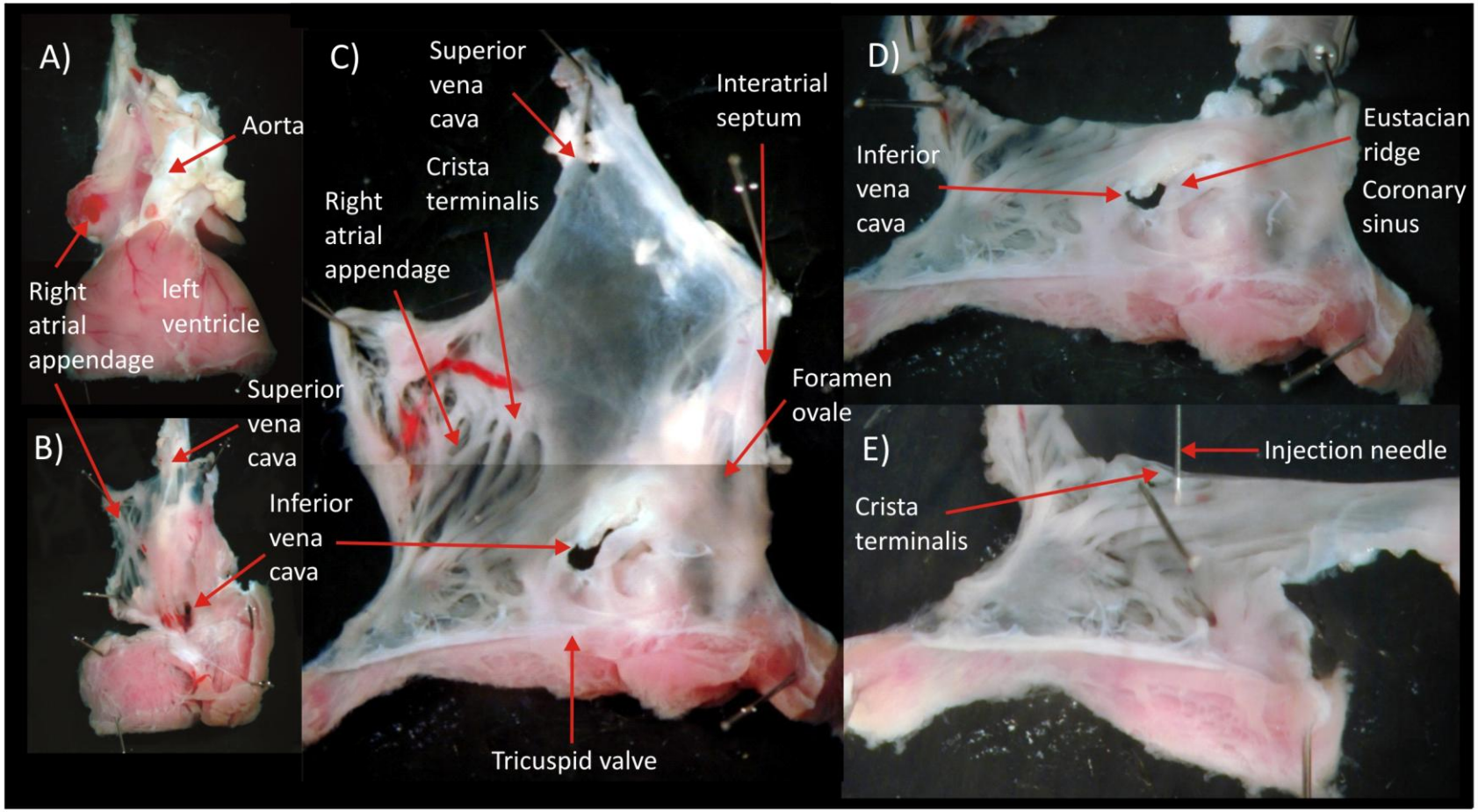

Figure 17. Method of preparation of the sick sinus syndrome model and injection of adenovirus. The heart was removed from the thorax and the right atrium was opened (A,B). Surrounding tissue was removed to leave the full sinoatrial node preparation (C). The SSS model was the inferior portion created by division of the preparation at the level of the fossa ovalis (D). Adenovirus was injected near the termination of the crista terminalis (E).

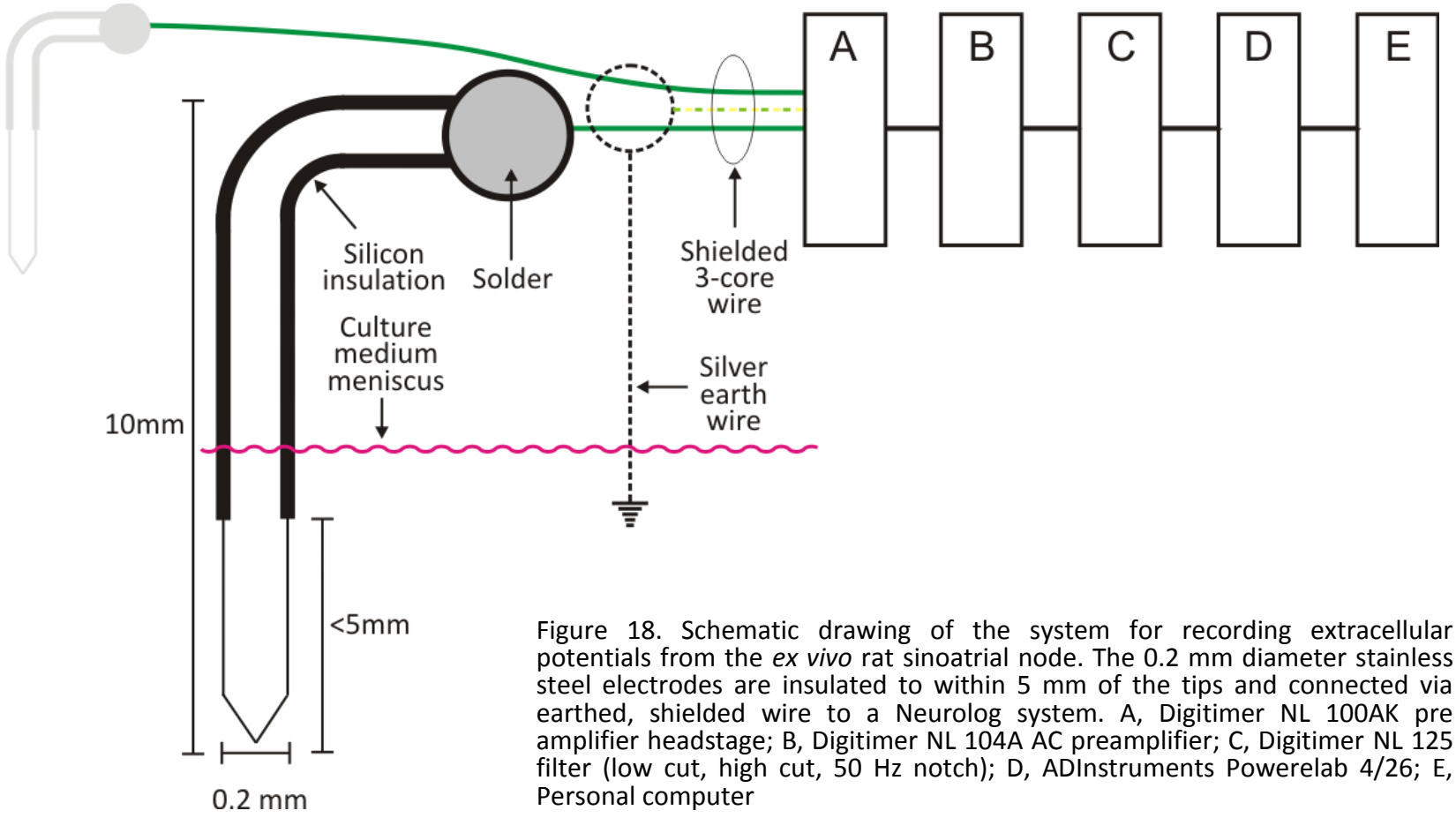

Figure 18. Schematic drawing of the system for recording extracellular potentials from the *ex vivo* rat sinoatrial node. The 0.2 mm diameter stainless steel electrodes are insulated to within 5 mm of the tips and connected via earthed, shielded wire to a Neurolog system. A, Digitimer NL 100AK pre amplifier headstage; B, Digitimer NL 104A AC preamplifier; C, Digitimer NL 125 filter (low cut, high cut, 50 Hz notch); D, ADInstruments Powerelab 4/26; E, Personal computer

(SigmaStat). The mean, maximum and minimum rates were calculated and compared to the control using 1-way ANOVA (SigmaStat).

2.6.2 Injection of recombinant adenovirus into sinoatrial node tissue

A graduated syringe (Nanofil, WPI) was attached to a micromanipulator (Naharshige) by a custom-designed aluminium rod and clamp. The syringe was filled with 5 µl of the RAd of interest prewarmed to 37°C then a 35 G needle was attached. The needle was flushed carefully with 1-2 µl of the RAd solution to ensure that no air bubbles were trapped in the system. The needle was positioned in the area of the superior aspect of the IVC (figure 17) and 1-2 µl RAd was injected to deliver ~ 1 x 10^7 pfu. The needle was left *in situ* for 2 min to promote dispersion of the RAd into the tissue and then carefully removed. The recording electrodes were inserted and the preparation was transferred to a 37°C/5% CO_2 incubator for monitoring of the pacing rate. The rate was averaged over 1 h and compared to the control and SSS syndrome preparations using 2-way ANOVA.

2.6.3 Camptothecin-induced apoptosis in sinoatrial node tissue

A stock solution of 0.1 M camptothecin (Fisher Scientific) was prepared in dimethyl sulfoxide (DMSO, Sigma) and sterilised by vacuum filtration (0.2 µm pore, Fisher Scientific). A SAN preparation was dissected as described in section 2.6 and transferred to SAN medium containing a final concentration of 6 µM camptothecin from the sterile stock. The SAN tissue was cultured for 24 h at 37°C/5% CO_2 for 24 h.

2.7 Activation mapping and rate response to isoprenaline and caesium

The activation sequence mapping was based on the recording of low frequency extracellular potentials from rabbit SAN, a technique described by Yamamoto et al.[364] Two pairs of bipolar electrodes were fashioned from two 100 µm stainless steel wires glued together and insulated to within 2 mm of the tip. The indifferent pole of each bipolar electrode was positioned 1 mm above the tip of the active pole. Rats were euthanised and the SAN dissected as described in section 2.6.1. The SAN was then transferred to a chamber constantly superfused with Tyrode's

solution via a peristaltic pump (Gilson Minipuls 3, Anachem) at 5 ml/min, 36°C and allowed to accommodate for 30 min.

Two bipolar electrodes were attached to *XYZ* micromanipulators (Naharshige) calibrated to 0.1 mm precision. The electrodes were gently touched to the endocardium and the potential difference between the active and indifferent poles was measured. The recording system comprised a Neurolog NL 100AK pre-amplifier headstage, NL 104A AC preamplifier and a NL 125 filter with 50 Hz notch filter and 0.5-30 Hz low frequency filter (Digitimer), and a Molecular Devices Digidata 1440A data acquisition unit attached to a PC with AxoScope software (Molecular Devices).

One electrode was used as a static reference electrode contacting the atrial muscle near the CT. The other electrode was used as a roving electrode to record extracellular potentials at 0.5-1 mm intervals and 100-150 coordinates. The time differences between the points of first depolarization were calculated using AxoScope software. The coordinates of the SAN tissue were measured using the tip of the roving electrode. SigmaPlot software (Systat) was used to construct a contour plot of the *XY* coordinates vs. time difference, which was overlaid on a plot of the SAN tissue coordinates. Hence the site of first activation and the activation sequence could be visualised. After the full SAN tissue had been mapped the SSS model was created as described in section 2.6.1, allowed to accommodate for 30 min and then mapped as above.

Using the same recording system but Spike software (ADInstruments) the rate of the SSS preparation was recorded for 5 min. The superfusing solution was then changed to Tyrode's solution containing CsCl 2 mM, allowed to accommodate for 30 min and the rate was recorded for 5 min. The preparation was washed by superfusing with normal Tyrode's for 30 min and the rate recorded for 5 min. Finally Tyrode's solution containing isoprenaline (Stockport NHS trust) 100 µM was used and after 30 min the rate was recorded for 5 min. The mean rate for each period was calculated and statistical analysis was performed by paired t-test (SigmaStat).

2.8 Histology, immunohistochemistry and immunocytochemistry

2.8.1 Preparation of tissue or cells

SAN tissue was encased in OCT and cooled to -50°C using isopentane (Fisher) cooled in liquid N_2 (BOC). The specimen was marked such that the orientation of the SVC and CT was known and then mounted onto a cork base. Transverse sections of 16 µm thickness were cut using a cryostat (Leica CM3050 S), then mounted onto Superfrost Plus slides (VWR) and stored at -80°C. Cell cultures to be used for immunocytochemistry were washed in 2 ml PBS, fixed in 10% buffered formalin (Sigma-Aldrich) for 5 min and then washed three times for 10 min in 0.01 M PBS.

2.8.2 Histology; Masson's trichrome staining

Tissue sections were removed from storage and fixed in room temperature Bouin's fluid (Sigma-Aldrich) overnight and then washed in 70% EtOH three times. Masson's trichrome staining was performed using commercially available solutions from Sigma-Aldrich. Slides were immersed in haematoxylin for 10 min, washed in tap water for 15 min and then the nuclear staining was checked by light microscopy. If further nuclear staining was required, the slide was placed back into haematoxylin solution for 2 min, rewashed and checked by light microscopy again. Further staining was performed with acid fuschin for 8 min, a rinse with distilled water, phosphomolybdic acid for 5 min, aniline blue for 6 min before a final rinse with distilled water. Stained sections were treated with 1% acetic acid (Sigma-Aldrich) for 2 min and then dehydrated through alcohols (70% EtOH 1 min, 90% EtOH 1 min, 100% EtOH 4 min). The samples were cleared with Histo-Clear (National Diagnostics) for 10 min and then cover slips (VWR) were fixed using DPX (Prolabo).

2.8.2 Immunohistochemistry with fluorescent conjugated secondary antibodies; sinoatrial node tissue

Slides were removed from -80°C storage and a ring was drawn around each section with a hydrophobic PAP pen (Sigma-Aldrich) leaving a ~ 5-10 mm gap from the tissue on each side. The tissue was then fixed in 10% buffered formalin for 30 min and then washed for 10 min three times in 0.01 M PBS. The cells were

permeabilised for 10 min using 0.1% Triton-X100 (Sigma-Aldrich) in 0.01 M PBS min then washed for 10 min three times in 0.01 M PBS. Following PBS washes, the sections were treated with the universal blocker 1% bovine serum albumin (BSA, Sigma-Aldrich) in 0.01M PBS for 30 min in order to block non-specific binding sites and reduce background fluorescence.

2.8.2.1 Primary antibodies

To allow selective binding of the secondary florescent conjugated antibody (see below) to the primary antibody only, a primary antibody was selected that had not been raised in the same species as the tissue of interest (i.e. rat). For double labelling, each primary antibody was raised in a different species (e.g., Cx43 IgG raised in mouse, HCN4 IgG raised in rabbit) and the antibodies were mixed and applied together in 1% BSA in 0.01 M PBS. Each antibody was diluted to its individual optimal concentration in the final mixture; for ion channels 1 in 50 and connexins 1 in 500.

Sufficient solution containing diluted primary antibody was added to cover each section within the PAP pen ring so that a meniscus was formed. The slides were placed in a sealed humid chamber to prevent evaporation of the antibody mixture and incubated overnight at 4°C and then washed twice for 10 min in 0.01 M PBS.

2.8.2.2 Fluorescent conjugated secondary antibodies

Sufficient solution containing diluted secondary antibody was added to cover each section within the PAP Pen ring. The tissue sections were incubated with the secondary antibody at room temperature for 2 h. The secondary antibodies were reconstituted according to the manufacturers' instructions and then diluted in 1% BSA in 0.01 M PBS to their working concentration.

The secondary antibody binds to the primary antibody with specificity for species and immunoglobulin type, e.g. if the primary antibody was IgG raised in rabbit, the secondary antibody was anti-rabbit IgG. The secondary antibody was conjugated to a fluorochrome enabling the visualisation of the bound antibody with fluorescence

confocal microscopy. For double labelling experiments, antibodies were selected to have differing excitation and emission spectra (shown in table 4).

2.8.3 Immunocytochemistry with fluorescent conjugated secondary antibodies; Cos7 cells

Cells to be used for immunocytochemistry were infected and cultured as described in section 2.4.4 and then prepared as described above. Cells were permeabilised by adding 0.1% Triton X-100 in PBS to each well for 10 min and then washed twice for 10 min with 0.01 M PBS. The cells were treated with 1% BSA in 0.01 M PBS for 30 min to block non-specific binding. Cover slips were removed from the wells and placed onto a microscope slide within a PAP pen ring. Sufficient primary antibody was added to cover the cover slip forming a meniscus. The cells were incubated for 1 h at room temperature in a sealed humid box and then washed twice for 10 min with 0.01 M PBS. The appropriate secondary antibody was applied (the principle is described in section 2.8.2.2) and the cells were incubated in a sealed humid box in the dark for 1 h at room temperature. The cells were then washed twice for 10 min with 0.01 M PBS. If nuclear staining was required, incubation with DAPI (Invitrogen) for 10 min was performed before a final washing step, twice for 10 min with 0.01 M PBS.

2.8.4 Mounting, storage and imaging

To avoid photo-bleaching during fluorescence confocal microscope scanning, the sections were mounted in Vectashield (Vectorlabs). The edges of the cover slips were sealed with acrylic nail varnish. Due to the instability of fluorochromes, immunofluorescence signals were captured as soon as the experiment was finished when possible, or the tissue sections were stored in the dark at 4°C and the images were captured within two weeks. Images were obtained using a laser scanning confocal microscope (Zeiss LSM 5) using the manufacturer-configured lasers and filter sets to provide the appropriate excitation wavelength and detection of emitted light.

Fluorophore	Absorption Peak (nm)	Emission Peak (nm)
Fluorescein, FITC	492	520
Indocarbocyanine, Cy3	550	570
Indodicarbocyanine, Cy5	650	670

Table 4. Absorption and emission spectra for the common fluorophores

When quantitative immunohistochemistry was required, the tissue sections were processed in batches so that the conditions were identical for all sections allowing comparison. The relative intensity of signals (above background fluorescence) was measured using Volocity software (Perkin Elmer) and compared using unpaired t-test or 1-way ANOVA. For cell size measurement, cells were selected that were cut in transverse section, the shortest axis was taken. The mean of 20 cells over three high power fields was taken for each sample. Data within a group (e.g. SAN versus RA cell size in control preparation) were compared using a paired t-test; comparison of data between groups (e.g. SAN versus SSS leading pacemaker) was performed by unpaired t-test.

2.8.5 X-Gal assay

To detect β-galactosidase activity in tissue infected with Ad5-LacZ, an X-Gal assay was performed. After 48 h culture the tissue was fixed; for whole tissue experiments the SAN preparation was fixed in 10% buffered formalin overnight and then washed twice in 0.01 M PBS for 10 min, or tissue sections were prepared as described in section 2.8.1. Cells were permeabilised using 0.1% Triton-X100 in 0.01 M PBS (1 h for whole tissue, 5 min for tissue sections) and then washed twice in 0.01 M PBS for 10 min. Staining was performed using freshly prepared X-Gal staining solution (see Appendix A1) for 1-3 h in the dark. The development of the blue staining was monitored by direct vision or light microscopy. When sufficient staining had occurred the reaction was stopped by washing twice for 10 min in 0.01 M PBS. Further histology or immunohistochemistry was performed as above if required.

3 Results

3.1 Recombinant adenovirus

3.1.1 Introduction

RAd based on Ad5 permit high efficiency of infection and transgene transfer.[331] Ad5 is a relatively safe vector. It is not oncogenic, but may cause mild respiratory disease or myocarditis in humans.[365] The safety of RAd is enhanced by the deletion of the E1 region of the genome rendering them replication deficient other than in specific complementing cell lines.[366] Their usefulness as a research tool lies in the ability to package large genes up to at least 7.5 kb and the ease of purification to high titres (up to 10^{13} virus particles per ml).[366]

Common approaches to construction of RAd employ the strategy of replacement of the E1 region of Ad5 viruses with the gene of interest. Recombination with the gene of interest requires homologous recombination between the E1 deleted Ad5 genome and DNA (such as a plasmid) containing the gene of interest.[367] This occurs in an E1-complementing mammalian cell line, usually 293 cells derived from human embryonic kidney cells transformed with sheared Ad5 DNA.[358, 368] This technique is labour intensive and the efficiency of homologous recombination in mammalian cells is low.

This latter problem has been circumvented by the use of *Escherichia coli* for the homologous recombination step. Recombination occurs between 1) a large plasmid containing the majority of the Ad5 genome, and 2) a plasmid containing the gene of interest plus the flanking regions and areas of sequence homology to the Ad5 genome. The resulting plasmid is then linearised and transfected into the E1-complementing cells. An example of this system is the AdEasy system.[351] Purification of the virions can be performed using CsCl gradient purification, column chromatography or anion exchange chromatography.[366] CsCl gradient purification yields high purity virus particles in small to medium quantities. Following purification the concentration of the virions can be quantified physically via SDS disruption and optical absorbance of the DNA at 260 nm, or biologically via

infection of a cell monolayer by serial dilutions of the purified virus.[369] Though more time consuming, the biological method has the advantage that it assesses the concentration of viable virions.

3.1.2 Ad5-GFP-HCN2

The virus Ad5-GFP-HCN2 was kindly provided by Dr Richard Robinson (Columbia University, USA). The virus was amplified and purified as described in section 2.4.

3.1.2.1 Validation of virus and HCN2 transgene

Cos7 cells were infected with Ad5-GFP-HCN2 at a MOI of 100. After 48 h incubation the cells were transferred to cover slips and patch clamp (n=5) or immunocytochemistry (n=3 separate experiments) was performed. The presence of HCN2 channel protein was confirmed as shown in figure 19. Figure 20 shows the current induced by HCN2 expression in Cos7 cells.

3.1.2.2 Determination of viral titre

The titre was determined by serial dilution at 4.1 x 10^{10} pfu/ml.

3.1.3 Ad5-GFP-HCN4Δ

3.1.3.1 Cloning

3.1.3.1.1 pShuttle-IRES-GFP-HCN4

The cDNA for mHCN4 was cloned into the shuttle vector as described in section 2.3 and Appendix A2. Verification of the correct gene insertion was by RE digest. It can be seen in figure 21A that RE digestion of pShuttle-IRES-GFP-HCN4Δ with NheI/XbaI should produce a 3.5 kb fragment, and that the correct insertion orientation of the mHCN4 cDNA should produce a 2.5 kb XbaI fragment on RE digestion with XbaI/SalI. In figure 21B 3.5 kb and 2.5 kb bands are seen on 1% agarose gel electrophoresis of the digestion products as expected.

3.1.3.1.2 pAd-GFP-HCN4

The predicted plasmid map for the plasmid resulting from homologous recombination as described is shown in figure 22A. The DNA between the PacI

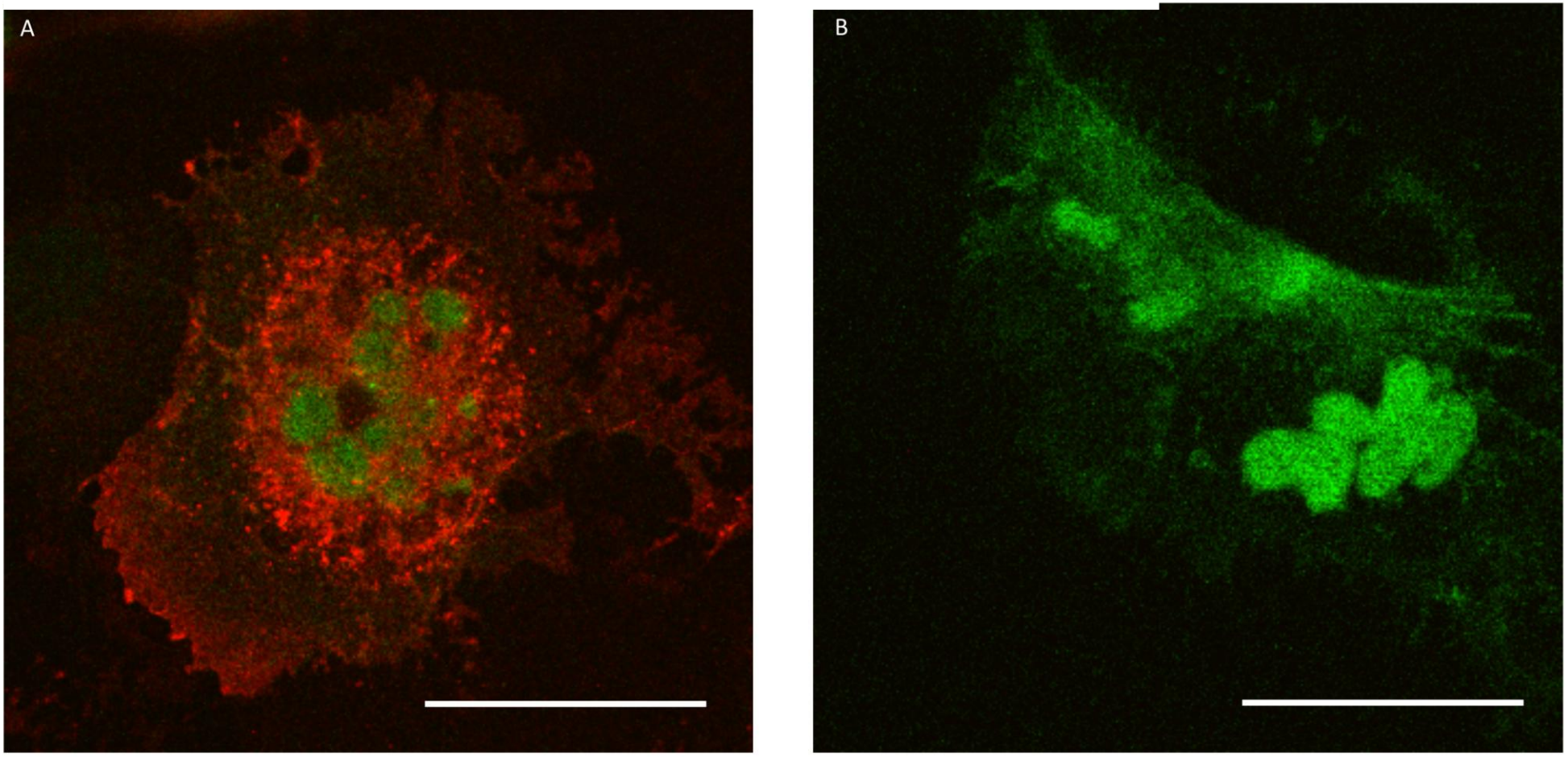

Figure 19. Adenovirus mediated expression of HCN2 in a Cos7 cell. Cos7 cells were infected with a recombinant adenovirus Ad5 GFP-HCN2 containing an internal ribosomal entry site allowing the expression of green fluorescent protein (GFP) and HCN2 under the control of the same CMV promoter (A),or Ad5-GFP expressing GFP via an internal ribosomal entry site and CMV promoter (B). The cells were labelled with a primary antibody to HCN2 (mouse anti-HCN2 IgG) and a secondary antibody, (donkey anti-mouse IgG conjugated to Cy3). HCN2 labelling is indicated by the red signal. The GFP gives the green signal. The image was captured using a confocal laser scanning microscope (Zeiss LSM5 PASCAL). Scale bars represent 50 µm.

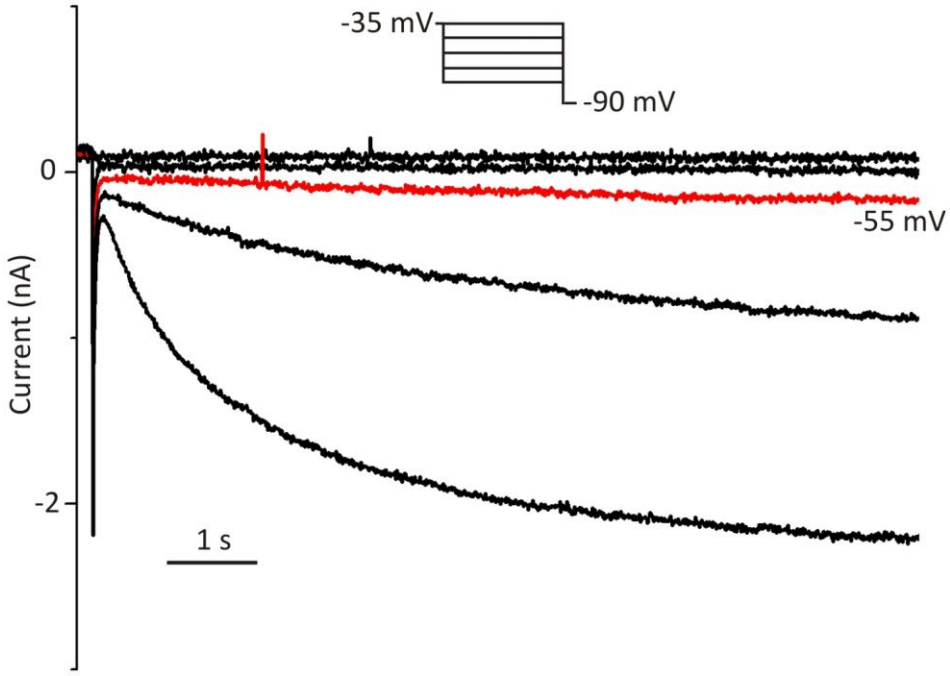

Figure 20. Representative inward current recorded from a 293 cell transduced with Ad5-GFP-HCN2. 293 cells were cultured as previously described and then infected with Ad5-GFP-HCN2 at a MOI of 5. Current was recorded 24 h later using a modification of the technique described by Qu et al. with a patch electrode in whole cell mode on cells superfused at 35 °C (n=5).[367] The extracellular solution (pH 7.4) contained 140 mM NaCl, 2.3 mM NaOH, 1 mM $MgCl_2$, 10 mM KCl, 1.0 mM $CaCl_2$, 5 mM HEPES, and 10 mM glucose. The pipette solution contained 130 mM aspartic acid, 146 mM KOH, 10 mM NaCl, 2 mM $CaCl_2$, 5 mM EGTA-KOH, 2 mM Mg-ATP, and 10 mM HEPES-KOH (pH 7.2). An Axopatch-200B amplifier and pClamp8 software (Axon Instruments) were used for acquisition and analysis. A 7 s hyperpolarizing step was applied ranging from -35 to -75 mV with decrements of -10 mV from a holding potential of -35 mV. The hyperpolarising step was followed by an 8 s step to -90 mV to record tail current and then a 0.5 s pulse to 5 mV to ensure full deactivation. Tail currents were measured at -90 mV (data not shown).

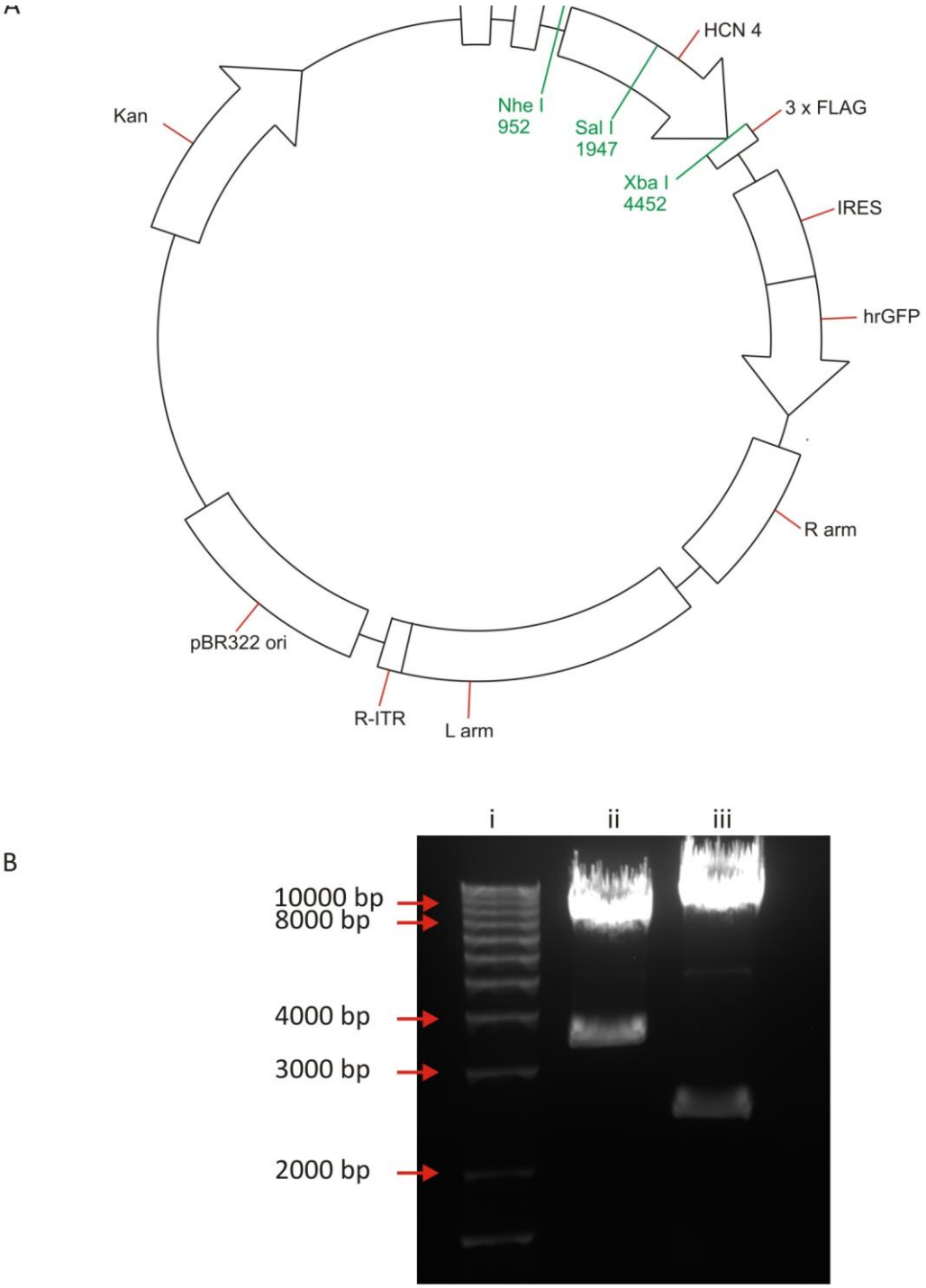

Figure 21. A) Plasmid map and restriction sites for pShuttle-IRES-GFP-HCN4 (12.4 kb). B) Restriction endonuclease digest of pShuttle-IRES-GFP-HCN4, i) 1 Kb ladder, ii) NheI/XbaI digest, iii) XbaI/SalI digest. Reference bands are marked by the red arrows with corresponding sizes in base pairs (bp). L/R-ITR, left/right inverted terminal repeat; ES, encapsidation signal; FLAG, Epitope tag N-DYKDDDDK-C; IRES, internal ribosomal entry site; hrGFP, humanised renilla green fluorescent protein; L/R arm, left/right region of homologous recombination; pBR322 ori, bacterial origin of replication; kan, kanamycin.

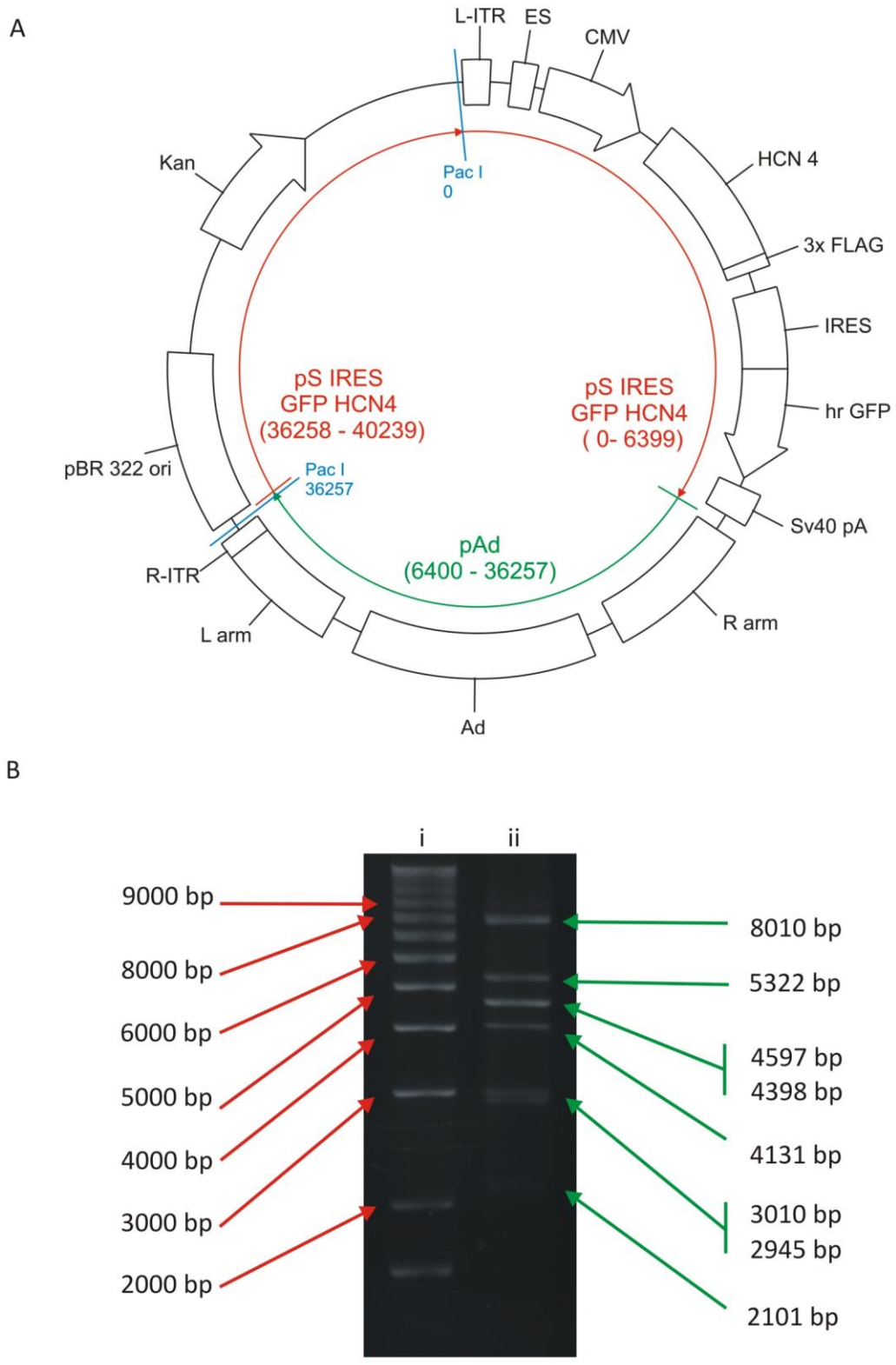

Figure 22. DNA analysis for pAd-hrGFP-HCN4. A) Plasmid map of pAd-GFP-HCN4. The plasmid is derived from pShuttle-hrGFP-HCN4 and pAd as indicated. Pac I restriction sites are shown in blue. B) 1% agarose gel electrophoresis. i) 1kb ladder; ii) HindIII digest of PacI fragment gel extracted from pAd-hrGFP-HCN4 DNA. Fragment sizes are marked in base pairs.Sv40 pA, Sv40 polyadenylation signal; Ad, Ad5 viral genome; other abbreviations as defined in legend for figure 21.

restriction sites (0 base pairs [bp] – 36257 bp) is used for the transfection of Ad293 cells and corresponds to the resulting Ad genome; the predicted HindIII RE digest pattern is shown in figure 23A. 1% agarose gel electrophoresis of the resulting RE digest fragments is shown in figure 22B. The 4398 bp band containing the mHCN4 cDNA is seen as a bright band with the 4597 bp band.

3.1.3.2 Validation of virus

3.1.3.2.1 Ad5-GFP-HCN4Δ viral DNA

Following extraction and purification of the viral DNA as described, the resultant fragments from HindIII RE digest were analysed by 1% agarose gel electrophoresis. The predicted digest pattern and agarose gel electrophoresis are shown in figure 23A and B. The resultant HindIII digest was used for southern blot analysis using a probe generated from the original plasmid pcDNA3-HCN4 (see Appendix A4). Figure 23A shows that the HCN4 gene should be within a 4.3 kb fragment. The probe binding to the 4.3 kb fragment is shown in figure 23Cii demonstrating the presence of the mHCN4 DNA sequence.

3.1.3.2.2 Validation of virus and HCN4 transgene

Cos7 cells were infected with Ad5-GFP-HCN4Δ at a MOI of 100 and then after 48 h incubation the cells were transferred to cover slips for patch clamp (n=6) or immunocytochemistry (n=3 separate experiments). In figure 24 immunocytochemistry appears to confirm the presence of HCN4 channel protein. However, If could not reliably be recorded from the cells at patch clamp (figure 25). Therefore the viral DNA was sequenced (MWG biotechnology, Germany) and compared to the reported sequence for Mus musculus HCN4 DNA (from http://www.ncbi.nlm.nih.gov/nuccore) using a BLAST query. Base pair deletions were seen between positions 845-1153 and 4577 – 4762; the sequence and mutation analysis is shown in Appendix A5.

3.1.3.3 Determination of viral titre

The titre was determined by serial dilution at 1.024×10^{10} pfu/ml.

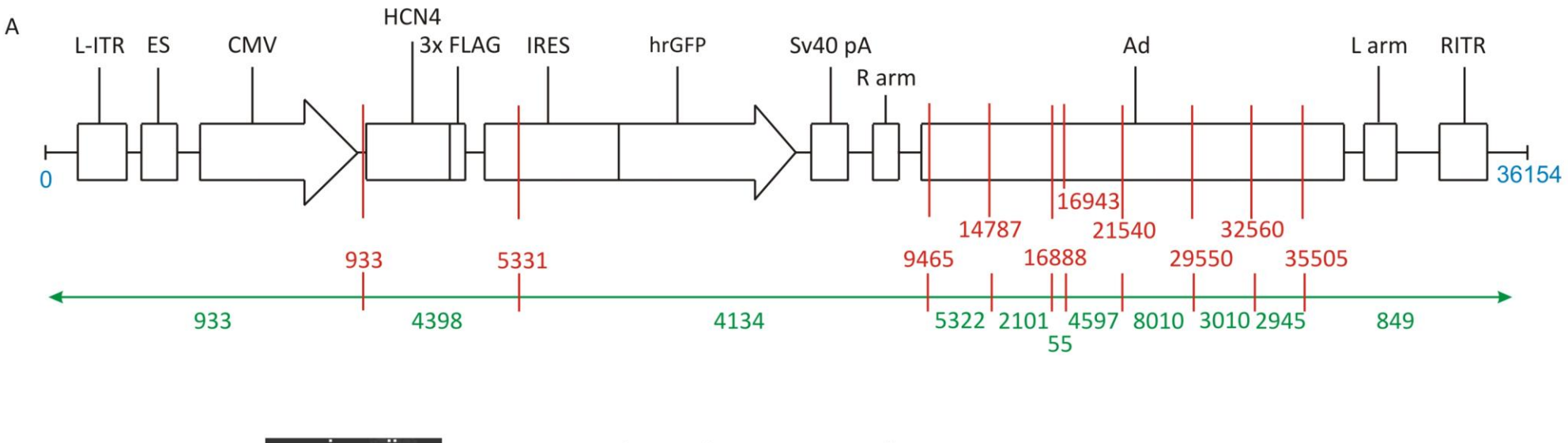

Figure 23. Viral DNA analysis for Ad5-GFP-HCN4Δ. A) Predicted HindIII restriction enzyme digest pattern for the viral DNA and the PacI segment of pAd-hrGFP-HCN4. HindIII sites are shown by the red numbers, fragment sizes by green numbers. B) 1% agarose gel electrophoresis. i) 1kb ladder; ii) HindIII digest of Ad5-GFP-HCN4Δ DNA. Fragment sizes are marked in base pairs. C) Southern blot with probe for HCN4 DNA. i) 1 kb ladder; ii) HindIII digest of Ad5-GFP-HCN4Δ. DNA Probe binding to 4.3 kb band marked by black arrow. iii) XbaI/XhoI digest of pcDNA3 HCN4. Positive control (original DNA used for probe generation) blue arrow. CMV, cytomegalovirus promoter; for other abbreviations see legends to figures 21 and 22.

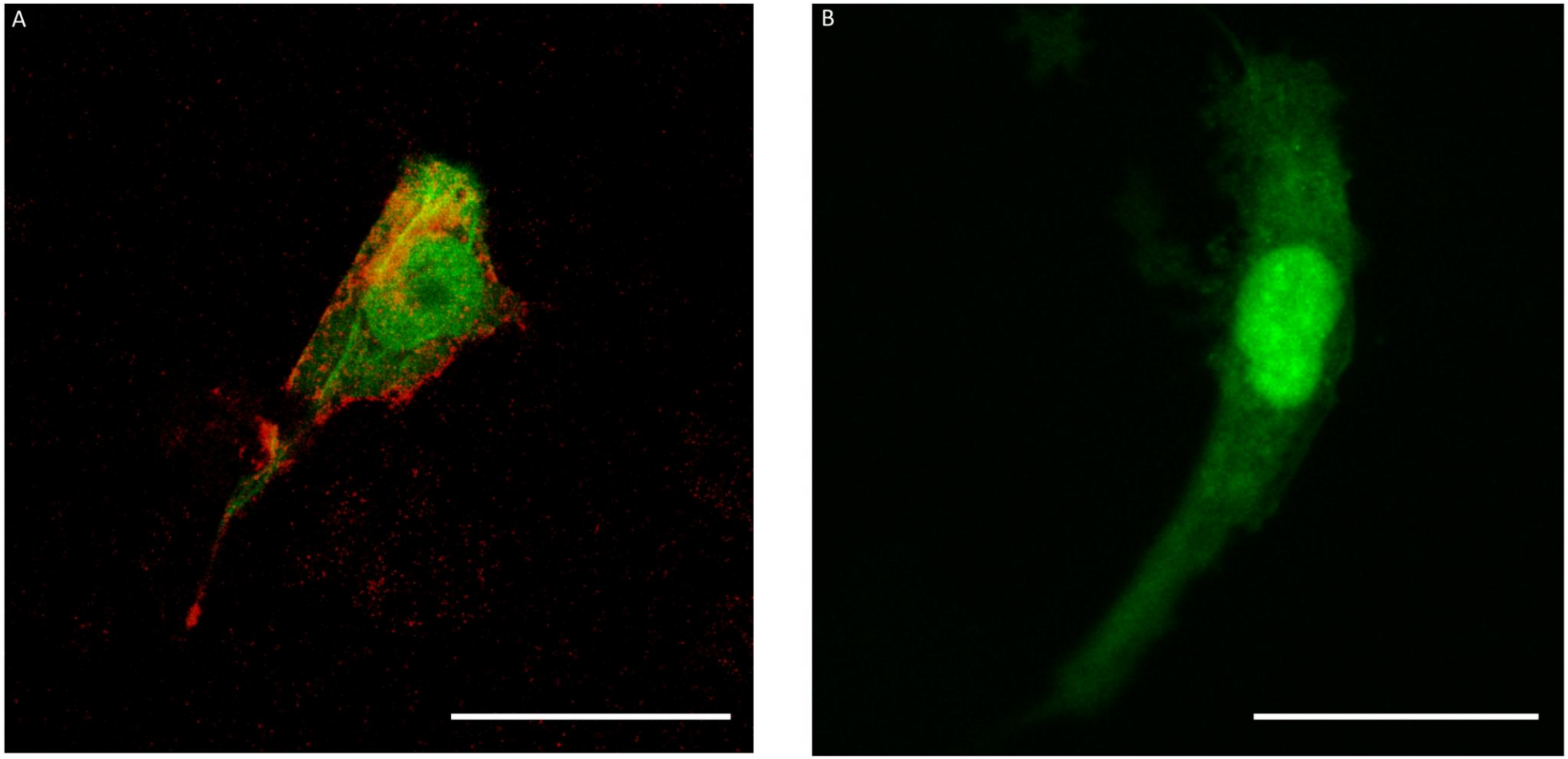

Figure 24. Adenovirus mediated expression of HCN4 in a Cos7 cell. Cos7 cells were infected with the recombinant adenovirus Ad5-GFP-HCN4Δ, containing an internal ribosomal entry site allowing the expression of green fluorescent protein (GFP) and HCN4 under the control of the same CMV promoter (A), or Ad5-GFP, expressing GFP via an internal ribosomal entry site and CMV promoter (B). The cells were labelled with a primary antibody to HCN4 (mouse anti-HCN4 IgG) and a secondary antibody, (donkey anti-mouse IgG conjugated to Cy3). HCN4 labelling is indicated by the red signal. The GFP gives the green signal. The image was captured using a confocal laser scanning microscope (Zeiss LSM5 PASCAL). Scale bars represent 50 µm.

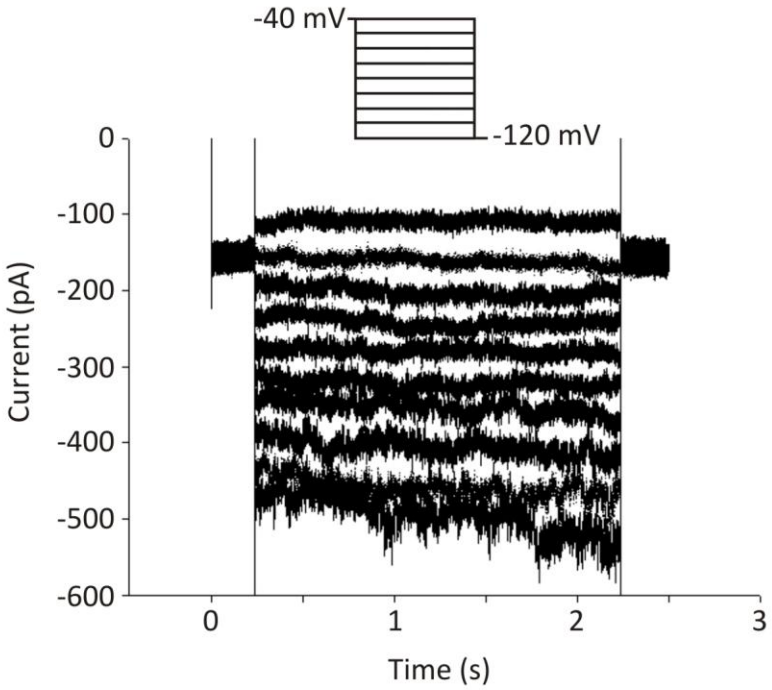

Figure 25. Representative inward current recorded from a Cos7 cell transduced with Ad5-GFP-HCN4Δ. Cos7 cells were cultured as previously described and then infected with Ad5-GFP-HCN4Δ at a MOI of 100. Current was recorded 48 h later with a patch electrode in whole cell mode on cells superfused at 35 °C (n=3). The extracellular solution (pH 7.4) contained 140 mM NaCl, 1 mM $MgCl_2$, 4 mM KCl, 1.8 mM $CaCl_2$, 10 mM HEPES, and 10 mM glucose. The pipette solution (pH 7.4) contained 0.1 mM GTP, 1 mM $MgCl_2$, 5 mM Na_2-phosphocreatine, 20 mM KCl, 10 mM HEPES, 110 mM aspartic acid, 5 mM EGTA, 5 mM Mg-ATP. An Axopatch-200B amplifier and pClamp8 software (Axon Instruments) were used for acquisition and analysis. A 2 s hyperpolarizing step was applied ranging from -40 to -120 mV with decrements of -10 mV from a holding potential of -40 mV.

3.1.4 Ad5-PREK-HCN4

3.1.4.1 Cloning

3.1.4.1.1 pShuttle-PREK-HCN4

The cDNA for mHCN4 was cloned into the shuttle vector as described in section 2.3 and Appendix A2. Verification of the correct gene insertion was by RE digest. It can be seen in figure 26A that RE digestion of pShuttle-PREK-HCN4 with XhoI/XbaI should produce a 3.5 kb fragment, and that the correct insertion orientation of the mHCN4 cDNA should produce a 2.6 kb fragment on RE digestion with XbaI/SalI. In figure 26B the expected 3.5 kb and 2.6 kb bands are seen on 1% agarose gel electrophoresis of the digestion products.

3.1.4.1.2 pAd-PREK-HCN4

The predicted plasmid map for the plasmid resulting from homologous recombination as described in section 2.4.1.2 is shown in figure 27A. The DNA between the PacI restriction sites (0 bp – 35149 bp) is used for the transfection of Ad293 cells and corresponds to the resulting Ad genome, the predicted HindIII RE digest pattern is shown in figure 28A. The expected pattern of RE digest fragments is seen on 1% agarose gel electrophoresis as shown in figure 27B. The fragment containing the mHCN cDNA is seen at 7320 bp.

3.1.4.2 Validation of virus

3.1.4.2.1 Ad5-PREK-HCN4 viral DNA

Following extraction and purification of the viral DNA as described in section 2.4.2.4, the resultant fragments from HindIII RE digest were analysed by 1% agarose gel electrophoresis. The predicted digest pattern and the expected RE digest fragments on agarose gel electrophoresis are shown in figure 28A and B. The resultant HindIII digest was used for southern blot analysis using a probe generated from the original plasmid pcDNA3-HCN4 (see Appendix A4). Figure 28A shows that the HCN4 gene should be within a 7.3 kb fragment; probe binding to the 7.3 kb

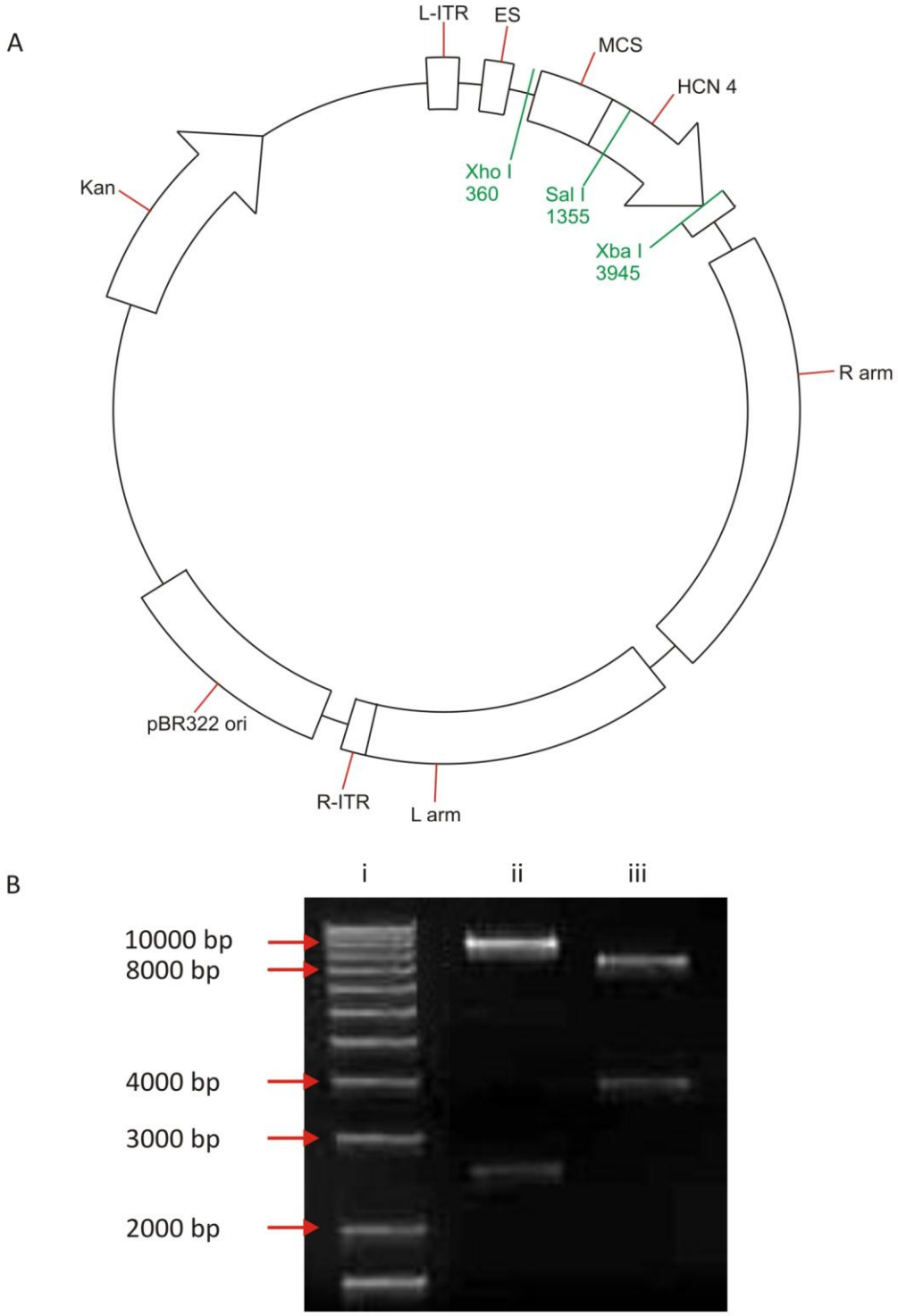

Figure 26. A) Plasmid map and restriction sites for pShuttle-PREK1-HCN4 (9.6kb).B) Restriction endonuclease digest of pShuttle-PREK1-HCN4. i) 1 Kb ladder; ii) SalI/XbaI digest; iii) XbaI/XhoI digest. Reference bands are marked by the red arrows with corresponding sizes in base pairs (bp). For abbreviations see figure 21 legend.

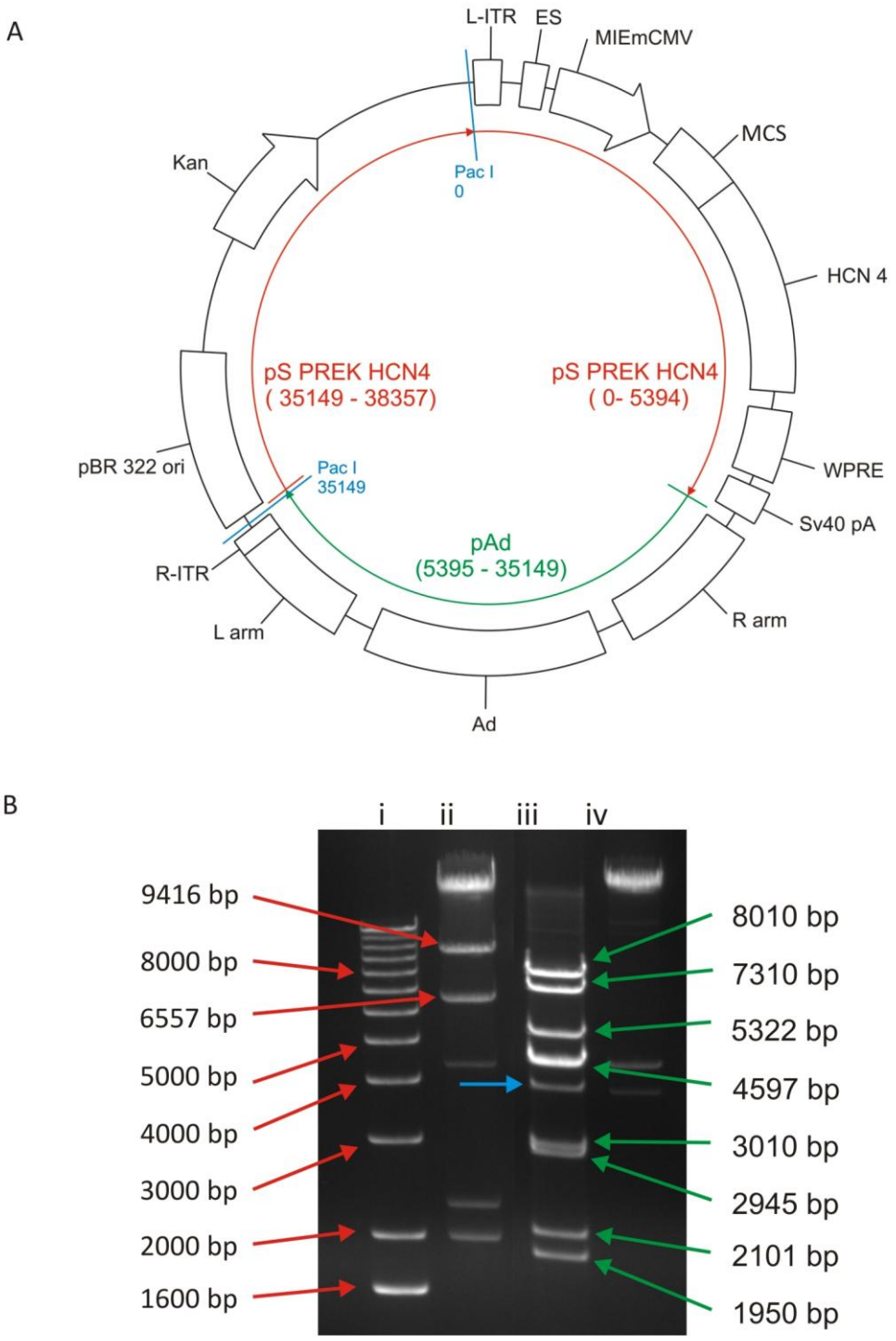

Figure 27. DNA analysis for pAd-PREK-HCN4. A) Plasmid map of pAd-PREK-HCN4 derived from pShuttle-PREK-HCN4 and pAd as indicated. PacI restriction sites are shown in blue. B) 1% agarose gel electrophoresis., i) 1kb ladder; ii) lambda phage ladder; iii) HindIII/PacI digest of pAd-PREK-HCN4 DNA; iv) PacI digest of pAd-PREK-HCN4 DNA. Fragment sizes are marked in base pairs. Blue arrow ~ 5 kb is from the initial PacI digest (bp 35149 - 0) and is also see in lane iv. This fragment is from outside the region of DNA used for transfection. MCS,multiple cloning site; WPRE, woodchuck hepatitis post-transcriptional regulatory element; for other abbreviations see legends to figures 21 and 22.

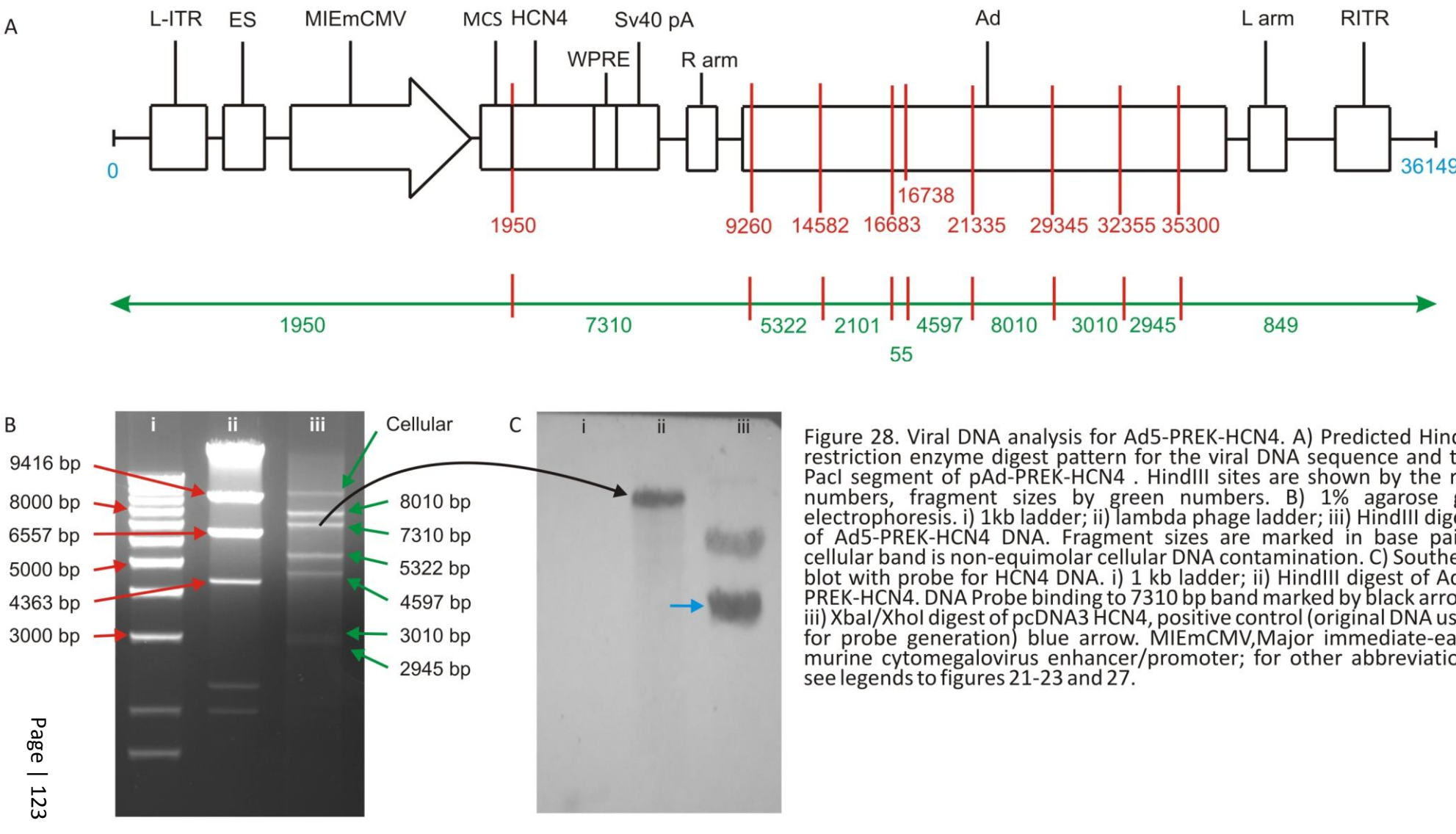

Figure 28. Viral DNA analysis for Ad5-PREK-HCN4. A) Predicted HindIII restriction enzyme digest pattern for the viral DNA sequence and the PacI segment of pAd-PREK-HCN4 . HindIII sites are shown by the red numbers, fragment sizes by green numbers. B) 1% agarose gel electrophoresis. i) 1kb ladder; ii) lambda phage ladder; iii) HindIII digest of Ad5-PREK-HCN4 DNA. Fragment sizes are marked in base pairs, cellular band is non-equimolar cellular DNA contamination. C) Southern blot with probe for HCN4 DNA. i) 1 kb ladder; ii) HindIII digest of Ad5-PREK-HCN4. DNA Probe binding to 7310 bp band marked by black arrow; iii) XbaI/XhoI digest of pcDNA3 HCN4, positive control (original DNA used for probe generation) blue arrow. MIEmCMV,Major immediate-early murine cytomegalovirus enhancer/promoter; for other abbreviations see legends to figures 21-23 and 27.

fragment is shown in figure 28Cii demonstrating the presence of the HCN4 DNA sequence.

3.1.4.2.2 Validation of virus and HCN4 transgene

Cos7 cells were infected with Ad5-PREK-HCN4 at a MOI of 100 and then after 48 h incubation the cells were transferred to cover slips for patch clamp (n=4) or immunocytochemistry (n=3 separate experiments). In figure 29 immunocytochemistry shows the presence of HCN4 channel protein. I_f recorded from the cells by patch clamp is shown in figure 30.

3.1.4.3 Determination of viral titre

The titre was determined by serial dilution at 5.1 x 10^9 pfu/ml.

3.1.5 Ad5-HCN212

3.1.5.1 Validation of virus and HCN212 transgene

HCN212 contains the transmembrane domain from HCN1 with the intracellular and extracellular domains of HCN2.[371] The primary antibody anti-HCN2 binds to its epitope at amino acids 147 – 161 of human HCN2 (see www.millipore.com). This epitope is preserved in HCN212 and therefore anti-HCN2 can be used for the detection of expressed HCN212. Cos7 cells were infected with Ad5-HCN212 at a MOI of 100 and then after 48 h incubation the cells were transferred to cover slips for immunocytochemistry. In figure 31 immunocytochemistry shows the presence of HCN212 channel protein (n=3 separate experiments). The expression of I_f resulting from infection with Ad5-HCN212 has been previously published.[372]

3.1.5.2 Determination of viral titre

The titre was determined by serial dilution at 2.05 x 10^{10} pfu/ml.

3.1.6 Ad5-GFP

The virus Ad5-GFP was prepared using the plasmid pShuttle-IRES-hrGFP. Homologous recombination of the plasmid with pAd was performed directly. The plasmid map for pShuttle-IRES-hrGFP is shown in Appendix A2. The predicted

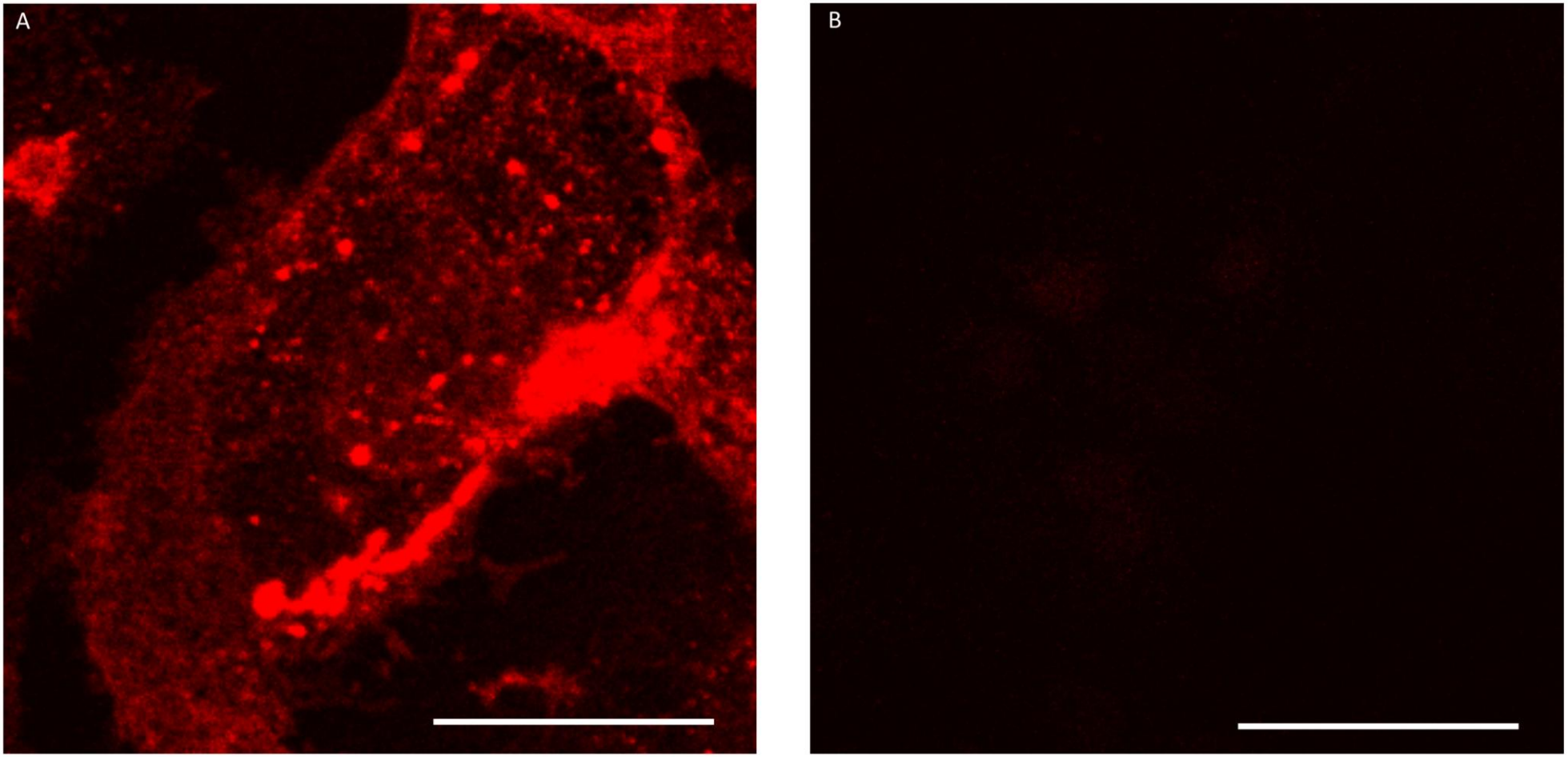

Figure 29. Adenovirus mediated expression of HCN4 in a Cos7 cell. Cos7 cells were infected with a recombinant adenovirus Ad5-PREK-HCN4 containing cDNA for mHCN4 allowing the expression of HCN4 under the control of the CMV promoter (A), or Ad5-PREK-LacZ expressing LacZ (B). The cells were labelled with a primary antibody to HCN4 (mouse anti-HCN4 IgG) and a secondary antibody, (donkey anti-mouse IgG conjugated to Cy3). HCN4 labelling is indicated by the red signal. The image was captured using a confocal laser scanning microscope (Zeiss LSM5 PASCAL) Scale bars represent 50 µm.

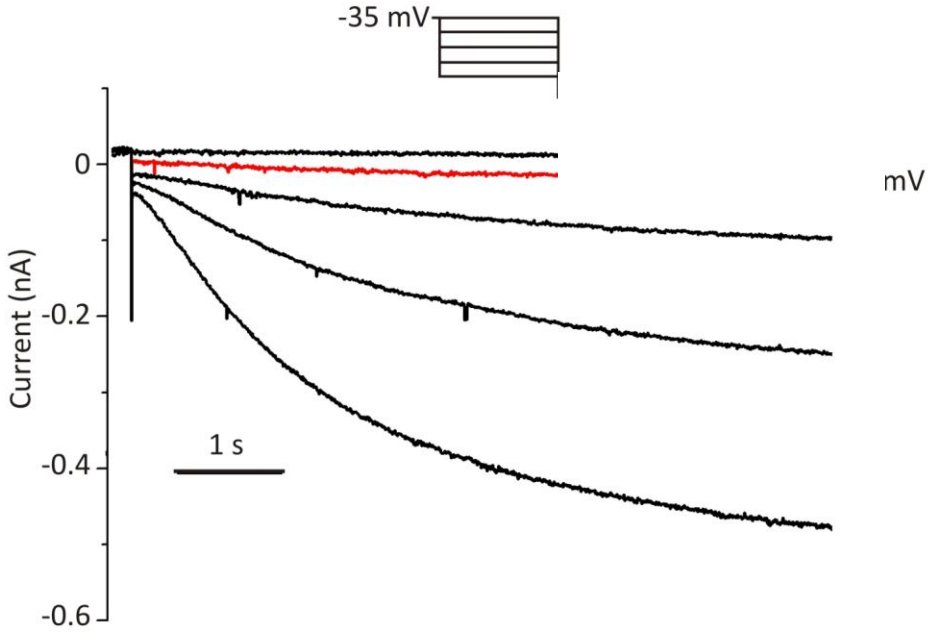

Figure 30. Representative inward current recorded from a 293 cell transduced with Ad5-PREK-HCN4. 293 cells were cultured as previously described and then infected with Ad5-PREK-HCN4 at a MOI of 5. Current was recorded 24 h later using a modification of the technique described by Qu et al. with a patch electrode in whole cell mode on cells superfused at 35 °C (n=4).[367] The extracellular solutions and protocol are as described in the legend to figure 20.

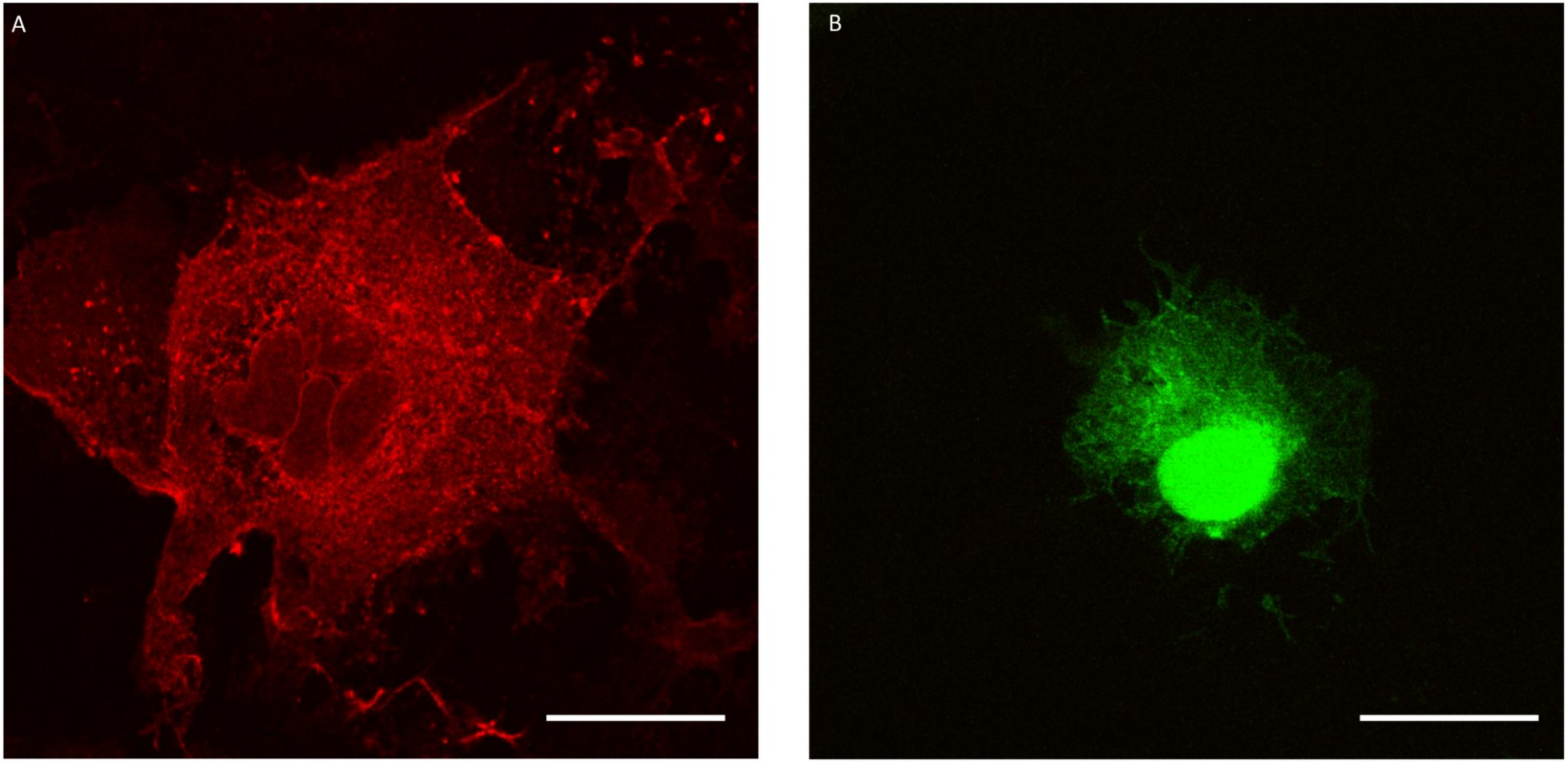

Figure 31. Adenovirus mediated expression of HCN212 in a Cos7 cell. Cos7 cells were infected with a recombinant adenovirus Ad5-PHCN212 containing cDNA for HCN212 allowing the expression of HCN212 under the control of the CMV promoter (A), or Ad5-GFP expressing GFP via an internal ribosomal entry site and CMV promoter (B). The cells were labelled with a primary antibody to HCN2 (mouse anti-HCN2 IgG) and a secondary antibody (donkey anti-mouse IgG conjugated to Cy3). HCN212/HCN2 labelling is indicated by the red signal. The GFP gives the green signal. The image was captured using a confocal laser scanning microscope (Zeiss LSM5 PASCAL). Scale bars represent 50 µm.

plasmid map for the plasmid resulting from this recombination is shown in figure 32A and the predicted HindIII RE digest pattern of the PacI fragment is shown in figure 33A. The expected HindIII digest pattern is seen on 1% agarose gel electrophoresis, as shown in figure 32B. Analysis of purified viral DNA by 1% agarose gel electrophoresis of HindIII RE digested DNA results in the expected pattern (figure 33). The absence of HCN channel protein following transduction of Cos7 cells with Ad5-GFP can be seen in figures 24 and 31 (anti-HCN4, n=3; anti-HCN2, n=3

3.2 Sinoatrial node culture

3.2.1 Introduction

The SAN is a complex heterogeneous region of the RA. The specialisation of the SAN is both electrophysiological and morphological, allowing for reliable generation and propagation of the cardiac action potential into the surrounding RA myocardium.[40] In comparison to the myocytes of the RA, SAN cells are smaller. Furthermore the action potential of isolated SAN cells displays diastolic depolarization and thus SAN cells show pacemaking (figure 5).[373] The generation of this specific pacemaker action potential is dependent on the expression of a specific set of ion channels in the SAN cells.[77] As discussed in detail in section 1.5, in the SAN there is abundance of $Ca_v1.3$, HCN1, HCN4 while $K_{ir}2.1$, RYR2 and $Na_v1.5$ are poorly expressed, leading to the complex interplay of the calcium and membrane clocks.[122] SAN cells have been isolated and propagated in culture.[374] This has facilitated the study of the nature of the SAN AP generation as well as manipulation of SAN cell function via transduction of genetic material.[49] The transduction of SAN specific genes into working myocytes allows the study of biopacemaking at a cellular level.[372]

However, the *in vivo* functioning SAN is more than a scattered collection of SAN cells throughout the RA posterior wall. Histologically the SAN is clearly defined as a collection of small loosely-packed cells. This area expresses high levels of HCN4 and displays an absence of the high conductance connexin, Cx43.[7] Moving from the centre to the periphery of the SAN there is a progression from a typical SAN AP towards that of the working myocardium.[223,159,375] This suggests either a change in

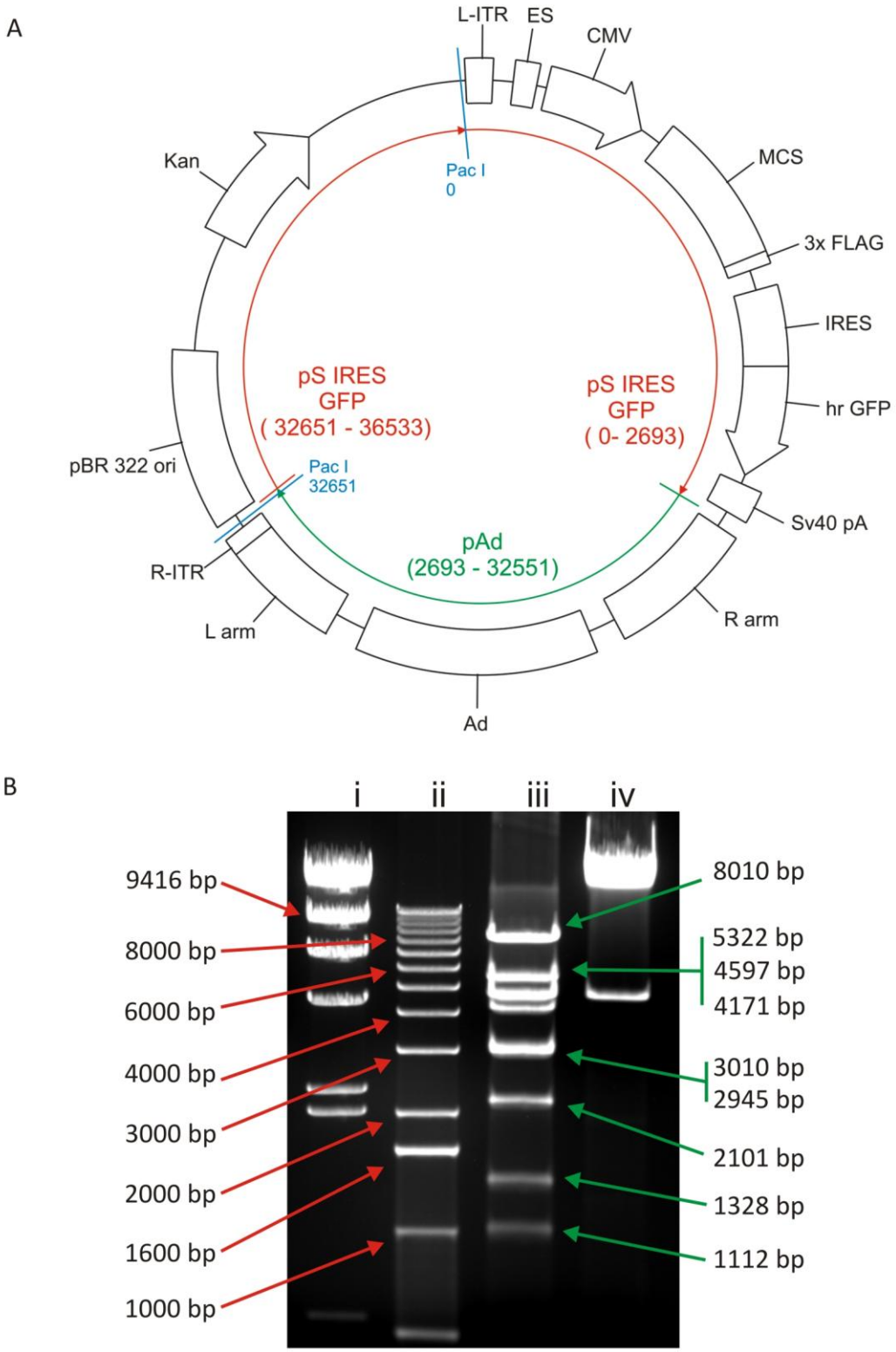

Figure 32. DNA analysis for pAd-hrGFP. A) Plasmid map of pAd-GFP. The plasmid is derived from pShuttle-IRES-hrGFP and pAd as indicated. PacI restriction sites are shown in blue. B) 1% agarose gel electrophoresis. i) Lambda phage ladder; ii) 1kb ladder; iii) HindIII/PacI digest of pAd-hrGFP-DNA; iv) PacI digest of pAd-hrGFP-DNA. Fragment sizes are marked in base pairs. For abbreviations see figures 21, 22 and 27.

A

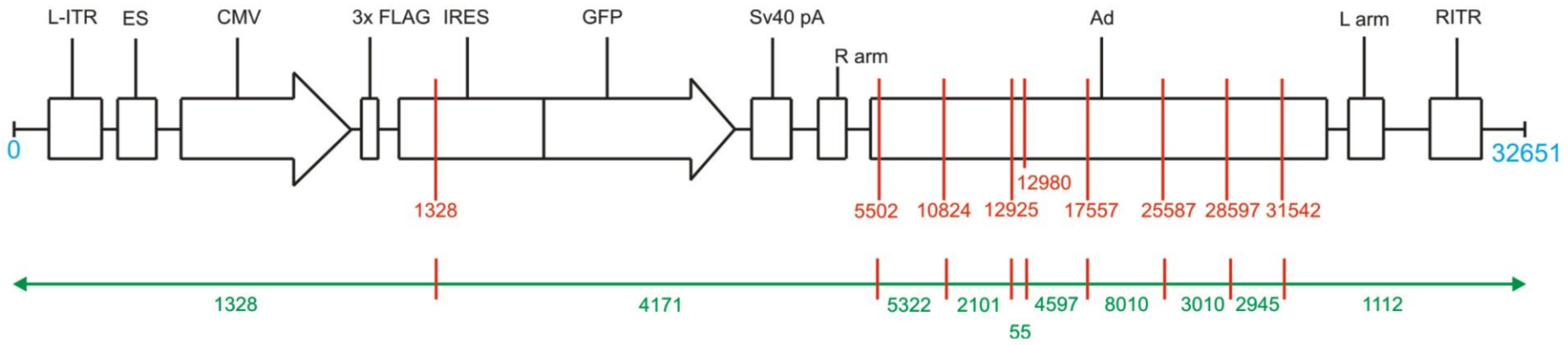

B

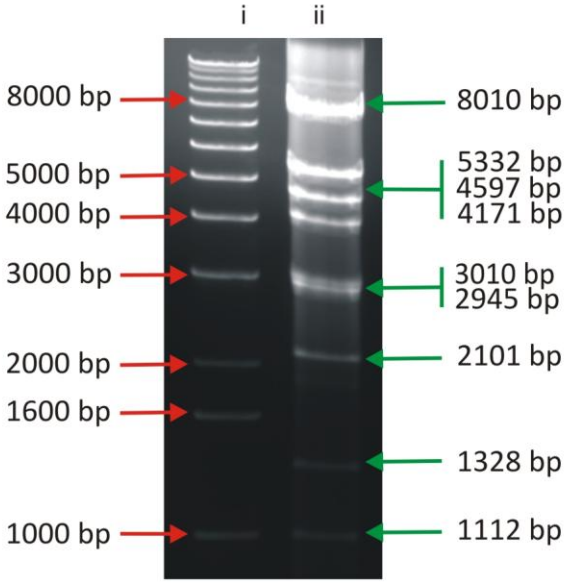

Figure 33. Viral DNA analysis for Ad5-GFP. A) Predicted HindIII restriction enzyme digest pattern for the virus and the PacI fragment of Ad-GFP. HindIII sites are shown by the red numbers, fragment sizes by green numbers. B) 1% agarose gel electrophoresis. i) 1kb ladder; ii) HindIII digest of Ad5-GFP DNA. Fragment sizes are marked in base pairs. For abbreviations see legends for figures 21-23.

the ratio of SAN/myocardial cells (mosaic model) or a progressive change in cell phenotype (gradient model).[39] Taking these factors into account, it is generally accepted that the intact SAN is a complex structure, and thus the normal function depends on more than simply cellular expression of specific ion channels.[40] Therefore to accurately study the effect of genetic transduction on SAN function, culture of intact SAN tissue is required. To date this has not been reported.

The following null hypotheses were tested:

1) The SAN from the rat, *Rattus rattus,* cannot be cultured *ex vivo* and the pacemaker activity cannot be sustained and monitored.

2) Tissue culture will induce no significant change in the level of ion channel and gap junction expression.

3) Tissue culture will induce no significant cellular apoptosis and no changes in cell or tissue histology.

3.2.2 Extracellular potential recordings from the sinoatrial node in culture

To investigate the feasibility of monitoring the pacing rate of the SAN *ex vivo*, extracellular potentials were recorded using 0.15 mm stainless steel bipolar electrodes. A representative trace and recording is shown in figures 34A and 34B respectively. Spontaneous pacing activity was maintained for a maximum of 260 h (10.8 days, figure 34) and was reliably maintained for 72 h (3 days); there was an increase in the pacing rate to 21 h and thereafter the rate declined (figure 35A). RAd experiments were planned to run over 24 – 48 h and thus further analysis was performed for this period. The mean six hour pacing rates are shown in figure 36A (n=6). The mean pacing rate during the first hour was 257 ± 21 bpm, the maximum rate was at 21 h (336 ± 14 bpm) and the minimum rate was at 45 h (201 ± 13 bpm) (figures 36 and 37). The maximal effect of the RAd mediated gene expression was expected to be around 16 h. Therefore, hourly mean pacing rates were calculated for the period 12-20 h (figure 36B); this covers the period of maximal effect but is prior to the decline in pacing rate evident in figures 35A and 36A.

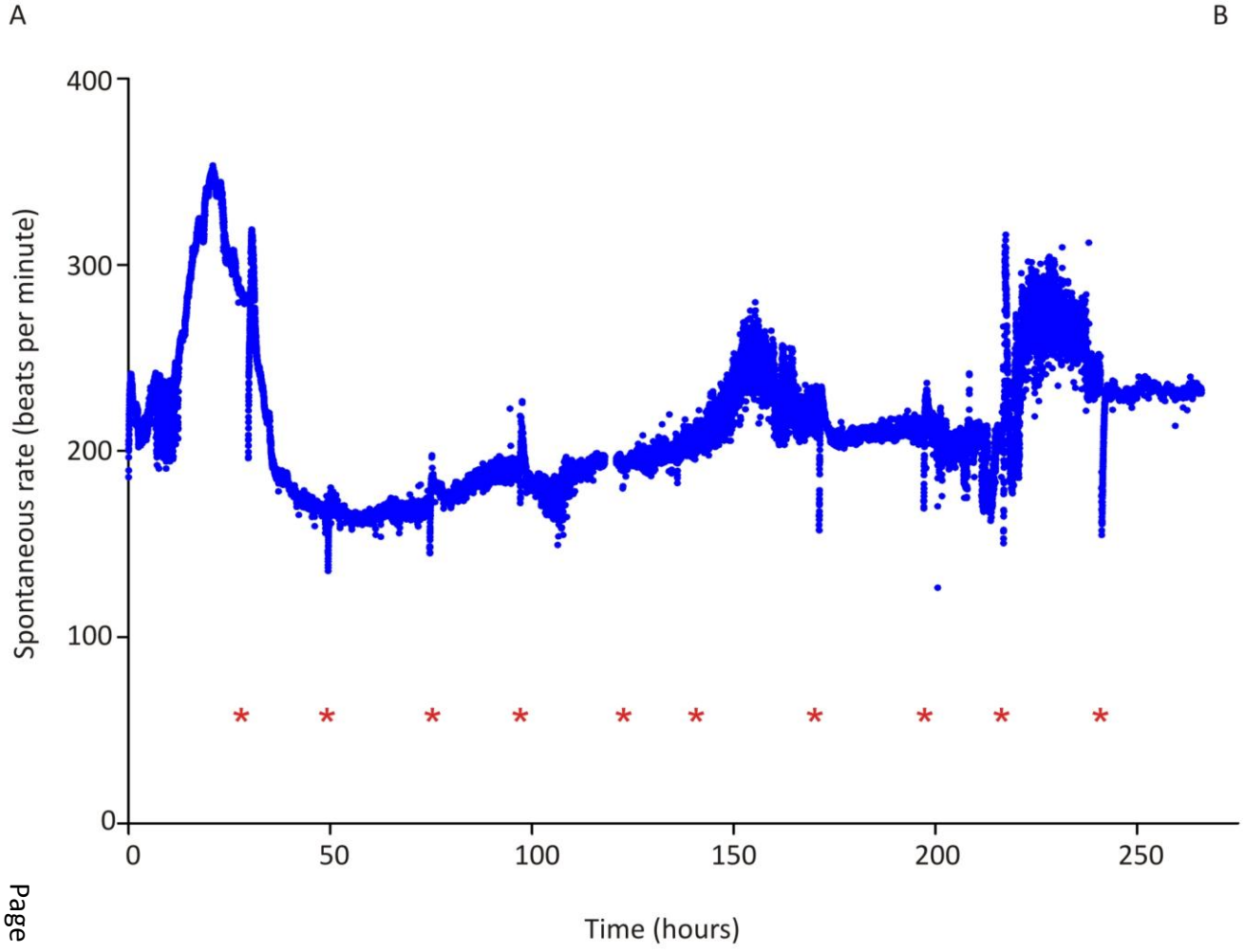

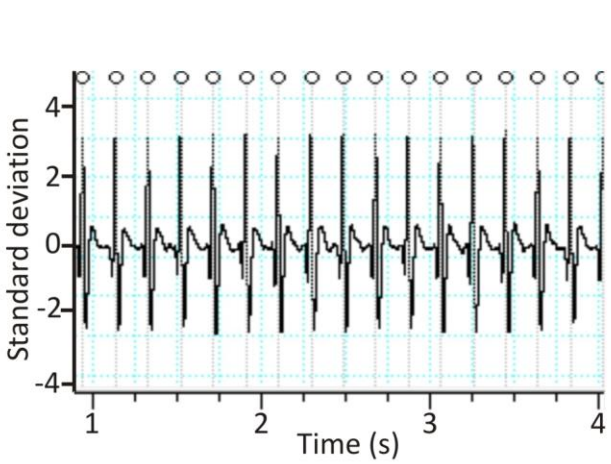

Figure 34. A) Representative rate of *ex vivo* rat sinoatrial node during tissue culture. Extracellular potentials were recorded using 0.2 mm stainless steel bipolar electrodes. Each blue dot is a 30 s average rate, media changes are indicated by red asterisks. B) Extracellular potentials were recorded and analysed using ADInstruments Chart software. A spike over 2.5 SD from the mean was detected as a 'beat' (circles) and the rate over 30 s was averaged.

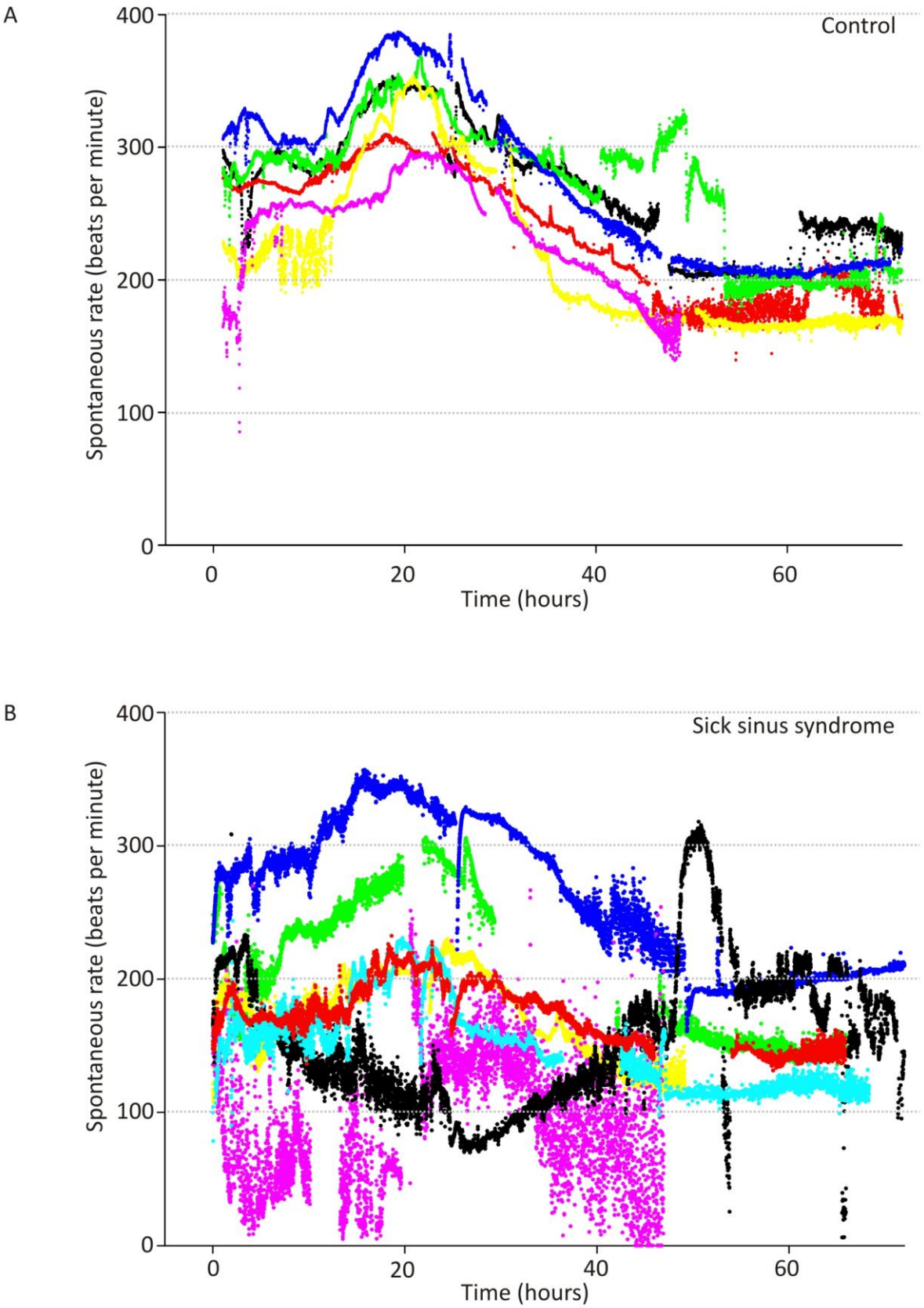

Figure 35. Spontaneous *ex vivo* pacing rates of control sinus node and the sick sinus syndrome model. (A) Control (full rat sinoatrial node, n=6) and (B) sick sinus syndrome (inferior rat sinoatrial node, n=7) preparations were cultured at 37°C as described. Extracellular potentials were recorded using 0.15 mm stainless steel bipolar electrodes. Each dot represents a 30 s average rate; differing colours distinguish different preparations.

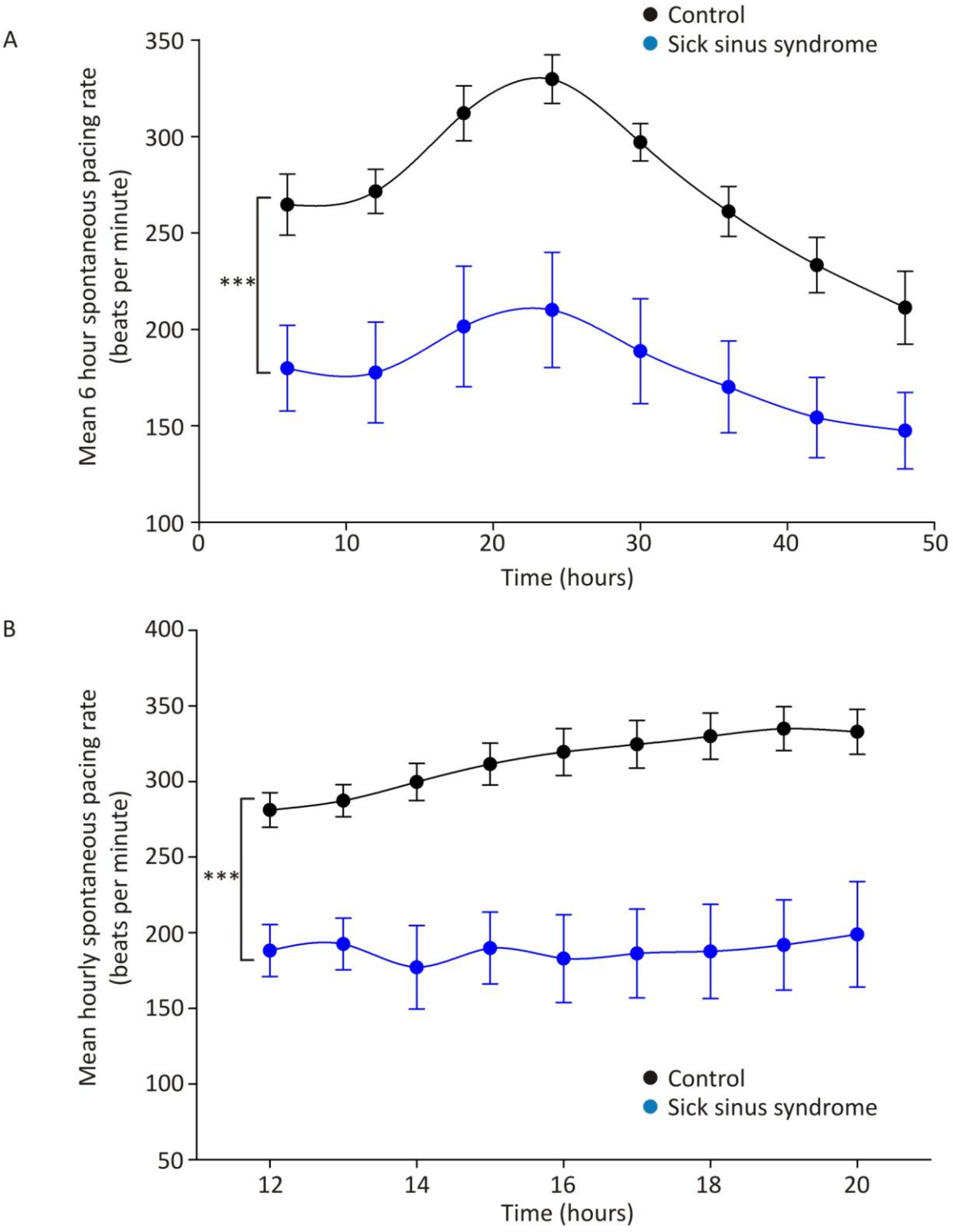

Figure 36. Average spontaneous *ex vivo* pacing rates of control sinoatrial node and the sick sinus syndrome model. Control (full rat sinoatrial node, black circles, n = 6) and sick sinus syndrome (inferior rat sinus node, blue circles, n = 7) preparations were cultured at 37°C as described. Extracellular potentials were recorded using 0.15 mm stainless steel bipolar electrodes. The pacing rate was averaged over six hours (A). One hour averages were calculated for the period 12 - 20 h (B). The peak effect of adenovirus mediated gene expression in later experiments is expected to fall in this time period and it is before the decline in rate seen in panel A. Data were analysed by 2-way ANOVA; *** $p<0.001$ for all time points.

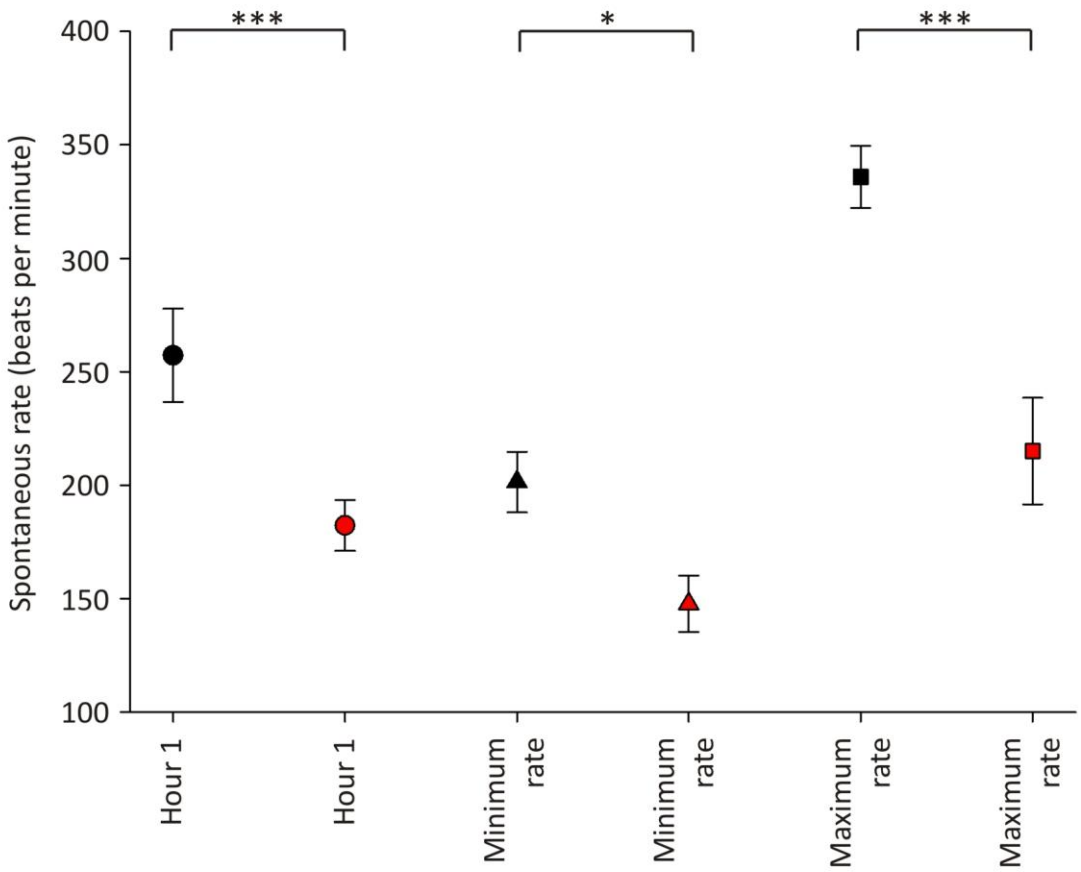

Figure 37. Initial, maximum and minimum rates for the control sinoatrial node and sick sinus syndrome model. Mean hourly average rates ± SEM were calculated for the first hour of culture. The maximum rate and the minimum rate during the first 72 h culture were also calculated. The control (full sinoatrial node, n = 6) is shown in black; the sick sinus syndrome model (inferior sinoatrial node, n = 6) is shown in red; circles, initial rate; triangle, minimum rate; square, maximum rate. Data were analysed by 1-way ANOVA; * $p<0.05$; ** $p<0.01$; *** $p<0.001$.

3.2.3 Histology and immunohistochemistry of the sinoatrial node following tissue culture

Morphological, histological and immunohistochemical analysis of the SAN was undertaken before and after 48 h tissue culture to assess the impact of culture on the node (n=6). Other than pallor, no macroscopic alterations in the appearance of the SAN tissue were observed (figure 38). Masson's trichrome staining of the cultured SAN shows patches of cells with loss of cytoplasmic staining and nuclear swelling (figure 39A and B). Similar appearances were seen in cultured RA, but to a lesser extent (figure 40A and B). Although SAN cells were significantly smaller than the RA cells (11.3 µm vs. 14.6 µm, respectively, $p<0.01$), tissue culture induced a significant change in size of the RA cells from 14.6 µm to 11.6 µm ($p<0.05$). However, no significant change was seen in the SAN cell size from 11.3 µm to 11.2 µm (p=NS) (figure 41). Quantitative immunohistochemistry was used to study the effect of tissue culture on gap junction and ion channel expression (figures 42 and 43). Tissue culture induced no significant change in the relative immunofluorescence of the gap junction channel Cx43 in the RA (42.5 ± 10.0 vs. 35.2 ± 4.0, arbitrary units; n=6, p = NS) or the ion channel HCN4 in the SAN (48.9 ± 7.8 vs. 46.7 ± 9.6, arbitrary units; n=6, p = NS).

Following culture with 6 µM camptothecin to induce apoptosis, Masson's trichrome staining revealed that the SAN tissue displayed large areas of cellular loss with increased presence of connective tissue (figure 39C). The effect on RA was less marked (figure 40C). Levels of apoptosis were measured via immunohistochemistry using a primary antibody to activated caspase-3. As shown in figure 44 there was no significant increase in the relative immunofluorescence of caspase-3 following tissue culture, but activated caspase-3 was detected in the camptothecin positive control (2.9 ± 1.0 vs. 4.7 ± 1.2, arbitrary units; n=6, p = NS).

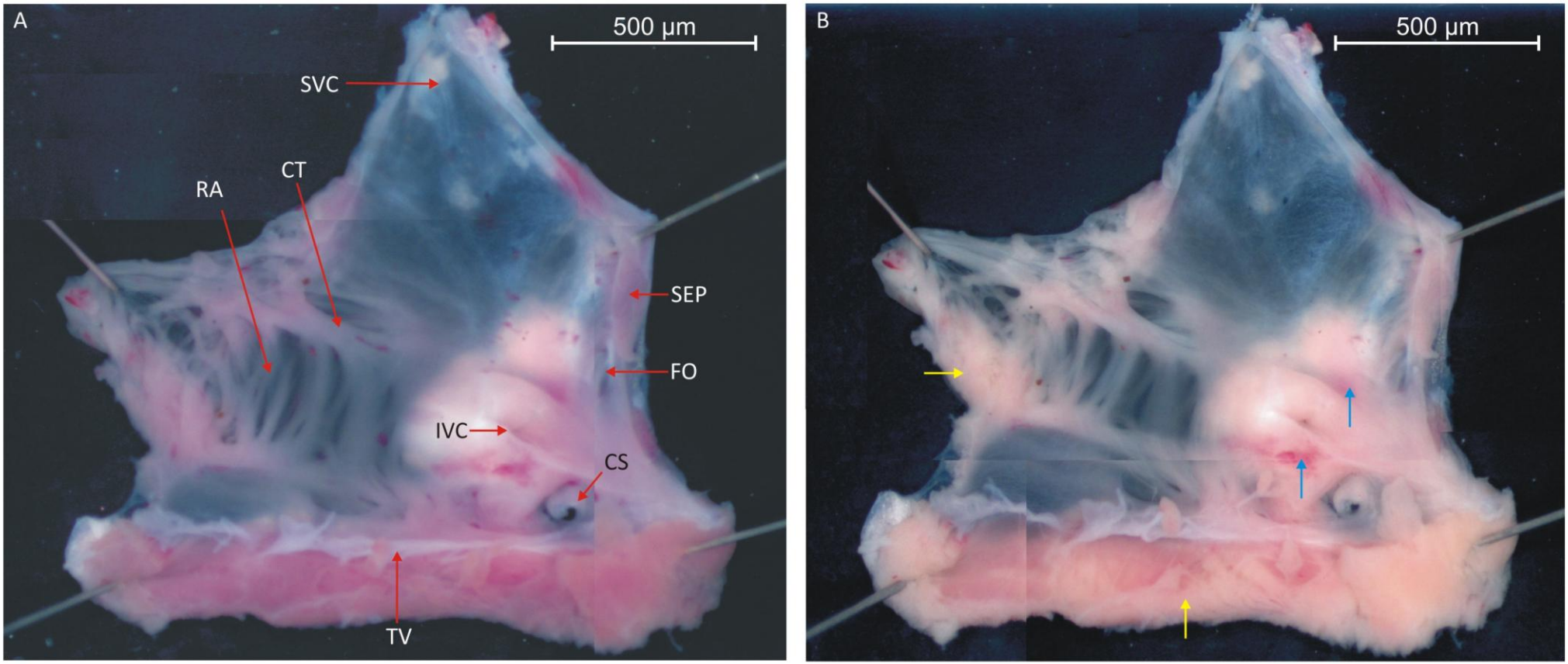

Figure 38. The effect of tissue culture on the gross morphology of the rat sinoatrial node tissue preparation (unstained). A) Prior to tissue culture. B) The same preparation following 48 h tissue culture. In panel B there is relative pallor of most of the muscular areas (yellow arrows), though some areas retain the pre-culture appearance (blue arrows). SVC, superior vena cava; CT, crista terminalis; RA, right atrium; Sep, interatral septum; FO, fossa ovalis; IVC, inferior vena cava; CS, coronary sinus; TV, tricuspid valve.

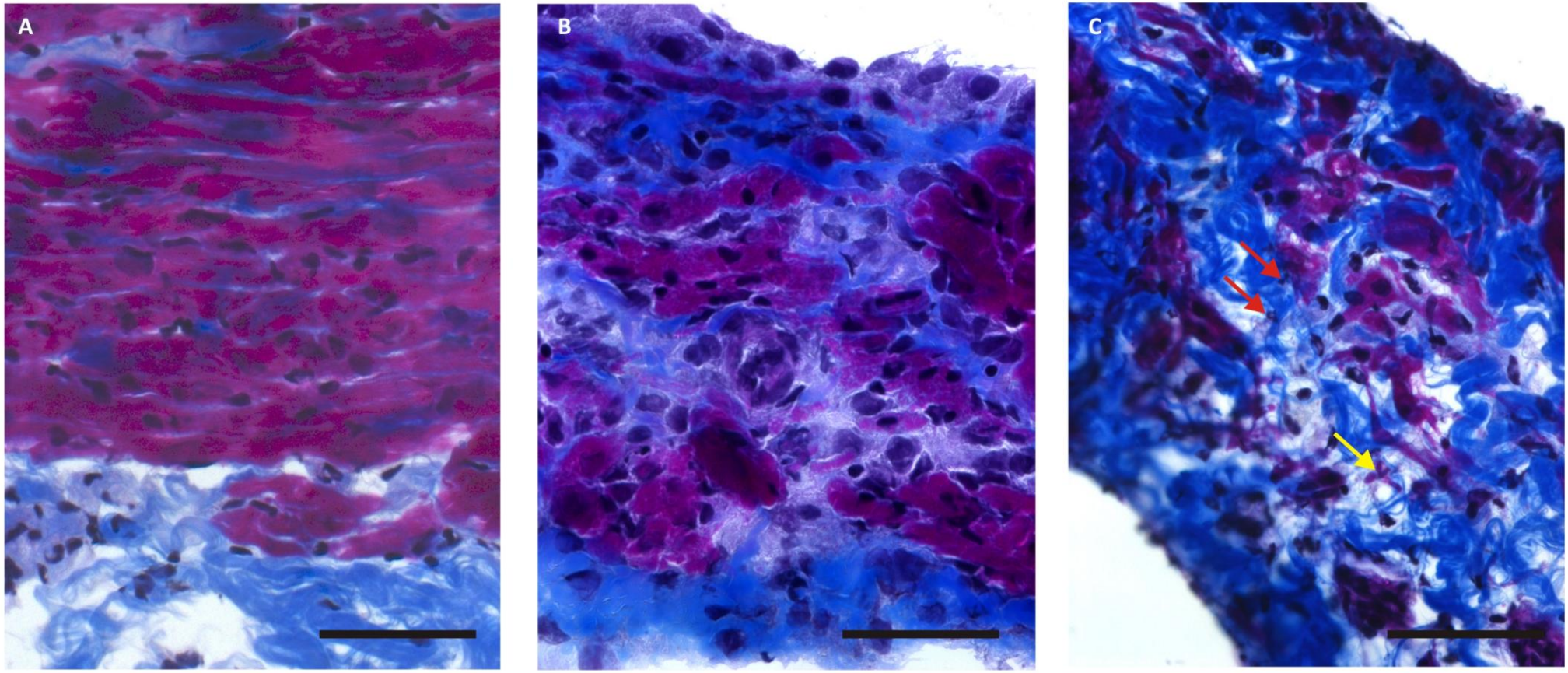

Figure 39. Histology of the rat sinoatrial node. Masson's trichrome staining was performed on 16 µm cryosections prepared from rat sinoatrial node. A) Uncultured sinoatrial node; B) sinoatrial node following 48 h tissue culture, C) sinoatrial node following 24 h tissue culture with 6 µM camptothecin. For all groups n=6. Nuclear fragmentation and cell membrane blebbing is seen in C (red arrows and yellow arrow respectively) indicating the presence of cellular apoptosis. Purple, myocytes; blue, connective tissue; scale bars represent 50 µm.

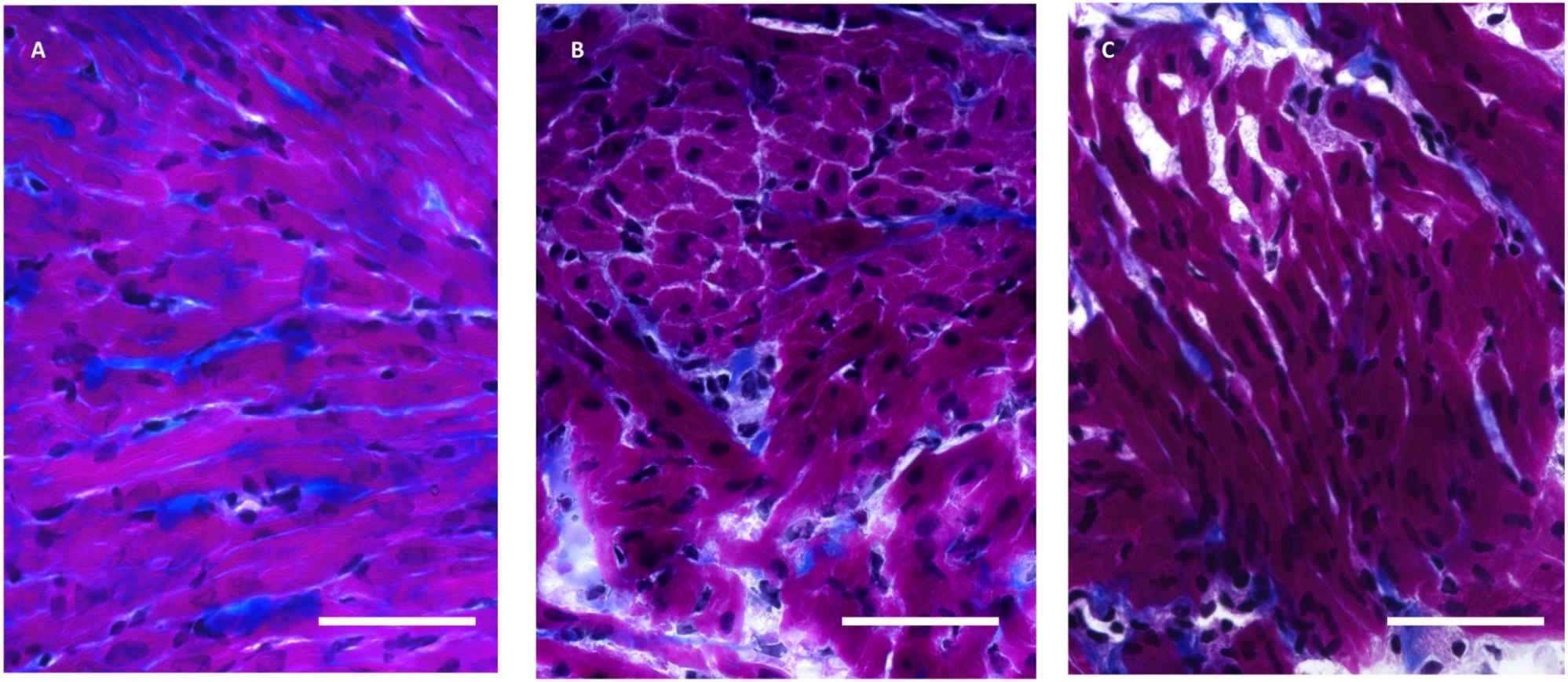

Figure 40. Histology of the rat right atrial muscle. Masson's trichrome staining was performed on 16 µm cryosections prepared from rat right atrial appendage. A) Uncultured right atrium; B) right atrium following 48 h tissue culture; C) right atrium following 24 h tissue culture with 6 µM camptothecin. For all groups n=6. Purple, myocytes; blue, connective tissue; scale bars represent 50 µm.

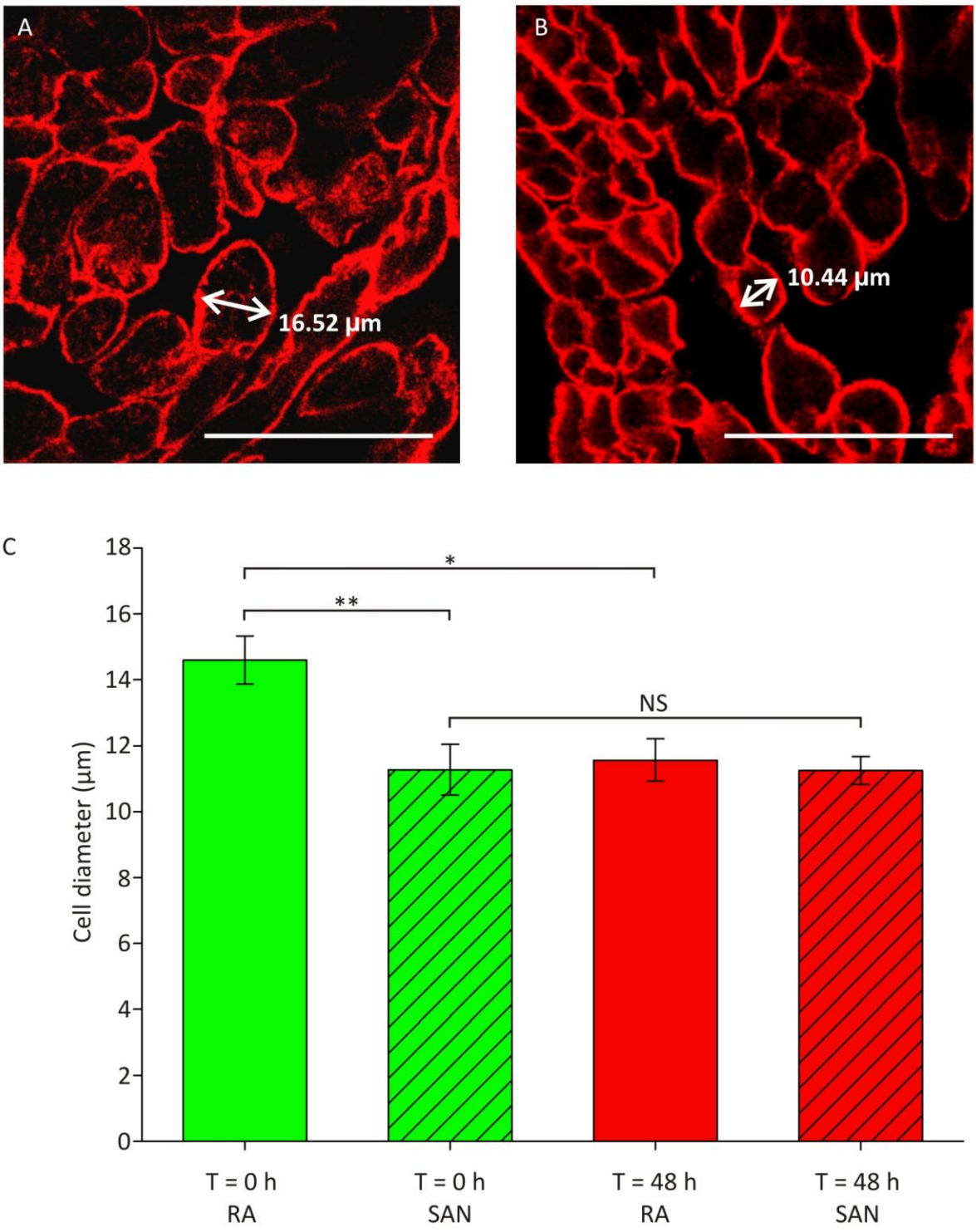

Figure 41. The effect of *ex vivo* tissue culture on cell size. The cell membranes of 16 µm cryosections of rat right atrial appendage (A) and sinoatrial node (B) were labelled using the cardiomyocyte-specific primary antibody rabbit anti-Cav3 IgG and the secondary antibody donkey anti-rabbit conjugated to Cy3, at the beginning of the experiment (time, [T] = 0 h) and following 48 h tissue culture (T = 48 h). Cell size was measured on cells cut in transverse section, the shortest axis was taken (examples in panels A and B). The mean of 20 cells over three high power fields was taken for each preparation (n=6 preparations per group). Scale bars in A and B represent 50 µm. C) Mean cell diameter +/- SEM for control (T = 0 h) and cultured (T= 48 h) cells from right atrium (open bars) and sinoatrial node (hashed bars). Data within each timepoint were compared using a paired t-test. Comparison of data between the two timepoints was performed by unpaired t-test. NS $p>0.05$, * $p<0.05$,** $p<0.01$.

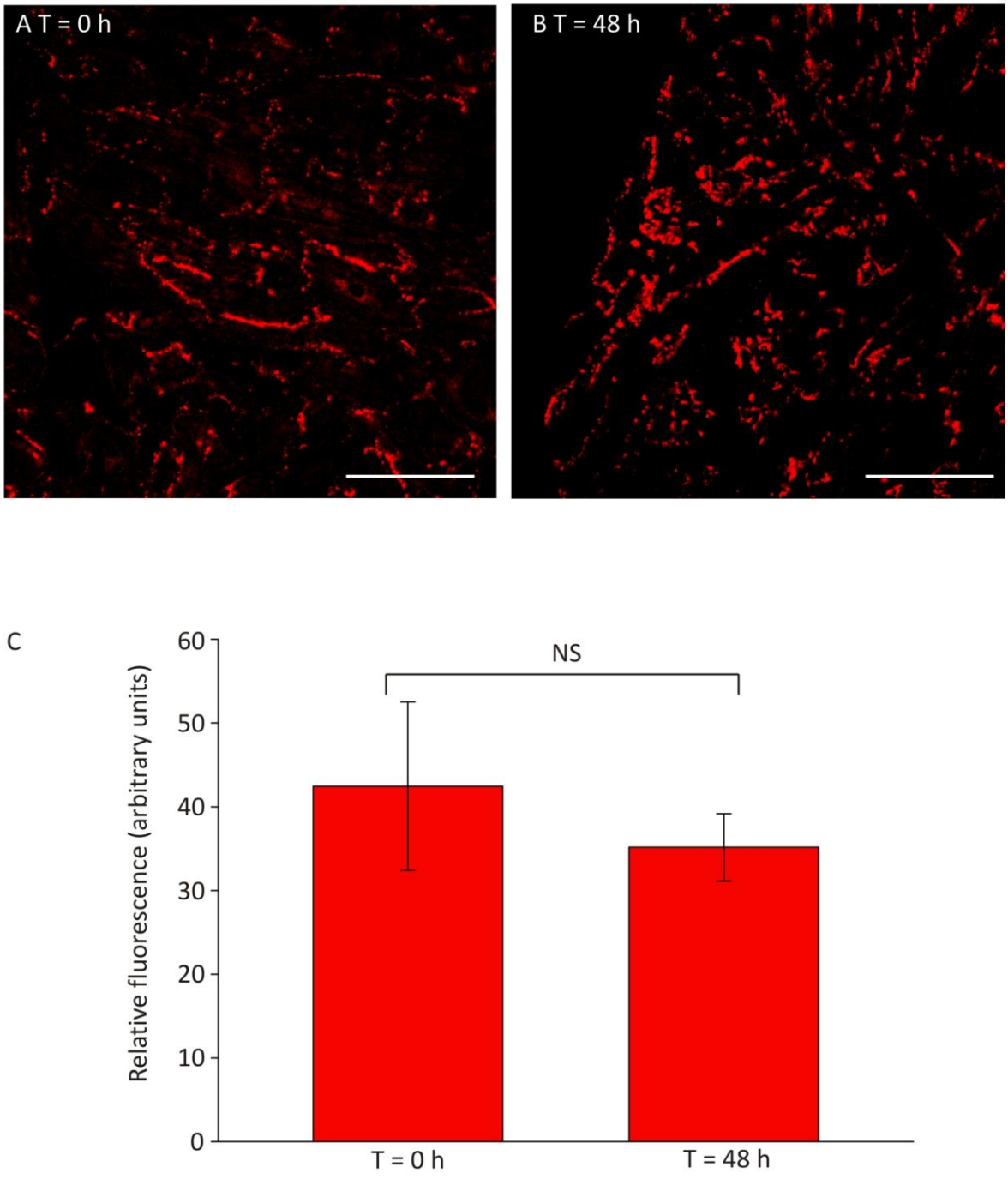

Figure 42. The effect of *ex vivo* tissue culture on gap junction expression. Using the primary antibody mouse anti-connexin-43 IgG and the secondary antibody donkey anti-mouse conjugated to Cy3, immunohistochemistry was performed on 16 µm cryosections of rat right atrial appendage. A) No tissue culture. B) Following 48 h tissue culture. Images were captured using a laser scanning confocal microscope. Immunohistochemistry was performed simultaneously and the same microscope settings were used for all pictures to allow quantitative comparison. C) Relative immunofluorescence of connexin-43 measured using Volocity software with no tissue culture and following 48 h tissue culture (preparations n=6 for each group, mean +/-SEM shown). Data were compared using unpaired t-test. Scale bars in panels A and B = 50 µm. NS, $p>0.05$.

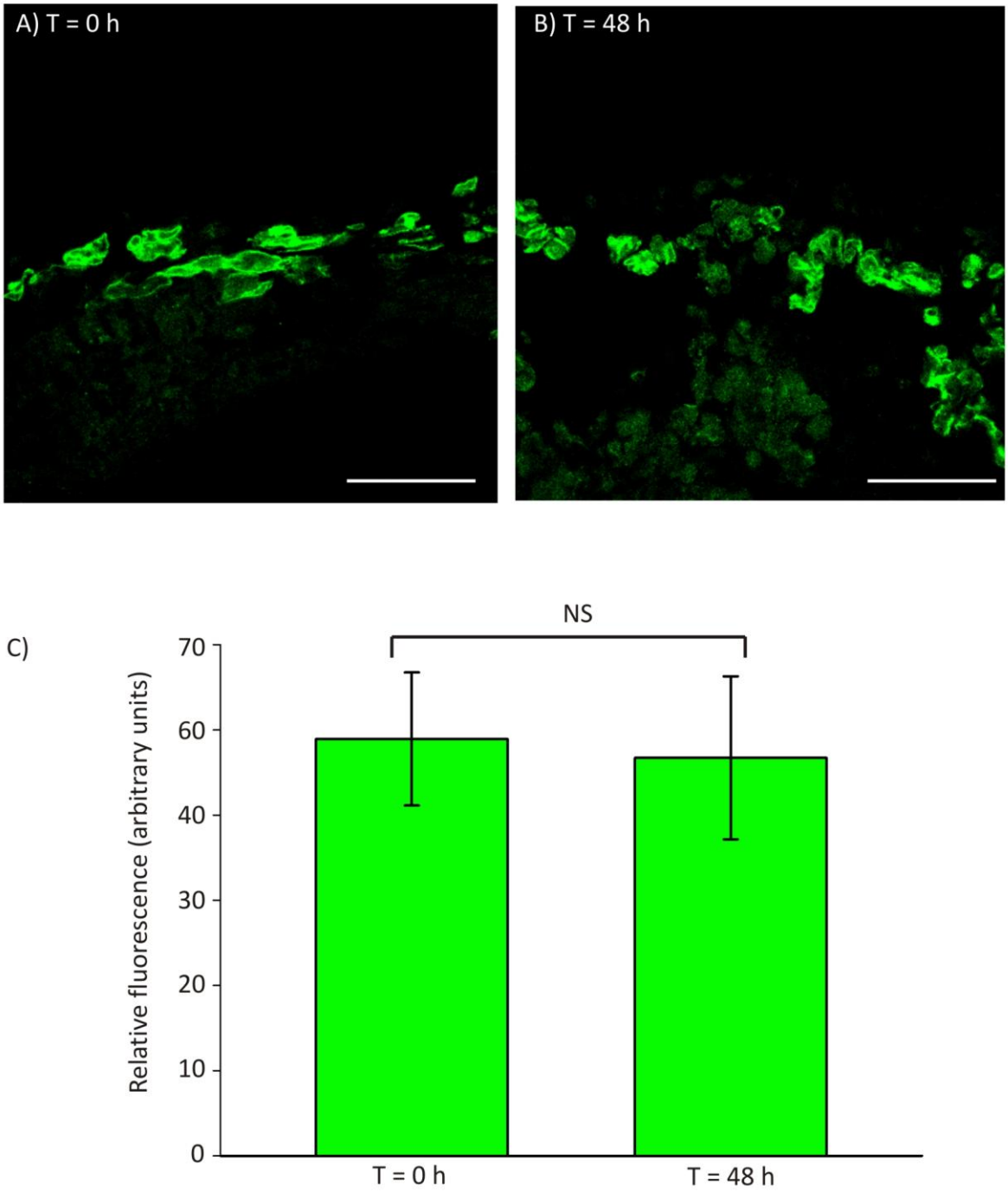

Figure 43. The effect of ex vivo tissue culture on ion channel expression. Using the primary antibody rabbit anti-HCN4 IgG and the secondary antibody donkey anti-rabbit conjugated to FITC, immunohistochemistry was performed on 16 µm cryosections of rat sinoatrial node. A) No tissue culture. B) Following 48 h tissue culture. Images were captured using a laser scanning confocal microscope. Immunohistochemistry was performed simultaneously and the same microscope settings were used for all pictures to allow quantitative comparison. C) Relative immunofluorescence of HCN4 measured using Volocity software with no tissue culture and following 48 h tissue culture (preparations n=6 for each group, mean +/-SEM shown). Data were compared using unpaired t-test. Scale bars in panels A and B = 50 µm. NS, p>0.05.

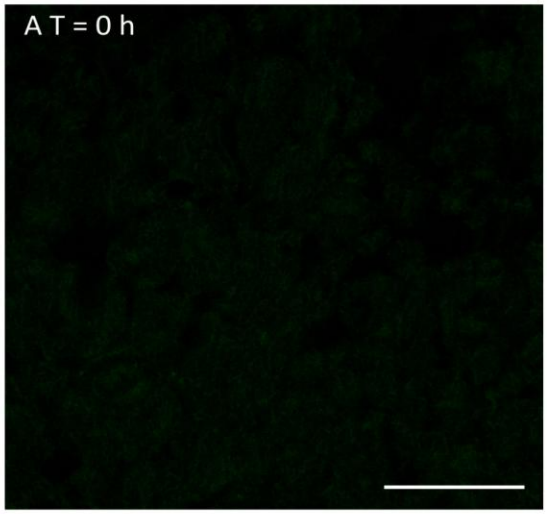

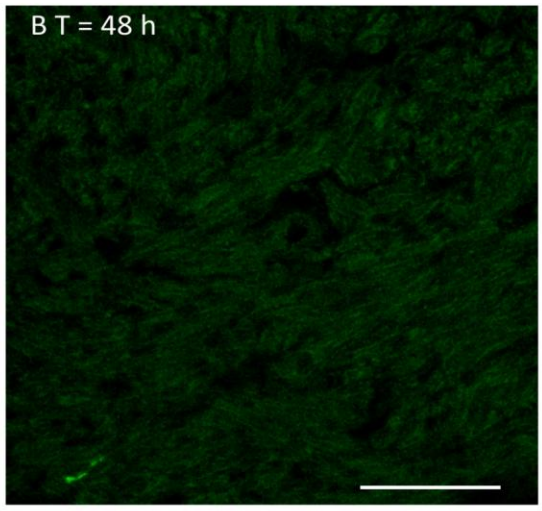

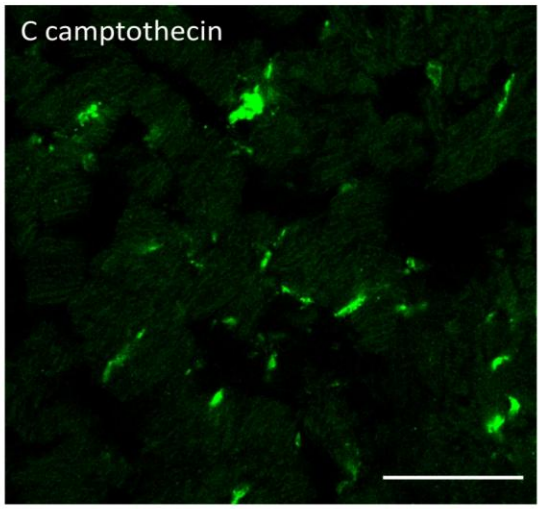

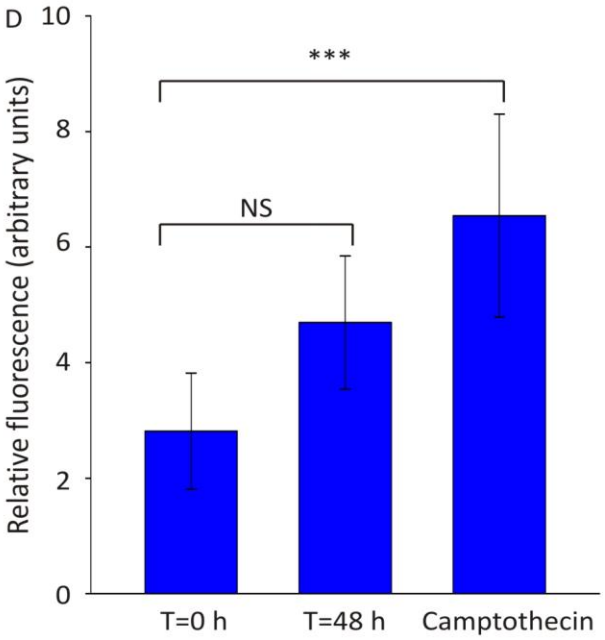

Figure 44. The effect of *ex vivo* tissue culture on cellular apoptosis. Apoptosis was detected by immunohistochemistry using the primary antibody rabbit anti-active caspase 3 IgG and the secondary antibody donkey anti-rabbit conjugated to FITC. Immunohistochemistry was performed on 16 µm cryosections of rat right atrial appendage. A) No tissue culture. B) Following 48 h tissue culture. C) Following 24 h tissue culture with 5 µm camptothecin to induce apoptosis. Images were captured using a laser scanning confocal microscope. Immuno-histochemistry was performed simultaneously and the same microscope settings were used for all pictures to allow quantitative comparison. Scale bars in panels A, B and C=50 µm. D) Relative immunofluorescence of active caspase 3 measured using Volocity software with no tissue culture, 48 h tissue culture and camptothecin (n=6 preparations for each group, mean +/ SEM shown). Data were compared to the uncultured control (T=0 h) using 1-way ANOVA. NS, $p>0.05$; *** $p<0.001$.

3.3 Sick sinus syndrome model

3.3.1 Introduction

SSS is a heterogeneous disease with a number of causes (see section 1.6). In this syndrome it is unclear where the leading pacemaker site lies. Though it is generally thought that the 'native' SAN is dysfunctional, there may actually be a shift to pacing from subsidiary pacemaker tissue. The wide distribution of SAN tissue and the common finding of ectopic atrial rhythms calls into question the exact nature of pacemaking sites away from the traditional site of the SAN at the junction of the SVC and RA.[210] For example, as previously discussed, electroanatomical mapping has demonstrated that what appears clinically to be SSS may be SAN exit block with an ectopic atrial leading pacemaker.[207] A slowing of the rate of the SAN may also unmask ectopic atrial rhythms.

The development of an *ex vivo* model of SSS utilising the presence of subsidiary pacemaker tissue could allow simple, rapid and inexpensive testing of pharmacological or genetic therapy for this disorder. It may also help define the nature of subsidiary pacemakers.

The following null hypotheses were tested:

1) The spontaneous pacing rate of the inferior portion of the SSS model is not significantly different to the intact RA (control) preparation.

2) The primary histological and immunohistochemical features of the subsidiary pacemaker do not differ from that of the SAN (i.e. small cell size, HCN4 positive, Cx43 negative).

3) There is no significant contribution of I_f to pacemaker activity in the subsidiary pacemaker.

4) The subsidiary pacemaker is not responsive to β-adrenergic stimulation.

3.3.2 Extracellular potential recordings

The spontaneous rates measured from the extracellular potential recordings made from the SSS model are shown in figure 35B (n=7). Of the seven preparations, six followed a similar pattern to the control preparations but at a slower rate, but one showed an initial slowing of the pacing rate with a later acceleration (figure 35B, black trace). Spontaneous pacing activity was reliably maintained for 72 h; in general there was an increase in the pacing rate to 21 h and thereafter the rate declined (figure 35B).

As above, further analysis was performed for the 0-48 h period. The mean six hour pacing rates are shown in figure 36A. When compared to the control, the SSS model was slower at all points (control, n=6; SSS, n=7; $p<0.001$). The mean pacing rate during the first hour was 182 ± 11 bpm, the maximum rate was at 21 h (214 ± 24 bpm) and the minimum rate was at 43 h (148 ± 13 bpm) (figures 36B and 37). The first hour, and maximum and minimum pacing rates were significantly slower than that of the control ($p<0.01$, $p<0.001$, $p<0.05$, respectively). Hourly mean pacing rates were calculated for the period 12-20 h (figure 36B); the SSS model was slower than the control at all timepoints ($p<0.001$).

3.3.3 Leading pacemaker site

The activation sequence was determined for six pairs of control and SSS preparations; representative records are shown in figure 45. The distribution of the leading pacemaker sites and preparation numbers are shown in figure 46. For the control preparations 2 through 6 the leading pacemaker was situated near the bifurcation of the sinoatrial node artery or in the SVC. The leading pacemaker site of preparation 1 was situated inferiorly, lateral to the IVC. Five of the leading pacemaker sites of the SSS model were located close to the superior aspect of the IVC (preparations 1 and 3 through 6). The leading pacemaker of preparation 2 was located inferior to the FO. Note that the leading pacemakers of preparation 1 (control and SSS) are very similar.

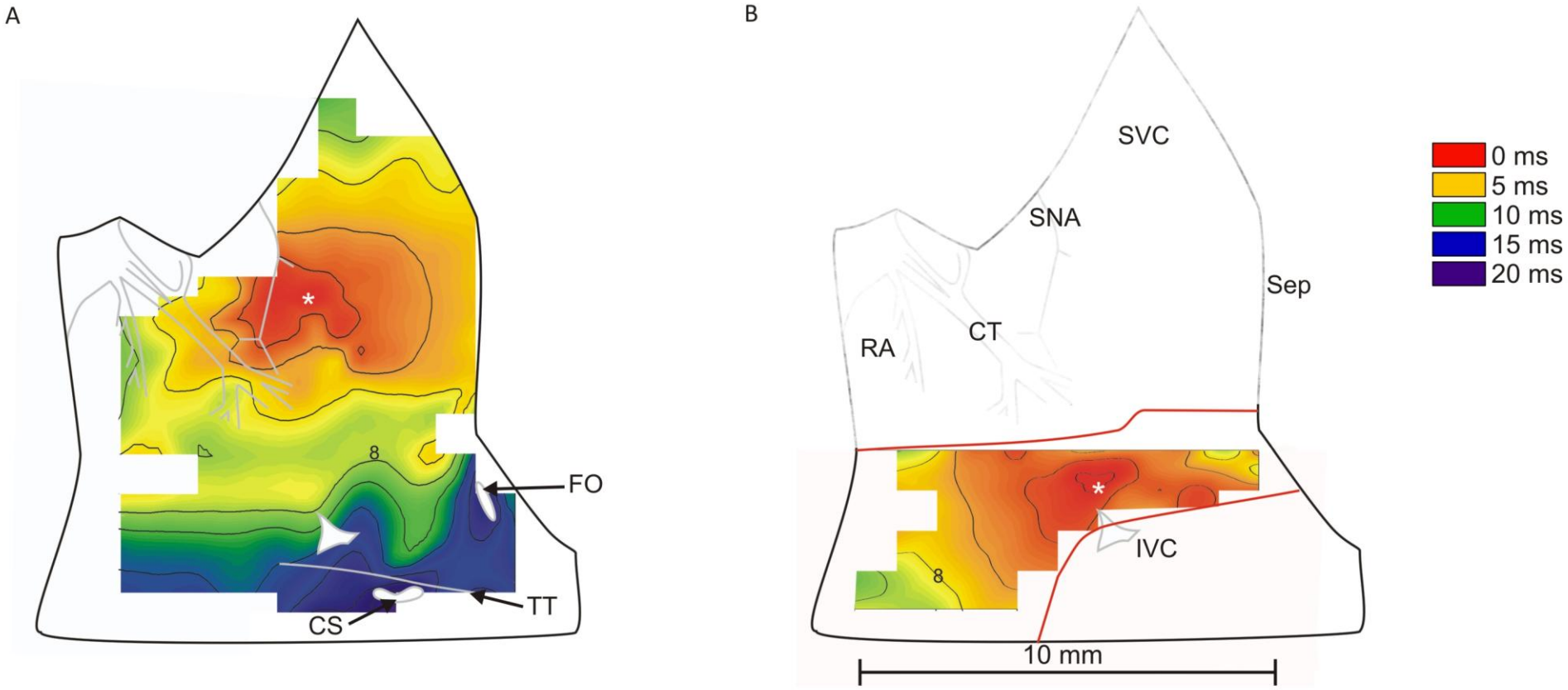

Figure 45. Representative activation maps of rat sinoatrial node preparations. Mapping was performed using a bipolar electrode to record surface potentials and the activation time was measured relative to a static reference electrode. The point of earliest electrical activity was taken as the leading pacemaker site (white asterisk). Following mapping of the full preparation, the tissue was cut (red lines) to make the sick sinus syndrome model. A) Activation map of intact (control) preparation. B) Activation map of sick sinus syndrome model. CT, crista terminalis; CS, coronary sinus; FO, foramen ovale; IVC, inferior vena cava; RA, right atrium; Sep, interatrial septum; SNA, sinus node artery; SVC,superior vena cava; TT, tendon of todaro. Black lines indicate 2 ms isochrones; the 8 ms isochrone is marked for reference. Colours represent the activation time relative to the leading pacemaker site at 0 ms. Areas within the preparation where extracellular potentials could not be reliably recorded are shown in white.

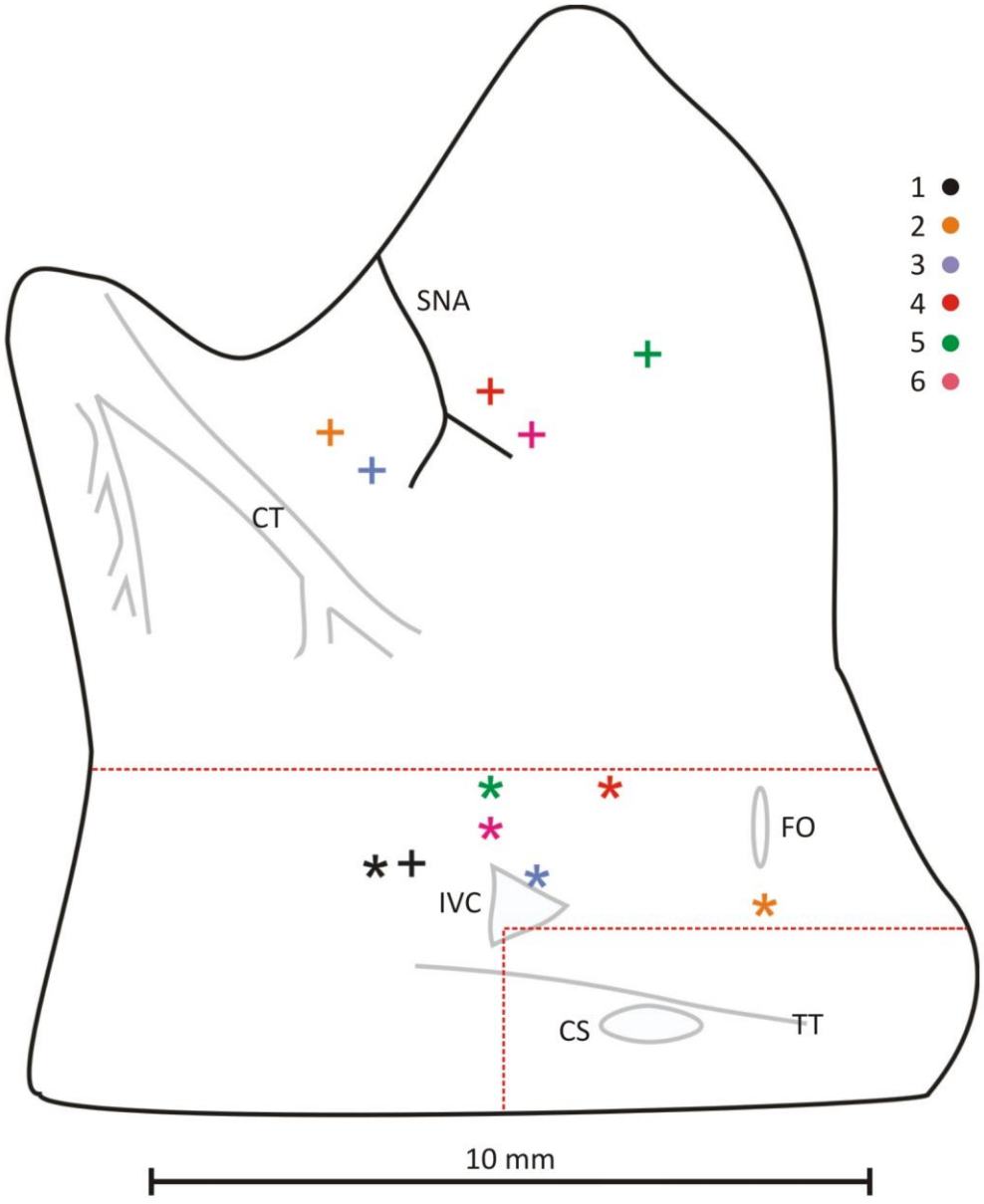

Figure 46. The distribution of leading pacemaker sites in pairs of control (intact rat sinoatrial node) and sick sinus syndrome (inferior rat sinoatrial node) preparations (n = 6). Activation mapping of a control preparation was performed at 36°C using a bipolar electrode; the site of earliest activation was taken as the leading pacemaker site. The leading pacemaker site of a control preparation is denoted by a cross, the position is calculated relative to the bifurcation of the sinoatrial node artery (SNA). The sinoatrial node was then divided to create the sick sinus syndrome model as previously described. Approximate lines of division are shown in red. The leading pacemaker site of the sick sinus syndrome model was then determined in the same manner. The leading pacemaker site of a sick sinus syndrome preparation is denoted by an asterisk; the position is calculated relative to the superior aspect of the inferior vena cava (IVC). Each pair of preparations are represented by an individual colour. Abbreviations as for figure 45.

Having identified the leading pacemaker of the SSS model, it was then possible to characterise it further. The SSS preparations were densely innervated with frequent ganglion cells ('G' in figure 47). Preparations 1, 2 and 4-6 were HCN4 negative and Cx43 positive; an example is shown in figure 47 (the remaining preparations are shown in Appendix A6). An HCN4 positive, Cx43 negative area was identified in preparation 3 (figure 48). Cell diameter at the leading pacemaker site in the SSS model was similar to the cell size of the SAN in control preparations (10.3 ± 0.6 µm vs. 11.3 ± 0.8 µm, respectively; p = NS). The cell diameter of the leading pacemaker site in the SSS model was significantly smaller than that of the surrounding RA (10.3 ± 0.6 µm vs. 13.6 ± 0.6 µm, respectively; $p<0.05$). RA cell size did not vary significantly between the superior (control) and inferior (SSS) samples (14.6 ± 0.7 µm vs. 13.6 ± 0.6 µm, respectively; p = NS; figures 41 and 49).

Inhibition of I_f by 2 mM CsCl induced a 37.8% increase in the cycle length of the SSS model cycle length from 221.0 ± 5.3 ms to 304.6 ± 20.4 ms, corresponding to a decrease in the pacing rate from 271.5 ± 6.5 bpm to 197.0 ± 13.2 bpm (n=6, $p<0.05$; figure 50). β-adrenergic stimulation of the same SSS preparations with 100 µM isoprenaline decreased the cycle length by 29.8% from 243.3 ± 10.6 ms to 170.8 ± 8.5 ms corresponding to an increase in the pacing rate from 246.6 ± 10.7 bpm to 351.3 ± 17.5 bpm (n=6, $p<0.01$; figure 50).

3.4 Adenovirus-mediated transgene expression in cardiac tissue

3.4.1 Introduction

Adenoviruses consist of an icosohedral protein capsid surrounding an inner DNA core; the genome is a linear double stranded DNA molecule of ~36 kb.[368] Infection of the host cell requires binding of the virus to the coxsackie and adenovirus receptor (CAR) at the cell surface and subsequent phagocytosis by the cell.[366] Binding to this receptor is a necessary step in cellular infection and thus expression of this receptor is one determinant of the susceptibility of each tissue type to Ad5 infection.[376] Once the virus escapes the endosome, the capsid is disrupted and the virus is transported to the nuclear membrane where the viral DNA passes through the nuclear pore into the cell nucleus; the viral DNA remains extra-chromosomal.[368]

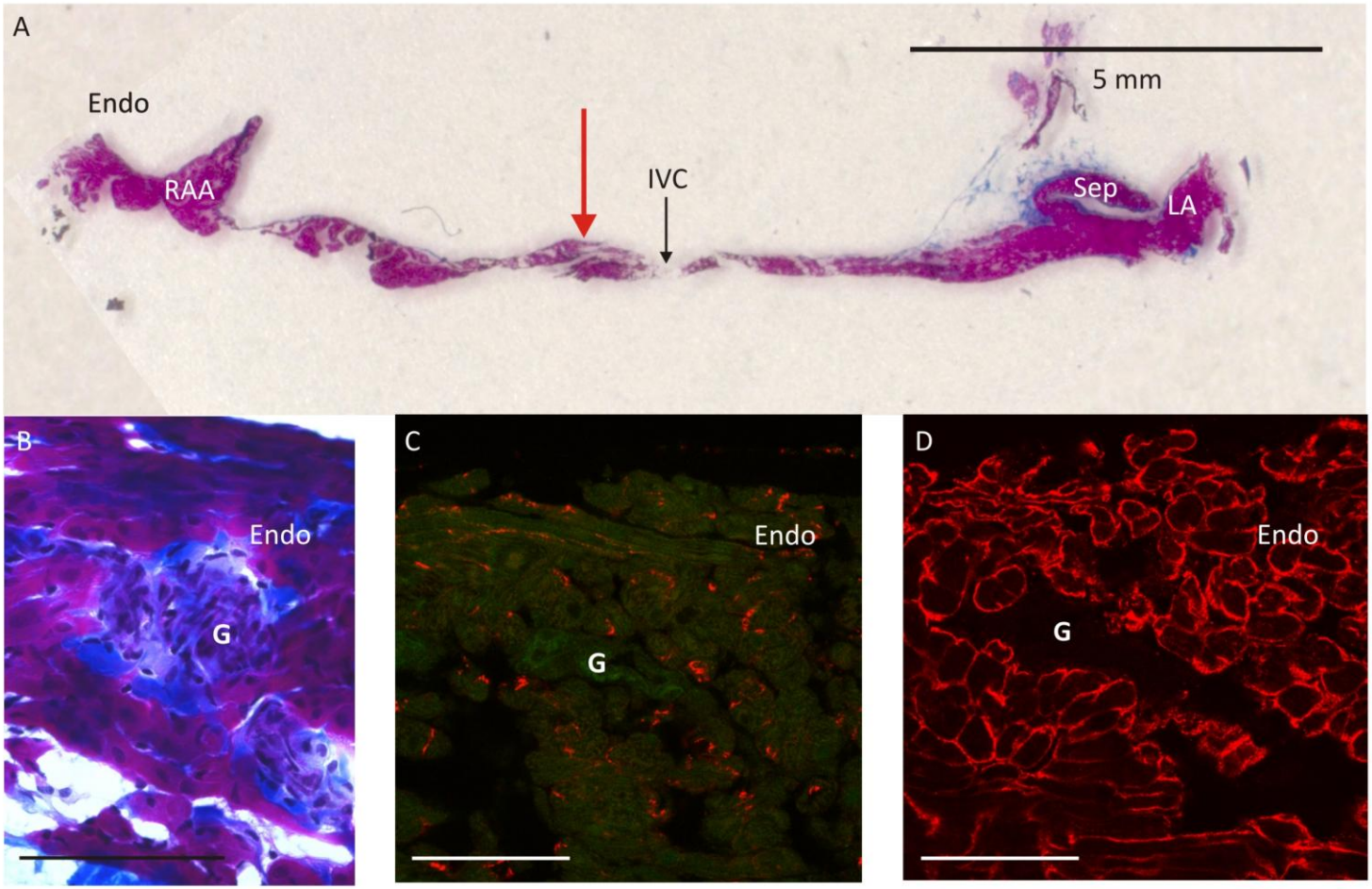

Figure 47. The histology and immunohistochemistry of the subsidiary pacemaker. Preparation 1 (see figure 46). A) Sick sinus syndrome preparations were mapped as previously described then frozen. 16 µm cryosections at the level of the leading pacemaker were stained with Masson's trichrome. The leading pacemaker is marked by the red arrow. B) Masson's trichrome staining of the leading pacemaker site. C) Ion channel and gap junction expression at the leading pacemaker site. Sections were labelled for HCN4 (green) and Cx43 (red). D) Cell size at the leading pacemaker site. The cell membrane of myocytes was labelled using an antibody to Caveolin 3. For Masson's trichrome: purple, myocytes; blue, connective tissue. Endo, endocardium; IVC, inferior vena cava; LA, left atrium; RAA, right atrial appendage; Sep, interatrial septum. Scale bar in panels B - D = 100 µm. 'G' denotes the site of neuronal ganglion cells.

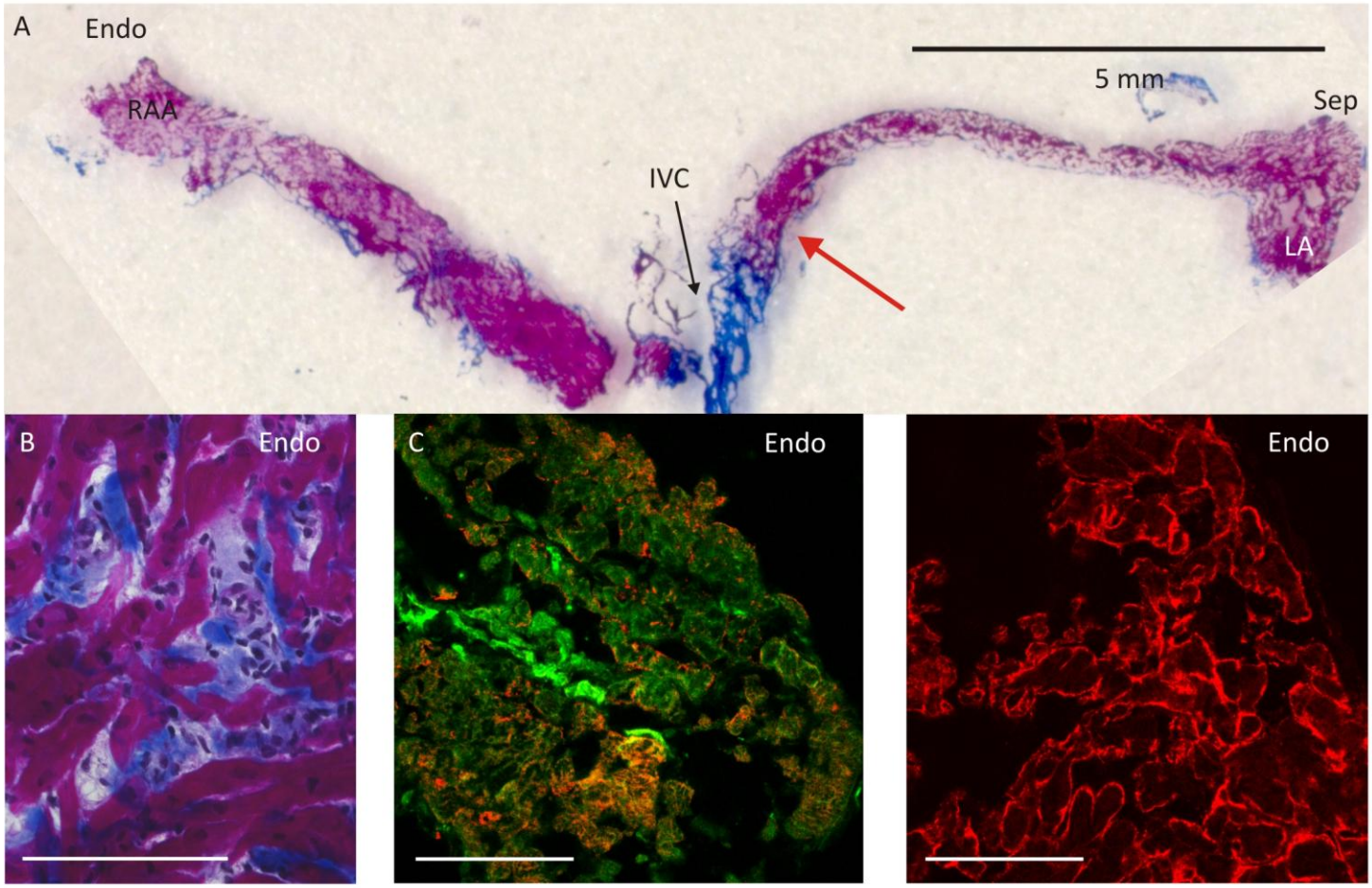

Figure 48. The histology and immunohistochemistry of the subsidiary pacemaker. Preparation 3 (see figure 46). A) Sick sinus syndrome preparations were mapped as previously described then frozen. 16 µm cryosections at the level of the leading pacemaker were stained with Masson's trichrome. The leading pacemaker is marked by the red arrow. B) Masson's trichrome staining of the leading pacemaker site. C) Ion channel and gap junction expression at the leading pacemaker site. Sections were labelled for HCN4 (green) and Cx43 (red). D) Cell size at the leading pacemaker site. The cell membrane of myocytes was labelled using an antibody to Caveolin 3. For Masson's trichrome: purple, myocytes; blue, connective tissue. Endo, endocardium; IVC, inferior vena cava; LA, left atrium; RAA, right atrial appendage; Sep, inter-atrial septum. Scale bar in panels B - D = 100 µm.

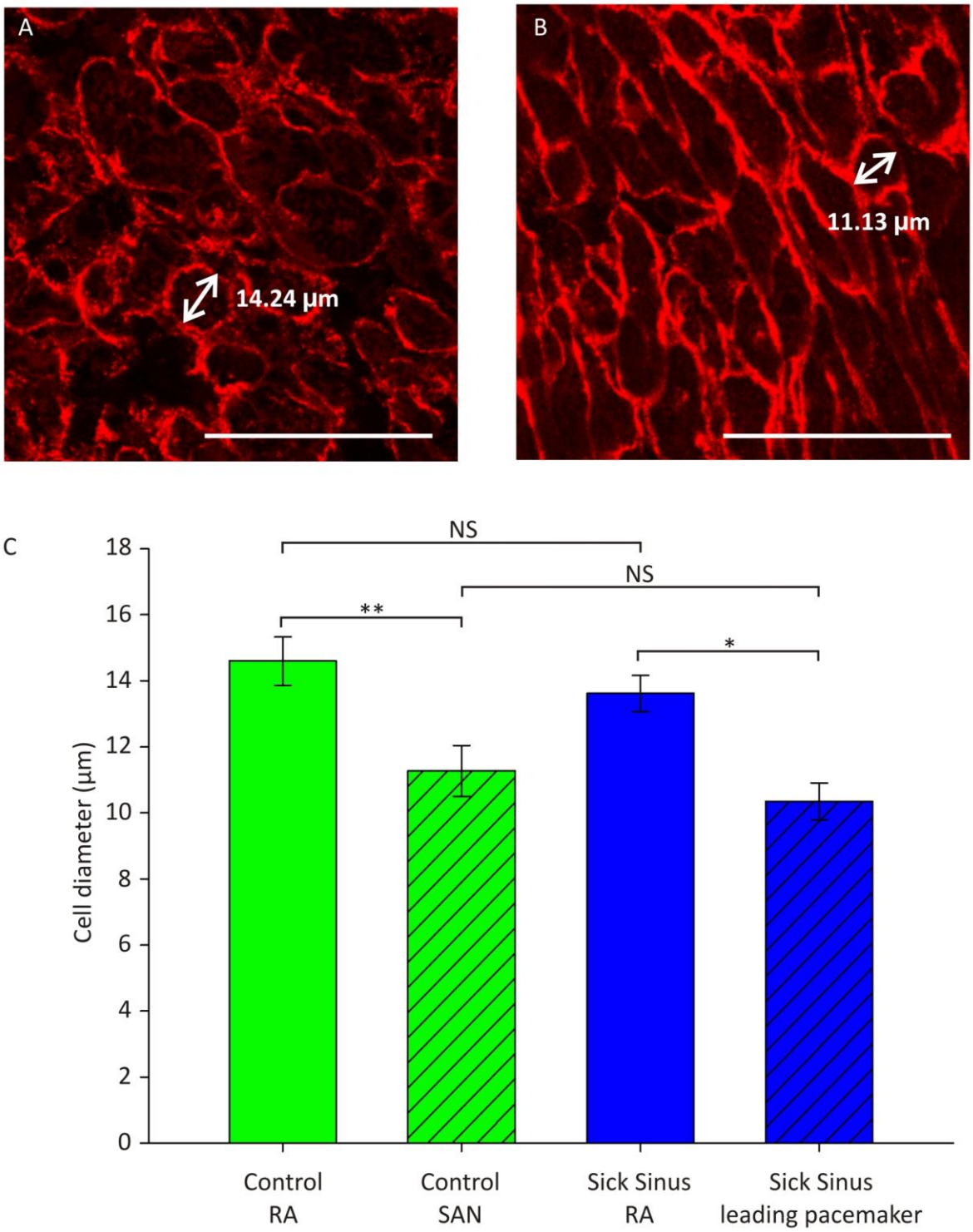

Figure 49. Cell size at the leading pacemaker site of the sick sinus syndrome model. Immunohistochemistry was performed on 16 µm cryosections of rat right atrial appendage (A) and the leading pacemaker site (B) of sick sinus syndrome preparations. Cell membranes were labelled using the cardiomyocyte-specific primary antibody rabbit anti-Cav3 IgG and the secondary antibody donkey anti-rabbit conjugated to Cy3. Cell size was measured on cells cut in transverse section, the shortest axis was taken (examples in panels A and B). The mean of 20 cells over three high power fields was taken for each preparation (n=6 preparations per group). Scale bars in A and B represent 50 µm. C) Mean cell diameter +/- SEM for control and sick sinus cells from right atrium (open bars) and sinoatrial node or leading pacemaker (hashed bars). Data within each group were compared using a paired t-test. Comparison of data between the two groups was performed by unpaired t-test. NS, $p>0.05$; * $p<0.05$; ** $p<0.01$.

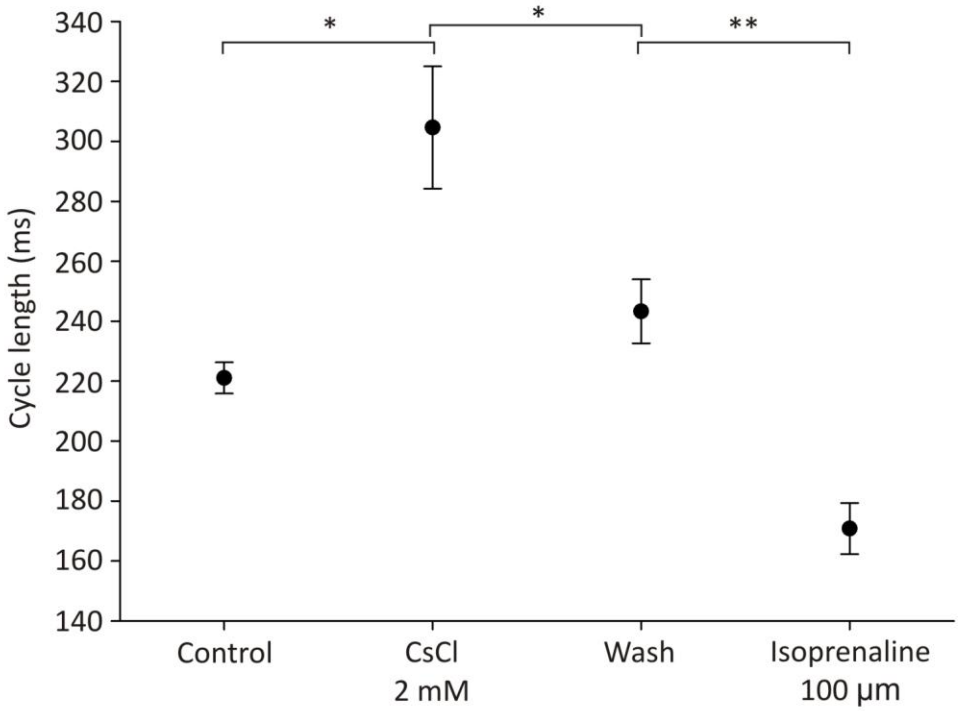

Figure 50. Pacemaking in the sick sinus syndrome model is partially dependent on I_f and is responsive to ß-adrenergic stimulation. A sick sinus syndrome preparation (inferior rat sinoatrial node) was superfused with normal Tyrode's solution at 37°C and spontaneous pacing activity was recorded using bipolar extracellular electrodes. 500 beats were averaged to give a mean cycle length under control conditions, with the addition of the I_f blocker 2 mM CsCl and in the presence of a maximal dose 100 µM isoprenaline . The graph represents mean +/- SEM (n=7). Data were analysed by paired t-test; * $p<0.05$; ** $p<0.01$.

The Ad5 genome region E1A is the first to be expressed in wild-type Ad5. The E1A proteins activate downstream transcription, induce the cell to enter the S phase and prevent apoptosis.[368] Deletion of the E1 region in RAd means that, generally speaking, only the DNA sequence between the inverted terminal repeats (usually the cDNA cloned in experimentally) is expressed.[366]

E1-deleted Ad5 has been used in a broad range of investigative and clinical applications. These include the expression of proteins from mammalian cell lines, gene transfer and gene therapy in animals and humans.[377, 378] They offer a high, though transient, level of protein expression but do display a degree of tissue tropism. The tropism is partly mediated by the availability of the CAR, for example airway epithelium, skeletal muscle and dendritic cells are CAR-deficient.[379-381] The expression of CAR in the heart and CCS is tightly regulated. Expression is maximal in neonatal heart muscle and wanes afterwards.[382] CAR -/- is lethal in transgenic mice, the cardiac development is abnormal leading to multiple areas of apoptosis and left ventricular rupture.[383] Interestingly, a cardiac specific CAR knockout mouse shows AV conduction defects with loss of Cx45 localisation to the gap junctions of the AV node.[384] Taken together these observations make it difficult to predict the response of SAN or subsidiary pacemaker cells to RAd infection.

The following null hypotheses were tested:

1) Adenovirus mediated gene expression in the sinoatrial node or subsidiary nodal tissue is not viable.

2) The RA intercaval area is not receptive to adenovirus mediated ion channel expression.

3.4.2 Adenovirus-mediated gene expression in nodal tissue

β-galactosidase expression was detected after 48 h culture (n=2, representative preparation shown in figure 51). To identify the nature of the tissue supporting transgene expression, immunohistochemistry was performed using markers for SAN tissue (HCN4) and RA tissue (ANP); β-galactosidase expression is seen in both (n=2, representative preparation shown in figure 52).

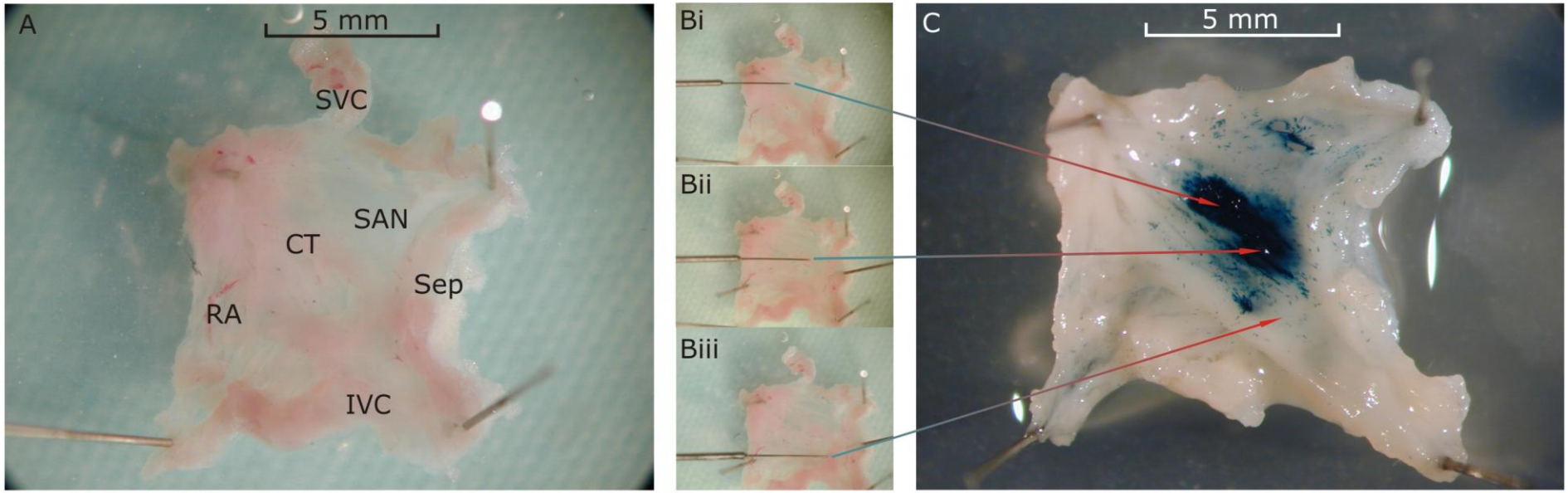

Figure 51. A) SN preparation from three month old male Wistar-Hanover rat. B) Injection of $1x10^8$ pfu of Ad-PREP-lacZ at three sites; superior, mid and inferior intercaval regions (Bi ,Bii and Biii respectively). C) Presence of β-galactosidase was confirmed by X-gal staining after 48 h incubation at 37 °C in a 95 % O_2/ 5 % CO_2 incubator. Localised β-galactosidase expression is seen at two sites (Bi and Bii). For abbreviations see legend to figure 38.

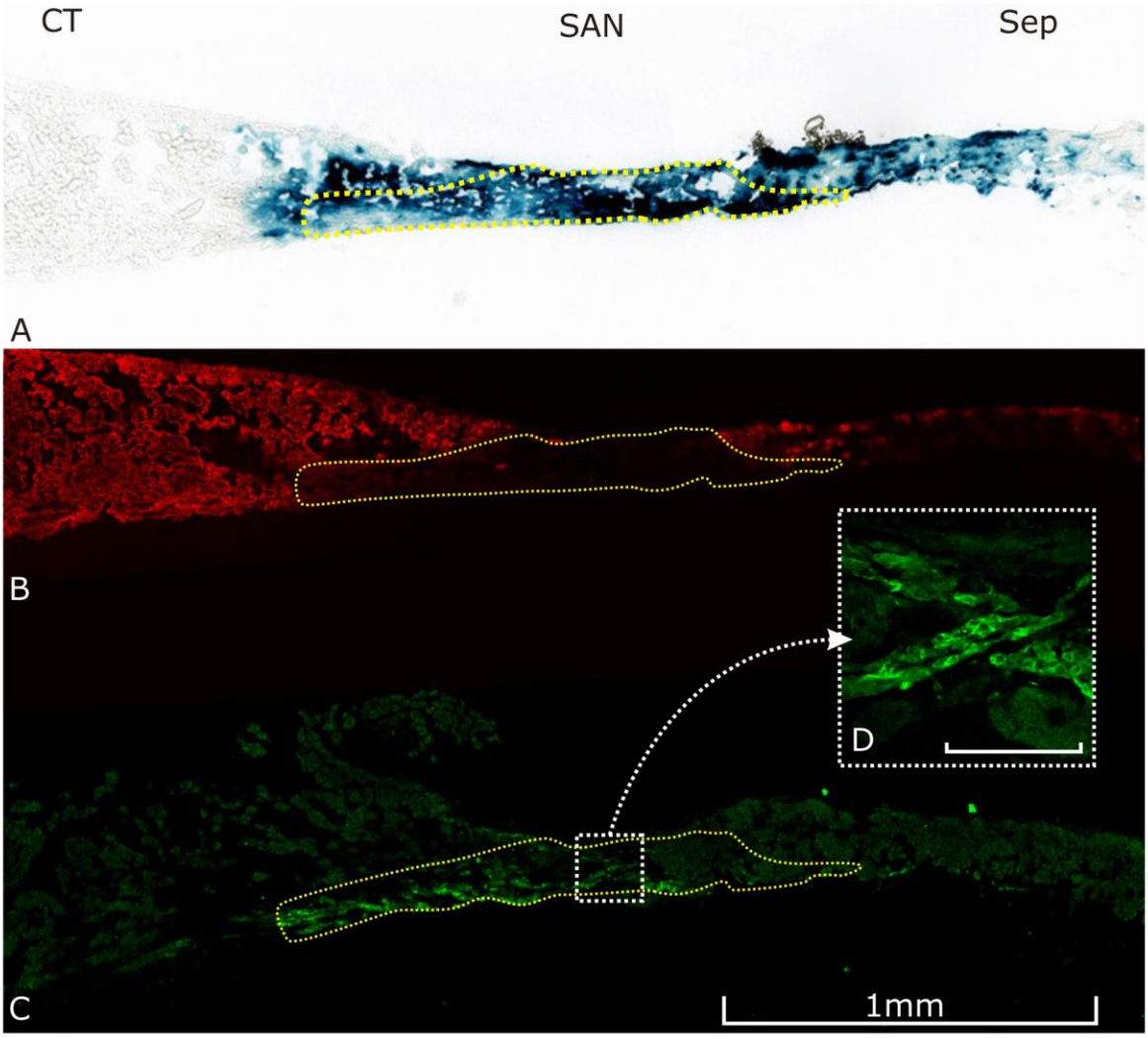

Figure 52. β-galactosidase expression in the sinoatrial node revealed by X-gal staining and immunohistochemistry of adjacent sections prepared from rat sinoatrial node following injection of $1x10^8$ pfu of Ad-PREP-lacZ and then tissue culture for 48 h. A) β-galactosidase expression assessed by X-gal staining (blue area). B, C) Immunolabelling for the negative marker for the sinoatrial node, ANP (B), and the positive marker for the sinoatrial node, HCN4 (C). D) High power image of immunolabelling for HCN4 in the area indicated by the dotted box. Scale bar in box D is 100 µm. The sinoatrial node area is indicated by the dotted yellow lines.

Injection of 1 x 10^8 pfu Ad5-GFP-HCN2 into the most common subsidiary pacemaker site, superior to the IVC, resulted in detectable GFP and HCN2 expression in whole SAN tissue (n=2, representative preparation shown in figure 53) Immunohistochemistry for HCN2 performed on 16 μm cryosections taken through the injection site confirmed that the HCN2 expression was localised to the cell membrane (n=2, representative findings shown in figure 54).

3.5 Biopacemaking

3.5.1 Introduction

Biopacemaking has been developed as an experimental treatment for bradycardia, it is an evolving field and multiple strategies have been tested (see section 1.7 for detailed review). All *in vivo* experimental work has used HCN channels as the biopacemaker substrate.[385] The bulk of published work has focussed on treatment of AV block with implantation of an adenovirus-mediated biopacemaker in the ventricular free wall or bundle of His.

Initial work demonstrated that subepicardial expression of HCN2 in the left atrial appendage of dogs provided a slow escape rhythm when complete SAN arrest was induced via vagal stimulation.[309] Improved pacing rates were seen when the same channel was expressed in the left bundle branch of dogs with experimentally induced AV block.[313] Pacing rates in these animals, although 'physiologically acceptable' remain slow. The context dependence of HCN channels means that, in these ectopic sites, induced I_f is likely to produce a slow rhythm. This is further emphasised by experiments using engineered HCN channels with fast kinetics. The use of mutant HCN2, mE324A, in the left bundle branch of dogs did not abolish the dependence on back up electronic pacing.[314] Furthermore, results of patch clamp experiments in rat ventricular myocytes presented show that mutant mE324a has a faster more positive pacemaker depolarization than mHCN2, yet the *in vivo* pacing rate of the two do not differ.[314] Another attempt to use engineered HCN channels in ventricular muscle had even more disastrous results, expression of HCN212 in canine left ventricle induced potentially lethal ventricular tachycardia.[319] Perhaps the context dependence of HCN channels cannot be effectively overcome in

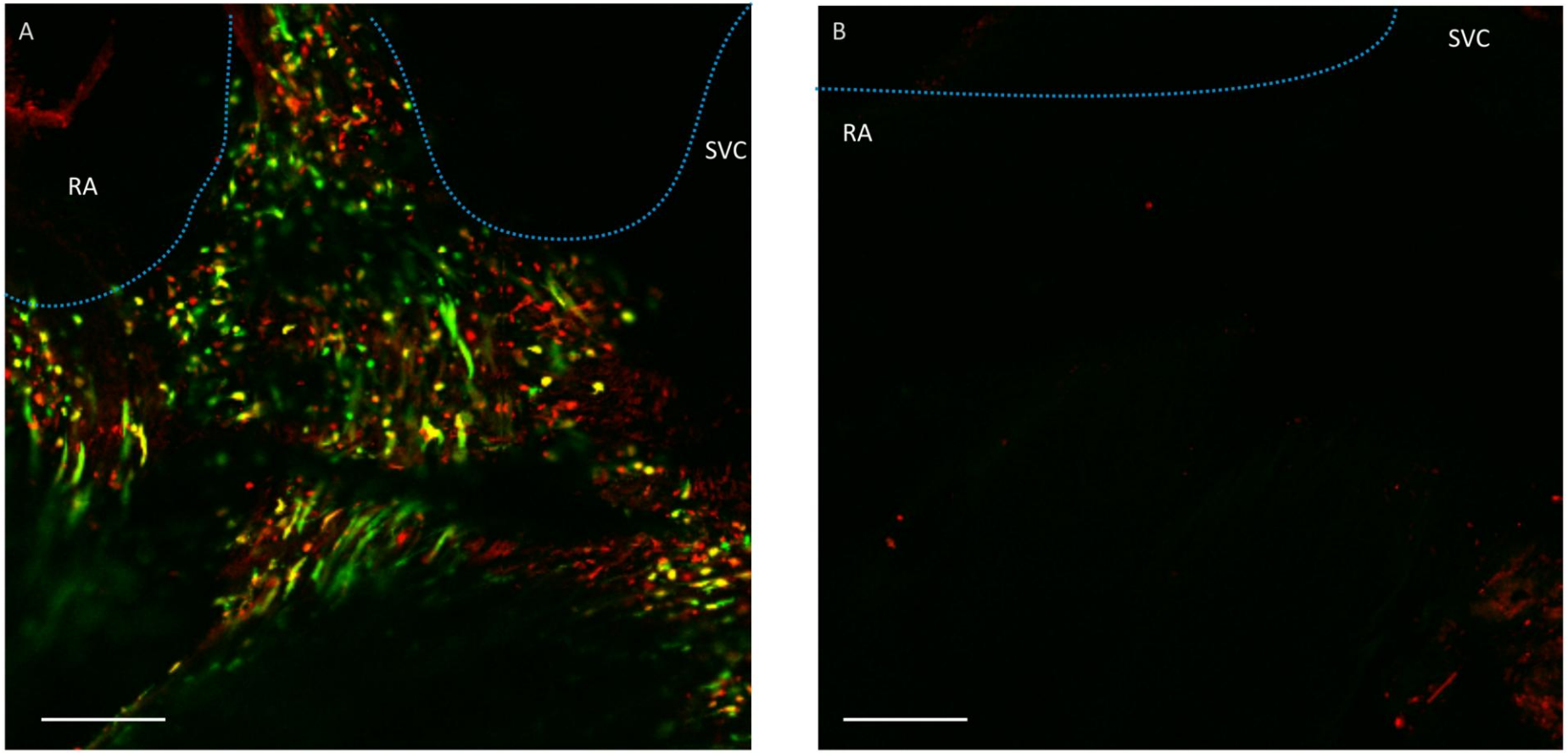

Figure 53. Adenovirus mediated expression of HCN2 in the rat sinoatrial node. Sinoatrial node preparations were injected with 1 x 10^8 pfu Ad5-GFP-HCN2 (A) or 1 x 10^8 pfu Ad5-PREK-LacZ (B). After 24 h tissue culture, immunohistochemistry was performed on the whole tissue using the primary antibody rabbit anti-HCN2 IgG and the secondary antibody donkey anti-rabbit conjugated to Cy3 (red). GFP gives the green signal. The images are taken looking down onto the endocardial surface, The blue lines indicate the superior aspect of the preparations, the lateral and inferior aspects are outside the area shown. RA, right atrium; SVC, superior vena cava. Scale bars in panels A and B = 100 µm.

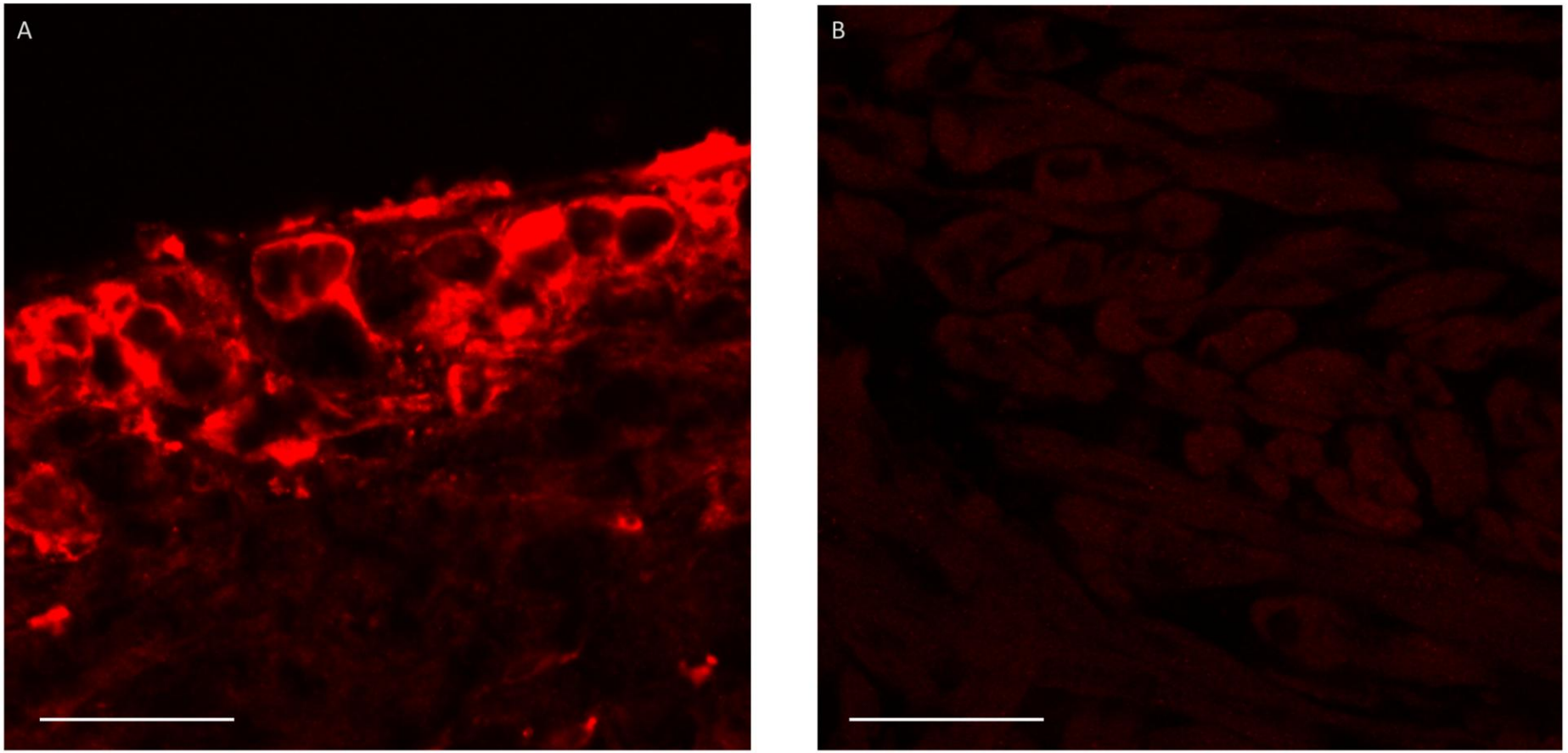

Figure 54. Adenovirus mediated expression of HCN2 in the rat sinoatrial node. Sinoatrial node preparations were injected with 1 x 10^8 pfu Ad5-GFP-HCN2 (A) or 1 x 10^8 pfu Ad5-PREK-LacZ (B). After 24 h tissue culture, immunohistochemistry was performed on 16 µm cryosections using the primary antibody rabbit anti-HCN2 IgG and the secondary antibody donkey anti-rabbit conjugated to Cy3 (red). Immunohistochemistry was performed simultaneously and the same microscope settings were used for both pictures. Scale bars in panels A and B = 50 µm.

ventricular myocytes without the co-expression of other 'nodal' ion channels such as $Ca_v1.3$, or I_K suppression.

There have been attempts to model SSS *in vivo* to allow the study of the utility of biopacemaking in this syndrome. The expression of mutant mHCN1 (mHCN1ΔΔΔ – favours channel opening) in the left atrial appendage of pigs reduced electronic pacemaker dependence following radiofrequency ablation of the SAN.[318] Repair of a diseased or dysfunctional SAN by gene therapy has not been studied.

The following null hypotheses were tested:

1) The spontaneous pacing rate of the SSS model will not be increased by injection of Ad5-HCN212 (containing the transgene for the chimaeric ion channel HCN212) or Ad5-PREK-HCN4 (containing the transgene for the ion channel HCN4).

2) The spontaneous pacing rate of the SSS model will not be increased by injection of Ad5-GFP or Ad5-GFP-HCN4Δ that do not carry transgenes for active ion channels.

3.5.2 Green fluorescent protein – Ad5-GFP

The extracellular potentials recorded from the SSS model injected with Ad5-GFP (n=8) are shown in figure 55. Six hour averages of the spontaneous pacing rates were compared to those of the control SAN (n=6) and uninjected SSS (n=7) preparations. The rate of the Ad5-GFP injected preparations was not significantly different to that of the uninjected SSS preparations (p=NS; figure 56); both were slower than the control SAN ($p<0.001$).

3.5.3 Mutant, non-functional, HCN – Ad5-GFP-HCN4Δ

The extracellular potentials recorded from the SSS model injected with Ad5-GFP-HCN4Δ (n=5) are shown in figure 57. Six hour averages of the spontaneous pacing rates were compared to those of the control SAN (n=6) and uninjected SSS (n=7) preparations. The rate of the Ad5-GFP-HCN4Δ injected preparations was not significantly different to that of the uninjected SSS preparations (p=NS; figure 58); both were slower than the control SAN ($p<0.001$).

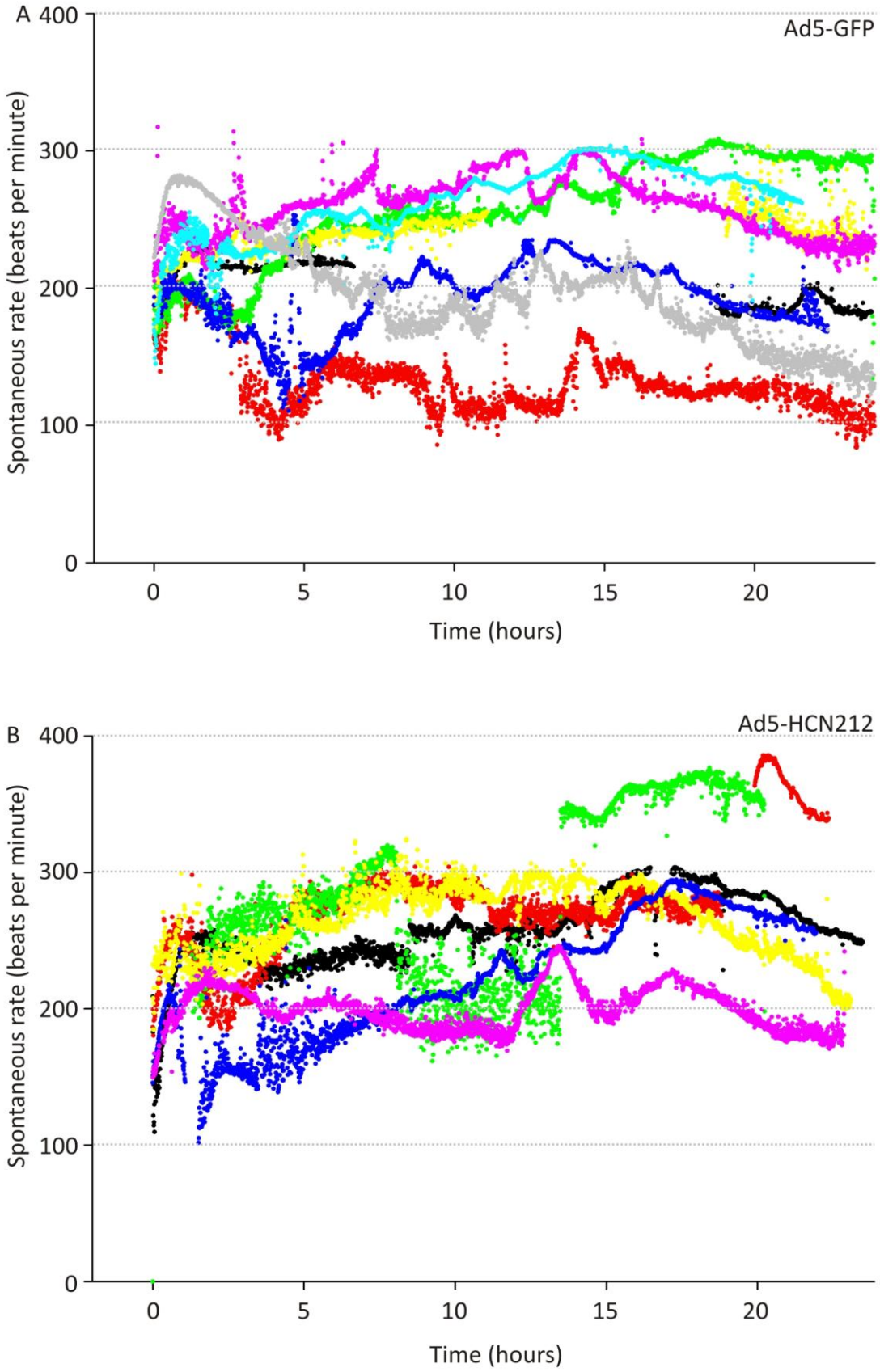

Figure 55. Spontaneous *ex vivo* pacing rates of the sick sinus syndrome model injected with Ad5-GFP or Ad5-HCN212. Sick sinus syndrome preparations were injected with 1 x 10^8 pfu Ad5-GFP (n=8) (A) or 1 x 10^8 pfu Ad5-HCN212 (n=6) (B) and then cultured at 37 °C as described. Extracellular potentials were continuously recorded using 0.15 mm stainless steel bipolar electrodes. Each dot represents a 30 s average rate. Differing colours distinguish individual preparations.

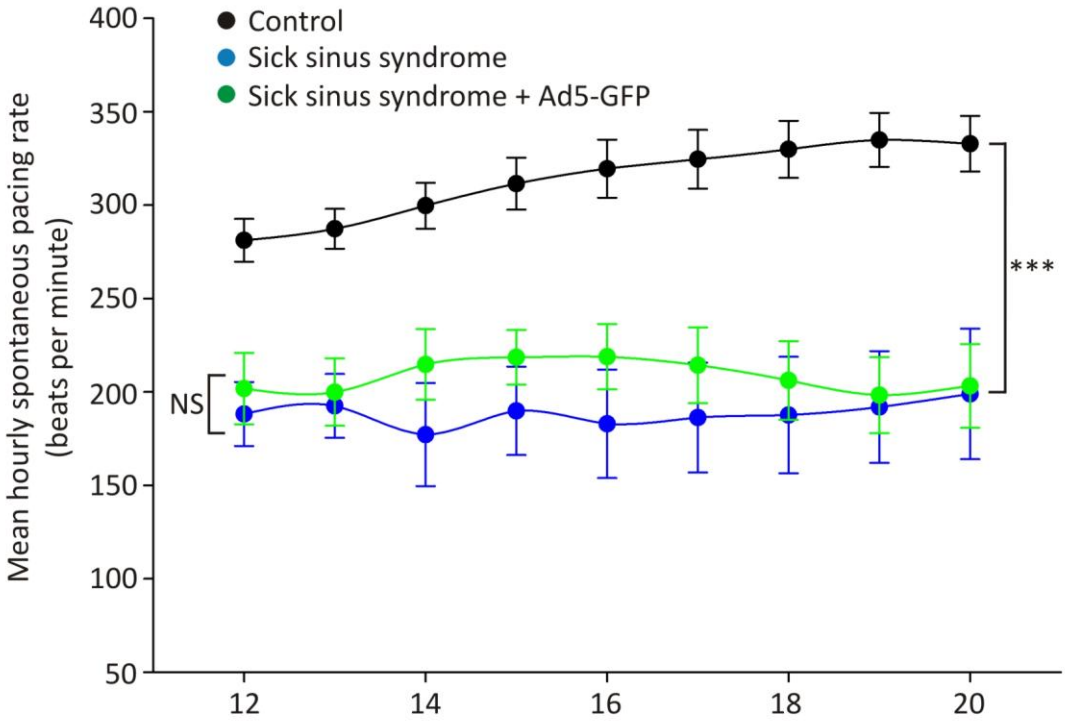

Figure 56. Average spontaneous *ex vivo* pacing rates of the control sinoatrial node, the sick sinus syndrome model and the Ad5-GFP-injected sick sinus syndrome model. Control preparations (full rat sinoatrial node, black circles, n=6), sick sinus syndrome preparations (inferior rat sinoatrial node, blue circles, n=7) and sick sinus syndrome preparations injected with 1 X 10^8 pfu Ad5-GFP (green circles, n=8) were cultured at 37°C as previously described. Extracellular potentials were recorded using 0.15 mm stainless steel bipolar electrodes. The pacing rate was averaged over each hour for the period 12-20 h. Data were analysed using 2-way ANOVA to compare the rate to that of the uninjected sick sinus syndrome model. *** $p<0.001$; NS, $p>0.05$ for all time points.

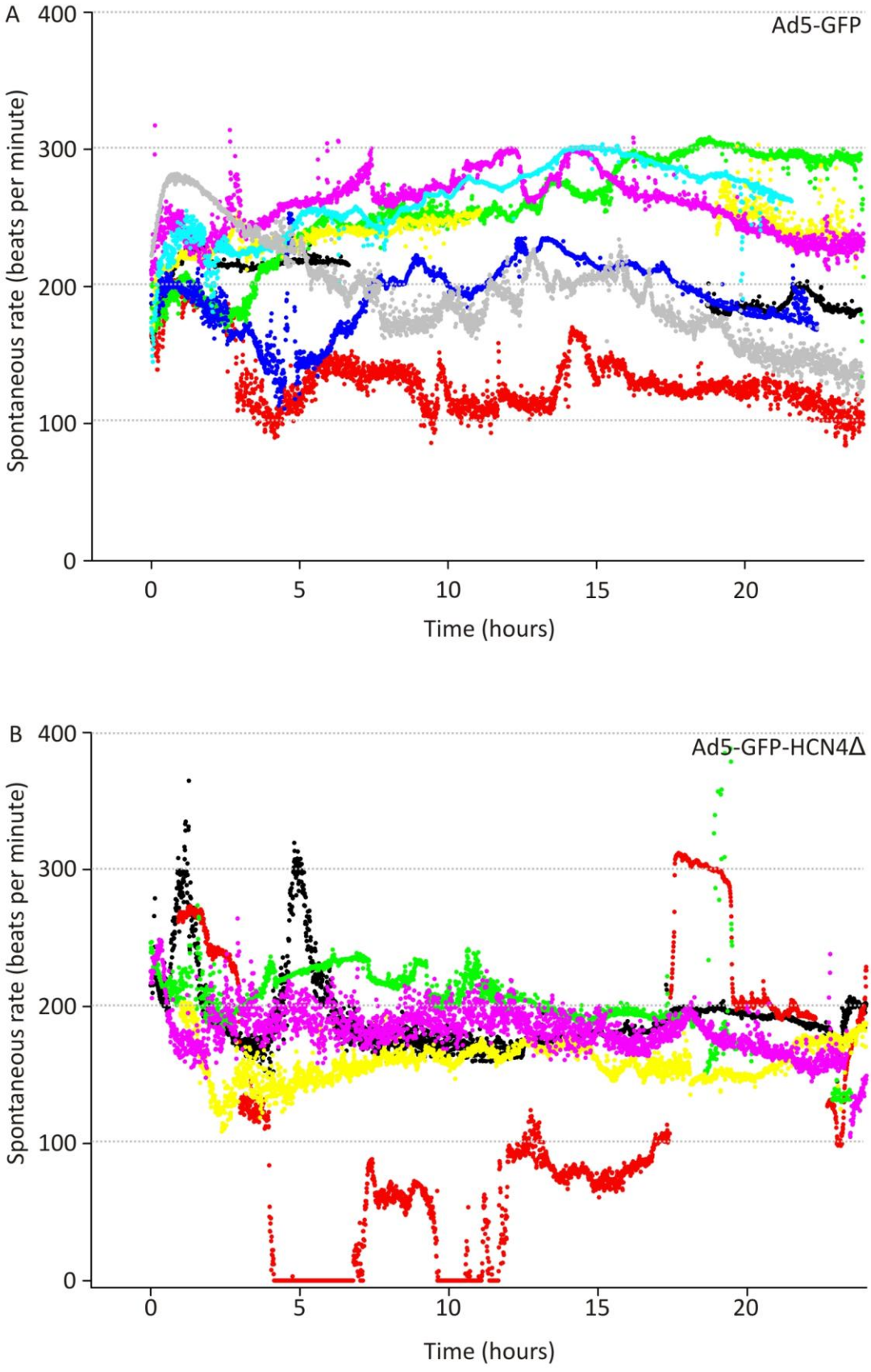

Figure 57. Spontaneous *ex vivo* pacing rates of the sick sinus syndrome model injected with Ad5-GFP or Ad5-GFP-HCN4Δ. Sick sinus syndrome preparations were injected with 1 x 10^8 pfu Ad5-GFP (n=8) (A) or 1 x 10^8 pfu Ad5-GFP-HCN4Δ (n=5) (B) and then cultured at 37 °C as described. Extracellular potentials were continuously recorded using 0.15 mm stainless steel bipolar electrodes. Each dot represents a 30 s average rate. Differing colours distinguish individual preparations.

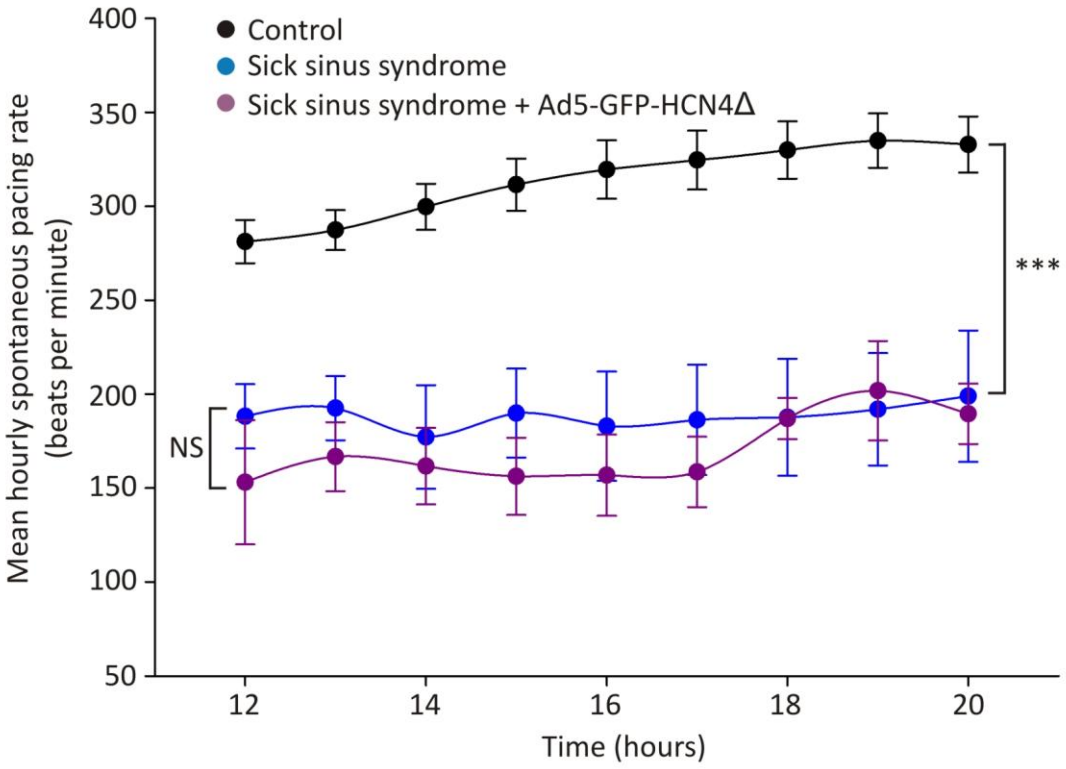

Figure 58. Average spontaneous *ex vivo* pacing rates of control sinus node, the sick sinus syndrome model and the Ad5-GFP-HCN4Δ-injected sick sinus syndrome model. Control preparations (full rat sinoatrial node, black circles, n=6), sick sinus syndrome preparations (inferior rat sinoatrial node, blue circles, n=7) and sick sinus syndrome preparations injected with 1 X 10^8 pfu Ad5-GFP-HCN4Δ (purple circles, n=5) were cultured at 37°C as previously described. Extracellular potentials were recorded using 0.15 mm stainless steel bipolar electrodes. The pacing rate was averaged over each hour for the period 12-20 h. Data were analysed using 2-way ANOVA to compare the rate to that of the uninjected sick sinus syndrome model. *** $p<0.001$; NS, $p > 0.05$ for all time points.

3.5.4 Chimaeric HCN – Ad5-HCN212

The spontaneous rate calculated from extracellular potentials recorded from the SSS model injected with Ad5-HCN212 (n=6) is shown in figure 55B. Six hour averages of the spontaneous pacing rates were compared to those of the control SAN (n=6), Ad5-GFP-injected (n=8) and uninjected SSS (n=7) preparations. The rate of the Ad5-HCN212 injected preparations was significantly faster than the Ad5-GFP injected and the uninjected SSS preparations ($p<0.001$; figure 59).

3.5.5 mHCN4 – Ad5-PREK-HCN4

The spontaneous rate calculated from extracellular potentials recorded from the SSS model injected with Ad5-PREK-HCN4 (n=6) are shown in figure 60A. Of the six injected preparations, three demonstrated unstable pacing activity (blue, yellow and green traces). The remaining three preparations that showed stable pacing were analysed further (n=3) and the rate compared to that of the uninjected SSS (n=7) preparations. Six hour averages of the spontaneous pacing rates are shown in figure 60. The rate of the Ad5-PREK-HCN4 injected preparations was not significantly different to the uninjected SSS preparations (figure 61, p=NS).

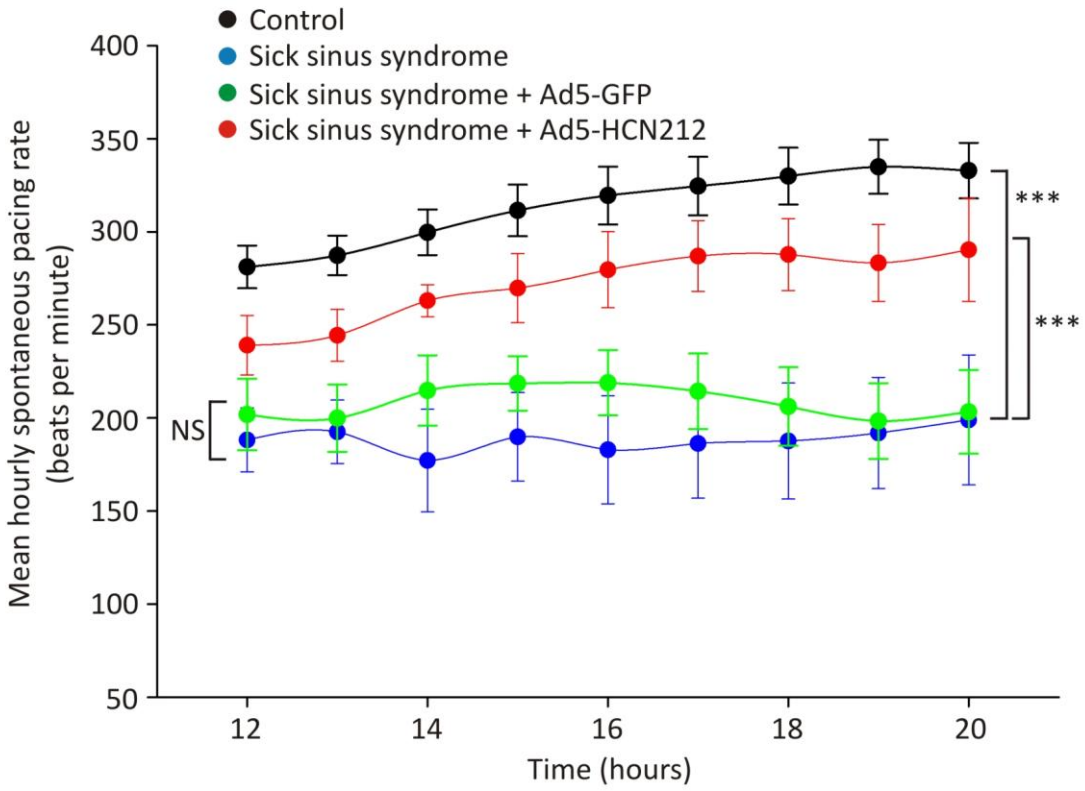

Figure 59. Average spontaneous *ex vivo* pacing rates of control sinoatrial node, the sick sinus syndrome model and the sick sinus syndrome model injected with Ad5-GFP or Ad5-HCN212. Control preparations (full rat sinoatrial node, black circles, n=6), sick sinus syndrome preparations (inferior rat sinoatrial node, blue circles, n=7) and sick sinus syndrome preparations injected with 1 X 10^8 pfu Ad5-GFP (green circles, n = 6) or 1 X 10^8 pfu Ad5-HCN212 (red circles, n=6) were cultured at 37°C as previously described. Extracellular potentials were recorded using 0.15 mm stainless steel bipolar electrodes. The pacing rate was averaged over each hour for the period 12-20 h. Data were analysed using 2-way ANOVA to compare the rate to that of the uninjected sick sinus syndrome model. *** $p<0.001$; NS, $p>0.05$ for all time points.

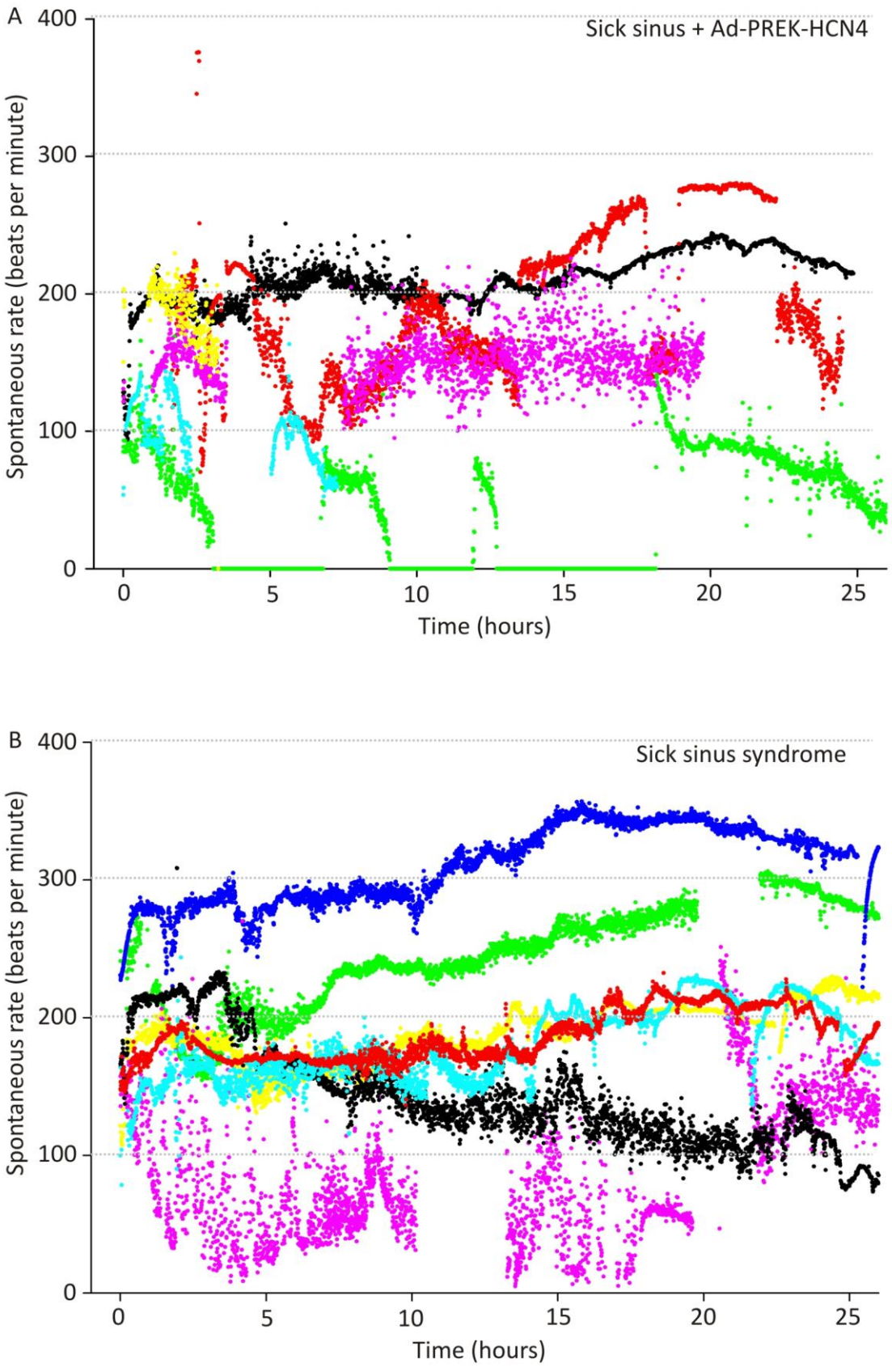

Figure 60. Spontaneous *ex vivo* pacing rates of the sick sinus syndrome model and the sick sinus syndrome model injected with Ad5-PREK-HCN4. (A) Ad5-PREK-HCN4 injected (n=6) and (B) uninjected sick sinus syndrome (inferior rat sinoatrial node, n=7) preparations were cultured at 37°C as described. Extracellular potentials were recorded using 0.15 mm stainless steel bipolar electrodes. Each dot represents a 30 second average rate. Differing colours distinguish individual preparations.

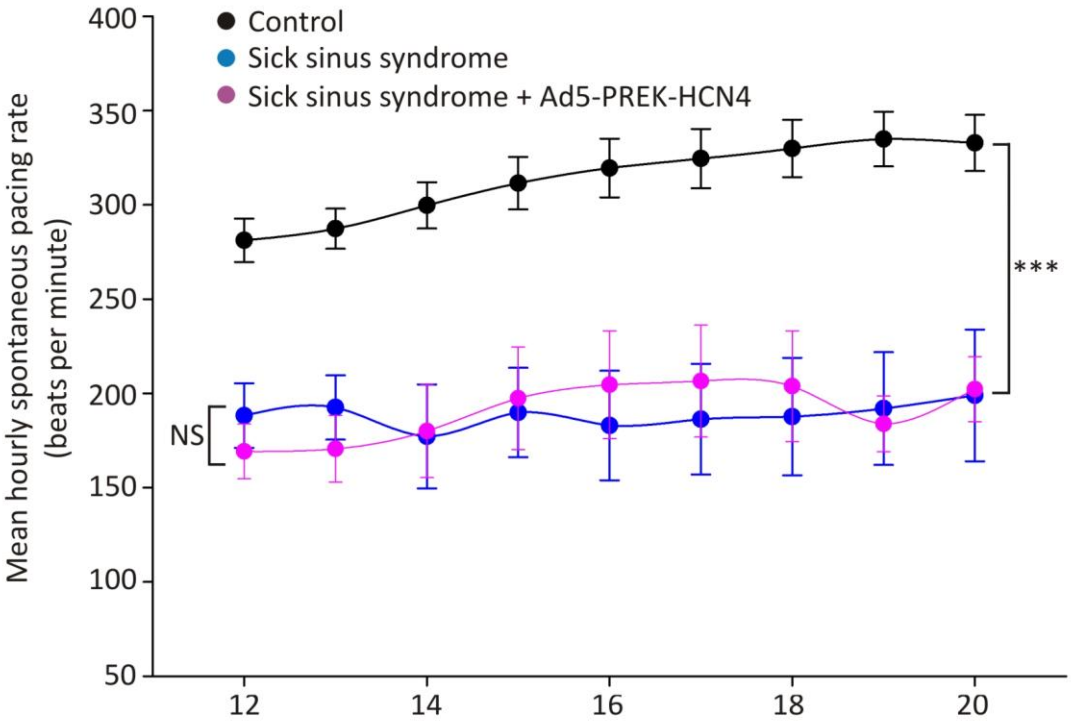

Figure 61. Average spontaneous *ex vivo* pacing rates of control sinoatrial node, the sick sinus syndrome model and the Ad5-PREK-HCN4-injected sick sinus syndrome model. Control preparations (full rat sinoatrial node, black circles, n=6), sick sinus syndrome preparations (inferior rat sinoatrial node, blue circles, n=7) and sick sinus syndrome preparations injected with 1 X 10^8 pfu Ad5-PREK-HCN4 (purple circles, n=3) were cultured at 37 °C as previously described. Extracellular potentials were recorded using 0.15 mm stainless steel bipolar electrodes. The pacing rate was averaged over each hour for the period 12-20 h. Data were analysed using 2-way ANOVA to compare the rate to that of the uninjected sick sinus syndrome model. *** $p<0.001$; NS, $p>0.05$ for all time points.

4. Discussion

4.1 Summary introduction

Biopacemaking is a dynamic research field that offers the hope of a cure for bradycardic heart rhythm disorders. The published literature demonstrates the capability of constructing a functional, if suboptimal, biopacemaker in the ventricular or atrial myocardium of whole animals.[385] The data presented here explores the feasibility of utilising an *ex vivo* model of SSS to study of biopacemaking via rejuvenation of a dysfunctional SAN. The use of an ex vivo experimental model would allow the rapid screening of potential biopacemaker target genes without the complexity and expense of large whole animal models. The novel approach of genetic manipulation of the SAN may be expected to be a superior strategy to generation of a *de novo* pacemaker in the working myocardium, due to the heterogeneity and specialisation of the SAN.[39]

4.2 Sinoatrial node culture

Experiments were performed to investigate the feasibility of *ex vivo* SAN culture and to assess whether culture induced significant changes or deterioration of the SAN tissue. Data presented here suggests that the cultures SAN tissue retains viable pacing function, continues to express ion channels plus functional gap junctions and does not undergo significant apoptosis or necrosis. Thus cultured SAN tissue should provide an acceptable substrate for the investigation of SAN function; this is discussed further in sections 4.2.1-4.2.4.

4.2.1 Null Hypothesis 1. The sinoatrial node from the rat, *Rattus rattus,* cannot be cultured *ex vivo* and the pacemaker activity cannot be sustained and monitored

Data presented in section 3.2.2 demonstrate the feasibility of SAN tissue culture *ex vivo* and the continuous monitoring of the extracellular potentials for experimental purposes thus supporting the rejection of this hypothesis. The spontaneous rate of the preparations followed a predictable pattern as seen in figures 34 and 35. There was an initial 23.5% acceleration of the rate over the first 21 h followed by a 42%

deceleration from the maximum between 21 and 45 h (figure 37). The changes in rate may be due to alterations in the level of ion channel expression or cell death, these possibilities are explored below. Alternatively the initial acceleration could be caused by death of the working myocardium of the RA attached to the preparation. The RA exerts a hyperpolarizing influence on the SAN thus shifting the MDP to a more negative value.[39] The consequence of this is that the diastolic depolarization takes longer to reach the threshold for AP activation and thus the cycle length is increased in a manner independent of the speed of the diastolic depolarization slope. Hence the loss of RA muscle might shift the MDP of the SAN to a more positive value and increase the pacing rate. This was not specifically investigated, but the idea is supported by the observation that in some peripheral portions of RA muscle thicker than 100 µm (away from the thinner areas that abut the SAN) there was loss of Cx43 expression in the central regions (figure 62). The expression of Cx43 has been noted to be sensitive to tissue culture previously in our laboratory.[386]

The most obvious explanation for the slowing of the rate seen after 21 h is tissue death or necrosis and this is addressed below. It might be expected that if this were the case then the rate would continue to decline with time rather than stabilising after 50 h as seen in figure 34. Perhaps this pattern could be explained by a reduction in cellular ATP levels (initially masked by the loss of the RA hyperpolarization)? Intuitively it might be argued that if this were the explanation then the rate should also continue to decline, but the level of cellular ATP might reach a steady state in culture that is lower than that *in vivo* where tissue perfusion via the microcirculation is optimal. An assay of cellular ATP levels was not undertaken.

4.2.2 Null hypothesis 2. Tissue culture will induce no significant change in the level of ion channel and gap junction expression of the sinoatrial node

The data in section 3.2.3 show no statistically significant change in the protein levels of the ion channel HCN4 or the gap junction Cx43 and therefore this hypothesis is accepted. The continued pacemaker activity and propagation of the

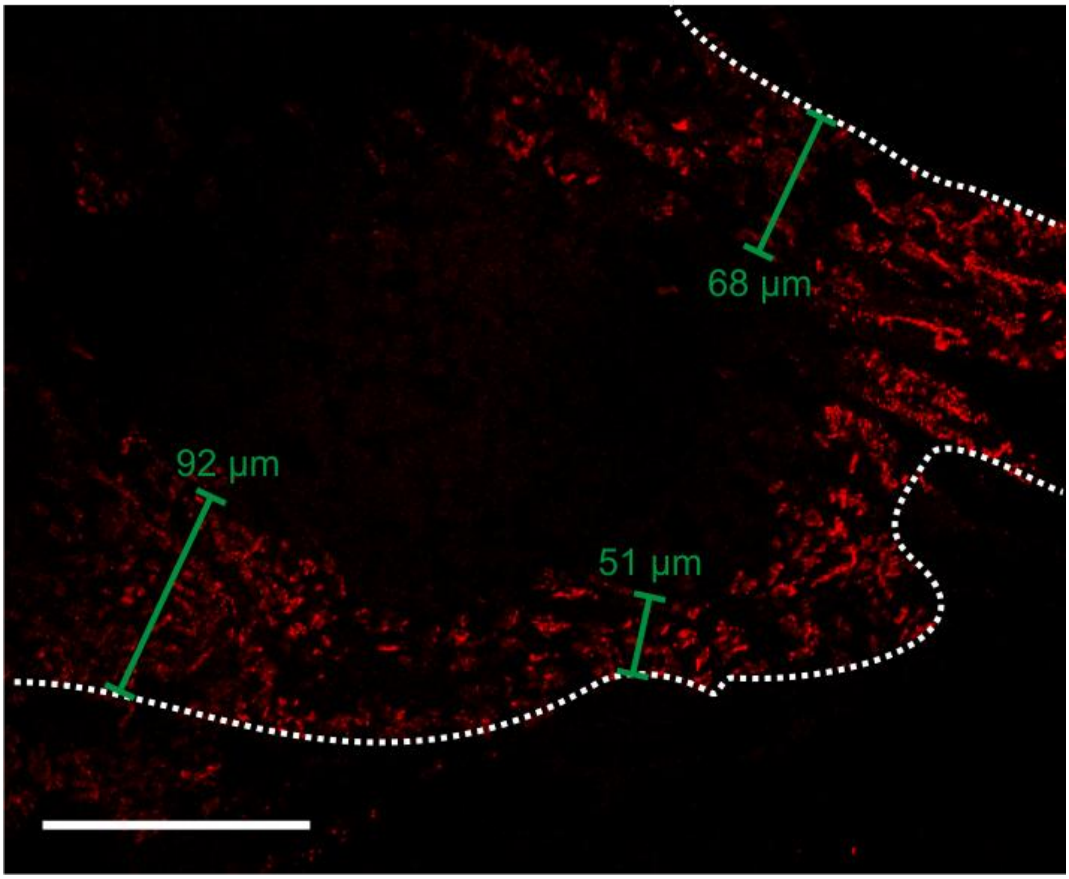

Figure 62. Loss of connexin-43 from the central region of the rat right atrial appendage during tissue culture. Following tissue culture for 48 h, 16 µm cryosections were prepared of the right atrial appendage. Immunohistochemistry reveals loss of connexin-43 expression from the central area of the muscle at depths beyond a maximum of 51-92 µm. This loss of connexin expression was not always seen (data not shown).

AP to the recording electrodes positioned in the RA muscle provides indirect evidence for the persisting presence of both the ion channels responsible for pacing activity and the gap junctions required for the transmission of the AP (figures 34-36). However, as mentioned above the pacing rate of the SAN tissue changes over at least the first 50 h in culture and one of the explanations for this observation could be changing levels of ion channel expression. Loss of Cx43 could uncouple the SAN from the RA thus removing the hyperpolarizing influence mentioned above. Theoretically, downregulation of HCN channels could lead to the reduction in pacing between 21 and 50 h.

The effective use of the tissue culture system to investigate the effects of RAd induced ion channel transduction requires a stable level of intrinsic gene expression. Quantitative immunohistochemistry did not demonstrate a statistically significant change in the expression levels of RA muscle (close to SAN) Cx43 or SAN HCN4 over 48 h of culture (figures 42 and 43). In addition to HCN4, there are many more ion channels, connexins and Ca^{2+} handing proteins involved in the generation of the diastolic depolarization and the AP in the SAN (see sections 1.4, 1.5 and Maltsev et al.[122]). It is possible that some of these other proteins are more sensitive to metabolic perturbations in the cells induced by tissue culture, but it was not feasible to investigate the full panel of these proteins. Furthermore, quantitative immunohistochemistry has limited sensitivity and poor internal controls. A more accurate assessment could have been performed using quantitative PCR normalised to a housekeeping gene such as GAPDH or ribosomal protein 28S. This technique is both time consuming and expensive. Furthermore immunohistochemistry was sufficient to provide reassurance that protein expression in the SAN tissue was not grossly altered to a level that would render the model ineffective.

For all of the above reasons we elected to perform the experiments between 16-20 h culture, during this time the spontaneous pacing rate was stable and there would be no appreciable change in ion channel expression (figures 36, 42 and 43).

4.2.3 Null hypothesis 3. Tissue culture will induce no cellular apoptosis in the sinoatrial node

The data presented in section 3.2.3 show that there were no observed morphological features of apoptosis and that levels of activated caspase-3 were not elevated in response to tissue culture for 48 h and thus this hypothesis is accepted. The histological sections in figures 39 and 40 do not show histological features of apoptosis (e.g. membrane blebbing, nuclear condensation, cell fragmentation and cell shrinkage). The positive control in figure 39C demonstrates nuclear fragmentation and cell membrane blebs induced by camptothecin. Other features are not present in the positive controls suggesting that the late features of apoptosis may not have developed by 48 h. Measurement of the cell diameter (figure 41) shows that there is a significant decrease in the cell size of RA cells during tissue culture, which could be interpreted as evidence of apoptosis, but the SAN cell size is unaffected.

In figure 44D there is a trend towards increased detection of activated caspase-3 in cultured RA tissue, though the difference is not statistically significant. Cardiomyocyte apoptosis is thought to occur only in disease and thus it would be expected that there are negligible levels of apoptosis at the start of the experiment (T=0).[387] There is detectable immunofluorescence seen in figure 44D suggesting that there is a degree of non-specific binding in this assay. Indeed, if figure 44B is compared to the positive control in figure 44C the pattern of fluorescence differs. It is possible that the apparent (non significant) increase in caspase-3 levels in after 48 h culture is due in part to the levels of non-specific antibody binding. It is difficult to control accurately for this phenomenon using this technique. An additional TUNEL assay of apoptosis may clarify these results. The data may be confounded by the existence of caspase independent pathways of apoptosis that would not be detected by the caspase-3 assay. However, the importance of these mechanisms is debated.[388]

4.2.4 Null hypothesis 4. Tissue culture will induce no changes in cell or tissue histology of the sinoatrial node or right atrial myocardium

The data in section 3.2.3 are conflicting, and in totality cannot lead one to convincingly accept or reject this hypothesis. The gross morphology of the node following 24 h of culture shows pallor that may suggest tissue oedema or loss of myoglobin from the tissue (figure 38). There is no structural deformation of the preparation. Analysis of the cell size during culture reveals that the cell diameter of the RA cells reduced during culture while the SAN cells were unaffected (figure 41). Masson's trichrome staining and light microscopy suggests that the histology of the RA tissue was similar to the control (at the beginning of the experiment), but the SAN cells appear pale with increased presence of connective tissue (figures 39 and 40).

The process of cryosectioning and histological staining of cultured tissue was difficult. Anecdotally, the tissue sections were more friable than uncultured tissue. Furthermore, following culture the uptake of the stains was patchy and unreliable. The consequence of this is that the utility of histology as a method of assessing the effect of tissue culture on the viability of the cultured SAN and RA tissue is questionable. The apparent increase in connective tissue is surprising; it seems unlikely that the process of gene activation, transcription and translation could occur in sufficient quantity to be seen by simple histological techniques and light microscopy by 48 h. Further analysis is required to provide reliable data in this aspect. Rather than reliance on visual inspection the SAN could be accurately identified using markers such as HCN4, ANP or Cx43 and the extracellular matrix could be accurately investigated using a picrosirus red stain for collagen, immunohistochemistry for collagen or a qPCR array for extracellular matrix and adhesion proteins. However, this detailed assessment is beyond the scope of the current work.

4.3 Sick sinus syndrome model

SSS is a heterogeneous disease with multiple causes (see section 1.6) and a varied clinical phenotype. One of the most important features is that of bradycardia,

hence the need for electronic pacing in these patients.[389] A whole animal model of SSS has been created by ablation of the leading pacemaker site in pigs.[318] In addition to the cost of large mammals, this approach requires the use of the CARTO mapping system (or similar) which requires significant set up costs, ongoing expensive consumables and considerable operator expertise. The development of an *ex vivo* system would allow cheap and rapid investigation of approaches to biopacemaking in SSS.

It has previously been established that the culture of SAN tissue is possible (sections 4.2.1 – 4.2.4). Data in this section demonstrates that it is possible to modify the SAN preparation to create a bradycardic SSS model that shares some, but not all, features of the SAN, depends partly on I_f for pacemaking and is responsive to β-adrenergic stimulation.

4.3.1 Null hypothesis 5. The spontaneous pacing rate of the sick sinus syndrome model is not significantly different to the intact (control) preparation

The very crux of this model is that the spontaneous pacing rate is slower than the control preparation that contains the body of the SAN. The data in section 3.3.2 demonstrate that the SSS model is significantly bradycardic at all time points when compared to the control SAN and hence this hypothesis is rejected (figures 35 – 37). It can be seen in figure 35 that the rate of the SSS model is more unpredictable than that of the control SAN. There may well be variation in the position of the fossa ovalis as well as the extent of the tail of the SAN down the CT such that the amount and phenotype of the remaining nodal tissue is disparate in the sample group. Indeed, the tail of the human SAN is certainly variable in nature.[26] Another contributor to this pattern of pacing activity may be that the subsidiary pacemaker tissue is less stable and reliable than the body of the SAN, the usual native pacemaker.

4.3.2 Null hypothesis 6. The primary histological and immunohistochemical features of the subsidiary pacemaker do not differ from that of the sinoatrial node

Taken as a whole, the data in section 3.3.3 show that the subsidiary pacemaker differs from the body of the SAN and therefore this hypothesis is rejected. Given that the pacemaker rate of this tissue is slower, and perhaps more unstable, than the true SAN it should be expected that the ion channel fingerprint will differ. What is also evident is that the subsidiary pacemaker tissue is distinct from the RA muscle at the same anatomical level.

As discussed in section 1.5, the molecular motif of the human SAN is characterised by (among other things) a high level of expression of HCN1, HCN4 and Cav1.3, with low or no expression of Cx43 and $Na_V1.5$. Qualitative immunohistochemistry revealed that the leading pacemaker site in 5/6 of the SSS models were HCN4 negative and Cx43 positive (figures 47, 48 and Appendix A6), quantitative data are not available.

It is known that SAN cells are smaller than RA working myocardial cells, central SAN cells are 5-10 μm in diameter (RA cells are 15-20 μm in diameter, section 1.3).[39] The cell diameter at the SSS leading pacemaker is similar to this at 10.3 ± 0.6 μm and was not significantly different to the body of the rat SAN (figure 49). Thus in this respect this subsidiary pacemaker tissue bears similarity to the SAN. The further implications of the immunohistochemistry and cell size data are discussed below.

4.3.3 Null hypothesis 7. There is no significant contribution of I_f to pacemaker activity in the subsidiary pacemaker

&

4.3.4 Null hypothesis 8. The subsidiary pacemaker is not responsive to β-adrenergic stimulation

The lack of immunohistological evidence for the presence of HCN4 at the subsidiary pacemaker site questions the importance of I_f for pacemaker activity in this tissue.

Furthermore, if this is the case, there may be little chronotropic adaptability of the SSS model due to the central role of HCN channels in mediating the pacing response to β–adrenergic stimulation. The data in section 3.3.3 demonstrate an unequivocal prolongation of the cycle length of the SSS preparation in the presence of I_f blockade by 2mM CsCl and shortening of the cycle length in the presence of 100 µM isoprenaline (figure 50). Under these conditions, the pacing rate was slowed by 37.8% and increased by 42.5% respectively. These data support the rejection of null hypotheses 7 and 8.

4.3.5. Summary and discussion of the characteristics of the sick sinus syndrome model

Blockage of I_f in intact rabbit SAN tissue has been previously reported to slow the pacing rate by between 12% and 16%.[390] However, the potency of this effect varies depending on the exact nature of the SAN tissue tested. The greatest effects are seen in peripheral SAN tissue - a rate decrease of 19% was observed in peripheral SAN tissue, but only 7% in central SAN tissue.[390] These published results represent SAN cells at a maximum of 2.5 mm from the leading pacemaker site in the rabbit, less than 50% of the distance to the IVC. Therefore the data presented here suggest that this gradient in characteristic away from the leading pacemaker site continues in the subsidiary pacemaker tissue that is found along the CT. The interpretation of these findings is that the contribution of I_f to DD (but not necessarily HCN4 expression levels – see below) is increased in peripheral SAN and subsidiary pacemaker tissue.

The effect of I_f blockade on the pacing rate demonstrates the importance of this current in pacemaker activity of the subsidiary pacemaker. So why is there no detectable HCN4 in the majority of these samples? Furthermore, a previous study using qPCR has failed to demonstrate HCN4 outside the central SAN, in the CT, in rabbits (subsidiary pacemaker regions were not specifically studied).[41] As previously discussed in section 1.5, HCN2 is the predominant isoform in the rat, hence the level of HCN4 in this subsidiary tissue may be below the threshold for detection by immunohistochemistry. The process of cellular pacing is not simply slave to I_f

density. The interplay between I_f and $I_{K,1}$ is discussed in detail in section 1.4, the ratio of the two currents is vitally important in the modulation of pacemaker activity, hence low levels of I_f could still be instrumental in pacemaking if other cellular ion channels, especially $I_{K,1}$, were appropriately down-regulated.[58]

In many respects the subsidiary pacemaker can be considered as the extreme periphery of the SAN. The phenotypic differences between central and peripheral SAN cells of the rabbit SAN have been a topic of significant research interest, though some of the evidence is conflicting. Central cells are thought to be smaller than the peripheral SAN cells, therefore immunohistochemistry and patch clamp experiments have been performed to compare the characteristics of low capacitance (small, central) and high capacitance (large, peripheral) SAN cells. Interestingly, peripheral cells appear to display faster pacing activity with a higher I_f and I_{Na} current densities when compared to central cells, and the I_{to} density (as well as other current densities) is positively correlated with cell size.[52, 53, 194] One study appears to show that the labelling of the Ca^{2+}-handling proteins SERCA, RYR, NCX and the L-type subunit α1C is increased in the periphery and is associated with a lower $I_{Ca,L}$ current density.[147] However these findings are disputed in a study of Ca^{2+} handling proteins in isolated rabbit SAN cells by Lyashkov et al who found no correlation between the density of NCX, RYR or SERCA proteins with cell size, they also failed to demonstrate any variation in AP morphology.[148] These findings are disputed by some on the basis that the sample may not have included true peripheral SAN cells.[391] Others have previously failed to demonstrate a correlation between $I_{Ca,L}$ and cell size.[194]

As mentioned above I_f blockade caused a profound decrease in the pacemaker rate of the SSS preparation in comparison to published data from the intact SAN of the rabbit. The response to isoprenaline is also in excess of that expected. Maximal dose isoprenaline caused an increase in the pacing rate of 20%-26% in isolated rabbit SAN cells.[392, 393] The variation in cellular pacing mechanisms discussed above may render these cells more sensitive to both I_f blockade and β-adrenergic stimulation. These findings could have implications for the mechanisms behind the induction of atrial arrhythmia by adrenergic stimulation. The potency of the effect

of isoprenaline may be explained by the apparent dominant contribution of I_f to pacemaking in this tissue - the co-application of CsCl and isoprenaline to the tissue may provide some clues as to the ionic currents mediating the chronotropic response in this tissue.

Work on subsidiary pacemaker tissues of the eustachian ridge and AV valves in cats and of the low right atrium in dogs have also demonstrated a dependence on, and sensitivity to, β-adrenergic stimulation.[208-211] The pacemaker mechanism in such tissues was proposed to be similar to that of the SAN, with early Cs^+-sensitive and late ryanodine-sensitive component to DD.[211] However, comment has not been previously made regarding the magnitude of this response in comparison to the SAN. Further work is needed on subsidiary pacemaker mechanisms.

It might initially seem surprising to find the presence of Cx43 in pacemaker tissue; however, this may be of significant physiological importance *in vivo*. Coupling to the RA muscle via high conductance gap junctions comprising Cx43 would potentially strongly hyperpolarise the subsidiary pacemaker tissues; ergo the pacing rate would be suppressed below that of the central SAN preventing atrial ectopic rhythms. This same concept may explain why large peripheral SAN cells (Cx43-positive) have a faster pacing rate when disaggregated, but the small central SAN cells (Cx43-negative) are the leading pacemakers in whole tissue samples. Cardiac conditional Cx43 knockout mice are principally susceptible to abnormal cardiac conduction leading to lethal ventricular arrhythmias.[394] However, knockout mice deficient in Cx40, the other high conductance gap junction in working myocardium, display atrial arrhythmia and ectopic atrial pacing foci.[181]

Though the data are mixed, the implication of all of the above is that there is significant variation in the ion channel expression and current density away from the centre of the SAN. Elucidation of the pacemaker mechanisms at play in the SSS model would require sensitive assays of the ion channel expression profile, perhaps using micro-dissection and qPCR. Comparison of the effect of a panel of channel blockers (for example CsCl, 4AP, TTX, ryanodine and nifedipine) may provide

interesting insights into the pacemaker mechanisms of peripheral and subsidiary pacemaker tissues.

4.4 Adenovirus-mediated transgene expression in cardiac tissue

The expression of functional ion channels in the working myocardium *in vivo* is a principle established by the published biopacemaker research.[385] Such gene expression has not to date been demonstrated in SAN tissue.

4.4.1 Null hypothesis 9. Adenovirus mediated gene expression in the sinoatrial node or subsidiary nodal tissue is not viable

The data in section 3.4.2 clearly demonstrate high levels of β-galactosidase expression in the intervacal area at the injection sites of Ad5-PREP-LacZ. Immunohistochemistry using markers for the SAN confirmed that this gene expression occurs in the SAN tissue. The β-galactosidase expression was not limited to the SAN tissue and there does not appear to be any obvious tissue tropism for the RA muscle or SAN tissue (figures 51 and 52). Therefore this hypothesis is rejected. The data from experiments using Ad-GFP-HCN2, discussed below, further supports this conclusion (figures 53 and 54).

4.4.2 Null hypothesis 10. The right atrium intercaval area is not receptive to adenovirus mediated ion channel expression

As shown in section 3.4.2, the injection of Ad5-GFP-HCN2 into the SSS model lead to localised expression of GFP and HCN2 and thus this hypothesis is rejected. The immunohistochemistry performed on cryosections also demonstrated that the HCN2 protein was correctly trafficked to the cell membrane (figure 54).

4.5 Biopacemaking

As discussed in section 1.7, there is mounting evidence that biopacemaking can reduce electronic pacemaker-dependence in animal models of AVN disease and SAN disease.[385] These approaches use the expression of HCN channels in working myocardium. Data presented here show that the use of subsidiary pacemaker tissue as the biopacemaker substrate is an alternative strategy.

4.5.1 Null hypothesis 11. The spontaneous pacing rate of the sick sinus syndrome model will not be increased by injection of adenovirus that carries a transgene for a functional ion channel (Ad5-HCN212 or Ad5-PREK-HCN4)

Expression of HCN4 in the SSS syndrome did not significantly impact on the pacing rate of the SSS (figures 60 and 61). Due to time constraints the Ad5-PREK-HCN4 experiments were curtailed at n=3, although $p>0.05$ the test is underpowered, increasing the risk of a type II statistical error, so this result should be interpreted with caution. However it appears in figure 60 that HCN4 expression appears to slow the pacing rate or stop it altogether in some preparations (green, blue and yellow traces – not included in the analysis figure 61. This pattern was not seen in any of the other RAd experiments. Given that HCN4 is the predominant isoform in many mammalian species, it might be expected that expression of HCN4 in the subsidiary pacemaker would have a profound effect on the pacing rate through acceleration of the membrane clock.

It is difficult to offer an explanation for the slowing of the rate and unstable pacing seen with Ad5-PREK-HCN4. Further experiments are required to ascertain whether this represents a real effect or experimental error. If the unstable pacing is reproducible, then one explanation could be that high levels of HCN4 expression suppress pacemaker activity via permanent hyperpolarization of the SAN cells. Through this mechanism, a high density of I_f has been demonstrated to silence biopacemakers created in RA myocytes.[395] If this were the case, then I_f blockade with increasing concentrations of ivabradine would first stabilise the pacemaking, then slow the rate of the SSS model injected with Ad5-PREK-HCN4.

HCN212 did significantly increase the pacing rate towards that of the control preparation (figure 59), which supports the rejection of this null hypothesis. How could this difference in effect between the two isoforms be explained? HCN4 has the slowest kinetics of the cardiac isoforms (section 1.4) and so may not be suited to the demands of pacing in small rodents with rapid heart rates. This could explain why the f-channels in rats comprise mainly of HCN2. The kinetics of HCN212 are

faster even than HCN2 as shown in figure 63.[372] In a small rodent with a heart rate of 300-400 bpm, the cycle length will be between 150-200 ms requiring f-channels with rapid kinetics for I_f to make a significant contribution to DD, the activation time constant of HCN4 is almost twice that of HCN2.[310] The development of biopacemakers for larger mammals will require careful consideration of this fact, and engineered pacemaker channels will be required to provide physiological pacing rates appropriate for humans.

The application of experimental animal data to the development of biopacemakers may prove difficult. There is ongoing debate regarding the mechanisms of cardiac pacemaking. [139, 396] The focus of much of this discussion is the membrane clock versus the Ca^{2+} clock.[123] It is clear that the membrane and Ca^{2+}clocks are interdependent, but their relative contributions to pacemaking are not known.

It is likely that the variation in pacing mechanisms between species leads to a large spread of data and thus to some of the difficulty in unifying the theories of pacemaking. Variation in cellular pacing mechanisms is to be expected when it is considered that the heart rate in small rodents is between 300-500 bpm, but in larger mammals is 50-100 bpm. Indeed inter-species variation of the contribution of the ionic currents to pacing has been noted. For example I_f is found in SAN cells of most species, $I_{K,1}$ can be recorded from SAN cells of the rat and monkey, thus theoretically reducing the contribution of I_f in these species.[397] Furthermore, while $I_{K,r}$ and $I_{K,s}$ decay contributes to DD in guinea-pig SAN cells, only $I_{K,s}$ is present in porcine SA nodal cells and only $I_{K,r}$ in the rat and rabbit.[397] Thus variation is also expected in the impact of blocking or reducing each current between species. While it is known that defective HCN4 causes significant bradycardia in zebra fish and humans (see section 1.4), an HCN4 knockout mouse does not show bradycardia (though subtle SAN dysfunction is detectable).[398] Such arguments also apply to the Ca^{2+}clock. The contribution of $I_{Ca,T}$ has an roughly inverse relationship to the heart rate; there is a large contribution of $I_{Ca,T}$ in the SAN of mice and rats, modest in rabbit SAN, minimal in canine SAN cells and none in swine SAN cells (which begs the question as to how the Ca^{2+}clock can be integrated into DD in the SAN of the pig).[124, 126, 396, 397]

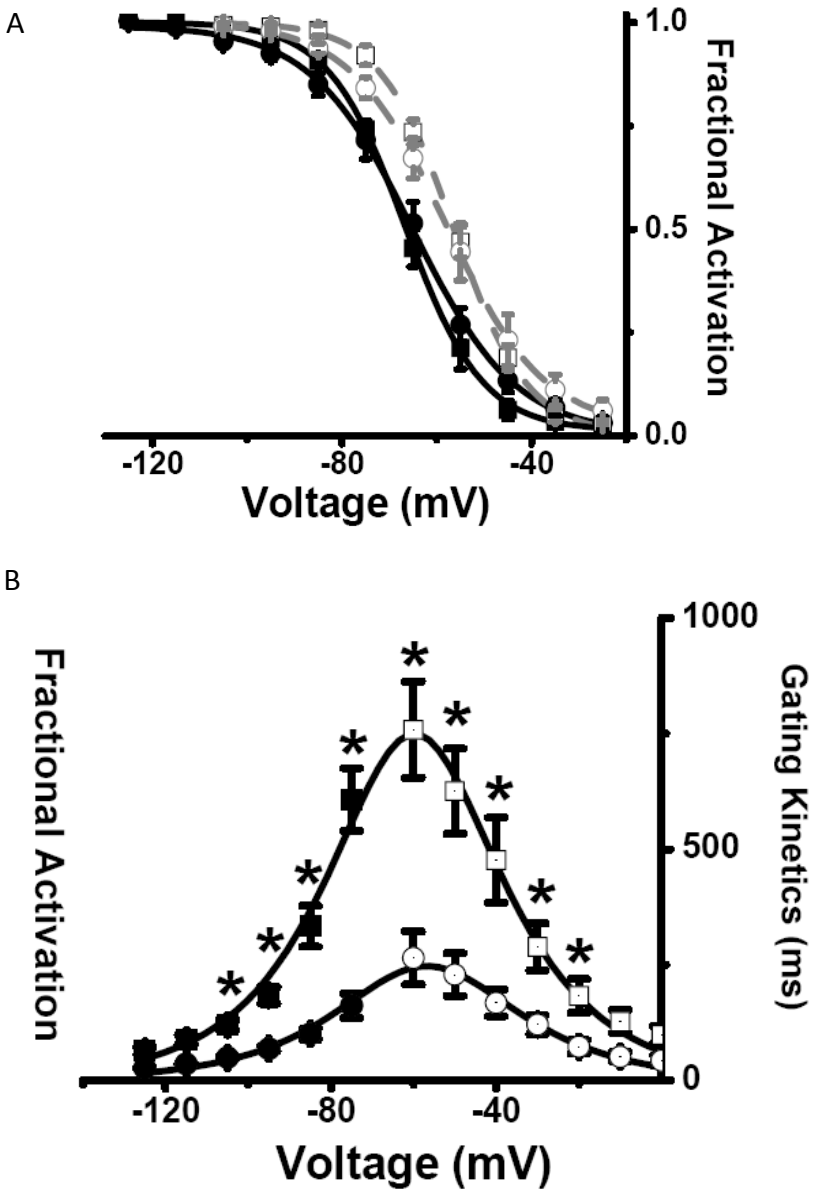

Figure 63. Steady-state properties of HCN2 and HCN212 in neonatal rat ventricular myocytes. A) Activation-voltage relation of HCN2 (squares) and HCN212 (circles) with (black symbols) and without (grey symbols) cAMP. B) Voltage dependence of activation (black symbols) and deactivation (white symbols) time constants of HCN2 (squares) and HCN212 (circles). From Xin et al.[372]

It is also not clear as to how much each clock influences the chronotropic response to autonomic modulation. β-adrenergic stimulation and acetylcholine cause a positive and negative shift the activation curve of I_f respectively.[79, 109] Furthermore, HCN channels are known to co-localise with β-receptors.[114] The consequent direct activation of HCN channels by cAMP provides a mechanism for autonomic modulation of the heart rate, but in some studies disabling the protein kinase-A phosphorylation-dependent Ca^{2+} cycling almost completely inhibits autonomic modulation, even though HCN channels are thought not to be phosphorylation-dependent.[153] In canine SAN cells, blockage of CICR by ryanodine has a profound effect on autonomic modulation of heart rate and the I_f blocker CsCl does not abolish autonomic modulation.[396, 399] So the development of a physiologically appropriate and adaptive biopacemaker may prove more demanding than currently expected.

4.5.2 Null hypothesis 12. The spontaneous pacing rate of the sick sinus syndrome model will not be increased by injection of adenovirus that does not carry a transgene for an active ion channel (Ad5-GFP or Ad5-GFP-HCN4Δ)

The control viruses for the biopacemaker experiments expressed green fluorescent protein or a non-functional ion channel, HCN4Δ. Neither Ad5-GFP or Ad5-GFP-HCN4Δ produced significant change in the pacing rate of the SSS model and therefore this null hypothesis is accepted. The patch clamp experiments in section 3.4.1.2.2 do not show convincing evidence of I_f (figure 25), and subsequent sequencing of the Ad5-GFP-HCN4Δ genome showed multiple deletions (Appendix A5).The immunohistochemistry does appear to show the HCN4 channel at the cell membrane of Cos7 cells (figure 24); the reason for this is not clear. The staining appears to be specific as there is no HCN4 signal in the control experiment using Ad5-GFP (figure 24B), an epitope of the HCN4 protein may have been preserved and trafficked to the cell membrane, although this seems unlikely as the DNA sequence predicts a mis-sense mutation.

5. Summary and future directions

Data presented here provide proof of concept for biopacemaking as a potential therapy for SAN disease. To further investigate this strategy, a large mammal, *in vivo* model of SSS requires development. It is hoped that expression of an HCN transgene in the modified SAN will increase the intrinsic heart rate of the experimental animal while retaining physiological autonomic control.

The use of the *ex vivo* model presented here allows inexpensive screening of potential transgenes and modes of delivery for use in biopacemaking. The selection of the biopacemaker strategy is increasingly recognised as an important and difficult process due to the context-dependence of cardiac ion channels.[299] The heterogeneity of the SAN means that ion channels previously demonstrated to provide effective pacemaking in RA or ventricular myocardium may not be suitable for SAN applications. Though previously shown to be ineffective in ventricular muscle, in this model mHCN212 appeared to be effective in the bradycardic SAN.[319]

The complex pacemaker mechanisms of the SAN not only mean that the selection of the biopacemaker gene is difficult, but also that there is a myriad of target genes. Using the model developed and presented here we aim to investigate biopacemaker mechanisms outside of the 'HCN axis' such as the Ca^{2+}-handling proteins, and to also explore the effectiveness of dual gene expression (e.g. I_f expression with I_K suppression). There is also the utility to explore additional vector systems including AAV and plasmid based systems.

The subsidiary pacemaker tissue identified as the biopacemaker target has been partly characterised here and shows some similarities to subsidiary pacemaker tissue previously described. As discussed in detail above, further work using microdissection, qPCR and functional assessment by channel blockade will help elucidate the details of the pacemaker mechanisms involved.

There are many exciting developments in the new field of biopacemaker research with hope of delivering a novel therapy for bradycardia within the next decade. The

acceleration of a diseased SAN, demonstrated for the first time here, is the first step down a new avenue of investigation.

Appendices

Appendix A1. Solutions and reagents

All reagents from Sigma-Aldrich unless stated otherwise.

Tyrode's solution

Tyrode's solution was prepared using 120 mM NaCl, 4 mM KCl, 1.3 mM $MgSO_4.7H_2O$, 1.2 mM $NaH_2PO_4.2H_2O$, 1.2 mM $CaCl_2$ (2.4 mM for electrophysiology experiments), 25.2 mM $NaHCO_3$ and 5.8 mM D-glucose (11 mM for electrophysiology experiments) in dH_2O. If required the solution was filter sterilised (Steritop 0.2 µm pore, Fisher Scientific)

20 x SSC

3M NaCl, 0.3 M NaCitrate, pH 7

Southern Blot Buffers

Pre-hybridisation solution: 5x SSC, 1% Blocking reagent (Roche), 0.1% N-lauroylsarcosine, 0.02% SDS. Heat to 60°C for 30 min, store at -20 °C.

Buffer 1: Tris-HCl 100 mM, NaCl 150 mM, pH 7.5

Buffer 2: Tris-HCl 100 mM, NaCl 150 mM, 1% Blocking reagent (Roche), pH 7.5. Heat to 60 °C for 30 min, store at -20°C.

Buffer 3: Tris-HCl 100 mM, NaCl 150 mM, $MgCl_2$ 50 mM, pH 9.5

Buffer 4: Tris-HCl 10mM, EDTA 1mM , pH 8.0

Colour substrate: 45 µl NBT solution (Roche), 200 µl reagent 9 (Roche), 35 µl X-Phosphate solution (Roche), 10ml buffer 3

Luria Bertani broth (LB broth)

400 ml dH_2O, 8 g Luria Bertani powder, sterilised by autoclaving, if required 0.05 mg/ml kanamycin or 0.05 mg/ml ampicillin was added.

Luria Bertani agar (LB agar)

400 ml dH_2O, 8 g Luria Bertani powder, 4 g agar (Invitrogen), sterilised by autoclaving. If required 0.05 mg/ml kanamycin or 0.05 mg/ml was added then 20-25 ml was poured into each of 20 sterile petri dishes (VWR) and allowed to set at room temperature. Petri dishes were stored at 4°C for a maximum of 14 days until required.

Phosphate buffered saline (PBS)

PBS was reconstituted from powder into 1 l dH_2O according to the manufacturer's instructions.

1% agarose gel

2 g of molecular biology grade agarose (Severn Biotech) was added to 200 ml tris-acetate-EDTA (TAE) buffer and the mixture was heated to boiling in a microwave. The solution was allowed to cool for 20-30 min and then poured carefully into a gel tray and allowed to set.

1 x TAE buffer

TAE buffer was prepared in dH_2O containing 40 mM Tris-acetate and 1 mM EDTA.

293 medium

500 ml minimum essential medium (MEM, Gibco) was supplemented with 5 ml 100x MEM non essential amino acids (Gibco), 50 ml foetal bovine serum (Gibco) 500 units/ml penicillin, 0.5 mg/ml streptomycin and 2 mM L-glutamine then stored at 4 °C.

SAN medium

500 ml UltraCULTURE medium (Biowhittaker) was supplemented with 2 µg/ml vitamin B12, 500 units/ml penicillin, 0.5 mg/ml streptomycin and 2 mM L-glutamine then sterile filtered (Steritop 0.2 µm pore) and stored at 4 °C.

CsCl gradient purification

Tris-EDTA buffer: 10 mM tris-hydrochloride with mM EDTA 1 in dH2O sterilised by autoclave.

CsCl buffer A: 10mM tris-hydrochloride, 1 mM $MgCl_2$, 135 mM NaCl in dH2O sterilised by autoclave.

CsCl buffer B: 10 mM tris-hydrochloride, 1mM $MgCl_2$, 135 mM NaCl in dH2O with 10 % glycerol sterilised by autoclave.

X-Gal staining solution

20 ml X-Gal staining solution was prepared in 0.01 M PBS containing 42 mg $C_6N_6FeK_4$ (potassium ferrocyanide), 32 mg $C_6N_6FeK_3$ (potassium ferricyanide), 8 mg $MgCl_2$, 20 mg 5-Bromo-4-Chloro-3-Indolyl-D-Galactoside (X-Gal) dissolved in 500µl DMSO.

Appendix A2. Cloning strategies

A) pShuttle-PREK-HCN4

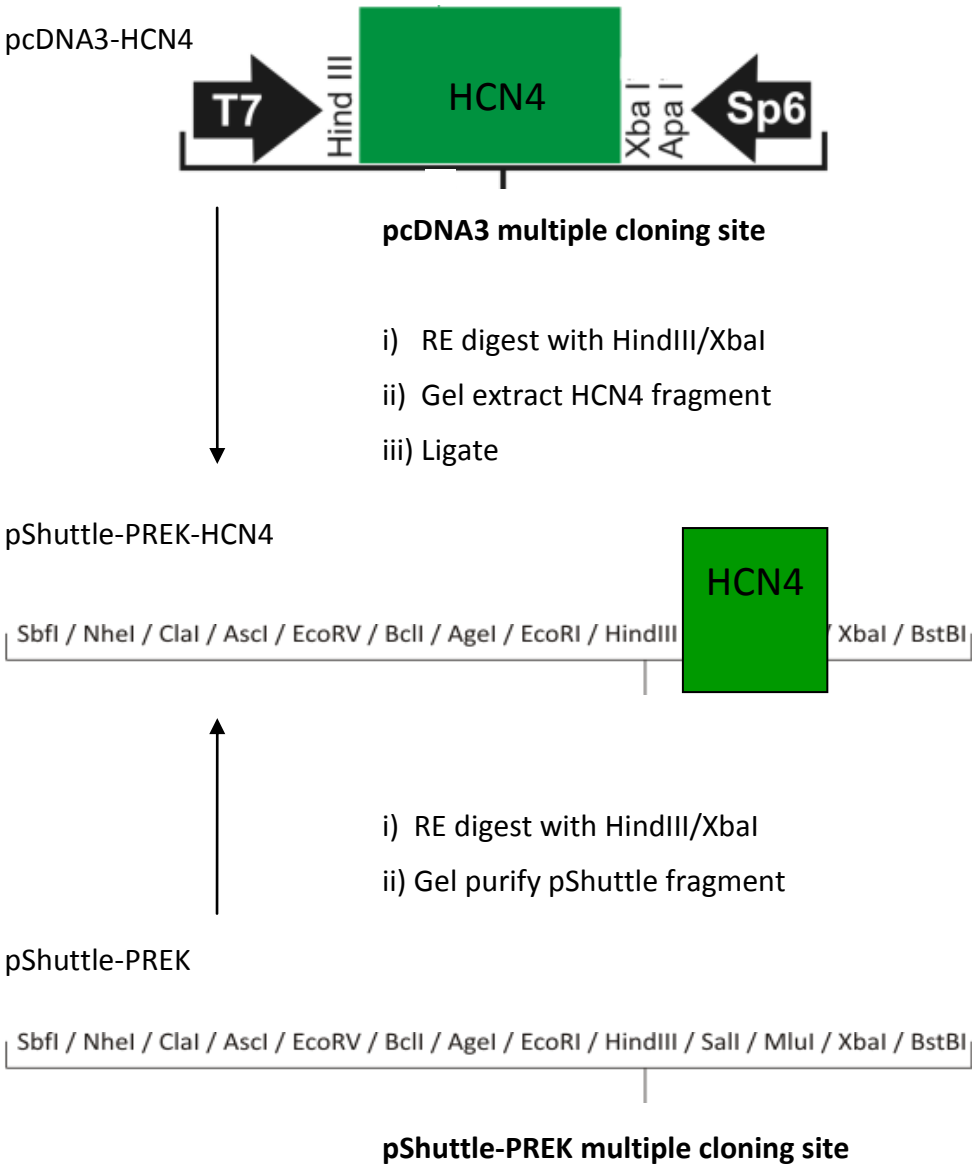

B) pShuttle-IRES-GFP-HCN4

pShuttle-PREK-HCN4

i) Digest with XbaI and BstBI

ii) Gel purify cut plasmid

iii) Ligate oligonucleotide Xba/Xho/BstBI

pShuttle-PREK1P-X-HCN4

i) Digest with NheI and XhoI

ii) Gel purify HCN4 fragment

iii) Ligate

pShuttle-GFP-HCN4

i) Digest with NheI and XhoI

ii) Gel purify cut plasmid

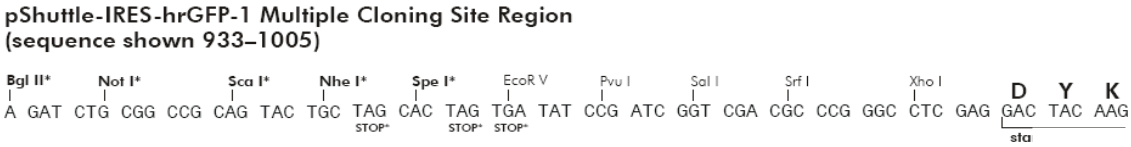

Figure 64. Cloning strategy for Ad5-GFP-HCN4 and Ad5-PREK-HCN4. A) (Previous page). Schematic representation of the cloning of pShuttle-PREK-HCN4. mHCN4 was isolated from pcDNA3-HCN4 by RE digestion with HindII/XbaI and gel extraction (top). The fragment was then ligated into the vector pShuttle-PREK that had been cut with HindIII/XbaI and gel purified (bottom) to provide complementary ends for mHCN4. B) Schematic representation of the cloning of pShuttle-IRES-GFP-HCN4. mHCN4 was isolated from pcDNA3-HCN4 by the introduction of a XhoI restriction site and then RE digestion with NheI/XhoI and gel extraction (top). The fragment was then ligated into the vector pShuttle-IRES-hrGFP that had been cut with NheI/XhoI and gel purified (bottom) to provide complementary ends for mHCN4.

Appendix A3. Oligonucleotides

The sequence of the oligonucleotide 'XbaI/XhoI/BstBI' used in the cloning of pShuttle-IRES-GFP-HCN4 is shown below.

XbaI XhoI BstBI

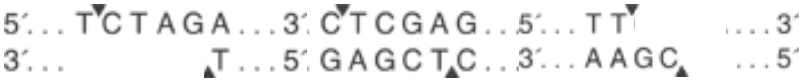

Appendix A4. Reference plasmids

pcDNA3-mHCN4

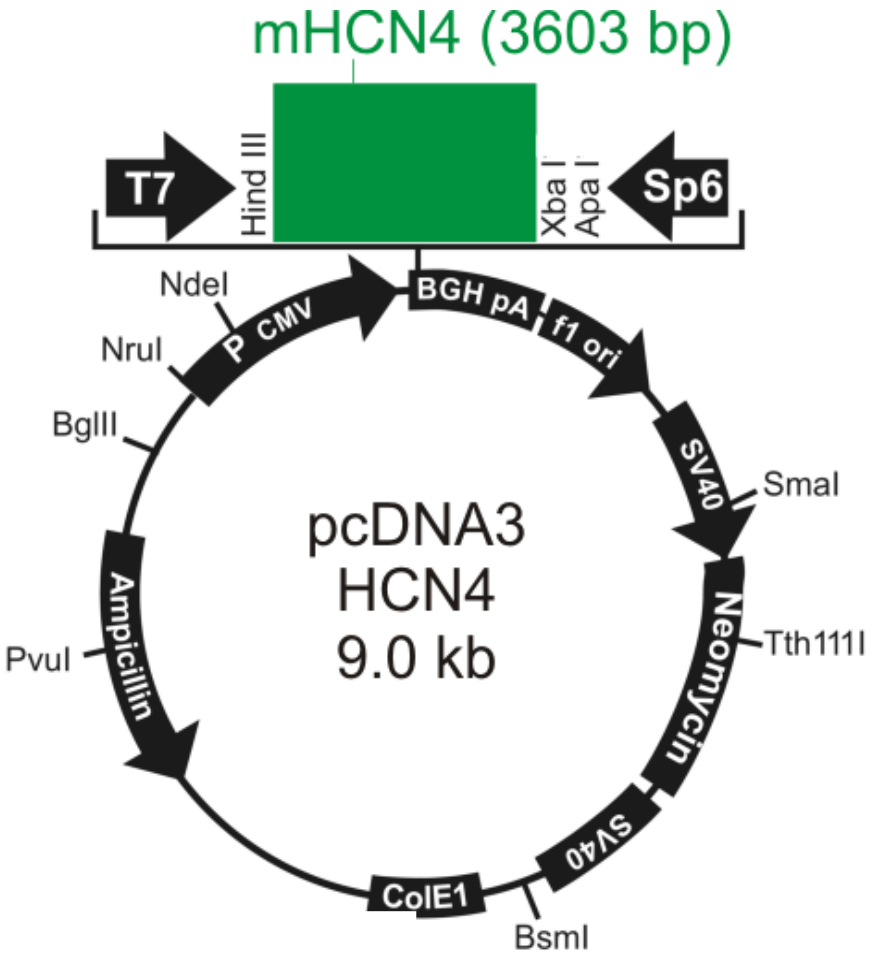

Figure 65. Plasmid map of pcDNA3-HCN4. BGH pA, bovine growth hormone polyadenylation signal; f1 ori, filamentous bacteriophage f1 origin of replication; SV40, simian vacuolating virus 40 polyadenylation signal; Neomycin, neomycin antibiotic resistance gene; ColE1, ColE1 origin of replication; ampicillin, ampicillin antibiotic resistance gene; pCMV, cytomegalovirus promoter; T7, bacteriophage T7 promoter; Sp6, bacteriophage SP6 promoter; remaining abbreviations refer to restriction endonuclease cleavage sites

pShuttle-PREK

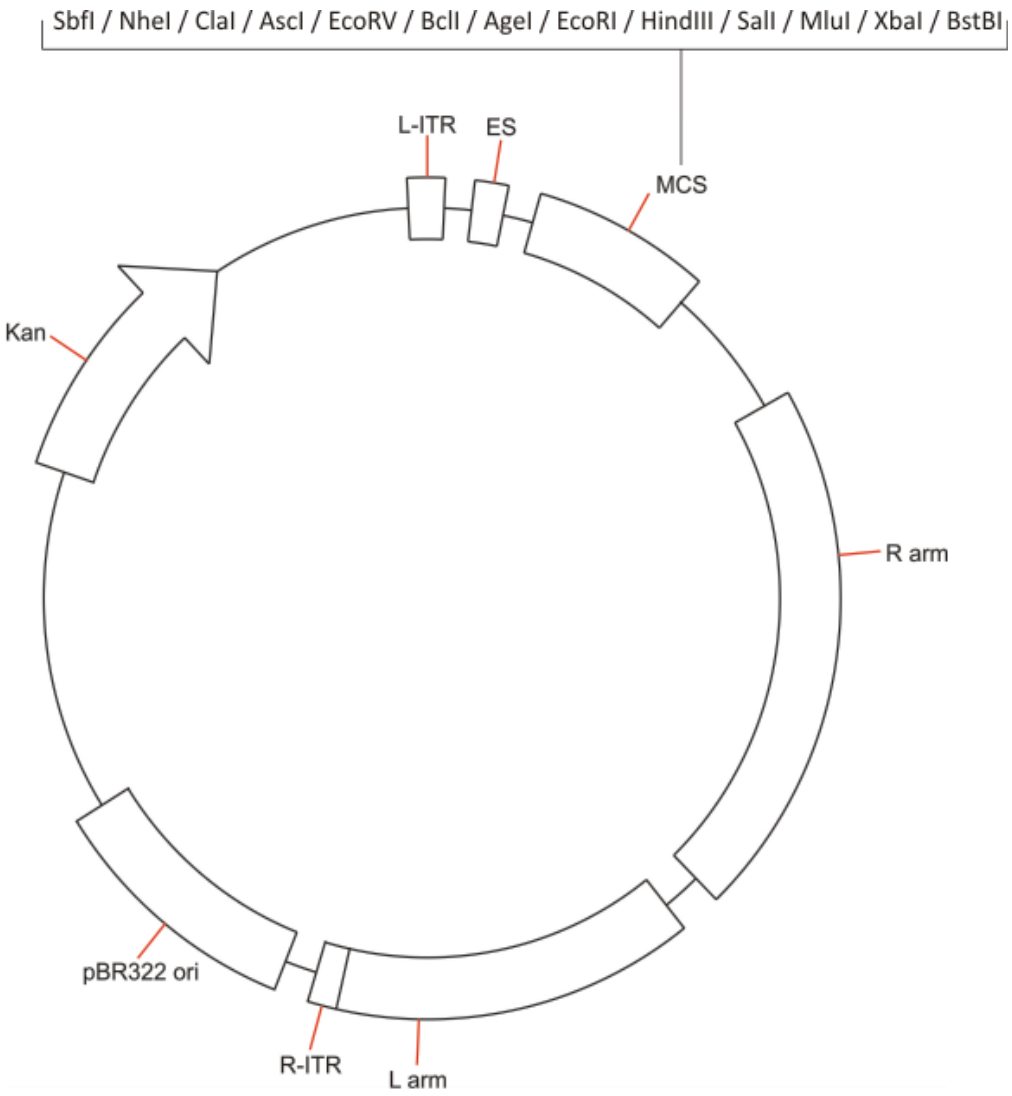

Figure 66. Plasmid map of pShuttle-PREK. Plasmid map of pShuttle-PREK with the restriction endonuclease sites in the multiple cloning site. ES, encapsidation signal; MCS, multiple cloning site; R-arm/L-arm, right/left arm homology; R-ITR/L-ITR, right/left inverted terminal repeats; pBR322, pBR322 plasmid origin; kanamycin, kanamycin antibiotic resistance gene.

pShuttle-GFP

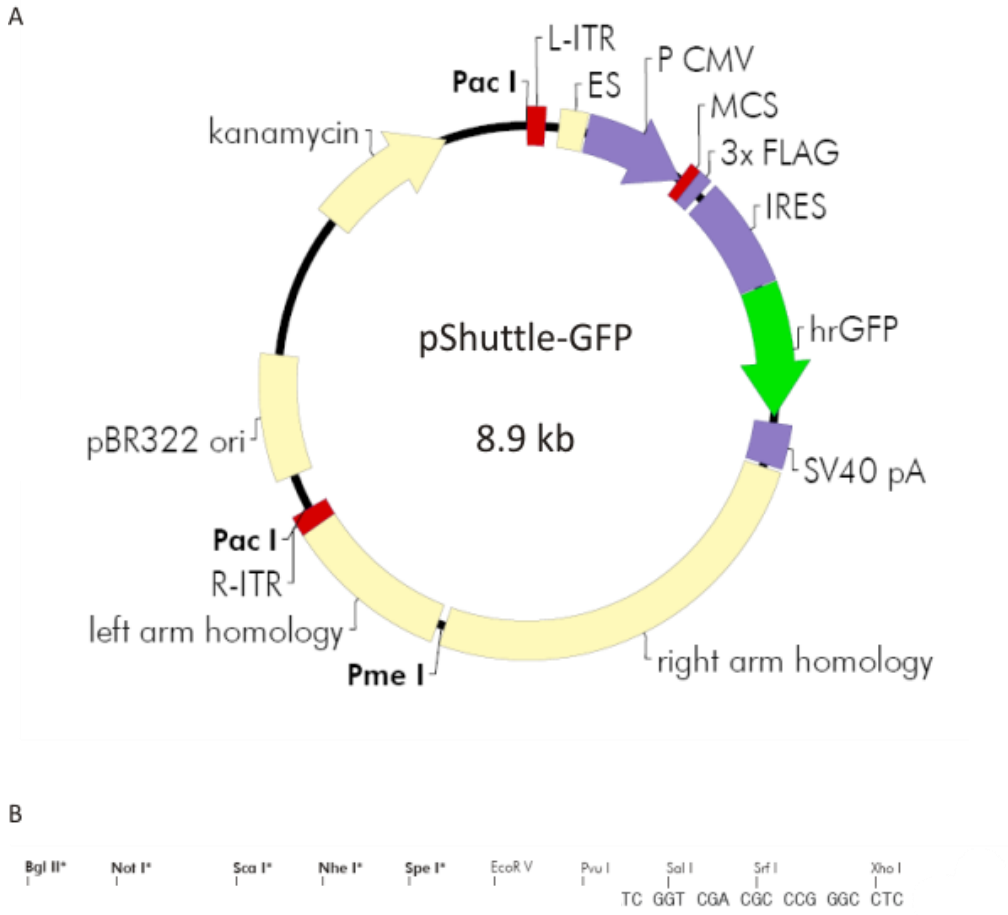

Figure 67. Plasmid map of pShuttle-GFP (Stratagene). A) Plasmid map of pShuttle-GFP B) restriction endonuclease sites in the multiple cloning site. ES, encapsidation signal; pCMV, cytomegalovirus promoter; MCS, multiple cloning site; 3 xFLAG, open reading frame for flag octapeptide ; IRES, internal ribosomal entry site; hrGFP, humanised renilla green fluorescent protein; sv40 pa, simian vacuolating virus 40 polyadenylation signal; R-ITR/L-ITR, right/left inverted terminal repeats; pBR322, pBR322 plasmid origin; kanamycin, kanamycin antibiotic resistance gene.

pAd-easy

pBR322 origin 1854–2521
ampicillin resistance (*bla*) ORF 2669–3529
Ad5 right arm homology 3716–5721
Ad5 left arm homology 32483–33471

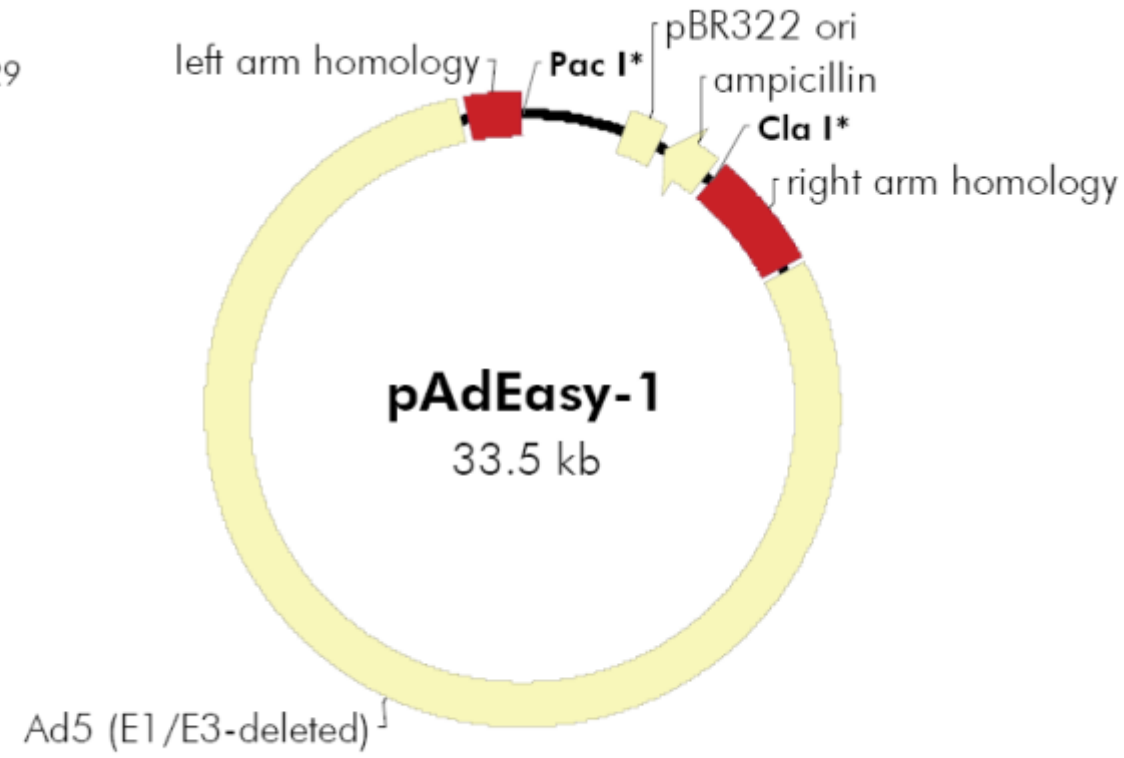

Figure 68. Plasmid map of pAd-easy

Appendix A5. Sequence and mutation analysis of Ad5-GFP-HCN4Δ viral DNA

The nucleotide base sequence of Ad5-GFP-HCN4 was sequenced (MWG biotech) Mutation analysis of the portion of DNA containing the gene insert was performed by comparison of the sequence to that of the DNA sequence of Mus musculus hyperpolarisation-activated, cyclic nucleotide-gated K^+ 4 (Hcn4) mRNA (available from Entrez Nucleotide, http://www.ncbi.nlm.nih.gov/nuccore). Sequences obtained from sequencing reactions were compared to the reference sequences using a nucleotide BLAST query (http://blast.ncbi.nlm.nih.gov/Blast.cgi). There are deletions between bases 845 and 1153 and 4577 and 4762. The primer sequences used are shown in table 5 (see end of sequence data).

Deletions = -

Mutations = A

Insertions = A shown above the letter that immediately precedes it

Coloured numbers represent the position in the DNA sequence.

Black letters and numbers (e.g. R1) denotes the primer (table 5).

Forward:

```
   1 atggacaagc tgccgccgtc catgcgcaag cggctctaca gccttccgca gcaggtgggg
  61 gccaaggcgt ggatcatgga cgaggaagag gatggtgagg aagaaggggc cgggggccgc
 121 caggacccca gccgaaggag catccggctg cggccgctgc cctcgccctc tccctcggtg
 181 gctgcgggct gctcggagtc ccggggtgcg gccctcgggg cgacagagag cgaggggccg
 241 ggccgcagcg ccggcaagtc cagcaccaac ggtgactgca ggcgcttccg cgggagtctg
 301 gcctcgctgg gcagccgggg cggcggcagt ggtggagcag ggggcggcag cagtctcggg
 361 cacctgcatg actccgcgga ggaacggcgg ctcatcgccg ctgagggcga tgcgtccccc
 421 ggcgaggaca ggacgccccc gggcctggcg accgaacccg agcgcccggc caccgcggca
 481 caacccgcag cctcgccgcc gccccagcag ccgccgcagc cggcctctgc ctcctgcgag
 541 cagccctcgg cggacaccgc tatcaaagtg gagggaggcg cggccgccag cgaccagatc
 601 ctccccgagg ccgaggtgcg cctgggccag agcggcttca tgcagcgcca gttcggtgcc
 661 atgctgcaac ctggggtcaa caaattctcc ctaaggatgt tcggcagcca gaaagcggtg
 721 gagcgcgagc aggagagggt taagtcagca gggttttgga ttatccaccc ctacagtgac
 781 ttcagatttt actgggacct gacgatgctg ttgctgatgg tggggaatct gatcatcata
 841 cccgtgggca tcaccttctt caaggatgag aacaccacac cctggatcgt cttcaatgtg
 901 gtgtcagaca cattcttcct cattgacttg gtcctcaact tccgcacggg gatcgtggtg
```

```
      961 gaggacaaca cagaaatcat ccttgacccg cagaggatca agatgaagta cctgaaaagc
     1021 tggtttgtgg tagatttcat ctcctccatc cctgtcgact acatcttcct tatagtggag
     1081 actcgcattg actcggaggt ctacaaaacc gctagggctc tgcgcattgt ccgtttcact
     1141 aagatcctca gcctcctgcg cctcttgagg ctttcccgcc tcattcgata cattcatcag
     1201 tgggaagaga tcttccacat gacctatgac ctggccagcg ccgtggtacg catcgtgaac
     1261 ctcattggca tgatgcttct gctgtgtcac tgggatggct gcctgcagtt cctagtgccc
     1321 atgctgcagg acttccccca tgactgctgg gtgtccatca atggcatggt gaataactcc
     1381 tgggggaagc agtattccta cgccctcttc aaggccatga gccacatgct gtgcattggg
     1441 tatggacggc aggcacccgt aggcatgtct gacgtctggc tcaccatgct cagcatgatc
     1501 gtgggggcca cctgctatgc catgttcatc ggccacgcca ctgccctcat ccagtcgcta
     1561 gactcctccc ggcgccagta ccaggagaag tataaacagg tggagcagta catgtccttc
     1621 cacaagctcc cgcctgacac ccgacagcgc atccatgact actatgaaca ccgctaccaa
     1681 ggcaagatgt ttgatgagga aagcatcctg ggtgagctga gtgagccact tcgagaggag
     1741 atcatcaact ttaactgccg aaagctggtg gcatccatgc cactgtttgc caacgcagat
     1801 cccaactttg tgacatccat gctgaccaag ttgcgtttcg aggtcttcca gcctggggat
     1861 tacatcatcc gcgaaggcac catcggcaag aagatgtact ttatccagca cggcgtggtc
     1921 agcgtgctca ctaagggcaa caaagagacc aagctggctg atggctccta ttttggagag
     1981 atctgcttgc tgacccgggg tcggcgcaca gccagcgtca gagcggatac ttattgccgc
     2041 ctctactcac tgagcgtgga caacttcaat gaggtgctgg aggagtatcc catgatgcgg
R5               CAC TGAACGTGG-  -AACTTC-AT GAGGTGCTGG AGGAGTATCC CATGATGCGG

     2101 agggccttcg agacggttgc gctggaccgc ctggaccgca taggcaagaa gaactccatc
R5        AGGGCCTTCG AGACGGTTGC GCTGGACCGC CTGGACCGCA TAGGCAAGAA GAACTCCATC

     2161 ctcctccaca aggtgcagca cgacctcaac tcaggcgtct tcaactacca agagaacgag
R5        CTCCTCCACA AGGTGCAGCA CGACCTCAAC TCAGGCGTCT TCAACTACCA AGAGAACGAG

     2221 atcatccagc agatcgtgcg gcatgaccgt gagatggccc actgtgctca ccgcgtccag
R5        ATCATCCAGC AGATCGTGCG GCATGACCGT GAGATGGCCC ACTGTGCTCA CCGCGTCCAG

     2281 gctgccgcct cagccacccc aacccccacg cctgttatat ggaccccgct gatccaggcg
R5        GCTGCCGCCTC AGCCACCCC AACCCCCACG CCTGTTATAT GGACCCCGCT GATCCAGGCG

     2341 ccactgcagg ctgctgctgc tactacttcg gtggccatag ccctcacaca ccacccccgc
R5        CCACTGCAGG CTGCTGCTGC TACTACTTCG GTGGCCATAG CCCTCACACA CCACCCCCGC

     2401 ctgcccgccg ccatcttccg gccccctccc ggacctgggc tgggcaacct tggggctgga
R5        CTGCCCGCCG CCATCTTCCG GCCCCCTCCC GGACCTGGGC TGGGCAACCT TGGGGCTGGA

     2461 cagacaccga ggcacccaag gaggctgcag tccttgatcc cttcagctct gggctctgct
R5        CAGACACCGAG GCACCCAAG GAGGCTGCAG TCCTTGATCC CTTCAGCTCT GGGCTCTGCT

     2521 tcacccgcca gcagcccctc acaggtggac acaccgtctt catcctcctt ccacatccaa
```

```
R5        TCACCCGCCA GCAGCCCCTC ACAGGTGGAC ACACCGTCTT CATCCTCCTT CCACATCCAA

     2581 cagctggctg gattctctgc acctcctgga ttgagccctc tcctgccctc ctctagctct
R5        CAGCTGGCTG GATTCTCTGC ACCTCCTGGA TTGAGCCCTC TCCTGCCCTC CTCTAGCTCT

     2641 tccccacctc caggagcctg cggttcccca ccagccccca caccctccac ctccactgcc
R5        TCCCCACCTC CAGGAGCCTG CGGTTCCCCA CCAGCCCCCA CACCCTCCAC CTCCACTGCC

     2701 gccgccgcct ccaccactgg gttcggccac tttcacaagg cgctgggtgg ctccctgtca
R5        GCCGCCGCCT CCACCACTG GGTTCGGCCAC TTTCACAAGG CGCTGGGTGG CTCCCTGTCA

     2761 tcctctgact ccccgctgct caccccactg caaccaggcg ctcgctctcc acaggctgcc
R5        TCCTCTGACT CCCCGCTGCT CACCCCACTG CAACCAGGCG CTCGCTCTCC ACAGGCTGCC

     2821 cagccaccac ccccactgcc tggggcccga ggaggtctgg gactcctgga gcacttcttg
R5        CAGCCACCAC CCCCACTGCC TGGGGCCCGA GGAGGTCTGG GACTCCTGGA GCACTTCTTG

     2881 ccgcccccac cctcctccag gtcaccatca tccagccctg ggcagctggg ccagcctcct
R5        CCGCCCCCAC CCTCCTCCAG GTCACCATCA TCCAGCCCTG GGCAGCTGGG CCAGCCTCCT

     2941 ggagagttgt ccctaggtct ggcagctggt ccatcaagta caccagagac acccccacgg
R5        GGAGAGTTGT CCCTAGGTCT GGCAGCTGGT CCATCAAGTA CACCAGAGAC ACCCCCACGG

     3001 cctgagcgac catccttcat ggcaggggcc tctggagggg cttctcctgt agcctttacc
R5        CCTGAGCGAC CATCCTTCAT GGCAGGG-C- TCTGGAGGG-CTTCTCCTGT AGCCTTTACC

     3061 ccccgaggag gcctcagtcc tccgggccac agcccggggc ccccaagaac tttcccgagt
R5        CCCCGAGGAG GCCTCAGTCC TC-GGGC-AC AGCCCGGG-C CCC-AAGAAC TTTCCCGAGT

     3121 gccccacccc gggcctctgg ctcccatggt tccctgctcc tgccacctgc atccagccct
                                                  T
R5        GCCCCACCC- GGGCCTCTGG CTCC-ATGGG TCCTTGCTC- TGCCAC-TGC ATC-AGCCTT

     3181 ccacctcccc aggtcccaca gcgcaggggc acaccacccc tcacccctgg ccgcctcaca
                                                  T          T
R5        C-ACCTCTCA AGGTCC-ACA GCGCAGGGGC AAACCACTCC -CACCCCTGG TCGCC-CTCA

     3241 caggacctga agctcatctc agcctctcag ccagccctcc cccaggatgg ggcacagact
               A
R5        CAGGACCTGA -GCTCATCTA A-CCTCTCAG TCA-CCTTTC CA-AGAATGG G-CAGA-ACT

     3301 ctccgcaggg cctcgcctca ctcctcaggg gagtcggtgg ctgccttctc actctacccc
R5        CTC
```

```
3361 agagctgggg gtggcagtgg gagtagtggg ggccttgggc ctcctggaag gccatatggt
3421 gccatcccag gccaacatgt cactttgcct cggaagacat cctcaggttc tttgccaccc
3481 ccactttctt tgtttggggc aagagccgcc tcttctggag ggccccctct gactactgct
3541 gcaccccaga gggaacctgg cgctaggtct gagccagtac gctccaaact gccgtctaat
3601 ttatgagctg ggccctccct ccctcttctt tttcttgctc ctttcttcct tcaggtttaa
3661 ctgtgattag gagatatacc aacaacaata ataaccataa aaaaacatac cccagaaaaa
3721 caaaaagaca gcagaaaata accaggtatt cttagagcta tagatttttg gtcacttgct
3781 tttatagact attttaat
```

Reverse:

```
   1 attaaaatag tctataaaag caagtgacca aaaatctata gctctaagaa tacctggtta
  61 ttttctgctg tctttttgtt tttctggggt atgtttttt atggttatta ttgttgttgg
 121 tatatctcct aatcacagtt aaacctgaag gaagaaagga gcaagaaaaa gaagagggag
 181 ggagggccca gctcataaat tagacggcag tttggagcgt actggctcag acctagcgcc
R8         CCCA GCTCATAAAT TAGACGGCAG TTTGGAGCGT ACTGGCTCAG ACCTAGCGCC

 241 aggttccctc tggggtgcag cagtagtcag agggggccct ccagaagagg cggctcttgc
R8     AGGTTCCCTC TGGGGTGCAG CAGTAGTCAG AGGGGGCCCT CCAGAAGAGG CGGCTCTTGC

 301 cccaaacaaa gaaagtgggg gtggcaaaga acctgaggat gtcttccgag gcaaagtgac
R8     CCCAAACAAA GAAAGTGGGG GTGGCAAAGA ACCTGAGGAT GTCTTCCGAG GCAAAGTGAC

 361 atgttggcct gggatggcac catatggcct tccaggaggc ccaaggcccc cactactccc
R8     ATGTTGGCCT GGGATGGCAC CATATGGCCT TCCAGGAGGC CCAAGGCCCC CACTACTCCC

 421 actgccaccc ccagctctgg ggtagagtga gaaggcagcc accgactccc ctgaggagtg
R7                                                       C CTGAGGAGTG
R8     ACTGCCACCC CCAGCTCTGG GGTAGAGTGA GAAGGCAGCC ACCGACTCCC CTGAGGAGTG

 481 aggcgaggcc ctgcggagag tctgtgcccc atcctggggg agggctggct gagaggctga
R7     AGGCGAGGCC CTGCGGAGAG TCTGTGCCCC ATCCTGGGGG AGGGCTGGCT GAGAGGCTGA
R8     AGGCGAGGCC CTGCGGAGAG TCTGTGCCCC ATCCTGGGGG AGGGCTGGCT GAGAGGCTGA

 541 gatgagcttc aggtcctgtg tgaggcggcc aggggtgagg ggtggtgtgc ccctgcgctg
R7     GATGAGCTTC AGGTCCTGTG TGAGGCGGCC AGGGGTGAGG GGTGGTGTGC CCCTGCGCTG
R8     GATGAGCTTC AGGTCCTGTG TGAGGCGGCC AGGGGTGAGG GGTGGTGTGC CCCTGCGCTG

 601 tgggacctgg ggaggtggag ggctggatgc aggtggcagg agcagggaac catgggagcc
R7     TGGGACCTGG GGAGGTGGAG GGCTGGATGC AGGTGGCAGG AGCAGGGAAC CATGGGAGCC
R8     TGGGACCTGG GGAGGTGGAG GGCTGGATGC AGGTGGCAGG AGCAGGGAAC CATGGGAGCC

 661 agaggcccgg ggtggggcac tcgggaaagt tcttgggggc cccgggctgt ggcccggagg
R7     AGAGGCCCGG GGTGGGGCAC TCGGGAAAGT TCTTGGGGGC CCCGGGCTGT GGCCCGGAGG
R8     AGAGGCCCGG GGTGGGGCAC TCGGGAAAGT TCTTGGGGGC CCCGGGCTGT GGCCCGGAGG

 721 actgaggcct cctcgggggg taaaggctac aggagaagcc cctccagagg cccctgccat
R7     ACTGAGGCCT CCTCGGGGGG TAAAGGCTAC AGGAGAAGCC CCTCCAGAGG CCCCTGCCAT
R8     ACTGAGGCCT CCTCGGGGGG TAAAGGCTAC AGGAGAAGCC CCTCCAGAGG CCCCTGCCAT

 781 gaaggatggt cgctcaggcc gtgggggtgt ctctggtgta cttgatggac cagctgccag
R7     GAAGGATGGT CGCTCAGGCC GTGGGGGTGT CTCTGGTGTA CTTGATGGAC CAGCTGCCAG
R8     GAAGGATGGT CGCTCAGGCC GTGGGGGTGT CTCTGGTGTA CTTGATGGAC CAGCTGCCAG

 841 acctagggac aactctccag gaggctggcc cagctgccca gggctggatg atggtgacct
R7     ACCTAGGGAC AACTCTCCAG GAGGCTGGCC CAGCTGCCCA GGGCTGGATG ATGGTGACCT
R8     ACCTAGGGACA ACTCTCCAG GAGGCTGGCC CAGCTGCCCA GGGCTGGATG ATGGTGACCT
```

```
      901 ggaggagggt gggggcggca agaagtgctc caggagtccc agacctcctc gggccccagg
R7        GGAGGAGGGT GGGGGCGGCA AGAAGTGCTC CAGGAGTCCC AGACCTCCTC GGGCCCCAGG
R8        GGAGGAGGGT GGGGGCGGCA AGAAGTGCTC CAGGAGTCCC AGACCTCCTC GGGCCCCAGG

      961 cagtgggggt ggtggctggg cagcctgtgg agagcgagcg cctggttgca gtggggtgag
R7        CAGTGGGGGT GGTGGCTGGG CAGCCTGTGG AGAGCGAGCG CCTGGTTGCA GTGGGGTGAG
R8        CAGTGGGGGT GGTGGCTGGG CAGCCTGTGG AGAGCGAGCG CCTGGTTGCA GTGGGGTGAG

     1021 cagcggggag tcagaggatg acagggagcc acccagcgcc ttgtgaaagt ggccgaaccc
R7        CAGCGGGGAG TCAGAGGATG ACAGGGAGCC ACCCAGCGCC TTGTGAAAGT GGCCGAACCC
R8        CAGCGGGGAG TCAGAGGATG ACAGGGAGCC ACCCAGCGCC TTGTGAAAGT GGCCGAACCA

     1081 agtggtggag gcggcggcgg cagtggaggt ggagggtgtg ggggctggtg gggaaccgca
R7        AGTGGTGGAG GCGGCGGCGG CAGTGGAGGT GGAGGGTGTG GTGGCCGGT
                                                             C
R8        AGTGGTGGAG GCGGCGGCG- CAGTGGAG-T GGAGG-TGTG GGGGCTGGTG GGGCACCGC

     1141 ggctcctgga ggtggggaag agctagagga gggcaggaga gggctcaatc caggaggtgc
             C
R8        AGCTCCTGGA GGTGGCGA-G AGCTCGAGGA GGCCAG-AGA TGCCTCA-TC CAG-AG-TGC

     1201 agagaatcca gccagctgtt ggatgtggaa ggaggatgaa gacggtgtgt ccacctgtga
R8        -GAGCATCAA -CCT-CTGTT GGATGTGGAC G-AGGATGA- GACG-TGTGT C

     1261 ggggctgctg gcgggtgaag cagagcccag agctgaaggg atcaaggact gcagcctcct
     1321 tgggtgcctc ggtgtctgtc cagccccaag gttgcccagc ccaggtccgg gaggggccg
     1381 gaagatggcg gcgggcaggc gggggtggtg tgtgagggct atggccaccg aagtagtagc

     1441 agcagcagcc tgcagtggcg cctggatcag cggggtccat ataacaggcg tgggggttgg
                                                                 T
R5                                                            GGGTTTG

     1501 ggtggctgag gcggcagcct ggacgcggtg agcacagtgg gccatctcac ggtcatgccg
R5        GG-GGCTGA- GCGGCAGCCT GGACGCGGTG AGCACAGTGG GCCATCTCAC GGTCATGCCG

     1561 cacgatctgc tggatgatct cgttctcttg gtagttgaag acgcctgagt tgaggtcgtg
R5        CACGATCTGC TGGATGATCT CGTTCTCTTG GTAGTTGAAG ACGCCTGAGT TGAGGTCGTG

     1621 ctgcaccttg tggaggagga tggagttctt cttgcctatg cggtccaggc ggtccagcgc
R5        CTGCACCTTG TGGAGGAGGA TGGAGTTCTT CTTGCCTATG CGGTCCAGGC GGTCCAGCGC

     1681 aaccgtctcg aaggccctcc gcatcatggg atactcctcc agcacctcat tgaagttgtc
R5        AACCGTCTCG AAGGCCCTCC GCATCATGGG ATACTCCTCC AGCACCTCAT TGAAGTTGTC

     1741 cacgctcagt gagtagaggc ggcaataagt atccgctctg acgctggctg tgcgccgacc
R5        CACGCTCAGT GAGTAGAGGC GGCAATAAGT ATCCGCTCTG ACGCTGGCTG TGCGCCGACC

     1801 ccgggtcagc aagcagatct ctccaaaata ggagccatca gccagcttgg tctctttgtt
R5        CCGGGTCAGC AAGCAGATCT CTCCAAAATA GGAGCCATCA GCCAGCTTGG TCTCTTTGTT

     1861 gcccttagtg agcacgctga ccacgccgtg ctggataaag tacatcttct tgccgatggt
R5        GCCCTTAGTG AGCACGCTGA CCACGCCGTG CTGGATAAAG TACATCTTCT TGCCGATGGT

     1921 gccttcgcgg atgatgtaat ccccaggctg gaagacctcg aaacgcaact tggtcagcat
R5        GCCTTCGCGG ATGATGTAAT CCCCAGGCTG GAAGACCTCG AAACGCAACT TGGTCAGCAT

     1981 ggatgtcaca aagttgggat ctgcgttggc aaacagtggc atggatgcca ccagctttcg
R5        GGATGTCACA AAGTTGGGAT CTGCGTTGGC AAACAGTGGC ATGGATGCCA CCAGCTTTCG

     2041 gcagttaaag ttgatgatct cctctcgaag tggctcactc agctcaccca ggatgctttc
R4                                                          CCA TGATGCTTTC
R5        GCAGTTAAAG TTGATGATCT CCTCTCGAAG TGGCTCACTC AGCTCACCCA GGATGCTTTC

     2101 ctcatcaaac atcttgcctt ggtagcggtg ttcatagtag tcatggatgc gctgtcgggt
R4        CTCATC-AAC ATCTTGCCTT GGTAGCGGTG TTCATAGTAG TCATGGATGC GCTGTCGGGT
R5        CTCATCAAAC ATCTTGCCTT GGTAGCGGTG TTCATAGTAG TCATGGATGC GCTGTCGGGT

     2161 gtcaggcggg agcttgtgga aggacatgta ctgctccacc tgtttatact tctcctggta
```

```
R4          GTCAGGCGGG AGCTTGTGGA AGGACATGTA CTGCTCCACC TGTTTATACT TCTCCTGGTA
R5          GTCAGGCGGG AGCTTGTGGA AGGACATGTA CTGCTCCACC TGTTTATACT TCTCCTGGTA

      2221  ctggcgccgg gaggagtcta gcgactggat gagggcagtg gcgtggccga tgaacatggc
R4          CTGGCGCCGG GAGGAGTCTA GCGACTGGAT GAGGGCAGTG GCGTGGCCGA TGAACATGGC
R5          CTGGCGCCGG GAGGAGTCTA GCGACTGGAT GAGGGCAGTG GCGTGGCCGA TGAACATGGC


      2281  atagcaggtg gcccccacga tcatgctgag catggtgagc cagacgtcag acatgcctac
R4          ATAGCAGGTG GCCCCCACGA TCATGCTGAG CATGGTGAGC CAGACGTCAG ACATGCCTAC
R5          ATAGCATGTG GCCCCCACGA TCATGCTGAG CATGGTGAGC CAGACGTCAG ACATGCCTAC

      2341  gggtgcctgc cgtccatacc caatgcacag catgtggctc atggccttga agagggcgta
R4          GGGTGCCTGC CGTCCATACC CAATGCACAG CATGTGGCTC ATGGCCTTGA AGAGGGCGTA
R5          GGGTGCCTGC CGTCCATACC CAATGCACAG CATGTGGCTC ATGGCCTTGA AgAGGGCGTA

      2401  ggaatactgc ttcccccagg agttattcac catgccattg atggacaccc agcagtcatg
R4          GGAATACTGC TTCCCCCAGG AGTTATTCAC CATGCCATTG ATGGACACCC AGCAGTCATG
R5          GGAATACTGC TTCCCCCAGG AGTTATTCAC CATGCCATTG ATGGACACCC AGCAGTCATG


      2461  ggggaagtcc tgcagcatgg gcactaggaa ctgcaggcag ccatcccagt gacacagcag
R4          GGGGAAGTCC TGCAGCATGG GCACTAGGAA CTGCAGGCAG CCATCCCAGT GACACAGCAG
R5          GGGGAAGTCC TGCAGCATGG GCACTAGGAA CTGCAGGCAG CCATCCCAGT GACACAGCAG

      2521  aagcatcatg ccaatgaggt tcacgatgcg taccacggcg ctggccaggt cataggtcat
R3                           GT T-ACGATGCG TACCACGGCG CTGGCCAGGT CATAGGTCAT
R4          AAGCATCATG CCAATGAGGT TCACGATGCG TACCACGGCG CTGGCCAGGT CATAGGTCAT
R5          AAGCATCATG CCAATGAGGT TCACGATGCG TACCACGGCG CTGGCCAGGT CATAGGTCAT

      2581  gtggaagatc tcttcccact gatgaatgta tcgaatgagg cgggaaagcc tcaagaggcg
R3          GTGGAAGATC TCTTCCCACT GATGAATGTA TCGAATGAGG CGGGAAAGCC TCAAGAGGCG
R4          GTGGAAGATC TCTTCCCACT GATGAATGTA TCGAATGAGG CGGGAAAGCC TCAAGAGGCG
                    C
R5          GTGGAAGATC TCT-CCCACT GATGA-TGTA TCGAATGAGG CGGGAAAGCC TCA-GAGGCG

      2641  caggaggctg aggatcttag tgaaacggac aatgcgcaga gccctagcgg ttttgtagac
R3          CAGGAGGCTG AGGATCTTAG TGAAACGGAC AATGCGCAGA GCCCTAGCGG TTTTGTAGAC
R4          CAGGAGGCTG AGGATCTTAG TGAAACGGAC AATGCGCAGA GCCCTAGCGG TTTTGTAGAC
R5          CAGAAGCCTG AGGATCT-AG TGAAACGGAC AAT

      2701  ctccgagtca atgcgagtct ccactataag gaagatgtag tcgacaggga tggaggagat
R3          CTCCGAGTCA ATGCGAGTCT CCACTATAAG GAAGATGTAG TCGACAGGGA TGGAGGAGAT
R4          CTCCGAGTCA ATGCGAGTCT CCACTATAAG GAAGATGTAG TCGACAGGGA TGGAGGAGAT

      2761  gaaatctacc acaaaccagc ttttcaggta cttcatcttg atcctctgcg ggtcaaggat
R3          GAAATCTACC ACAAACCAGC TTTTCAGGTA CTTCATCTTG ATCCTCTGCG GGTCAAGGAT
R4          GAAATCTACC ACAAACCAGC TTTTCAGGTA CTTCATCTTG ATCCTCTGCG GGTCAAGGAT

      2821  gatttctgtg ttgtcctcca ccacgatccc cgtgcggaag ttgaggacca agtcaatgag
R3          GATTTCTGTG TTGTCCTCCA CCACGATCCC CGTGCGGAAG TTGAGGACCA AGTCAATGAG
R4          GATTTCTGTG TTGTCCTCCA CCACGATCCC CGTGCGGAAG TTGAGGACCA AGTCAATGAG

      2881  gaagaatgtg tctgacacca cattgaagac gatccagggt gtggtgttct catccttgaa
R3          GAAGAATGTG TCTGACACCA CATTGAAGAC GATCCAGGGT GTGGTGTTCT CATCCTTGAA
R4          GAAGAATGTG TCTGACACCA CATTGAAGAC GATCCAGGGT GTGGTGTTCT CATCCTTGAA

      2941  gaaggtgatg cccacgggta tgatgatcag attccccacc atcagcaaca gcatcgtcag
R3          GAAGGTGATG CCCACGGGTA TGATGATCAG ATTCCCCACC ATCAGCAACA GCATCGTCAG
R4          GAAGGTGATG CCCACGGGTA TGATGATCAG ATTCCCCACC ATCAGCAACA GCATCGTCAG

      3001  gtcccagtaa aatctgaagt cactgtaggg gtggataatc caaaaccctg ctgacttaac
R2                                     GG GTGG--AATC C-AAACCCTG CTGACTTAAC
R3          GTCCCAGTAA AATCTGAAGT CACTGTAGGG GTGGATAATC CAAAACCCTG CTGACTTAAC
R4          GTCCCAGTAA AATCTGAAGT CACTGTAGGG GTGGATAATC CAAAACCCTG CTGACTTAAC

      3061  cctctcctgc tcgcgctcca ccgctttctg gctgccgaac atccttaggg agaatttgtt
R2          CCTCTCCTGC TCGCGCTCCA CCGCTTTCTG GCTGCCGAAC ATCCTTAGGG AGAATTTGTT
```

```
R3          CCTCTCCTGC TCGCGCTCCA CCGCTTTCTG GCTGCCGAAC ATCCTTAGGG AGAATTTGTT
R4          CCTCTCCTGC TCGCGCTCCA CCGCTTTCTG GCTGCCGAAC ATCCTTAGGG AGAATTTGTT

      3121  gaccccaggt tgcagcatgg caccgaactg gcgctgcatg aagccgctct ggcccaggcg
R2          GACCCCAGGT TGCAGCATGG CACCGAACTG GCGCTGCATG AAGCCGCTCT GGCCCAGGCG
R3          GACCCCAGGT TGCAGCATGG CACCGAACTG GCGCTGCATG AAGCCGCTCT GGCCCAGGCG
                    A
R4          GACCCCAGGT TGCAGCATGG CACCGAACTG GCGCTGCATG A-GCCGCTCT GGCCCAG-CG

      3181  cacctcggcc tcggggagga tctggtcgct ggcggccgcg cctccctcca ctttgatagc
R2          CACCTCGGCC TCGGGGAGGA TCTGGTCGCT GGCGGCCGCG CCTCCCTCCA CTTTGATAGC
R3          CACCTCGGCC TCGGGGAGGA TCTGGTCGCT GGCGGCCGCG CCTCCCTCCA CTTTGATAGC
                                                      T   T
R4          CACCTCGGCC TCGGGGAGGA TCTGGTCGCT GGCGGCCGCG CCTCCCTCCA CT
      3241  ggtgtccgcc gagggctgct cgcaggaggc agaggccggc tgcggcggct gctggggcgg
R2          GGTGTCCGCC GAGGGCTGCT CGCAGGAGGC AGAGGCCGGC TGCGGCGGCT GCTGGGGCGG
R3          GGTGTCCGCC GAGGGCTGCT CGCAGGAGGC AGAGGCCGGC TGCGGCGGCT GCTGGGGCGG

      3301  cggcgaggct gcgggttgtg ccgcggtggc cgggcgctcg ggttcggtcg ccaggcccgg
R2          CGGCGAGGCT GCGGGTTGTG CCGCGGTGGC CGGGCGCTCG GGTTCGGTCG CCAGGCCCGG
R3          CGGCGAGGCT GCGGGTTGTG CCGCGGTGGC CGGGCGCTCG GGTTCGGTCG CCAGGCCCGG

      3361  gggcgtcctg tcctcgccgg gggacgcatc gccctcagcg gcgatgagcc gccgttcctc
R2          GGGCGTCCTG TCCTCGCCGG GGGACGCATC GCCCTCAGCG GCGATGAGCC GCCGTTCCTC
R3          GGGCGTCCTG TCCTCGCCGG GGGACGCATC GCCCTCAGCG GCGATGAGCC GCCGTTCCTC

      3421  cgcggagtca tgcaggtgcc cgagactgct gccgcccccc gctccaccac tgccgccgcc
R1                                                        CCT GCT-C-CCAC TGCCGCCGCC
R2          CGCGGAGTCA TGCAGGTGCC CGAGACTGCT GCCGCCCCCT GCTCCACCAC TGCCGCCGCC
R3          CGCGGAGTCA TGCAGGTGCC CGAGACTGCT GCCGCCCCCT GCTCCACCAC TGCCGCCGCC

      3481  ccggctgccc agcgaggcca gactcccgcg gaagcgcctg cagtcaccgt tggtgctgga
R1          CCGGCTGCCC AGCGAGGCCA GACTCCCGCG GAAGCGCCTG CAGTCACCGT TGGTGCTGGA
R2          CCGGCTGCCC AGCGAGGCCA GACTCCCGCG GAAGCGCCTG CAGTCACCGT TGGTGCTGGA
R3          CCGGCTGCCC AGCGAGGCCA GACTCCCGCG GAAGCGCCTG CAGTCACCGT TGGTGCTGGA

      3541  cttgccggcg ctgcggcccg gcccctcgct ctctgtcgcc ccgagggccg caccccggga
R1          CTTGCCGGCG CTGCGGCCCG GCCCCTCGCT CTCTGTCGCC CCGAGGGCCG CACCCCGGGA
R2          CTTGCCGGCG CTGCGGCCCG GCCCCTCGCT CTCTGTCGCC CCGAGGGCCG CACCCCGGGA
                    C
R3          CTTGCCG-CG CTGCGGCCCG GCCCCTCGCT CTCTGTCGCC C-GAGGGCCG CACCCCGGGA

      3601  ctccgagcag cccgcagcca ccgagggaga gggcgagggc agcggccgca gccggatgct
R1          CTCCGAGCAG
R2          CTCCGAGCAG
R3          CTC-GAGCAG

      3661  ccttcggctg gggtcctggc ggcccccggc cccttcttcc tcaccatcct cttcctcgtc
      3721  catgatccac gccttggccc ccacctgctg cggaaggctg tagagccgct tgcgcatgga
      3781  cggcggcagc ttgtcca
```

Primer direction	Primer name	Binding site	Primer sequence
Reverse Primer	HCN4-R1	374	GCGGAGTCATGCAGGTG
Reverse Primer	HCN4-R2	796	TCAGGTCCCAGTAAAATCTG
Reverse Primer	HCN4-R3	1292	ATCCCAGTGACACAGCAG
Reverse Primer	HCN4-R4	1740	GATGATCTCCTCTCGAAGTG
Reverse Primer	HCN4-R5	2324	CGGGGTCCATATAACAGG
Forward Primer	HCN4-R5A	2031	TCAGAGCGGATACTTATTGC
Reverse Primer	HCN4-R8	3688	TCGTCATCATCCTTATAGTCC
Reverse Primer	HCN4-R7	3358	CTCTGGGGTAGAGTGAGAAG
Forward Primer	HCN4-F3	3159	ATGGTTCCCTGCTCCTG
Forward Primer	HCN4-F2	3384	GTGGCAGTGGGAGTAGTG
Reverse Primer	HCN4-R9	5000	AATGCTCGTCAAGAAGACAG

Table 5. Primers used for the sequencing of Ad5-GFP-HCN4Δ

The following sequencing reactions cover the first deletion between the bases 845 and 1153:

Ad5GFPHCN_HCN4-R1

Ad5GFPHCN_HCN4-R2

The following sequencing reactions cover the second deletion between the bases 4577 and 4762:

Ad5GFPHCN_HCN4-F2

Ad5GFPHCN_HCN4-F3

Ad5GFPHCN_HCN4-R9

Appendix A6. The leading pacemaker of individual sick sinus syndrome preparations; histology and immunohistochemistry

The leading pacemaker site of the SSS syndrome preparation was identified by activation mapping as described in section 2.6. Masson's trichrome staining and immunohistochemistry was then performed as described in section 2.7. The relative location of the leading pacemaker site for each SSS preparation is shown in figure 46, numbers in the figure legends refer to these sites. These data are presented in detail in section 3.3.3.

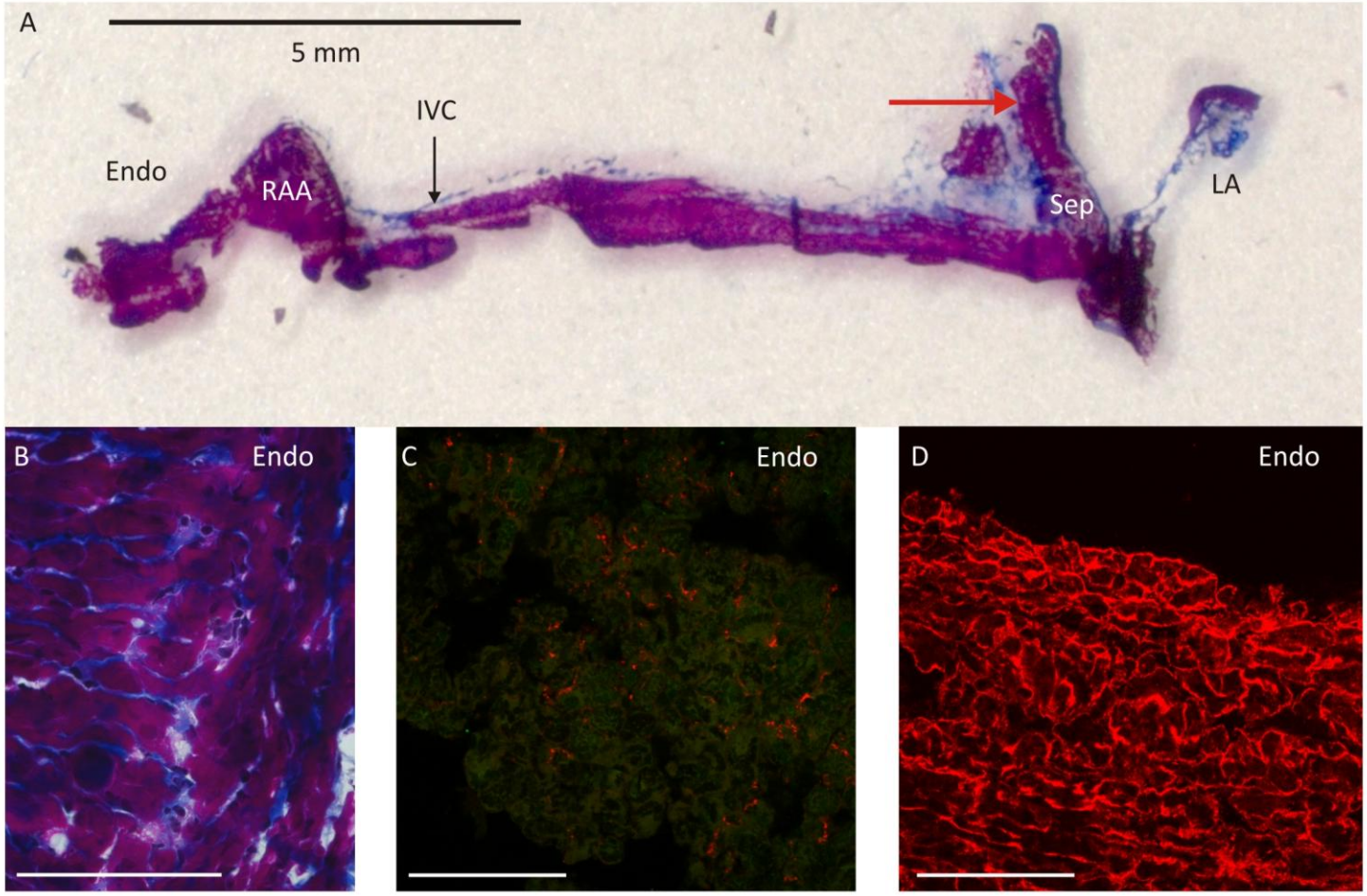

Figure 69. The histology and immunohistochemistry of the subsidiary pacemaker. Preparation 2. A) Sick sinus syndrome preparations were mapped as previously described and then frozen. 16 µm cryosections at the level of the leading pacemaker were stained withMasson's trichrome. The leading pacemaker is marked by the red arrow. B) Masson's trichrome staining of the leading pacemaker site. C) Ion channel and gap junction expression at the leading pacemaker site. Sections were labelled for HCN4 (green) and Cx43 (red). D) Cell size at the leading pacemaker site. The cell membrane of myocytes was labelled using an antibody to caveolin-3. For Masson's trichrome: purple, myocytes; blue, connective tissue. Endo, endocardium; IVC, inferior vena cava; LA, left atrium,RAA, right atrial appendage; Sep, interatrial septum. Scale bar in panels B - D = 100 µm.

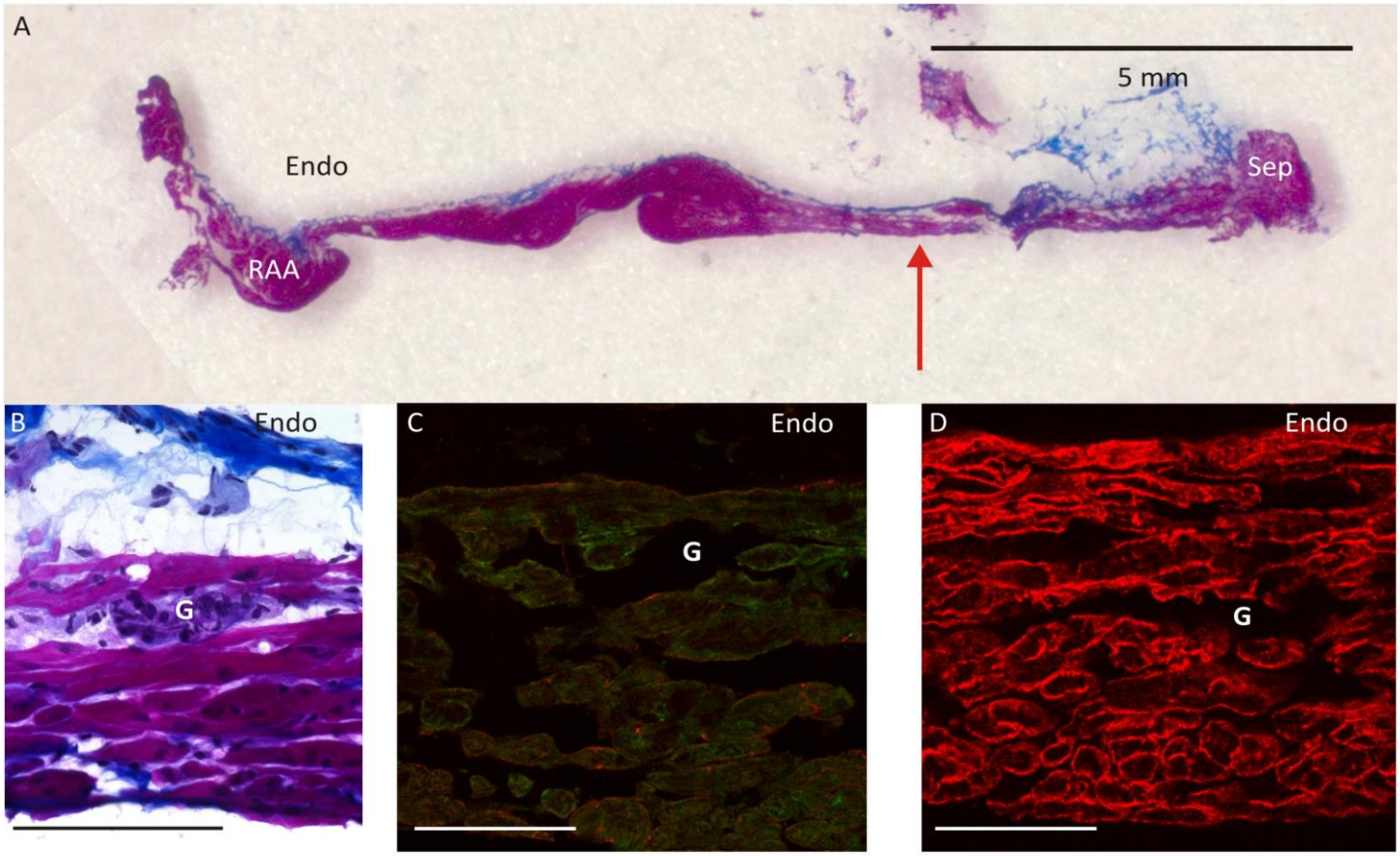

Figure 70. The histology and immunohistochemistry of the subsidiary pacemaker. Preparation 4. A) Sick sinus preparations were mapped as previously described and then frozen. 16 µm cryosections at the level of the leading pacemaker were stained with Masson's trichrome. The leading pacemaker is marked by the red arrow. B) Masson's trichrome staining of the leading pacemaker site. C) Ion channel and gap junction expression at the leading pacemaker site. Sections were labelled for HCN4 (green) and Cx43 (red). D) Cell size at the leading pacemaker site. The cell membrane of myocytes was labelled using an antibody to caveolin-3. For Masson's trichrome: purple, myocytes; blue, connective tissue. Endo, endocardium; RAA, right atrial appendage; Sep, inter-atrial septum. Scale bar in panels B - D = 100 µm. 'G' denotes the site of neuronal ganglion cells.

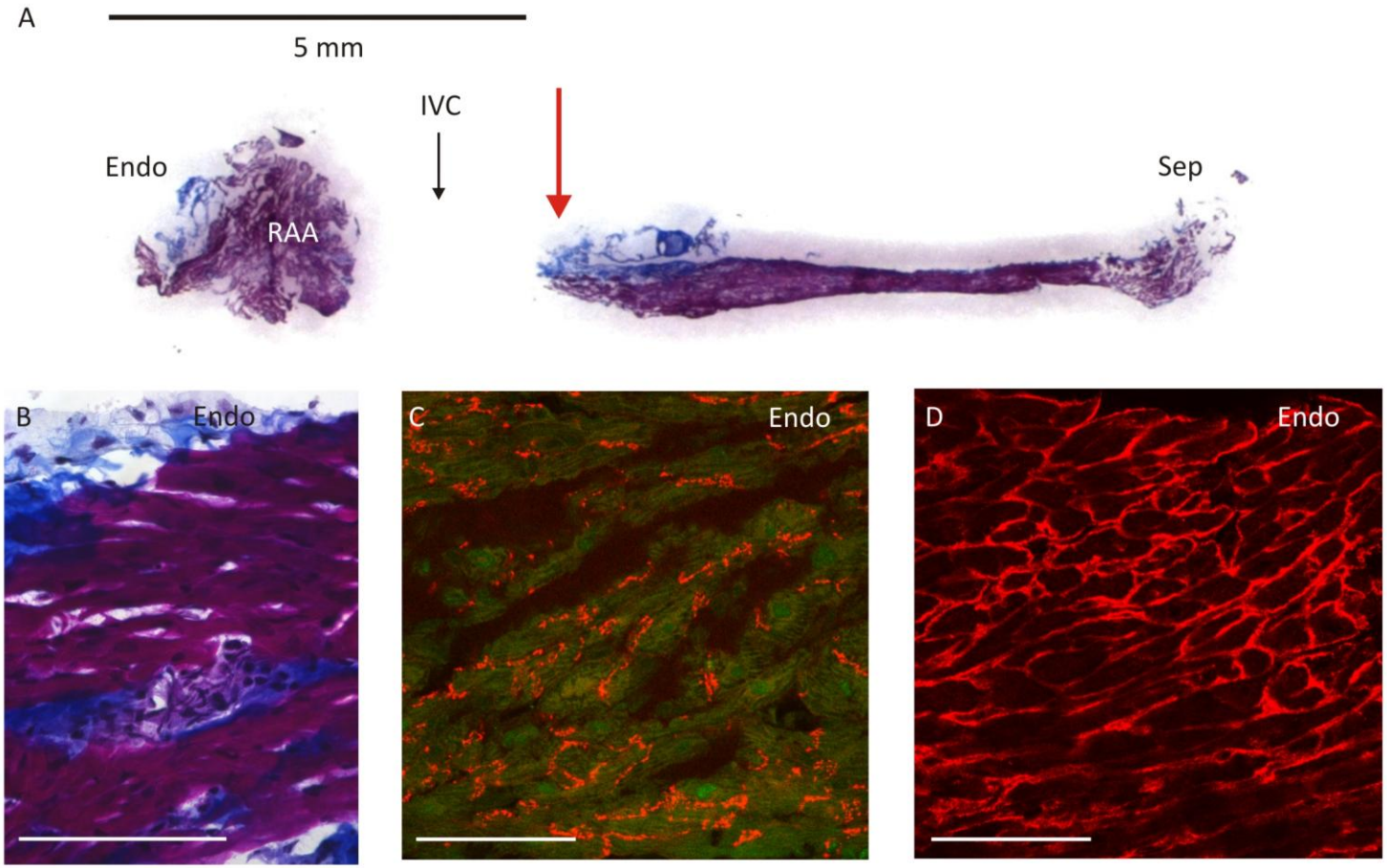

Figure 71. The histology and immunohistochemistry of the subsidiary pacemaker. Preparation 5. A) Sick sinus preparations were mapped as previously described and then frozen. 16 µm cryosections at the level of the leading pacemaker were stained with Masson's trichrome. The leading pacemaker is marked by the red arrow. B) Masson's trichrome staining of the leading pacemaker site. C) Ion channel and gap junction expression at the leading pacemaker site. Sections were labelled for HCN4 (green) and Cx43 (red). D) Cell size at the leading pacemaker site. The cell membrane of myocytes was labelled using an antibody to caveolin-3. For Masson's trichrome: purple, myocytes; blue, connective tissue. Endo, endocardium; IVC, inferior vena cava; LA, left atrium, RAA, right atrial appendage; Sep, interatrial septum. Scale bar in panels B - D = 100 µm.

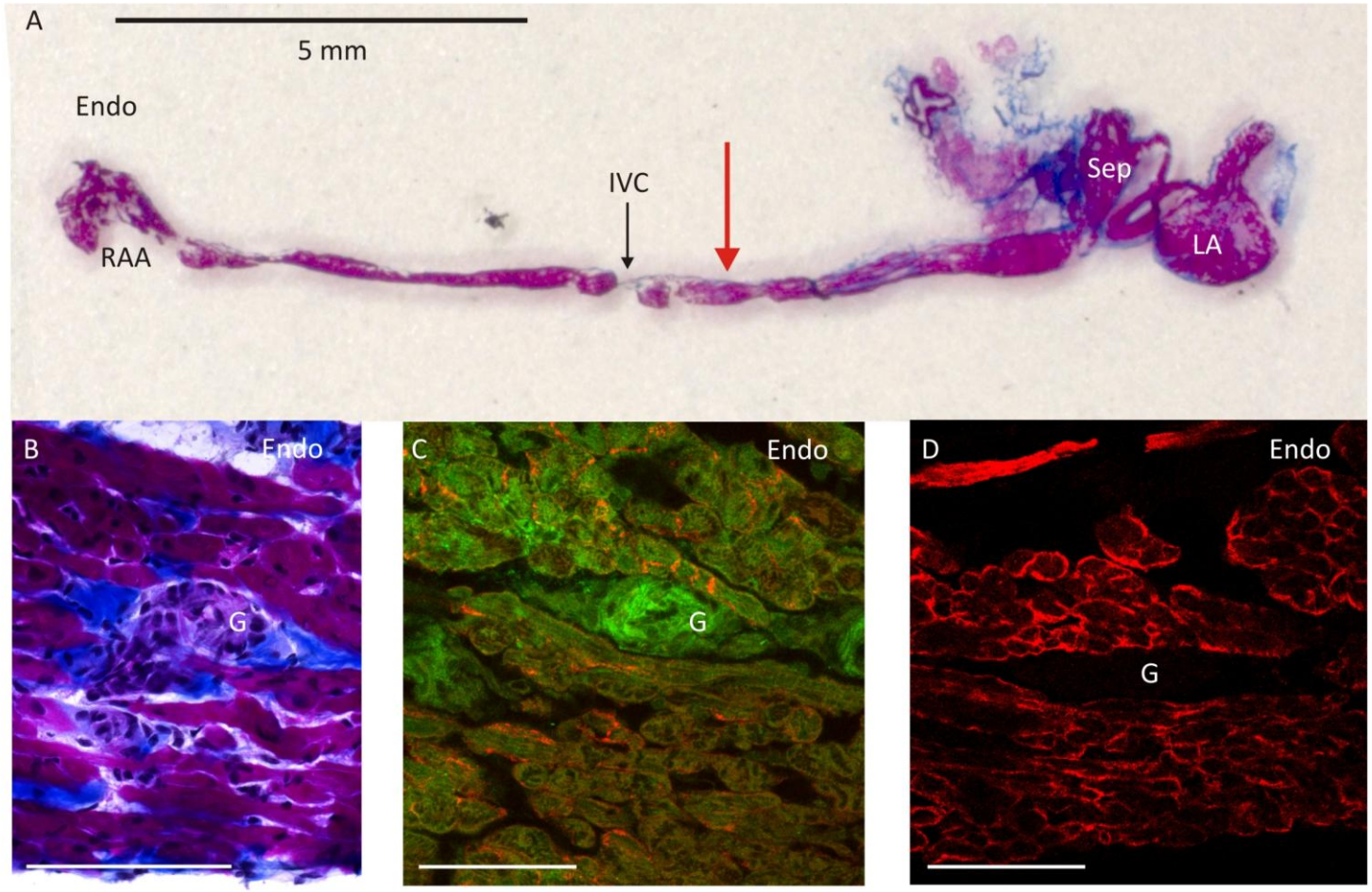

Figure 72. The histology and immunohistochemistry of the subsidiary pacemaker. Preparation 6. A) Sick sinus preparations were mapped as previously described then frozen. 16 µm cryosections at the level of the leading pacemaker were stained with Masson's trichrome. The leading pacemaker is marked by the red arrow. B) Masson's trichrome staining of the leading pacemaker site. C) Ion channel and gap junction expression at the leading pacemaker site. Sections were labelled for HCN4 (green) and Cx43 (red). D) Cell size at the leading pacemaker site. The cell membrane of myocytes was labelled using an antibody to caveolin-3. For Masson's trichrome: purple, myocytes; blue, connective tissue. Endo, endocardium; IVC, inferior vena cava; LA, left atrium, RAA, right atrial appendage; Sep, interatrial septum. Scale bar in panels B - D = 100 µm.

The author

Qualifications

MRCP (UK)

MA (Oxon)

BMBCh (Oxxon)

BA (Oxon, Physiological Sciences, 2i)

Prizes and awards

Turnberg cup (clinical academic trainees award), University of Manchester, 2010

AstraZeneca clinical research prize finalist, 2010

University of Manchester school of clinical and laboratory sciences research showcase. Poster presentation 2nd prize, 2009

Andrew Hopley Prize, University of Oxford. Best research dissertation, 1998

Wellcome Trust Scholarship for vacation research, 1998

St Edmund Hall, University of Oxford. Open scholarship for academic achievement. 1996 and 1997

Selected abstracts and publications

Morris GM, et al. Detection and Measurement of Cardiac Ion Channels. *Cardiac electrophysiology, methods and models.* Sigg D 2010 (Ed). *Springer.*New York.

Morris GM, et al. The Anatomy and Physiology of the Sinoatrial Node – A Contemporary Review. *PACE*. 2010;33:1392

Morris GM, et al. Perspectives -- biological pacing, a clinical reality? *Ther Adv Cardiovasc Dis.* 2009;3:479-483

Morris GM, et al. The association of heart valve diseases with coronary artery dominance. *J Heart Valve Dis*. 2010;19:389

Morris GM, et al. Retroperitoneal hematoma after diagnostic coronary angiography caused by collateralization of a chronic common femoral artery occlusion secondary to childhood femoral cannulation. *Circ Cardiovasc Interv*. 2009;2:580

Morris GM, et al. A cardiac biopacemaker created by acceleration of a subsidiary pacemaker via adenovirus mediated expression of a chimaeric pacemaker channel, HCN212. *Eur Heart J*. 2010;31(suppl 1):1

Morris GM, et al. Accelerated Activity of a Subsidiary Cardiac Pacemaker Induced by Adenovirus-Mediated Expression of a Chimeric Pacemaker Channel, HCN212. *Hum Gene Ther.* 2010;21:506

Morris GM, et al. The association of valve disease and a dominant left coronary circulation. *Eur Heart J.* 2009;30(Abstract Supplement),1039

Morris GM, et al. Adenovirus-mediated transgene expression in the sinus node and development of a bradycardic model for the *in vitro* study of biopacemaking in sick sinus syndrome. *Proc Physiol Soc 8*.(2007);PC36.

Grants

British Heart Foundation project grant (co-applicant): Effect of athletic training on the cardiac conduction system, ups and downs. Professor M.R. Boyett (PI). 2010-2013

References

1. Siegel RA. *Galen's System of Physiology and Medicine*. New York: Karger; 1968.

2. Gaskell WH. The contraction of cardiac muscle. In: Schafer EA, ed. *Textbook of Physiology*. Edinburgh: Pentland; 1899.

3. Gaskell WH. On the innervation of the heart, with especial reference to the heart of the tortoise. *J Physiol.* 1883;4:43-230.

4. His W, Jr. The story of the atrioventricular bundle with remarks concerning embryonic heart activity. *J Hist Med Allied Sci.* 1949;4:319-333.

5. Tawara S. *Das reizleitungssystem des sauetierherzens*: Gustav Fischer; 1906.

6. Schweitzer P. Jan Evangelista Purkinje. *Clin Cardiol.* 1991;14:85-86.

7. Keith A, Flack M. The form and nature of the muscular connections between the primary divisions of the vertebrate heart. *J Anat Physiol.* 1907;41:172-189.

8. Lewis T. The excitation wave in the heart. In: Lewis T, ed. *Lectures on the Heart*. New York: Paul B. Hoeber; 1915.

9. Christoffels VM, Smits GJ, Kispert A, Moorman AF. Development of the pacemaker tissues of the heart. *Circ Res.* 2010;106:240-254.

10. Christoffels VM, Moorman AFM. Development of the Cardiac Conduction System: Why Are Some Regions of the Heart More Arrhythmogenic Than Others? *Circ Arrhythm Electrophysiol.* 2009;2:195-207.

11. de Jong F, Opthof T, Wilde AA, Janse MJ, Charles R, Lamers WH, Moorman AF. Persisting zones of slow impulse conduction in developing chicken hearts. *Circ Res.* 1992;71:240-250.

12. Paff GH, Boucek RJ, Harrell TC. Observations on the development of the electrocardiogram. *Anat Rec.* 1968;160:575-582.

13. Moorman AF, Christoffels VM. Cardiac chamber formation: development, genes, and evolution. *Physiol Rev.* 2003;83:1223-1267.

14. van den Berg G, Abu-Issa R, de Boer BA, Hutson MR, de Boer PA, Soufan AT, Ruijter JM, Kirby ML, van den Hoff MJ, Moorman AF. A caudal proliferating growth center contributes to both poles of the forming heart tube. *Circ Res.* 2009;104:179-188.

15. Van Mierop LH. Location of pacemaker in chick embryo heart at the time of initiation of heartbeat. *Am J Physiol.* 1967;212:407-415.

16. Mommersteeg MTM, Hoogaars WMH, Prall OWJ, de Gier-de Vries C, Wiese C, Clout DEW, Papaioannou VE, Brown NA, Harvey RP, Moorman AFM, Christoffels VM. Molecular Pathway for the Localized Formation of the Sinoatrial Node. *Circ Res.* 2007;100:354-362.

17. Franco D, Campione M. The role of Pitx2 during cardiac development. Linking left-right signaling and congenital heart diseases. *Trends Cardiovasc Med.* 2003;13:157-163.

18. Yamada M, Revelli JP, Eichele G, Barron M, Schwartz RJ. Expression of chick Tbx-2, Tbx-3, and Tbx-5 genes during early heart development: evidence for BMP2 induction of Tbx2. *Dev Biol.* 2000;228:95-105.

19. Christoffels VM, Hoogaars WM, Tessari A, Clout DE, Moorman AF, Campione M. T-box transcription factor Tbx2 represses differentiation and formation of the cardiac chambers. *Dev Dyn.* 2004;229:763-770.

20. Harrelson Z, Kelly RG, Goldin SN, Gibson-Brown JJ, Bollag RJ, Silver LM, Papaioannou VE. Tbx2 is essential for patterning the atrioventricular canal and for morphogenesis of the outflow tract during heart development. *Development.* 2004;131:5041-5052.

21. Hoogaars WM, Tessari A, Moorman AF, de Boer PA, Hagoort J, Soufan AT, Campione M, Christoffels VM. The transcriptional repressor Tbx3 delineates the developing central conduction system of the heart. *Cardiovasc Res.* 2004;62:489-499.

22. Rutenberg JB, Fischer A, Jia H, Gessler M, Zhong TP, Mercola M. Developmental patterning of the cardiac atrioventricular canal by Notch and Hairy-related transcription factors. *Development.* 2006;133:4381-4390.

23. Kokubo H, Miyagawa-Tomita S, Nakazawa M, Saga Y, Johnson RL. Mouse hesr1 and hesr2 genes are redundantly required to mediate Notch signaling in the developing cardiovascular system. *Dev Biol.* 2005;278:301-309.

24. Kistler PM, Fynn SP, Haqqani H, Stevenson IH, Vohra JK, Morton JB, Sparks PB, Kalman JM. Focal atrial tachycardia from the ostium of the coronary sinus: electrocardiographic and electrophysiological characterization and radiofrequency ablation. *J Am Coll Cardiol.* 2005;45:1488-1493.

25. Kalman JM, Olgin JE, Karch MR, Hamdan M, Lee RJ, Lesh MD. "Cristal tachycardias": origin of right atrial tachycardias from the crista terminalis identified by intracardiac echocardiography. *J Am Coll Cardiol.* 1998;31:451-459.

26. Sanchez-Quintana D, Cabrera JA, Farre J, Climent V, Anderson RH, Ho SY. Sinus node revisited in the era of electroanatomical mapping and catheter ablation. *Heart.* 2005;91:189-194.

27. James TN, Sherf L, Fine G, Morales AR. Comparative ultrastructure of the sinus node in man and dog. *Circulation.* 1966;34:139-163.

28. Masson-Pevet M, Bleeker WK, Mackaay AJ, Bouman LN, Houtkooper JM. Sinus node and atrium cells from the rabbit heart: a quantitative electron microscopic description after electrophysiological localization. *J Mol Cell Cardiol.* 1979;11:555-568.

29. Opthof T, de Jonge B, Mackaay AJC, Bleeker WK, Masson-Pevet M, Jongsma HJ, Bouman LN. Functional and morphological organization of the guinea-pig

sinoatrial node compared with the rabbit sinoatrial node. *J Mol Cell Cardiol.* 1985;17:549-564.

30. Lowe JE, Hartwich T, Takla M, Schaper J. Ultrastructure of electrophysiologically identified human sinoatrial nodes. *Basic Res Cardiol.* 1988;83:401-409.

31. Opthof T, de Jonge B, Masson-Pevet M, Jongsma HJ, Bouman LN. Functional and morphological organization of the cat sinoatrial node. *J Mol Cell Cardiol.* 1986;18:1015-1031.

32. Alings AM, Abbas RF, Bouman LN. Age-related changes in structure and relative collagen content of the human and feline sinoatrial node. A comparative study. *Eur Heart J.* 1995;16:1655-1667.

33. Opthof T. *The Mammalian Sinoatrial Node. A Comparative Morphological and Electrophysiological Study*, University of Amsterdam; 1986.

34. James TN. Anatomy of the human sinus node. *Anat Rec.* 1961;141:109-139.

35. Truex RC, Smythe MQ, Taylor MJ. Reconstruction of the human sinoatrial node. *Anat Rec.* 1967;159:371-378.

36. Boineau JP, Canavan TE, Schuessler RB, Cain ME, Corr PB, Cox JL. Demonstration of a widely distributed atrial pacemaker complex in the human heart. *Circulation.* 1988;77:1221-1237.

37. Anderson KR, Ho SY, Anderson RH. Location and vascular supply of sinus node in human heart. *Br Heart J.* 1979;41:28-32.

38. Dobrzynski H, Li J, Tellez J, Greener ID, Nikolski VP, Wright SE, Parson SH, Jones SA, Lancaster MK, Yamamoto M, Honjo H, Takagishi Y, Kodama I, Efimov IR, Billeter R, Boyett MR. Computer three-dimensional reconstruction of the sinoatrial node. *Circulation.* 2005;111:846-854.

39. Boyett MR, Honjo H, Kodama I. The sinoatrial node, a heterogeneous pacemaker structure. *Cardiovasc Res.* 2000;47:658-687.

40. Boyett MR, Dobrzynski H, Lancaster MK, Jones SA, Honjo H, Kodama I. Sophisticated architecture is required for the sinoatrial node to perform its normal pacemaker function. *J Cardiovasc Electrophysiol.* 2003;14:104-106.

41. Brioschi C, Micheloni S, Tellez JO, Pisoni G, Longhi R, Moroni P, Billeter R, Barbuti A, Dobrzynski H, Boyett MR, DiFrancesco D, Baruscotti M. Distribution of the pacemaker HCN4 channel mRNA and protein in the rabbit sinoatrial node. *J Mol Cell Cardiol.* 2009;47:221-227.

42. Oosthoek PW, Viragh S, Lamers WH, Moorman AF. Immunohistochemical delineation of the conduction system. II: The atrioventricular node and Purkinje fibers. *Circ Res.* 1993;73:482-491.

43. Cabo C, Pertsov AM, Baxter WT, Davidenko JM, Gray RA, Jalife J. Wave-front curvature as a cause of slow conduction and block in isolated cardiac muscle. *Circ Res.* 1994;75:1014-1028.

44. Fedorov VV, Schuessler RB, Hemphill M, Ambrosi CM, Chang R, Voloshina AS, Brown K, Hucker WJ, Efimov IR. Structural and functional evidence for discrete exit pathways that connect the canine sinoatrial node and atria. *Circ Res.* 2009;104:915-923.

45. Bozler E. The initation of impulses in cardiac muscle. *Am J Physiol.* 1943;138:273-282.

46. West TC. Ultramicroelectrode recording from the cardiac pacemaker. *J Pharmacol Exp Ther.* 1955;115:283-290.

47. Harmar AJ, Hills RA, Rosser EM, Jones M, Buneman OP, Dunbar DR, Greenhill SD, Hale VA, Sharman JL, Bonner TI, Catterall WA, Davenport AP, Delagrange P, Dollery CT, Foord SM, Gutman GA, Laudet V, Neubig RR, Ohlstein EH, Olsen RW, Peters J, Pin J-P, Ruffolo RR, Searls DB, Wright MW, Spedding M. IUPHAR-DB: the IUPHAR database of G protein-coupled receptors and ion channels. *Nucl Acids Res.* 2009;37:D680-685.

48. Chandler NJ, Greener ID, Tellez JO, Inada S, Musa H, Molenaar P, Difrancesco D, Baruscotti M, Longhi R, Anderson RH, Billeter R, Sharma V, Sigg DC, Boyett MR, Dobrzynski H. Molecular architecture of the human sinus node: insights into the function of the cardiac pacemaker. *Circulation.* 2009;119:1562-1575.

49. Miake J, Marban E, Nuss HB. Biological pacemaker created by gene transfer. *Nature.* 2002;419:132-133.

50. Ito H, Ono K. A rapidly activating delayed rectifier K^+ channel in rabbit sinoatrial node cells. *Am J Physiol Heart Circ Physiol.* 1995;269:H443-452.

51. Anumonwo JM, Freeman LC, Kwok WM, Kass RS. Delayed rectification in single cells isolated from guinea pig sinoatrial node. *Am J Physiol Heart Circ Physiol.* 1992;262:H921-925.

52. Lei M, Brown HF. Two components of the delayed rectifier potassium current, I_K, in rabbit sino-atrial node cells. *Experimental Physiology.* 1996;81:725-741.

53. Lei M, Honjo H, Kodama I, Boyett MR. Heterogeneous expression of the delayed-rectifier K^+ currents $I_{K,r}$ and $I_{K,s}$ in rabbit sinoatrial node cells. *J Physiol.* 2001;535:703-714.

54. Verheijck EE, van Ginneken ACG, Bourier J, Bouman LN. Effects of delayed rectifier current blockade by E-4031 on impulse generation in single sinoatrial nodal myocytes of the rabbit. *Circ Res.* 1995;76:607-615.

55. Irisawa H, Brown HF, Giles W. Cardiac pacemaking in the sinoatrial node. *Physiol Rev.* 1993;73:197-227.

56. Ono K, Ito H. Role of rapidly activating delayed rectifier K^+ current in sinoatrial node pacemaker activity. *Am J Physiol Heart Circ Physiol.* 1995;269:H453-462.

57. Brahmajothi MV, Morales MJ, Reimer KA, Strauss HC. Regional Localization of ERG, the Channel Protein Responsible for the Rapid Component of the Delayed Rectifier, K^+ Current in the Ferret Heart. *Circ Res.* 1997;81:128-135.

58. Chan YC, Siu CW, Lau YM, Lau CP, Li RA, Tse HF. Synergistic effects of inward rectifier (I_K) and pacemaker (I_f) currents on the induction of bioengineered cardiac automaticity. *J Cardiovasc Electrophysiol.* 2009.

59. Brown AM. Drugs, hERG and sudden death. *Cell Calcium.* 2004;35:543-547.

60. Sanguinetti MC, Jiang C, Curran ME, Keating MT. A mechanistic link between an inherited and an acquired cardiac arrthytmia: HERG encodes the $I_{K,r}$ potassium channel. *Cell.* 1995;81:299-307.

61. Trudeau MC, Warmke JW, Ganetzky B, Robertson GA. HERG, a human inward rectifier in the voltage-gated potassium channel family. *Science.* 1995;269:92-95.

62. Sanguinetti MC, Tristani-Firouzi M. hERG potassium channels and cardiac arrhythmia. *Nature.* 2006;440:463-469.

63. Nerbonne JM, Kass RS. Molecular physiology of cardiac repolarization. *Physiol. Rev.* 2005;85:1205-1253.

64. Sanguinetti MC, Jurkiewicz NK. Two components of cardiac delayed rectifier K^+ current. Differential sensitivity to block by class III antiarrhythmic agents. *J Gen Physiol.* 1990;96:195-215.

65. Shibasaki T. Conductance and kinetics of delayed rectifier potassium channels in nodal cells of the rabbit heart. *J Physiol.* 1987;387:227-250.

66. Zhou Z, Gong Q, Ye B, Fan Z, Makielski JC, Robertson GA, January CT. Properties of HERG Channels Stably Expressed in HEK 293 Cells Studied at Physiological Temperature. *Biophys J.* 1998;74:230-241.

67. Hancox JC, McPate MJ, El Harchi A, Zhang Yh. The hERG potassium channel and hERG screening for drug-induced torsades de pointes. *Pharmacol Therapeut.* 2008;119:118-132.

68. Smith PL, Baukrowitz T, Yellen G. The inward rectification mechanism of the HERG cardiac potassium channel. *Nature.* 1996;379:833-836.

69. Spector PS, Curran ME, Zou A, Keating MT, Sanguinetti MC. Fast inactivation causes rectification of the $I_{K,r}$ channel. *J Gen Physiol.* 1996;107:611-619.

70. Noble D, Tsien RW. The kinetics and rectifier properties of the slow potassium current in cardiac Purkinje fibres. *J Physiol.* 1968;195:185-214.

71. Brown GL, Eccles JC. The action of a single vagal volley on the rhythm of the heart beat. *J Physiol.* 1934;82:211-241.

72. DiFrancesco D. A new interpretation of the pace-maker current in calf Purkinje fibres. *J Physiol.* 1981;314:359-376.

73. Brown HF, DiFrancesco D, Noble SJ. How does adrenaline accelerate the heart? *Nature.* 1979;280:235-236.

74. Bois P, Bescond J, Renaudon B, Lenfant J. Mode of action of bradycardic agent, S 16257, on ionic currents of rabbit sinoatrial node cells. *Br J Pharmacol.* 1996;118:1051-1057.

75. Baker K, Warren KS, Yellen G, Fishman MC. Defective "pacemaker" current (I_h) in a zebrafish mutant with a slow heart rate. *Proc Natl Acad Sci USA.* 1997;94:4554-4559.

76. DiFrancesco D. Serious workings of the funny current. *Prog Biophys Mol Biol.* 2006;90:13-25.

77. Chandler NJ, Greener ID, Tellez JO, Inada S, Musa H, Molenaar P, Difrancesco D, Baruscotti M, Longhi R, Anderson RH, Billeter R, Sharma V, Sigg DC, Boyett MR, Dobrzynski H. Molecular architecture of the human sinus node: insights into the function of the cardiac pacemaker. *Circulation.* 2009;119:1562-1575.

78. DiFrancesco D. The Role of the Funny Current in Pacemaker Activity. *Circ Res.* 2009;106:434-446.

79. DiFrancesco D, Tromba C. Inhibition of the hyperpolarization-activated current (I_f) induced by acetylcholine in rabbit sino-atrial node myocytes. *J Physiol.* 1988;405:477-491.

80. Robinson RB, Siegelbaum SA. Hyperpolarization-activated cation currents: from molecules to physiological function. *Annu Rev Physiol.* 2003;65:453-480.

81. Pape HC. Queer current and pacemaker: the hyperpolarization-activated cation current in neurons. *Annu Rev Physiol.* 1996;58:299-327.

82. Attwell D, Wilson M. Behaviour of the rod network in the tiger salamander retina mediated by membrane properties of individual rods. *J Physiol.* 1980;309:287-315.

83. Edman A, Gestrelius S, Grampp W. Current activation by membrane hyperpolarization in the slowly adapting lobster stretch receptor neurone. *J Physiol.* 1987;384:671-690.

84. DiFrancesco D. A study of the ionic nature of the pace-maker current in calf Purkinje fibres. *J Physiol.* 1981;314:377-393.

85. Angstadt JD, Calabrese RL. A hyperpolarization-activated inward current in heart interneurons of the medicinal leech. *J Neurosci.* 1989;9:2846-2857.

86. Solomon JS, Nerbonne JM. Two kinetically distinct components of hyperpolarization-activated current in rat superior colliculus-projecting neurons. *J Physiol.* 1993;469:291-313.

87. Corotto FS, Michel WC. A hyperpolarization-activated cation conductance in lobster olfactory receptor neurons. *J Neurophysiol.* 1994;72:360-365.

88. DiFrancesco D. Characterization of single pacemaker channels in cardiac sino-atrial node cells. *Nature.* 1986;324:470-473.

89. Yanagihara K, Irisawa H. Inward current activated during hyperpolarization in the rabbit sinoatrial node cell. *Pflugers Arch.* 1980;385:11-19.

90. van Ginneken AC, Giles W. Voltage clamp measurements of the hyperpolarization-activated inward current I_f in single cells from rabbit sino-atrial node. *J Physiol.* 1991;434:57-83.

91. Brown H, Kimura J, Noble S. Evidence that the current I_f in the sino-atrial node has a potassium component (Abstract). *J Physiol.* 1980;308:33P - 34P.

92. Nakayama T, Kurachi Y, Noma A, Irisawa H. Action potential and membrane currents of single pacemaker cells of the rabbit heart. *Pflugers Arch.* 1984;402:248-257.

93. Nathan RD. Role of I_f in pacemaker activity of the sinoatrial node (abstract). *Biophys J.* 1987;51:263a.

94. Denyer JC, Brown HF. Pacemaking in rabbit isolated sino-atrial node cells during Cs^+ block of the hyperpolarization-activated current I_f. *J Physiol.* 1990;429:401-409.

95. DiFrancesco D. Pacemaker mechanisms in cardiac tissue. *Annu Rev Physiol.* 1993;55:455-472.

96. DiFrancesco D. Block and activation of the pace-maker channel in calf Purkinje fibres: effects of potassium, caesium and rubidium. *J Physiol.* 1982;329:485-507.

97. Fox K, Ford I, Steg PG, Tendera M, Ferrari R. Ivabradine for patients with stable coronary artery disease and left-ventricular systolic dysfunction (BEAUTIFUL): a randomised, double-blind, placebo-controlled trial. *Lancet.* 2008;372:807-816.

98. Stieber J, Herrmann S, Feil S, Loster J, Feil R, Biel M, Hofmann F, Ludwig A. The hyperpolarization-activated channel HCN4 is required for the generation of pacemaker action potentials in the embryonic heart. *Proc Natl Acad Sci USA.* 2003;100:15235-15240.

99. Ueda K, Nakamura K, Hayashi T, Inagaki N, Takahashi M, Arimura T, Morita H, Higashiuesato Y, Hirano Y, Yasunami M, Takishita S, Yamashina A, Ohe T, Sunamori M, Hiraoka M, Kimura A. Functional characterization of a trafficking-defective HCN4 mutation, D553N, associated with cardiac arrhythmia. *J Biol Chem.* 2004;279:27194-27198.

100. Milanesi R, Baruscotti M, Gnecchi-Ruscone T, DiFrancesco D. Familial sinus bradycardia associated with a mutation in the cardiac pacemaker channel. *N Engl J Med.* 2006;354:151-157.

101. Schulze-Bahr E, Neu A, Friederich P, Kaupp UB, Breithardt G, Pongs O, Isbrandt D. Pacemaker channel dysfunction in a patient with sinus node disease. *J Clin Invest.* 2003;111:1537-1545.

102. Santoro B, Tibbs GR. The HCN gene family: molecular basis of the hyperpolarization-activated pacemaker channels. *Ann N Y Acad Sci.* 1999;868:741-764.

103. Kaupp UB, Seifert R. Molecular diversity of pacemaker ion channels. *Annu Rev Physiol.* 2001;63:235-257.

104. Biel M, Schneider A, Wahl C. Cardiac HCN channels: structure, function, and modulation. *Trends Cardiovasc Med.* 2002;12:206-212.

105. Chen S, Wang J, Siegelbaum SA. Properties of hyperpolarization-activated pacemaker current defined by coassembly of HCN1 and HCN2 subunits and basal modulation by cyclic nucleotide. *J Gen Physiol.* 2001;117:491-504.

106. Wainger BJ, DeGennaro M, Santoro B, Siegelbaum SA, Tibbs GR. Molecular mechanism of cAMP modulation of HCN pacemaker channels. *Nature.* 2001;411:805-810.

107. DiFrancesco D, Tortora P. Direct activation of cardiac pacemaker channels by intracellular cyclic AMP. *Nature.* 1991;351:145-147.

108. DiFrancesco D, Ducouret P, Robinson RB. Muscarinic modulation of cardiac rate at low acetylcholine concentrations. *Science.* 1989;243:669-671.

109. DiFrancesco D, Ferroni A, Mazzanti M, Tromba C. Properties of the hyperpolarizing-activated current (I_f) in cells isolated from the rabbit sino-atrial node. *J Physiol.* 1986;377:61-88.

110. Altomare C, Terragni B, Brioschi C, Milanesi R, Pagliuca C, Viscomi C, Moroni A, Baruscotti M, Difrancesco D. Heteromeric HCN1-HCN4 channels: a comparison with native pacemaker channels from the rabbit sinoatrial node. *J Physiol.* 2003;549:347-359.

111. Barbuti A, Baruscotti M, DiFrancesco D. The pacemaker current: from basics to the clinics. *J Cardiovasc Electrophysiol.* 2007;18:342-347.

112. Yu H, Wu J, Potapova I, Wymore RT, Holmes B, Zuckerman J, Pan Z, Wang H, Shi W, Robinson RB, El-Maghrabi MR, Benjamin W, Dixon J, McKinnon D, Cohen IS, Wymore R. MinK-related peptide 1: A beta subunit for the HCN ion channel subunit family enhances expression and speeds activation. *Circ Res.* 2001;88:E84-E87.

113. Barbuti A, Gravante B, Riolfo M, Milanesi R, Terragni B, DiFrancesco D. Localization of pacemaker channels in lipid rafts regulates channel kinetics. *Circ Res.* 2004;94:1325-1331.

114. Barbuti A, Terragni B, Brioschi C, DiFrancesco D. Localization of f-channels to caveolae mediates specific beta2-adrenergic receptor modulation of rate in sinoatrial myocytes. *J Mol Cell Cardiol.* 2007;42:71-78.

115. Pian P, Bucchi A, Robinson RB, Siegelbaum SA. Regulation of gating and rundown of HCN hyperpolarization-activated channels by exogenous and endogenous PIP2. *J Gen Physiol.* 2006;128:593-604.

116. Poolos NP, Bullis JB, Roth MK. Modulation of h-channels in hippocampal pyramidal neurons by p38 mitogen-activated protein kinase. *J Neurosci.* 2006;26:7995-8003.

117. Zong X, Eckert C, Yuan H, Wahl-Schott C, Abicht H, Fang L, Li R, Mistrik P, Gerstner A, Much B, Baumann L, Michalakis S, Zeng R, Chen Z, Biel M. A novel mechanism of modulation of hyperpolarization-activated cyclic nucleotide-gated channels by Src kinase. *J Biol Chem.* 2005;280:34224-34232.

118. Moosmang S, Stieber J, Zong X, Biel M, Hofmann F, Ludwig A. Cellular expression and functional characterization of four hyperpolarization-activated pacemaker channels in cardiac and neuronal tissues. *Eur J Biochem.* 2001;268:1646-1652.

119. Shi W, Wymore R, Yu H, Wu J, Wymore RT, Pan Z, Robinson RB, Dixon JE, McKinnon D, Cohen IS. Distribution and prevalence of hyperpolarization-activated cation channel (HCN) mRNA expression in cardiac tissues. *Circ Res.* 1999;85:e1-e6.

120. Shi WY, H. Wu, J. Zuckerman, J. Wymore R. The distribution and prevalence of HCN isoforms in the canine heart and their relation to the voltage dependence of I_f (Abstract). *Biophys J.* 2000;78:353A.

121. Azene EM, Xue T, Marban E, Tomaselli GF, Li RA. Non-equilibrium behavior of HCN channels: insights into the role of HCN channels in native and engineered pacemakers. *Cardiovasc Res.* 2005;67:263-273.

122. Maltsev VA, Lakatta EG. Dynamic interactions of an intracellular Ca^{2+} clock and membrane ion channel clock underlie robust initiation and regulation of cardiac pacemaker function. *Cardiovasc Res.* 2008;77:274-284.

123. Lakatta EG, DiFrancesco D. What keeps us ticking: a funny current, a calcium clock, or both? *J Mol Cell Cardiol.* 2009;47:157-170.

124. Hagiwara N, Irisawa H, Kameyama M. Contribution of two types of calcium currents to the pacemaker potentials of rabbit sino-atrial node cells. *J Physiol.* 1988;395:233-253.

125. Lacinova L. Voltage-dependent calcium channels. *Gen Physiol Biophys.* 2005;24 Suppl 1:1-78.

126. Ono K, Iijima T. Pathophysiological significance of T-type Ca^{2+} channels: properties and functional roles of T-type Ca^{2+} channels in cardiac pacemaking. *J Pharmacol Sci.* 2005;99:197-204.

127. Mangoni ME, Traboulsie A, Leoni AL, Couette B, Marger L, Le Quang K, Kupfer E, Cohen-Solal A, Vilar J, Shin HS, Escande D, Charpentier F, Nargeot J, Lory P. Bradycardia and slowing of the atrioventricular conduction in mice lacking $Ca_V3.1$/alpha1G T-type calcium channels. *Circ Res.* 2006;98:1422-1430.

128. Cribbs LL, Gomora JC, Daud AN, Lee JH, Perez-Reyes E. Molecular cloning and functional expression of $Ca_V3.1c$, a T-type calcium channel from human brain. *FEBS Lett.* 2000;466:54-58.

129. Dolphin AC, Page KM, Berrow NS, Stephens GJ, Canti C. Dissection of the calcium channel domains responsible for modulation of neuronal voltage-

dependent calcium channels by G proteins. *Ann N Y Acad Sci.* 1999;868:160-174.

130. Staes M, Talavera K, Klugbauer N, Prenen J, Lacinova L, Droogmans G, Hofmann F, Nilius B. The amino side of the C-terminus determines fast inactivation of the T-type calcium channel alpha1G. *J Physiol.* 2001;530:35-45.

131. Trafford AW, O'Neill SC, Eisner DA. Factors affecting the propagation of locally activated systolic Ca transients in rat ventricular myocytes. *Pflugers Arch.* 1993;425:181-183.

132. Fabiato A. Calcium-induced release of calcium from the cardiac sarcoplasmic reticulum. *Am J Physiol.* 1983;245:C1-14.

133. Franzini-Armstrong C, Protasi F, Ramesh V. Shape, size, and distribution of Ca^{2+} release units and couplons in skeletal and cardiac muscles. *Biophys J.* 1999;77:1528-1539.

134. Stern MD. Theory of excitation-contraction coupling in cardiac muscle. *Biophys J.* 1992;63:497-517.

135. Wang SQ, Song LS, Lakatta EG, Cheng H. Ca^{2+} signalling between single L-type Ca^{2+} channels and ryanodine receptors in heart cells. *Nature.* 2001;410:592-596.

136. Hamilton SL, Serysheva, II. Ryanodine receptor structure: progress and challenges. *J Biol Chem.* 2009;284:4047-4051.

137. Song LS, Guatimosim S, Gomez-Viquez L, Sobie EA, Ziman A, Hartmann H, Lederer WJ. Calcium biology of the transverse tubules in heart. *Ann N Y Acad Sci.* 2005;1047:99-111.

138. Ayettey AS, Navaratnam V. The T-tubule system in the specialized and general myocardium of the rat. *J Anat.* 1978;127:125-140.

139. Maltsev VA, Vinogradova TM, Lakatta EG. The emergence of a general theory of the initiation and strength of the heartbeat. *J Pharmacol Sci.* 2006;100:338-369.

140. Lakatta EG. Functional implications of spontaneous sarcoplasmic reticulum Ca^{2+} release in the heart. *Cardiovasc Res.* 1992;26:193-214.

141. Schwartz A, Sordahl LA, Entman ML, Allen JC, Reddy YS, Goldstein MA, Luchi RJ, Wyborny LE. Abnormal biochemistry in myocardial failure. *Am J Cardiol.* 1973;32:407-422.

142. Fabiato A, Fabiato F. Calcium-induced release of calcium from the sarcoplasmic reticulum of skinned cells from adult human, dog, cat, rabbit, rat, and frog hearts and from fetal and new-born rat ventricles. *Ann N Y Acad Sci.* 1978;307:491-522.

143. Cheng H, Lederer WJ, Cannell MB. Calcium sparks: elementary events underlying excitation-contraction coupling in heart muscle. *Science.* 1993;262:740-744.

144. Bogdanov KY, Vinogradova TM, Lakatta EG. Sinoatrial nodal cell ryanodine receptor and Na^+-Ca^{2+} exchanger: molecular partners in pacemaker regulation. *Circ Res.* 2001;88:1254-1258.

145. Vinogradova TM, Zhou YY, Maltsev V, Lyashkov A, Stern M, Lakatta EG. Rhythmic ryanodine receptor Ca^{2+} releases during diastolic depolarization of sinoatrial pacemaker cells do not require membrane depolarization. *Circ Res.* 2004;94:802-809.

146. Chen B, Wu Y, Mohler PJ, Anderson ME, Song LS. Local control of Ca^{2+}-induced Ca^{2+} release in mouse sinoatrial node cells. *J Mol Cell Cardiol.* 2009;47:706-715.

147. Musa H, Lei M, Honjo H, Jones SA, Dobrzynski H, Lancaster MK, Takagishi Y, Henderson Z, Kodama I, Boyett MR. Heterogeneous expression of Ca^{2+} handling proteins in rabbit sinoatrial node. *J Histochem Cytochem.* 2002;50:311-324.

148. Lyashkov AE, Juhaszova M, Dobrzynski H, Vinogradova TM, Maltsev VA, Juhasz O, Spurgeon HA, Sollott SJ, Lakatta EG. Calcium cycling protein density and functional importance to automaticity of isolated sinoatrial nodal cells are independent of cell size. *Circ Res.* 2007;100:1723-1731.

149. Huser J, Blatter LA, Lipsius SL. Intracellular Ca^{2+} release contributes to automaticity in cat atrial pacemaker cells. *J Physiol.* 2000;524 Pt 2:415-422.

150. Nakayama H, Wilkin BJ, Bodi I, Molkentin JD. Calcineurin-dependent cardiomyopathy is activated by TRPC in the adult mouse heart. *FASEB J.* 2006;20:1660-1670.

151. Beech DJ, Xu SZ, McHugh D, Flemming R. TRPC1 store-operated cationic channel subunit. *Cell Calcium.* 2003;33:433-440.

152. Ju YK, Chu Y, Chaulet H, Lai D, Gervasio OL, Graham RM, Cannell MB, Allen DG. Store-Operated Ca^{2+} Influx and Expression of TRPC Genes in Mouse Sinoatrial Node. *Circ Res.* 2007;100:1605-1614.

153. Vinogradova TM, Lyashkov AE, Zhu W, Ruknudin AM, Sirenko S, Yang D, Deo S, Barlow M, Johnson S, Caffrey JL, Zhou YY, Xiao RP, Cheng H, Stern MD, Maltsev VA, Lakatta EG. High basal protein kinase A-dependent phosphorylation drives rhythmic internal Ca^{2+} store oscillations and spontaneous beating of cardiac pacemaker cells. *Circ Res.* 2006;98:505-514.

154. Vinogradova TM, Lyashkov AE, Zhu W, Spurgeon H, Maltsev VA, Lakatta EG. Constitutive phosphodiesterase activity confers negative feedback on intrinsic cAMP PKA regulation of local rhythmic subsarcolemmal calcium releases and spontaneous beating in rabbit sinoatrial nodal cells (abstract). *Biophys J.* 2005;88:303a

155. Ju YK, Allen DG. Intracellular calcium and Na^+-Ca^{2+} exchange current in isolated toad pacemaker cells. *J Physiol.* 1998;508 (Pt 1):153-166.

156. Iwamoto T. Sodium-calcium exchange inhibitors: therapeutic potential in cardiovascular diseases. *Future Cardiol.* 2005;1:519-529.

157. Hilgemann DW. The cardiac Na-Ca exchanger in giant membrane patches. *Ann N Y Acad Sci.* 1996;779:136-158.

158. Tellez JO, Dobrzynski H, Greener ID, Graham GM, Laing E, Honjo H, Hubbard SJ, Boyett MR, Billeter R. Differential expression of ion channel transcripts in atrial muscle and sinoatrial node in rabbit. *Circ Res.* 2006;99:1384-1393.

159. Kodama I, Nikmaram MR, Boyett MR, Suzuki R, Honjo H, Owen JM. Regional differences in the role of the Ca^{2+} and Na^{+} currents in pacemaker activity in the sinoatrial node. *Am J Physiol.* 1997;272:H2793-H2806.

160. Striessnig J. Pharmacology, structure and function of cardiac L-type Ca^{2+} channels. *Cell Physiol Biochem.* 1999;9:242-269.

161. Mangoni ME, Couette B, Bourinet E, Platzer J, Reimer D, Striessnig J, Nargeot J. Functional role of L-type $Ca_v1.3$ Ca^{2+} channels in cardiac pacemaker activity. *Proc Natl Acad Sci USA.* 2003;100:5543-5548.

162. Platzer J, Engel J, Schrott-Fischer A, Stephan K, Bova S, Chen H, Zheng H, Striessnig J. Congenital deafness and sinoatrial node dysfunction in mice lacking class D L-type Ca^{2+} channels. *Cell.* 2000;102:89-97.

163. Abriel H, Kass RS. Regulation of the Voltage-Gated Cardiac Sodium Channel Nav1.5 by Interacting Proteins. *Trends in Cardiovascular Medicine.* 2005;15:35-40.

164. Dobrzynski H, Boyett MR, Anderson RH. New insights into pacemaker activity: promoting understanding of sick sinus syndrome. *Circulation.* 2007;115:1921-1932.

165. Lei M, Jones SA, Liu J, Lancaster MK, Fung SS, Dobrzynski H, Camelliti P, Maier SK, Noble D, Boyett MR. Requirement of neuronal- and cardiac-type sodium channels for murine sinoatrial node pacemaking. *J Physiol.* 2004;559:835-848.

166. Maier SK, Westenbroek RE, Yamanushi TT, Dobrzynski H, Boyett MR, Catterall WA, Scheuer T. An unexpected requirement for brain-type sodium channels for control of heart rate in the mouse sinoatrial node. *Proc Natl Acad Sci USA.* 2003;100:3507-3512.

167. Lei M, Goddard C, Liu J, Leoni AL, Royer A, Fung SS, Xiao G, Ma A, Zhang H, Charpentier F, Vandenberg JI, Colledge WH, Grace AA, Huang CL. Sinus node dysfunction following targeted disruption of the murine cardiac sodium channel gene Scn5a. *J Physiol.* 2005;567:387-400.

168. Benson DW, Wang DW, Dyment M, Knilans TK, Fish FA, Strieper MJ, Rhodes TH, George AL, Jr. Congenital sick sinus syndrome caused by recessive mutations in the cardiac sodium channel gene (SCN5A). *J Clin Invest.* 2003;112:1019-1028.

169. Bezzina C, Veldkamp MW, van Den Berg MP, Postma AV, Rook MB, Viersma JW, van Langen IM, Tan-Sindhunata G, Bink-Boelkens MT, van Der Hout AH, Mannens MM, Wilde AA. A single Na^{+} channel mutation causing both long-QT and Brugada syndromes. *Circ Res.* 1999;85:1206-1213.

170. Groenewegen WA, Firouzi M, Bezzina CR, Vliex S, van Langen IM, Sandkuijl L, Smits JP, Hulsbeek M, Rook MB, Jongsma HJ, Wilde AA. A cardiac sodium channel mutation cosegregates with a rare connexin40 genotype in familial atrial standstill. *Circ Res.* 2003;92:14-22.

171. Smits JP, Koopmann TT, Wilders R, Veldkamp MW, Opthof T, Bhuiyan ZA, Mannens MM, Balser JR, Tan HL, Bezzina CR, Wilde AA. A mutation in the human cardiac sodium channel (E161K) contributes to sick sinus syndrome, conduction disease and Brugada syndrome in two families. *J Mol Cell Cardiol.* 2005;38:969-981.

172. Veldkamp MW, Wilders R, Baartscheer A, Zegers JG, Bezzina CR, Wilde AA. Contribution of sodium channel mutations to bradycardia and sinus node dysfunction in LQT3 families. *Circ Res.* 2003;92:976-983.

173. Verkerk AO, Wilders R, van Borren MM, Tan HL. Is sodium current present in human sinoatrial node cells? *Int J Biol Sci.* 2009;5:201-204.

174. Sohl G, Willecke K. Gap junctions and the connexin protein family. *Cardiovasc Res.* 2004;62:228-232.

175. Laird DW. Life cycle of connexins in health and disease. *Biochem J.* 2006;394:527-543.

176. Saez JC, Berthoud VM, Branes MC, Martinez AD, Beyer EC. Plasma membrane channels formed by connexins: their regulation and functions. *Physiol Rev.* 2003;83:1359-1400.

177. Solan JL, Lampe PD. Connexin43 phosphorylation: structural changes and biological effects. *Biochem J.* 2009;419:261-272.

178. Boyett MR, Inada S, Yoo S, Li J, Liu J, Tellez J, Greener ID, Honjo H, Billeter R, Lei M, Zhang H, Efimov IR, Dobrzynski H. Connexins in the sinoatrial and atrioventricular nodes. *Adv Cardiol.* 2006;42:175-197.

179. Hagendorff A, Schumacher B, Kirchhoff S, Luderitz B, Willecke K. Conduction disturbances and increased atrial vulnerability in Connexin40-deficient mice analyzed by transesophageal stimulation. *Circulation.* 1999;99:1508-1515.

180. Kirchhoff S, Kim JS, Hagendorff A, Thonnissen E, Kruger O, Lamers WH, Willecke K. Abnormal cardiac conduction and morphogenesis in connexin40 and connexin43 double-deficient mice. *Circ Res.* 2000;87:399-405.

181. Kirchhoff S, Nelles E, Hagendorff A, Kruger O, Traub O, Willecke K. Reduced cardiac conduction velocity and predisposition to arrhythmias in connexin40-deficient mice. *Curr Biol.* 1998;8:299-302.

182. Paznekas WA, Boyadjiev SA, Shapiro RE, Daniels O, Wollnik B, Keegan CE, Innis JW, Dinulos MB, Christian C, Hannibal MC, Jabs EW. Connexin 43 (GJA1) mutations cause the pleiotropic phenotype of oculodentodigital dysplasia. *Am J Hum Genet.* 2003;72:408-418.

183. Bleeker WK, Mackaay AJ, Masson-Pevet M, Bouman LN, Becker AE. Functional and morphological organization of the rabbit sinus node. *Circ Res.* 1980;46:11-22.

184. Boineau JP, Miller CB, Schuessler RB, Roeske WR, Autry LJ, Wylds AC, Hill DA. Activation sequence and potential distribution maps demonstrating multicentric atrial impulse origin in dogs. *Circ Res.* 1984;54:332-347.

185. Bromberg BI, Hand DE, Schuessler RB, Boineau JP. Primary negativity does not predict dominant pacemaker location: implications for sinoatrial conduction. *Am J Physiol.* 1995;269:H877-887.

186. Opthof T. The mammalian sinoatrial node. *Cardiovasc Drugs Ther.* 1988;1:573-597.

187. Schuessler RB, Boineau JP, Bromberg BI. Origin of the sinus impulse. *J Cardiovasc Electrophysiol.* 1996;7:263-274.

188. Boineau JP, Schuessler RB, Hackel DB, Miller CB, Brockus CW, Wylds AC. Widespread distribution and rate differentiation of the atrial pacemaker complex. *Am J Physiol.* 1980;239:H406-415.

189. Boineau JP, Schuessler RB, Mooney CR, Wylds AC, Miller CB, Hudson RD, Borremans JM, Brockus CW. Multicentric origin of the atrial depolarization wave: the pacemaker complex. Relation to dynamics of atrial conduction, P-wave changes and heart rate control. *Circulation.* 1978;58:1036-1048.

190. Boyett MR, Honjo H, Yamamoto M, Nikmaram MR, Niwa R, Kodama I. Regional differences in effects of 4-aminopyridine within the sinoatrial node. *Am J Physiol.* 1998;275:H1158-H1168.

191. Mondal T. Personal Communication. 2009.

192. Verheijck EE, Wessels A, van Ginneken AC, Bourier J, Markman MW, Vermeulen JL, de Bakker JM, Lamers WH, Opthof T, Bouman LN. Distribution of atrial and nodal cells within the rabbit sinoatrial node: models of sinoatrial transition. *Circulation.* 1998;97:1623-1631.

193. Lei M, Musa H, Honjo H. Regional differences in expression of Ca^{2+} handling proteins in sinoatrial node. *Biophys J.* 2000;78:106A.

194. Honjo H, Boyett MR, Kodama I, Toyama J. Correlation between electrical activity and the size of rabbit sino-atrial node cells. *J Physiol.* 1996;496:795-808.

195. Alings AM, Abbas RF, de Jonge B, Bouman LN. Structure and function of the simian sinoatrial node (Macaca fascicularis). *J Mol Cell Cardiol.* 1990;22:1453-1466.

196. Opthof T, de Jonge B, Jongsma HJ, Bouman LN. Functional morphology of the pig sinoatrial node. *J Mol Cell Cardiol.* 1987;19:1221-1236.

197. Matsuyama TA, Inoue S, Kobayashi Y, Sakai T, Saito T, Katagiri T, Ota H. Anatomical diversity and age-related histological changes in the human right atrial posterolateral wall. *Europace.* 2004;6:307-315.

198. Mandel W, Hayakawa H, Danzig R, Marcus HS. Evaluation of sino-atrial node function in man by overdrive suppression. *Circulation.* 1971;44:59-66.

199. Boyett MR, Fedida D. Changes in the electrical activity of dog cardiac Purkinje fibres at high heart rates. *J Physiol.* 1984;350:361-391.

200. Yamamoto M, Dobrzynski H, Tellez J, Niwa R, Billeter R, Honjo H, Kodama I, Boyett MR. Extended atrial conduction system characterised by the expression of the HCN4 channel and connexin45. *Cardiovasc Res.* 2006;72:271-281.

201. Yanni J, Boyett MR, Anderson RH, Dobrzynski H. The extent of the specialized atrioventricular ring tissues. *Heart Rhythm.* 2009;6:672-680.

202. Kistler PM, Sanders P, Fynn SP, Stevenson IH, Hussin A, Vohra JK, Sparks PB, Kalman JM. Electrophysiological and electrocardiographic characteristics of focal atrial tachycardia originating from the pulmonary veins: acute and long-term outcomes of radiofrequency ablation. *Circulation.* 2003;108:1968-1975.

203. Hillock RJ, Singarayar S, Kalman JM, Sparks PB. Tale of two tails: The tip of the atrial appendages is an unusual site for focal atrial tachycardia. *Heart Rhythm.* 2006;3:467-469.

204. Marrouche NF, SippensGroenewegen A, Yang Y, Dibs S, Scheinman MM. Clinical and electrophysiologic characteristics of left septal atrial tachycardia. *Journal of the American College of Cardiology.* 2002;40:1133-1139.

205. Nakahara S, Seino M, Sakai Y, Takayanagi K. A unique iatrogenic organized left atrial tachycardia with a gap conduction in previously ablated lesions. *Journal of Cardiology.*55:139-142.

206. Kistler PM, Sanders P, Hussin A, Morton JB, Vohra JK, Sparks PB, Kalman JM. Focal atrial tachycardia arising from the mitral annulus: electrocardiographic and electrophysiologic characterization. *J Am Coll Cardiol.* 2003;41:2212-2219.

207. Matsuo S, Yamane T, Date T, Yoshimura M. Spontaneously isolated sinus node activation in sick sinus syndrome as revealed by a three-dimensional mapping system. *Heart Rhythm.* 2010;7:856-857.

208. Rozanski GJ, Lipsius SL. Electrophysiology of functional subsidiary pacemakers in canine right atrium. *Am J Physiol.* 1985;249:H594-603.

209. Rozanski GJ, Lipsius SL, Randall WC, Jones SB. Alterations in subsidiary pacemaker function after prolonged subsidiary pacemaker dominance in the canine right atrium. *J Am Coll Cardiol.* 1984;4:535-542.

210. Rubenstein DS, Fox LM, McNulty JA, Lipsius SL. Electrophysiology and ultrastructure of eustachian ridge from cat right atrium: a comparison with SA node. *J Mol Cell Cardiol.* 1987;19:965-976.

211. Rubenstein DS, Lipsius SL. Mechanisms of automaticity in subsidiary pacemakers from cat right atrium. *Circ Res.* 1989;64:648-657.

212. Zhou Z, Lipsius SL. Properties of the pacemaker current I_f in latent pacemaker cells isolated from cat right atrium. *J Physiol.* 1992;453:503-523.

213. Zhou Z, Lipsius SL. Delayed rectifier potassium current I_K in latent atrial pacemaker cells isolated from cat right atrium. *Pflugers Arch.* 1994;426:341-347.

214. Bassani RA, Bassani JW, Lipsius SL, Bers DM. Diastolic SR Ca efflux in atrial pacemaker cells and Ca-overloaded myocytes. *Am J Physiol Heart Circ Physiol.* 1997;273:H886-892.

215. Zhou Z, Lipsius SL. Na^+-Ca^{2+} exchange current in latent pacemaker cells isolated from cat right atrium. *J Physiol.* 1993;466:263-285.

216. Marionneau C, Couette B, Liu J, Li H, Mangoni ME, Nargeot J, Lei M, Escande D, Demolombe S. Specific pattern of ionic channel gene expression associated with pacemaker activity in the mouse heart. *J Physiol.* 2005;562:223-234.

217. Verkerk AO, Wilders R, van Borren MMGJ, Peters RJG, Broekhuis E, Lam K, Coronel R, de Bakker JMT, Tan HL. Pacemaker current I_f in the human sinoatrial node. *Eur Heart J.* 2007;20:2472-2478.

218. Verkerk AO, van Borren MM, Peters RJ, Broekhuis E, Lam KY, Coronel R, de Bakker JM, Tan HL, Wilders R. Single cells isolated from human sinoatrial node: action potentials and numerical reconstruction of pacemaker current. *Conf Proc IEEE Eng Med Biol Soc.* 2007;2007:904-907.

219. Dobrev D. Ion Channel Portrait of the Human Sinus Node: Useful for a Better Understanding of Sinus Node Function and Dysfunction in Humans? *Circulation.* 2009;119:1556-1558.

220. Bourassa MG, Cote P, Theroux P, Tubau JF, Genain C, Waters DD. Hemodynamics and coronary flow following diltiazem administration in anesthetized dogs and in humans. *Chest.* 1980;78:224-230.

221. Levine TB, Bernink PJ, Caspi A, Elkayam U, Geltman EM, Greenberg B, McKenna WJ, Ghali JK, Giles TD, Marmor A, Reisin LH, Ammon S, Lindberg E. Effect of mibefradil, a T-type calcium channel blocker, on morbidity and mortality in moderate to severe congestive heart failure: the MACH-1 study. Mortality assessment in congestive heart failure trial. *Circulation.* 2000;101:758-764.

222. Essin K, Gollasch M. Role of ryanodine receptor subtypes in initiation and formation of calcium sparks in arterial smooth muscle: comparison with striated muscle. *J Biomed Biotechnol.* 2009;2009:135249.

223. Boyett MR, Honjo H, Yamamoto M, Nikmaram MR, Niwa R, Kodama I. Downward gradient in action potential duration along conduction path in and around the sinoatrial node. *Am J Physiol.* 1999;276:H686-H698.

224. Monfredi OJ, Wisloff U, Boyett MR. The effect of endurance training on the intrinsic heart rate and sinus node function of *Rattus rattus.* Trondheim, Norway; 2010.

225. Yanni J, Tellez JO, Sutyagin PV, Boyett MR, Dobrzynski H. Structural remodelling of the sinoatrial node in obese old rats. *J Mol Cell Cardiol.* 2010;48:653-662.

226. Huang X, Yang P, Du Y, Zhang J, Ma A. Age-related down-regulation of HCN channels in rat sinoatrial node. *Basic Res Cardiol.* 2007;102:429-435.

227. Cunningham AD. *Report for European Heart Rhythm Association*: National Pacemaker Database; 2007.

228. Adan V, Crown LA. Diagnosis and treatment of sick sinus syndrome. *Am Fam Physician.* 2003;67:1725-1732.

229. Lamas GA, Lee K, Sweeney M, Leon A, Yee R, Ellenbogen K, Greer S, Wilber D, Silverman R, Marinchak R, Bernstein R, Mittleman RS, Lieberman EH, Sullivan C, Zorn L, Flaker G, Schron E, Orav EJ, Goldman L. The mode selection trial (MOST) in sinus node dysfunction: design, rationale, and baseline characteristics of the first 1000 patients. *Am Heart J.* 2000;140:541-551.

230. Kulbertus HE, De Leval-Rutten F, Demoulin JC. Sino-atrial disease: a report on 13 cases. *J Electrocardiol.* 1973;6:303-312.

231. Thery C, Gosselin B, Lekieffre J, Warembourg H. Pathology of sinoatrial node. Correlations with electrocardiographic findings in 111 patients. *Am Heart J.* 1977;93:735-740.

232. Alings AMW, Abbas RF, Bouman LN. Age-related changes in structure and relative collagen content of the human and feline sinoatrial node: A comparative study. *Eur Heart J.* 1995;16:1655-1667.

233. Lakatta EG, Sollott SJ. The "heartbreak" of older age. *Mol Interv.* 2002;2:431-446.

234. Kistler PM, Sanders P, Fynn SP, Stevenson IH, Spence SJ, Vohra JK, Sparks PB, Kalman JM. Electrophysiologic and electroanatomic changes in the human atrium associated with age. *J Am Coll Cardiol.* 2004;44:109-116.

235. Alings AM, Bouman LN. Electrophysiology of the ageing rabbit and cat sinoatrial node - a comparative study. *Eur Heart J.* 1993;14:1278-1288.

236. Lev M. Aging changes in the human sinoatrial node. *J Gerontol.* 1954;9:1-9.

237. Davies MJ, Pomerance A. Quantitative study of ageing changes in the human sinoatrial node and internodal tracts. *Br Heart J.* 1972;34:150-152.

238. Shiraishi I, Takamatsu T, Minamikawa T, Onouchi Z, Fujita S. Quantitative histological analysis of the human sinoatrial node during growth and aging. *Circulation.* 1992;85:2176-2184.

239. Baruscotti M, DiFrancesco D, Robinson RB. Na^+ current contribution to the diastolic depolarization in newborn rabbit SA node cells. *Am J Physiol Heart Circ Physiol.* 2000;279:H2303-H2309.

240. Tellez JO, Dobrzynski H, Yanni J, Billeter R, Boyett MR. Effect of aging on gene expression in the rat sinoatrial node. *J Mol Cell Cardiol.* 2006;40:982-982.

241. Jones SA, Lancaster MK, Boyett MR. Ageing-related changes of connexins and conduction within the sinoatrial node. *J Physiol.* 2004;560:429-437.

242. Jones SA, Boyett MR, Lancaster MK. Declining into failure: the age-dependent loss of the L-type calcium channel within the sinoatrial node. *Circulation.* 2007;115:1183-1190.

243. Shaw DB, Linker NJ, Heaver PA, Evans R. Chronic sinoatrial disorder (sick sinus syndrome): a possible result of cardiac ischaemia. *Br Heart J.* 1987;58:598-607.

244. Rokseth R, Hatle L. Sinus arrest in acute myocardial infarction. *Br Heart J.* 1971;33:639-642.

245. Brueck M, Bandorski D, Kramer W. Incidence of coronary artery disease and necessity of revascularization in symptomatic patients requiring permanent pacemaker implantation. *Med Klin (Munich).* 2008;103:827-830.

246. Yabek SM, Jarmakani JM. Sinus node dysfunction in children, adolescents, and young adults. *Pediatrics.* 1978;61:593-598.

247. Radford DJ, Izukawa T. Sick sinus syndrome. Symptomatic cases in children. *Arch Dis Child.* 1975;50:879-885.

248. Kugler JD, Gillette PC, Mullins CE, McNamara DG. Sinoatrial conduction in children: an index of sinoatrial node function. *Circulation.* 1979;59:1266-1276.

249. Ector H, Van der Hauwaert LG. Sick sinus syndrome in childhood. *Br Heart J.* 1980;44:684-691.

250. Beder SD, Gillette PC, Garson A, Jr., Porter CB, McNamara DG. Symptomatic sick sinus syndrome in children and adolescents as the only manifestation of cardiac abnormality or associated with unoperated congenital heart disease. *Am J Cardiol.* 1983;51:1133-1136.

251. Lahat H, Eldar M, Levy-Nissenbaum E, Bahan T, Friedman E, Khoury A, Lorber A, Kastner DL, Goldman B, Pras E. Autosomal recessive catecholamine- or exercise-induced polymorphic ventricular tachycardia: clinical features and assignment of the disease gene to chromosome 1p13-21. *Circulation.* 2001;103:2822-2827.

252. Uretsky BF, Sheahan RG. Primary prevention of sudden cardiac death in heart failure: will the solution be shocking? *J Am Coll Cardiol.* 1997;30:1589-1597.

253. Stevenson WG, Stevenson LW, Middlekauff HR, Saxon LA. Sudden death prevention in patients with advanced ventricular dysfunction. *Circulation.* 1993;88:2953-2961.

254. Faggiano P, d'Aloia A, Gualeni A, Gardini A, Giordano A. Mechanisms and immediate outcome of in-hospital cardiac arrest in patients with advanced heart failure secondary to ischemic or idiopathic dilated cardiomyopathy. *Am J Cardiol.* 2001;87:655-657, A610-651.

255. Sanders P, Kistler PM, Morton JB, Spence SJ, Kalman JM. Remodeling of sinus node function in patients with congestive heart failure: reduction in sinus node reserve. *Circulation.* 2004;110:897-903.

256. Sparks PB, Mond HG, Vohra JK, Jayaprakash S, Kalman JM. Electrical remodeling of the atria following loss of atrioventricular synchrony: a long-term study in humans. *Circulation.* 1999;100:1894-1900.

257. Morton JB, Sanders P, Vohra JK, Sparks PB, Morgan JG, Spence SJ, Grigg LE, Kalman JM. Effect of chronic right atrial stretch on atrial electrical remodeling in patients with an atrial septal defect. *Circulation.* 2003;107:1775-1782.

258. Zicha S, Fernandez-Velasco M, Lonardo G, L'Heureux N, Nattel S. Sinus node dysfunction and hyperpolarization-activated (HCN) channel subunit remodeling in a canine heart failure model. *Cardiovasc Res.* 2005;66:472-481.

259. Elvan A, Wylie K, Zipes DP. Pacing-induced chronic atrial fibrillation impairs sinus node function in dogs. Electrophysiological remodeling. *Circulation.* 1996;94:2953-2960.

260. Kumagai K, Akimitsu S, Kawahira K, Kawanami F, Yamanouchi Y, Hiroki T, Arakawa K. Electrophysiological properties in chronic lone atrial fibrillation. *Circulation.* 1991;84:1662-1668.

261. Manios EG, Kanoupakis EM, Mavrakis HE, Kallergis EM, Dermitzaki DN, Vardas PE. Sinus pacemaker function after cardioversion of chronic atrial fibrillation: is sinus node remodeling related with recurrence? *J Cardiovasc Electrophysiol.* 2001;12:800-806.

262. Hadian D, Zipes DP, Olgin JE, Miller JM. Short-term rapid atrial pacing produces electrical remodeling of sinus node function in humans. *J Cardiovasc Electrophysiol.* 2002;13:584-586.

263. Joung B, Tang L, Maruyama M, Han S, Chen Z, Stucky M, Jones LR, Fishbein MC, Weiss JN, Chen P-S, Lin S-F. Intracellular calcium dynamics and acceleration of sinus rhythm by beta-adrenergic stimulation. *Circulation.* 2009;119:788-796.

264. Yeh Y-H, Burstein B, Qi XY, Sakabe M, Chartier D, Comtois P, Wang Z, Kuo C-T, Nattel S. Funny current downregulation and sinus node dysfunction associated with atrial tachyarrhythmia. A molecular basis for tachycardia-bradycardia syndrome. *Circulation.* 2009;119:1576-1585.

265. Hocini M, Sanders P, Deisenhofer I, Jais P, Hsu LF, Scavee C, Weerasoriya R, Raybaud F, Macle L, Shah DC, Garrigue S, Le Metayer P, Clementy J, Haissaguerre M. Reverse remodeling of sinus node function after catheter

ablation of atrial fibrillation in patients with prolonged sinus pauses. *Circulation.* 2003;108:1172-1175.

266. Estes NA, 3rd, Link MS, Cannom D, Naccarelli GV, Prystowsky EN, Maron BJ, Olshansky B. Report of the NASPE policy conference on arrhythmias and the athlete. *J Cardiovasc Electrophysiol.* 2001;12:1208-1219.

267. Boyett MR. 'And the beat goes on.' The cardiac conduction system: the wiring system of the heart. *Exp Physiol.* 2009;94:1035-1049.

268. Baldesberger S, Bauersfeld U, Candinas R, Seifert B, Zuber M, Ritter M, Jenni R, Oechslin E, Luthi P, Scharf C, Marti B, Attenhofer Jost CH. Sinus node disease and arrhythmias in the long-term follow-up of former professional cyclists. *Eur Heart J.* 2008;29:71-78.

269. Stein R, Medeiros CM, Rosito GA, Zimerman LI, Ribeiro JP. Intrinsic sinus and atrioventricular node electrophysiologic adaptations in endurance athletes. *J Am Coll Cardiol.* 2002;39:1033-1038.

270. Sigvardsson K, Svanfeldt E, Kilbom A. Role of the adrenergic nervous system in development of training-induced bradycardia. *Acta Physiol Scand.* 1977;101:481-488.

271. Ordway GA, Charles JB, Randall DC, Billman GE, Wekstein DR. Heart rate adaptation to exercise training in cardiac-denervated dogs. *J Appl Physiol.* 1982;52:1586-1590.

272. Wasada T, Katsumori K, Hasumi S, Kasanuki H, Arii H, Saeki A, Kuroki H, Saito S, Omori Y. Association of sick sinus syndrome with hyperinsulinemia and insulin resistance in patients with non-insulin-dependent diabetes mellitus: report of four cases. *Intern Med.* 1995;34:1174-1177.

273. Podlaha R, Falk A. The prevalence of diabetes mellitus and other risk factors of atherosclerosis in bradycardia requiring pacemaker treatment. *Horm Metab Res Suppl.* 1992;26:84-87.

274. Howarth FC, Jacobson M, Shafiullah M, Adeghate E. Effects of insulin treatment on heart rhythm, body temperature and physical activity in streptozotocin-induced diabetic rat. *Clin Exp Pharmacol Physiol.* 2006;33:327-331.

275. Howarth FC, Jacobson M, Shafiullah M, Adeghate E. Long-term effects of streptozotocin-induced diabetes on the electrocardiogram, physical activity and body temperature in rats. *Exp Physiol.* 2005;90:827-835.

276. Hicks KK, Seifen E, Stimers JR, Kennedy RH. Effects of streptozotocin-induced diabetes on heart rate, blood pressure and cardiac autonomic nervous control. *J Auton Nerv Syst.* 1998;69:21-30.

277. Howarth F, Nowotny N, Zilahi E, El Haj M, Lei M. Altered expression of gap junction connexin proteins may partly underlie heart rhythm disturbances in the streptozotocin-induced diabetic rat heart. *Molecular and Cellular Biochemistry.* 2007;305:145-151.

278. Gregoratos G, Abrams J, Epstein AE, Freedman RA, Hayes DL, Hlatky MA, Kerber RE, Naccarelli GV, Schoenfeld MH, Silka MJ, Winters SL, Gibbons RI, Antman EM, Alpert JS, Hiratzka LF, Faxon DP, Jacobs AK, Fuster V, Smith SC, Jr. ACC/AHA/NASPE 2002 guideline update for implantation of cardiac pacemakers and antiarrhythmia devices: summary article. A report of the American College of Cardiology/American Heart Association Task Force on Practice Guidelines (ACC/AHA/NASPE Committee to Update the 1998 Pacemaker Guidelines). *J Cardiovasc Electrophysiol.* 2002;13:1183-1199.

279. Hayes DL, Zipes DP, Jalife J. Implantable Pacemakers. *Cardiac Electrophysiology From Cell To Bedside.* Vol 4: Saunders; 2006:1000-1010.

280. AVID. A comparison of antiarrhythmic-drug therapy with implantable defibrillators in patients resuscitated from near-fatal ventricular arrhythmias. *New Engl J Med.* 1997;337:1576-1584.

281. Grier D, Cook PG, Hartnell GG. Chest radiographs after permanent pacing. Are they really necessary? *Clin Radiol* 1990;42:244-249.

282. Connolly SJ, Gent M, Roberts RS, Dorian P, Roy D, Sheldon RS, Mitchell LB, Green MS, Klein GJ, O'Brien B. Canadian implantable defibrillator study (CIDS) : a randomized trial of the implantable cardioverter defibrillator against amiodarone. *Circulation.* 2000;101:1297-1302.

283. Boerth RC, Covell JW. Mechanical performance and efficiency of the left ventricle during ventricular stimulation. *Am J Physiol.* 1971;221:1686-1691.

284. Burkhoff D, Oikawa RY, Sagawa K. Influence of pacing site on canine left ventricular contraction. *Am.J.Physiol.* 1986;251:H428-H435.

285. Zile MR, Blaustein AS, Shimizu G, Gaasch WH. Right ventricular pacing reduces the rate of left ventricular relaxation and filling. *J Am Coll Cardiol.* 1987;10:702-709.

286. Askenazi J, Alexander JH, Koenigsberg DI, Belic N, Lesch M. Alteration of left ventricular performance by left bundle branch block simulated with atrioventricular sequential pacing. *Am J Cardiol.* 1984;53:99-104.

287. Bedotto JB, Grayburn PA, Black WH, Raya TE, McBride W, Hsia HH, Eichhorn EJ. Alterations in left ventricular relaxation during atrioventricular pacing in humans. *J Am Coll Cardiol.* 1990;15:658-664.

288. Betocchi S, Piscione F, Villari B, Pace L, Ciarmiello A, Perrone-Filardi P, Salvatore C, Salvatore M, Chiariello M. Effects of induced asynchrony on left ventricular diastolic function in patients with coronary artery disease. *J Am Coll Cardiol.* 1993;21:1124-1131.

289. Stojnic BB, Stojanov PL, Angelkov L, Pavlovic SU, Radjen GS, Velimirovic DB. Evaluation of asynchronous left ventricular relaxation by doppler echocardiography during ventricular pacing with AV synchrony (VDD): comparison with atrial pacing (AAI). *Pacing Clin Electrophysiol.* 1996;19:940-944.

290. Aronow WS. Epidemiology, pathophysiology, prognosis, and treatment of systolic and diastolic heart failure. *Cardiol Rev.* 2006;14:108-124.

291. Karpawich PP, Rabah R, Haas JE. Altered cardiac histology following apical right ventricular pacing in patients with congenital atrioventricular block. *Pacing Clin Electrophysiol.* 1999;22:1372-1377.

292. Adomian GE, Beazell J. Myofibrillar disarray produced in normal hearts by chronic electrical pacing. *Am Heart J.* 1986;112:79-83.

293. Ichiki H, Oketani N, Hamasaki S, Ishida S, Kataoka T, Ogawa M, Saihara K, Okui H, Fukudome T, Shinasato T, Kubozono T, Ninomiya Y, Matsushita T, Otsuji Y, Tei C. Effect of right ventricular apex pacing on the Tei index and brain natriuretic peptide in patients with a dual-chamber pacemaker. *Pacing Clin Electrophysiol.* 2006;29:985-990.

294. Tei C, Dujardin KS, Hodge DO, Kyle RA, Tajik AJ, Seward JB. Doppler index combining systolic and diastolic myocardial performance: clinical value in cardiac amyloidosis. *J Am Coll Cardiol.* 1996;28:658-664.

295. Dujardin KS, Tei C, Yeo TC, Hodge DO, Rossi A, Seward JB. Prognostic value of a Doppler index combining systolic and diastolic performance in idiopathic-dilated cardiomyopathy. *Am J Cardiol.* 1998;82:1071-1076.

296. Frohlig G, Schwaab B, Kindermann M. Selective site pacing: the right ventricular approach. *Pacing Clin Electrophysiol.* 2004;27:855-861.

297. Andersen HR, Nielsen JC, Thomsen PE, Thuesen L, Mortensen PT, Vesterlund T, Pedersen AK. Long-term follow-up of patients from a randomised trial of atrial versus ventricular pacing for sick-sinus syndrome. *Lancet.* 1997;350:1210-1216.

298. Heldman D, Mulvihill D, Nguyen H, Messenger JC, Rylaarsdam A, Evans K, Castellanet MJ. True incidence of pacemaker syndrome. *Pacing Clin Electrophysiol.* 1990;13:1742-1750.

299. Zhang H, David HL, Shlapakova I, Zhao X, Danilo P, Jr., Robinson RB, Cohen IS, Qu D, Xu Z, Rosen MR. Implantation of Sionatrial Node Cells into Canine Right Ventricle:Biological Pacing Appears Limited by the Substrate. Columbia University; 2010.

300. Cerbai E, Barbieri M, Li Q, Mugelli A. Ionic basis of action potential prolongation of hypertrophied cardiac myocytes isolated from hypertensive rats of different ages. *Cardiovasc Res.* 1994;28:1180-1187.

301. Cerbai E, Barbieri M, Mugelli A. Characterization of the hyperpolarization-activated current, I_f, in ventricular myocytes isolated from hypertensive rats. *J Physiol.* 1994;481:585-591.

302. Cerbai E, Barbieri M, Mugelli A. Occurrence and properties of the hyperpolarization-activated current I_f in ventricular myocytes from normotensive and hypertensive rats during aging. *Circulation.* 1996;94:1674-1681.

303. Stilli D, Sgoifo A, Macchi E, Zaniboni M, De Iasio S, Cerbai E, Mugelli A, Lagrasta C, Olivetti G, Musso E. Myocardial remodeling and arrhythmogenesis in moderate cardiac hypertrophy in rats. *Am J Physiol Heart Circ Physiol.* 2001;280:H142-150.

304. Fernandez-Velasco M, Goren N, Benito G, Blanco-Rivero J, Bosca L, Delgado C. Regional distribution of hyperpolarization-activated current I_f and hyperpolarization-activated cyclic nucleotide-gated channel mRNA expression in ventricular cells from control and hypertrophied rat hearts. *J Physiol.* 2003;553:395-405.

305. Edelberg JM, Aird WC, Rosenberg RD. Enhancement of murine cardiac chronotropy by the molecular transfer of the human beta2 adrenergic receptor cDNA. *J Clin Invest.* 1998;101:337-343.

306. Edelberg JM, Huang DT, Josephson ME, Rosenberg RD. Molecular enhancement of porcine cardiac chronotropy. *Heart.* 2001;86:559-562.

307. Wobus AM, Rohwedel J, Maltsev V, Hescheler J. Development of cardiomyocytes expressing cardiac-specific genes, action potentials, and ionic channels during embryonic stem cell-derived cardiogenesis. *Ann N Y Acad Sci.* 1995;752:460-469.

308. Piron J, Quang KL, Briec F, Amirault JC, Leoni AL, Desigaux L, Escande D, Pitard B, Charpentier F. Biological pacemaker engineered by nonviral gene transfer in a mouse model of complete atrioventricular block. *Mol Ther.* 2008;16:1937-1943.

309. Qu J, Plotnikov AN, Danilo P, Jr., Shlapakova I, Cohen IS, Robinson RB, Rosen MR. Expression and function of a biological pacemaker in canine heart. *Circulation.* 2003;107:1106-1109.

310. Qu J, Altomare C, Bucchi A, DiFrancesco D, Robinson R. Functional comparison of HCN isoforms expressed in ventricular and HEK 293 cells. *Pflug Arch Eur J Phy.* 2002;444:597-601.

311. Peters CJ, Chow SS, Angoli D, Nazzari H, Cayabyab FS, Morshedian A, Accili EA. In situ co-distribution and functional interactions of SAP97 with sinoatrial isoforms of HCN channels. *J Mol Cell Cardiol.* 2009;46:636-643.

312. Qu J, Barbuti A, Protas L, Santoro B, Cohen IS, Robinson RB. HCN2 overexpression in newborn and adult ventricular myocytes: distinct effects on gating and excitability. *Circ Res.* 2001;89:E8-14.

313. Plotnikov AN, Sosunov EA, Qu J, Shlapakova IN, Anyukhovsky EP, Liu L, Janse MJ, Brink PR, Cohen IS, Robinson RB, Danilo P, Jr., Rosen MR. Biological pacemaker implanted in canine left bundle branch provides ventricular escape rhythms that have physiologically acceptable rates. *Circulation.* 2004;109:506-512.

314. Bucchi A, Plotnikov AN, Shlapakova I, Danilo P, Jr., Kryukova Y, Qu J, Lu Z, Liu H, Pan Z, Potapova I, KenKnight B, Girouard S, Cohen IS, Brink PR, Robinson RB, Rosen MR. Wild-type and mutant HCN channels in a tandem biological-electronic cardiac pacemaker. *Circulation.* 2006;114:992-999.

315. Chadda KD, Banka VS, Bodenheimer MM, Helfant RH. Corrected sinus node recovery time. Experimental physiologic and pathologic determinants. *Circulation.* 1975;51:797-801.

316. Lin D, Callans DJ, Zipes DP, Jalife J. Sinus Rhythm Abnormalities. *Cardiac Electrophysiology From Cell To Bedside.* Vol Fourth: Saunders; 2006:479-484.

317. Chen J, Mitcheson JS, Tristani-Firouzi M, Lin M, Sanguinetti MC. The S4-S5 linker couples voltage sensing and activation of pacemaker channels. *Proc Natl Acad Sci USA.* 2001;98:11277-11282.

318. Tse HF, Xue T, Lau CP, Siu CW, Wang K, Zhang QY, Tomaselli GF, Akar FG, Li RA. Bioartificial sinus node constructed via in vivo gene transfer of an engineered pacemaker HCN Channel reduces the dependence on electronic pacemaker in a sick-sinus syndrome model. *Circulation.* 2006;114:1000-1011.

319. Plotnikov AN, Bucchi A, Shlapakova I, Danilo P, Jr., Brink PR, Robinson RB, Cohen IS, Rosen MR. HCN212-channel biological pacemakers manifesting ventricular tachyarrhythmias are responsive to treatment with I_f blockade. *Heart Rhythm.* 2008;5:282-288.

320. Bucchi A, Tognati A, Milanesi R, Baruscotti M, DiFrancesco D. Properties of ivabradine-induced block of HCN1 and HCN4 pacemaker channels. *J Physiol.* 2006;572:335-346.

321. Cho HC, Kashiwakura Y, Marban E. Creation of a Biological Pacemaker by Cell Fusion. *Circ Res.* 2007;100:1112-1115.

322. Kehat I, Amit M, Gepstein A, Huber I, Itskovitz-Eldor J, Gepstein L. Development of cardiomyocytes from human ES cells. *Methods Enzymol.* 2003;365:461-473.

323. Kehat I, Khimovich L, Caspi O, Gepstein A, Shofti R, Arbel G, Huber I, Satin J, Itskovitz-Eldor J, Gepstein L. Electromechanical integration of cardiomyocytes derived from human embryonic stem cells. *Nat Biotechnol.* 2004;22:1282-1289.

324. Xue T, Cho HC, Akar FG, Tsang SY, Jones SP, Marban E, Tomaselli GF, Li RA. Functional integration of electrically active cardiac derivatives from genetically engineered human embryonic stem cells with quiescent recipient ventricular cardiomyocytes: insights into the development of cell-based pacemakers. *Circulation.* 2005;111:11-20.

325. Kehat I, Kenyagin-Karsenti D, Snir M, Segev H, Amit M, Gepstein A, Livne E, Binah O, Itskovitz-Eldor J, Gepstein L. Human embryonic stem cells can differentiate into myocytes with structural and functional properties of cardiomyocytes. *J Clin Invest.* 2001;108:407-414.

326. Satin J, Kehat I, Caspi O, Huber I, Arbel G, Itzhaki I, Magyar J, Schroder EA, Perlman I, Gepstein L. Mechanism of spontaneous excitability in human embryonic stem cell derived cardiomyocytes. *J Physiol.* 2004;559:479-496.

327. Plotnikov AN, Shlapakova I, Szabolcs MJ, Danilo P, Jr., Lorell BH, Potapova IA, Lu Z, Rosen AB, Mathias RT, Brink PR, Robinson RB, Cohen IS, Rosen MR. Xenografted Adult Human Mesenchymal Stem Cells Provide a Platform for Sustained Biological Pacemaker Function in Canine Heart. *Circulation.* 2007;116:706-713.

328. Potapova I, Plotnikov A, Lu Z, Danilo P, Jr., Valiunas V, Qu J, Doronin S, Zuckerman J, Shlapakova IN, Gao J, Pan Z, Herron AJ, Robinson RB, Brink PR, Rosen MR, Cohen IS. Human mesenchymal stem cells as a gene delivery system to create cardiac pacemakers. *Circ Res.* 2004;94:952-959.

329. Cai J, Lin G, Jiang H, Yang B, Jiang X, Yu Q, Song J. Transplanted neonatal cardiomyocytes as a potential biological pacemaker in pigs with with complete atrioventricular block. *Transplantation.* 2006;81:1022-1026.

330. Assessment of adenoviral vector safety and toxicity: report of the National Institutes of Health Recombinant DNA Advisory Committee. *Hum Gene Ther.* 2002;13:3-13.

331. Wright MJ, Wightman LM, Lilley C, de AM, Hart SL, Miller A, Coffin RS, Thrasher A, Latchman DS, Marber MS. In vivo myocardial gene transfer: optimization, evaluation and direct comparison of gene transfer vectors. *Basic Res Cardiol.* 2001;96:227-236.

332. Muller OJ, Katus HA, Bekeredjian R. Targeting the heart with gene therapy-optimized gene delivery methods. *Cardiovasc Res.* 2006;73:453-462.

333. Jooss K, Yang Y, Fisher KJ, Wilson JM. Transduction of dendritic cells by DNA viral vectors directs the immune response to transgene products in muscle fibers. *J Virol.* 1998;72:4212-4223.

334. Yang Y, Nunes FA, Berencsi K, Furth EE, Gonczol E, Wilson JM. Cellular immunity to viral antigens limits E1-deleted adenoviruses for gene therapy. *Proc Natl Acad Sci USA.* 1994;91:4407-4411.

335. Volpers C, Kochanek S. Adenoviral vectors for gene transfer and therapy. *J Gene Med.* 2004;6 Suppl 1:S164-S171.

336. Kass-Eisler A, Leinwand L, Gall J, Bloom B, Falck-Pedersen E. Circumventing the immune response to adenovirus-mediated gene therapy. *Gene Ther.* 1996;3:154-162.

337. Chu D, Sullivan CC, Weitzman MD, Du L, Wolf PL, Jamieson SW, Thistlethwaite PA. Direct comparison of efficiency and stability of gene transfer into the mammalian heart using adeno-associated virus versus adenovirus vectors. *J Thorac Cardiovasc Surg.* 2003;126:671-679.

338. Vassalli G, Bueler H, Dudler J, von Segesser LK, Kappenberger L. Adeno-associated virus (AAV) vectors achieve prolonged transgene expression in mouse myocardium and arteries in vivo: a comparative study with adenovirus vectors. *Int J Cardiol.* 2003;90:229-238.

339. Muller OJ, Leuchs B, Pleger ST, Grimm D, Franz WM, Katus HA, Kleinschmidt JA. Improved cardiac gene transfer by transcriptional and transductional targeting of adeno-associated viral vectors. *Cardiovasc.Res.* 2006;70:70-78.

340. Miyake K, Suzuki N, Matsuoka H, Tohyama T, Shimada T. Stable integration of human immunodeficiency virus-based retroviral vectors into the chromosomes of nondividing cells. *Hum Gene Ther.* 1998;9:467-475.

341. Sakoda T, Kasahara N, Hamamori Y, Kedes L. A high-titer lentiviral production system mediates efficient transduction of differentiated cells including beating cardiac myocytes. *J Mol Cell Cardiol.* 1999;31:2037-2047.

342. Wu X, Burgess SM. Integration target site selection for retroviruses and transposable elements. *Cell Mol Life Sci.* 2004;61:2588-2596.

343. French BA, Mazur W, Geske RS, Bolli R. Direct in vivo gene transfer into porcine myocardium using replication-deficient adenoviral vectors. *Circulation.* 1994;90:2414-2424.

344. Buttrick PM, Kass A, Kitsis RN, Kaplan ML, Leinwand LA. Behavior of genes directly injected into the rat heart in vivo. *Circ Res.* 1992;70:193-198.

345. Deshmukh PM, Romanyshyn M. Direct His-bundle pacing: present and future. *Pacing Clin Electrophysiol.* 2004;27:862-870.

346. Cosio FG, Martin-Penato A, Pastor A, Nunez A, Montero MA, Cantale CP, Schames S. Atrial activation mapping in sinus rhythm in the clinical electrophysiology laboratory: observations during Bachmann's bundle block. *J Cardiovasc Electrophysiol.* 2004;15:524-531.

347. Shohet RV, Chen S, Zhou YT, Wang Z, Meidell RS, Unger RH, Grayburn PA. Echocardiographic destruction of albumin microbubbles directs gene delivery to the myocardium. *Circulation.* 2000;101:2554-2556.

348. Simpson D, Dudley SC, Jr. Lost in translation: what is limiting cardiomyoplasty and can tissue engineering help? *Curr Stem Cell Res Ther.* 2009;4:210-223.

349. Swijnenburg RJ, Tanaka M, Vogel H, Baker J, Kofidis T, Gunawan F, Lebl DR, Caffarelli AD, de Bruin JL, Fedoseyeva EV, Robbins RC. Embryonic stem cell immunogenicity increases upon differentiation after transplantation into ischemic myocardium. *Circulation.* 2005;112:I166-172.

350. Laflamme MA, Chen KY, Naumova AV, Muskheli V, Fugate JA, Dupras SK, Reinecke H, Xu C, Hassanipour M, Police S, O'Sullivan C, Collins L, Chen Y, Minami E, Gill EA, Ueno S, Yuan C, Gold J, Murry CE. Cardiomyocytes derived from human embryonic stem cells in pro-survival factors enhance function of infarcted rat hearts. *Nat Biotechnol.* 2007;25:1015-1024.

351. Stratagene. AdEasy Adenoviral Vector System. 2006/01/01/. Available at: http://www.stratagene.com/manuals/240009.pdf.

352. Zakeri Z, Lockshin RA. Cell death: history and future. *Adv Exp Med Biol.* 2008;615:1-11.

353. Kaufmann SH. Cell death induced by topoisomerase-targeted drugs: more questions than answers. *Biochim Biophys Acta.* 1998;1400:195-211.

354. Kingston PA, Sinha S, Appleby CE, David A, Verakis T, Castro MG, Lowenstein PR, Heagerty AM. Adenovirus-mediated gene transfer of transforming growth factor-beta3, but not transforming growth factor-beta1, inhibits constrictive remodeling and reduces luminal loss after coronary angioplasty. *Circulation.* 2003;108:2819-2825.

355. Qiagen. QIAGEN Handbooks & Protocols. 2005/01/11. Available at: http://www.qiagen.com/literature/default.aspx?WT.svl=m.

356. Biolabs NE. Technical reference. *New England Biolabs*. Available at: http://www.neb.com/nebecomm/tech_reference/restriction_enzymes/default.asp, 2010.

357. Promega cloning technical reference. Available at: http://www.promega.com/applications/cloning/.

358. Graham FL, Smiley J, Russell WC, Nairn R. Characteristics of a human cell line transformed by DNA from human adenovirus type 5. *J Gen Virol.* 1977;36:59-74.

359. Gluzman Y. SV40-transformed simian cells support the replication of early SV40 mutants. *Cell.* 1981;23:175-182.

360. Revab F. Gene transfer into the central and peripheral nervous system using adenoviral vectors. In: Enquist L, ed. *Protocols for Gene Transfer in Neuroscience: Towards Gene Therapy of Neurological Disorders*: John Wiley and Sons; 1996:81 - 92.

361. Maniatis T, Fritsch EF, Sambrook J. Appendix A: Biochemical Techniques *Molecular Cloning: a Laboratory Manual*: Cold Spring Harbour Laboratory; 1984:456.

362. Mahy BWJ. *Virology: A Practical Approach*. Oxford: IRL Press; 1991.

363. Act SASP. Available at: http://apc.homeoffice.gov.uk/reference/schedule-1-report.pdf.

364. Yamamoto M, Honjo H, Niwa R, Kodama I. Low-frequency extracellular potentials recorded from the sinoatrial node. *Cardiovasc Res.* 1998;39:360-372.

365. Kovesdi I, Brough DE, Bruder JT, Wickham TJ. Adenoviral vectors for gene transfer. *Curr Opin Biotechnol.* 1997;8:583-589.

366. Douglas JT. Adenoviral vectors for gene therapy. *Mol Biotechnol.* 2007;36:71-80.

367. Bett AJ, Haddara W, Prevec L, Graham FL. An efficient and flexible system for construction of adenovirus vectors with insertions or deletions in early regions 1 and 3. *Proc Natl Acad Sci USA.* 1994;91:8802-8806.

368. Shenk T. Adenoviridae: the viruses and their replication. In: Fields BN, ed. *Fields virology*. Philidelphia: Lippincott-Raven; 1996.

369. Mittereder N, March KL, Trapnell BC. Evaluation of the concentration and bioactivity of adenovirus vectors for gene therapy. *J Virol.* 1996;70:7498-7509.

370. Qu J, Kryukova Y, Potapova IA, Doronin SV, Larsen M, Krishnamurthy G, Cohen IS, Robinson RB. MiRP1 modulates HCN2 channel expression and gating in cardiac myocytes. *J Biol Chem.* 2004;279:43497-43502.

371. Wang J, Chen S, Siegelbaum SA. Regulation of Hyperpolarization-Activated HCN Channel Gating and Camp Modulation Due to Interactions of Cooh Terminus and Core Transmembrane Regions. *J Gen Physiol.* 2001;118:237-250.

372. Xin Z, Bucchi A, Oren RV, Kryukova Y, Dun W, Clancy CE, Robinson RB. In vitro characterization of HCN channel kinetics and frequency-dependence in myocytes predicts biological pacemaker functionality. *J Physiol.* 2009:jphysiol.2008.163444.

373. Denyer JC, Brown HF. Rabbit sino-atrial node cells: isolation and electrophysiological properties. *J Physiol.* 1990;428:405-424.

374. Marvin WJ, Jr., Chittick VL, Rosenthal JK, Sandra A, Atkins DL, Hermsmeyer K. The isolated sinoatrial node cell in primary culture from the newborn rat. *Circ Res.* 1984;55:253-260.

375. Kodama I, Boyett MR. Regional differences in the electrical activity of the rabbit sinus node. *Pflug Arch Eur J Phy* 1985;404:214-226.

376. Wang X, Bergelson JM. Coxsackievirus and adenovirus receptor cytoplasmic and transmembrane domains are not essential for coxsackievirus and adenovirus infection. *J Virol.* 1999;73:2559-2562.

377. Berkner KL. Development of adenovirus vectors for the expression of heterologous genes. *Biotechniques.* 1988;6:616-629.

378. Curiel DT, Douglas JT. *Adenoviral vectors for gene therapy*. New York: Academic Press; 2002.

379. Tillman BW, de Gruijl TD, Luykx-de Bakker SA, Scheper RJ, Pinedo HM, Curiel TJ, Gerritsen WR, Curiel DT. Maturation of dendritic cells accompanies high-efficiency gene transfer by a CD40-targeted adenoviral vector. *J Immunol.* 1999;162:6378-6383.

380. Nalbantoglu J, Pari G, Karpati G, Holland PC. Expression of the primary coxsackie and adenovirus receptor is downregulated during skeletal muscle maturation and limits the efficacy of adenovirus-mediated gene delivery to muscle cells. *Hum Gene Ther.* 1999;10:1009-1019.

381. Zabner J, Freimuth P, Puga A, Fabrega A, Welsh MJ. Lack of high affinity fiber receptor activity explains the resistance of ciliated airway epithelia to adenovirus infection. *J Clin Invest.* 1997;100:1144-1149.

382. Ito M, Kodama M, Masuko M, Yamaura M, Fuse K, Uesugi Y, Hirono S, Okura Y, Kato K, Hotta Y, Honda T, Kuwano R, Aizawa Y. Expression of

coxsackievirus and adenovirus receptor in hearts of rats with experimental autoimmune myocarditis. *Circ Res.* 2000;86:275-280.

383. Asher DR, Cerny AM, Weiler SR, Horner JW, Keeler ML, Neptune MA, Jones SN, Bronson RT, Depinho RA, Finberg RW. Coxsackievirus and adenovirus receptor is essential for cardiomyocyte development. *Genesis.* 2005;42:77-85.

384. Lim BK, Xiong D, Dorner A, Youn TJ, Yung A, Liu TI, Gu Y, Dalton ND, Wright AT, Evans SM, Chen J, Peterson KL, McCulloch AD, Yajima T, Knowlton KU. Coxsackievirus and adenovirus receptor (CAR) mediates atrioventricular-node function and connexin 45 localization in the murine heart. *J Clin Invest.* 2008;118:2758-2770.

385. Morris GM, Boyett MR. Perspectives - biological pacing, a clinical reality? *Ther Adv Cardiovasc Dis.* 2009;3:479-483.

386. Dobryzinski H. Personal Communication. 2009.

387. Cook SA, Poole-Wilson PA. Cardiac myocyte apoptosis. *Eur Heart J.* 1999;20:1619-1629.

388. Schrader K, Huai J, Jockel L, Oberle C, Borner C. Non-caspase proteases: triggers or amplifiers of apoptosis? *Cell Mol Life Sci.*67:1607-1618.

389. Haqqani HM, Kalman JM. Aging and sinoatrial node dysfunction: musings on the not-so-funny side. *Circulation.* 2007;115:1178-1179.

390. Nikmaram MR, Boyett MR, Kodama I, Suzuki R, Honjo H. Variation in effects of Cs^+, UL-FS-49, and ZD-7288 within sinoatrial node. *Am J Physiol.* 1997;272:H2782-2792.

391. Boyett MR, Honjo H, Kodama I, Lancaster MK, Lei M, Musa H, Zhang H. The sinoatrial node: cell size does matter. *Circ Res.* 2007;101:e81-82.

392. Lei M, Brown HF, Terrar DA. Modulation of delayed rectifier potassium current, I_K, by isoprenaline in rabbit isolated pacemaker cells. *Exp Physiol.* 2000;85:27-35.

393. Choi HS, Wang DY, Noble D, Lee CO. Effect of isoprenaline, carbachol, and Cs^+ on Na^+ activity and pacemaker potential in rabbit SA node cells. *Am J Physiol.* 1999;276:H205-214.

394. Danik SB, Liu F, Zhang J, Suk HJ, Morley GE, Fishman GI, Gutstein DE. Modulation of cardiac gap junction expression and arrhythmic susceptibility. *Circ Res.* 2004;95:1035-1041.

395. Lieu DK, Chan YC, Lau CP, Tse HF, Siu CW, Li RA. Overexpression of HCN-encoded pacemaker current silences bioartificial pacemakers. *Heart Rhythm.* 2008;5:1310-1317.

396. Gao Z, Chen B, Joiner M-lA, Wu Y, Guan X, Koval OM, Chaudhary AK, Cunha SR, Mohler PJ, Martins JB, Song L-S, Anderson ME. $\underline{I_f}$ and SR Ca^{2+} release both contribute to pacemaker activity in canine sinoatrial node cells. *Journal of Molecular and Cellular Cardiology.*In Press, Uncorrected Proof.

397. Satoh H. Sino-atrial nodal cells of mammalian hearts: ionic currents and gene expression of pacemaker ionic channels. *J Smooth Muscle Res.* 2003;39:175-193.

398. Herrmann S, Stieber J, Stockl G, Hofmann F, Ludwig A. HCN4 provides a 'depolarization reserve' and is not required for heart rate acceleration in mice. *EMBO J.* 2007;26:4423-4432.

399. Liu YM, Yu H, Li CZ, Cohen IS, Vassalle M. Cesium effects on I_f and I_k in rabbit sinoatrial node myocytes: implications for SA node automaticity. *J Cardiovasc Pharmacol.* 1998;32:783-790.